Characterising the structural, functional and metabolomic changes occurring in human corneal cells due to *Acanthamoeba castellanii* secretome and amelioration of infection using cerium oxide nanoparticles

Abdullah Alhazmi

School of Medicine

PhD thesis, University of Nottingham

2020-2021

Abstract

Acanthamoeba keratitis (AK) is a severe corneal infection that poses a public health problem. Treatment of AK remains challenging because it relies on prolonged therapeutic regimens often utilising drug combinations. The considerable damage to human ocular tissue of patients with AK is partially mediated by soluble factors present in the protozoan *Acanthamoeba castellanii's* secretome. The two aims of this thesis were to characterise the structural, functional and metabolomic changes occurring in human corneal cells caused by *A. castellanii* secretome and to investigate the potential amelioration of infection using cerium oxide nanoparticles (CeO_2NPs).

Human SV40 immortalised corneal epithelial cells (ihCECs) and corneal stromal cells (CSCs) were treated with various concentrations of *A. castellanii*-conditioned medium (ACCM) for different exposure times. ACCM significantly decreased cell viability, triggered apoptosis, disrupted the cell actin cytoskeleton and altered the ultrastructural properties of corneal cells, in a time- and concentration-dependant manner. These ACCM-related cellular alterations were mediated by *A. castellanii* proteases. Amino acid analysis of ACCM showed that serine and cysteine proteases are secreted by *A. castellanii.* ACCM also altered the levels of elements within CSCs, including changes in the abundance of potassium, sodium and calcium. However, ACCM exposure did not affect the DNA concentration of CSC cells. Liquid chromatography/mass spectrometry-based metabolomic analysis showed that ACCM induced alterations in nucleotide and amino acid contents in CSCs.

CeO_2NPs adversely compromised the proliferation and structural integrity, and encystation ability of *A. castellanii* in a dose-

dependent manner, they had no significant effect on corneal cells when utilised at doses up to 200 µg/mL. These results reaffirm previous findings and provide new insight into the adverse impact caused by *A. castellanii* secretome on corneal cells. The promising anti-*A. castellanii* effect of CeO_2NPs warrants further validation including testing their cytotoxic potential against human ocular tissue.

Contents

Dedication

All gratefulness to Allah, the most merciful and gracious for providing me the fortitude, forbearance and ability to complete my studies during this critical period of my life. I dedicate my thesis to my loving mother for her ongoing supplication to successfully complete the work as well as to my late father for praying for me before passing away in the last year of my PhD, may Allah, forgive and have mercy on him; as well as my dearest wife for her unlimited support and patience at all times; and lastly, my daughters and sons for their loyalty and support.

Acknowledgements

I would like to express my heartfelt gratitude and appreciation to all of my supervisors, Dr. Hany Elsheikha for his endless support, invaluable advice and useful ideas throughout the entire project, and to Dr. Laura Sidney and Dr. Andrew Hopkinson for their help, guidance and support during my studies.

I want also to express my thanks to all my colleagues, peers, post-doctoral researchers and technicians who were members of my research groups at Queen's Medical Centre and Sutton Bonington Campus for their friendship and support.

Thanks again to all the technicians (within and outside the Schools of Medicine and Veterinary Medicine) who helped me in performing some analysis by running the samples through instruments.

Finally, special thanks to Umm Al-Qura University for funding my PhD programme, and to the University of Nottingham for offering me the opportunity to develop new skills, learn more about conducting scientific research, and produce the results presented in this thesis.

List of Abbreviations

aa-tRNA	aminoacyl-tRNA
ACCM	*Acanthamoeba castellanii*-conditioned medium
ACCM-M199	ACCM mixed with M199 medium
ACCM-Epilife	ACCM mixed with Epilife medium
AcCP	Cysteine protease of *A. castellanii*
ADP	Adenosine diphosphate
AMP	Adenosine monophosphate
ATP	Adenosine triphosphate
AO	Acridine orange
AK	Acanthamoeba keratitis
ANOVA	Analysis of variance
BBB	Blood-brain barrier
BCA	Bicinchoninic acid assay
BSA	Bovine serum albumin
°C	Celsius
CA	Cutaneous acanth-amoebiasis
Ca^{2+}	Calcium
CeO_2NPs	Cerium oxide nanoparticles
CHX	Chlorhexidine
CMP	Cytidine monophosphate
CNS	Central nervous system
CO_2	Carbon dioxide
CSCs	Corneal stromal cells
CSF	Cerebrospinal fluid
DAPI	4',6-diamidino-2-phenylindole
DMSO	Dimethylsulfoxide
DNA	Deoxyribonucleic acid
ECM	Extracellular matrix
FBS	Fetal bovine serum
F-actin	Filamentous actin
GAE	Granulomatous amoebic encephalitis
G-actin	Globular actin

HKGS	Human keratinocyte growth supplement
HIV/AIDS	Human immunodeficiency virus
ihCECs	Immortalised human corneal epithelial cells
kDa	Kilo Daltons
KEGG	Kyoto Encyclopedia of Genes and Genomes
KSS	Kearns-Sayre Syndrome
ICP-MS	Inductively coupled plasma-mass spectrometry
LC-MS	Liquid chromatography-mass spectrometry
LDH	Lactate dehydrogenase
LogFC	Log Fold Change
MBP	Mannose-binding protein
MS	Mass spectrometry
MTT	(3-(4,5-dimethyl-2-thiazolyl)-2,5-diphenyl-2H-tetrazolium bromide)
NADH	Nicotinamide adenine dinucleotide-hydrogen
NM	Normal medium
NPs	Nanoparticles
PALS	Pathway Activity Level Scoring
PBS	Phosphate buffered saline
PCA	Principal Component Analysis
PCR	Polymerase chain reaction
PFA-ST	Perfluoroalkoxy nebulizer ST
PHMB	Polyhexamethylene biguanide
PiMP	Polyomics integrated Metabolomics Pipeline
Ppb	Part-per-billion
Ppm	Part-per-million
Propox	Propylene oxide
PYG	Medium (Peptone-Yeast Extract-Glucose)
QC	Quality control
RNA	Ribonucleic acid
rRNA	Ribosomal ribonucleic acid
ROS	Reactive oxygen species
SD	Standard deviation
SDS	Sodium dodecyl sulphate

SRB	Sulforhodamine B
SSA	Sulphosalicylic acid
TCA	Trichloroacetic acid
TEM	Transmission electron microscope
T0	Time 0 group
T48hCTRL	Time 48 h control group
T48hINF	Time 48 h infected group
UV	Ultraviolet radiation
w/v	Weight by volume

List of Figures

List of Tables

1. Chapter One: Literature Review

1.1 The research problem

Acanthamoeba species are free-living, single-celled eukaryotes and ubiquitous protozoa. Some *Acanthamoeba* species can be opportunistic human pathogens. For example, *Acanthamoeba castellanii* genotype T4 is the agent that causes Acanthamoeba keratitis (AK), a serious ocular condition that compromises the sight (Carnt *et al.*, 2018; Marciano-Cabral and Cabral, 2003).

The pathogenesis mechanism associated with eye infection as a result of *Acanthamoeba* is uncertain. However, it is necessary to understand the mechanisms related to this organism's pathogenic potential, in order to develop new and more effective therapeutic interventions. Existing drugs have a limited effect, and numerous challenges are encountered as a result of frequent application with adverse side effects, especially during the late infection phases. Modern, long-term treatment uses a combination of drugs which have few effects, many of which are insignificant. Although chemotherapy is particularly costly, and results in detrimental and toxicity concerns as well as drug resistance, it remains the preferred treatment (Lorenzo-Morales, Khan and Walochnik, 2015). Consequently, the aim of this thesis is to create and characterise new and significant information in order to elucidate the molecular mechanism of AK pathogenicity.

Given the current limitations of anti-Acanthamoebic drugs, this thesis also aims to test a new preventive agent against *A. castellanii*.

1.2 General aspects of *Acanthamoeba*

1.2.1 History of discovery

In 1930, *Acanthamoeba* was initially defined by Castellanii as a eukaryote of contaminated culture from fungal culture (Marciano-Cabral and Cabral, 2003; Visvesvara, 1991; Castellanii, 1930). Sawyer and Griffin (1975), placed the *Acanthamoeba* genus in the Acanthamoebidae family (Sawyer and Griffin, 1975; Fuerst, Booton and Crary, 2015). In 1958, Culbertson produced the first hypothesis concerning the infectious nature of *Acanthamoeba* (Marciano-Cabral and Cabral, 2003; Culbertson, Smith and Minner, 1958). Nagington et al, were first to report AK in the UK (Nagington *et al.*, 1974), and Jones et al, were the first to document AK in the USA (Jones, Visvesvara and Robinson, 1975). Following this, numerous studies have defined the place of *Acanthamoeba* in AK, revealing that contact lenses are a major risk factor for AK because of lens contamination (Visvesvara, 1991; Radford, Minassian and Dart, 2002; Lindsay *et al.*, 2007).

1.2.2 Classification of *Acanthamoeba*

Acanthamoeba is in the Protista Kingdom as shown in Table 1-1. The *Acanthamoeba* taxonomy mainly emanated from morphological studies in trophozoite and cyst (Visvesvara, 1991). A minimum of 10 species had been detected and recorded by 1977. In the same year, Pussard and Pons recognised variation in cyst morphology and recorded at least 18 species (Visvesvara, 1991; Khan, 2006; Pussard and Pons, 1977). Booton *et al*, (2005) documented 25 *Acanthamoeba* genus species with pathogenic attributes, which included *A. castellanii,* as well as other *Acanthamoeba* species (Booton *et al.*, 2005). The *Acanthamoeba* classification genus was previously limited to the morphological identification, mainly concerning the morphology and size of the cysts. Nevertheless, this categorisation may now be considered fallible. Therefore, in order to categorise *Acanthamoeba* spp. correctly, new identification processes have been developed recently.

Table 1-1 The taxonomic classification of *Acanthamoeba* (Martinez and Visvesvara, 1997).

Kingdom	**Protista**
Subkingdom	Protozoa
Phylum	Sarcomastigophora
Subphylum	Sarcodina
Superclass	Rhizopoda
Class	Lobosea
Subclass	Gymnamoeba
Order	Amoebida
Suborder	Acanthopodina
Family	Acanthamoebidae
Genus	Acanthamoeba

As molecular tools have advanced, the classification basis of the *Acanthamoeba* genus' categorisation basis has moved to the gene sequences of ribosomal ribonucleic acid (rRNA). The *Acanthamoeba* genus is currently categorised into 20 different isolates bearing genotypes (T1-T20) (Fuerst, Booton and Crary, 2015; Corsaro *et al.*, 2015). Each of these shows a difference in sequences with the others of at least >5 (Siddiqui and Khan, 2012). This categorisation shows that 90 per cent of keratitis cases are the result of *Acanthamoeba castellanii*, particularly genotype T4.

1.2.3 Life cycle and morphology of *Acanthamoeba*

The *Acanthamoeba* species' life cycle involves two phases: the metabolically active trophozoites and the cyst, which is the

dormant phase (Figure 1-1). During the trophozoites stage, they replicate by mitosis. Since trophozoites are active, they are considered to be infective types of *Acanthamoeba* whose size is between 12 and 35 µm, whereas the length of the cyst is between 5 and 20 µm (Khan, 2006). A central nucleolus is enclosed with the nucleus of the trophozoites, and their cytoplasm, includes contractile vacuoles (Marciano-Cabral and Cabral, 2003; Khan, 2006). They carry on their surfaces, spine-like configurations known as acanthopodia which give *Acanthamoeba* its broadly applied and accepted name. Acanthopodia are the outward extension developing from the cytoplasm allowing the organism movement and adherence to the host cell's surface (Marciano-Cabral and Cabral, 2003; Bowers and Korn, 1968; Khan, 2006).

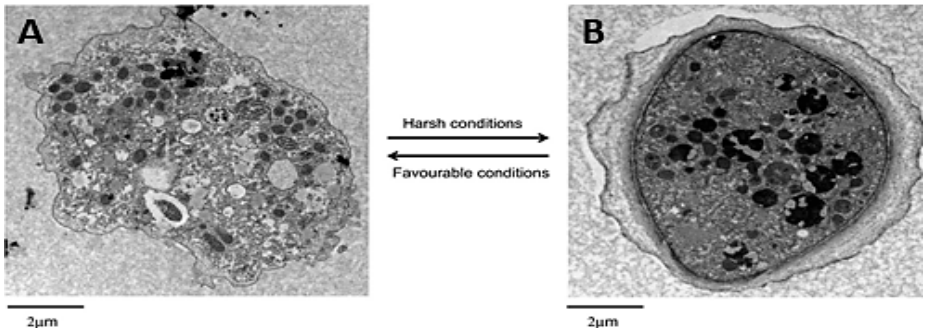

Figure 1-1 *Acanthamoeba* has two major stages in its life cycle: trophozoite and cyst forms. The trophozoite is the infective form of *Acanthamoeba* (A). Under unfavourable conditions, the trophozoite transforms into a cyst (B). (Siddiqui and Khan, 2012).

It is known that trophozoites, being the infectious and active form of *Acanthamoeba*, obtain their nutrition by feeding on other environmental micro-organisms, including bacterial cells and other micro-organisms on the surfaces to which they attach themselves (Marciano-Cabral and Cabral, 2003; Khan, 2006). To manage extremely, adverse environmental conditions, *Acanthamoeba* change to their dormant form to the cyst. It has been recorded that in exceptional environmental conditions including the presence of biocides, high temperature and high/low pH, induce the development of cysts through a procedure known as encystment is induced. The encystment process involves monoclonal antibodies binding to specific membrane proteins in *A. castellanii* (Marciano-Cabral and Cabral, 2003; Villemez, Carlo and Russell, 1985) and serves as a mechanism for parasite protection and survival. When environmental conditions become favourable, the cysts change back into the active trophozoites; a process known as excystment.

Infections occur when *Acanthamoeba* cysts or trophozoites come into contact with eyes, wounds or skin lesions, or the respiratory tract. Once inside the body, they move with the bloodstream into other vital body parts, proliferating and causing infection and proliferation (Figure 1-2) (Marciano-Cabral and

Cabral, 2003; Schuster and Visvesvara, 2004). It must be understood that *Acanthamoeba* species do not require a host in order to complete their life cycle. Since *Acanthamoeba* is able to survive as an infectious organism by infecting both humans and animals, or as a free-living amoeba, it functions as an opportunistic organism (Martinez and Visvesvara, 1997).

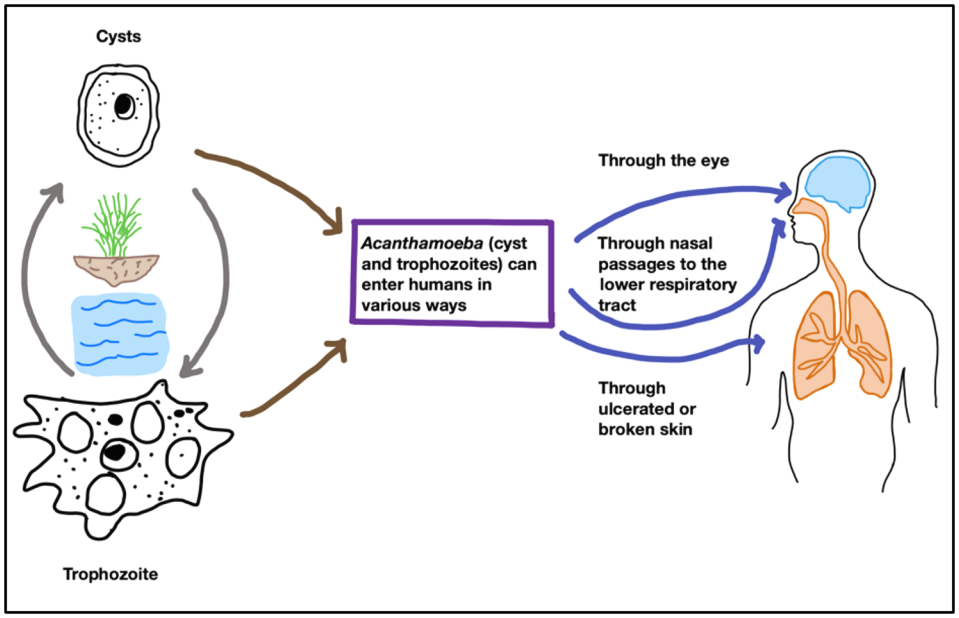

Figure 1-2 *Acanthamoeba* life cycle: *Acanthamoeba* has two specific stages: trophozoite and cysts. The trophozoite is the infective form of this parasite, which attacks the eyes, the respiratory tract or skin. *Acanthamoeba* eye infection can result in AK. When *Acanthamoeba* enters the body through skin wounds or through the respiratory system, it can lead to encephalitis, and also cause cutaneous infections. The cystic stage is formed when the trophozoite is subjected to stressful conditions.

1.2.4 Epidemiology of *Acanthamoeba*

Acanthamoeba species are extensively scattered in nature, especially in water and soil environments, as a free-living amoeba. Bacteria in these environments is a significant factor in maintaining these parasites because the bacteria are a food source (Marciano-Cabral and Cabral, 2003; Schuster and Visvesvara, 2004). Despite *Acanthamoeba* worldwide distribution and it being impossible to avoid contact with the parasite, the number of *Acanthamoeba* infections is comparatively small. It has been demonstrated by past studies that Anti-*Acanthamoeba* antibodies are present in about 80% of humans (Chappell *et al.*, 2001; Ahmed Khan, 2003), thereby showing the ability of healthy persons to resist being infected by *Acanthamoeba*.

The survival of *A. castellanii* is associated with their ability to adapt easily to various host environments to remain viable for long periods. The organism can survive extreme conditions of pH, moist heat of 60°C, irradiation, chemical conditions, and even freezing temperatures for years without any destruction or impairment (Sriram *et al.*, 2008). *Acanthamoeba* can transform into the cyst stage during adverse conditions, particularly during food outages and exposure to a chemical such as disinfectants.

Therefore, survival is sustained by ensuring the cysts are resistant to adverse environments.

1.2.5 *Acanthamoeba* T4 genotype

Acanthamoeba T4 genotype is commonly used in studies investigating the pathogenicity of *Acanthamoeba* spp. as it is involved in the pathogenicity of the majority of AK cases (Siddiqui and Khan, 2012; Maghsood *et al.*, 2005), The T4 genotype strain used in the present work was isolated from a clinical AK case and thus is highly relevant for the study of pathogenic effect of *A. castellanii* on corneal cells.

1.3 Structure of the human cornea: the target organ of *Acanthamoeba*

The human cornea is a dome-shaped, avascular transparent tissue located at the front of the eye that is directly exposed to the external environment (Figure 1-3). The human cornea allows light to enter the eye, then refracts the rays onto the retina (Baylis *et al.*, 2011; Klausner *et al.*, 2007). The cornea's surface protects the eye from external agents which have the potential to cause diseases and to damage deeper structures. Although at first glance the corneal tissue appears to lack substance, it is in fact a highly organised tissue comprising collagen fibrils, proteins and numerous cells. The corneal cells acquire oxygen and nutrients from the adjacent environment by a diffusion process

which also involves tear fluid and aqueous humour (Shafaie *et al.*, 2016; Alzubaidi *et al.*, 2016). As the major property of the cornea is transparency, it does not contain blood vessels like other body tissue. Therefore, nutrients diffuse directly from the tear fluid on the external environment and the aqueous humour in the internal environment (Sridhar, 2018). A histological cross-section shows that the cornea has six specific layers: 1) epithelium, 2) Bowman's membrane, 3) stroma, 4) Dua's layer, 5) Descemet's membrane, and 6) endothelium (Figure 1-4).

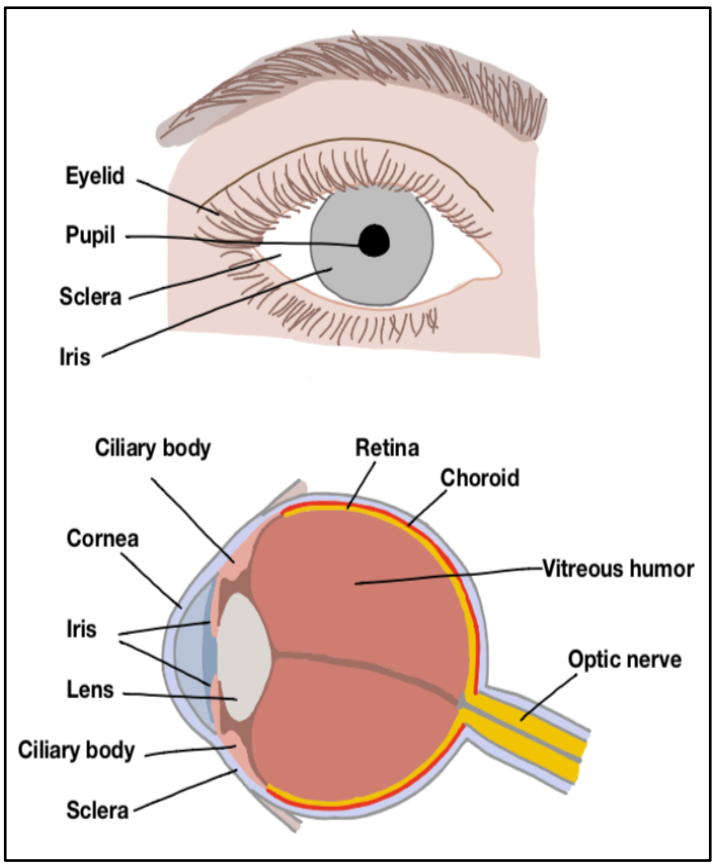

Figure 1-3 Schematic of the human eye.

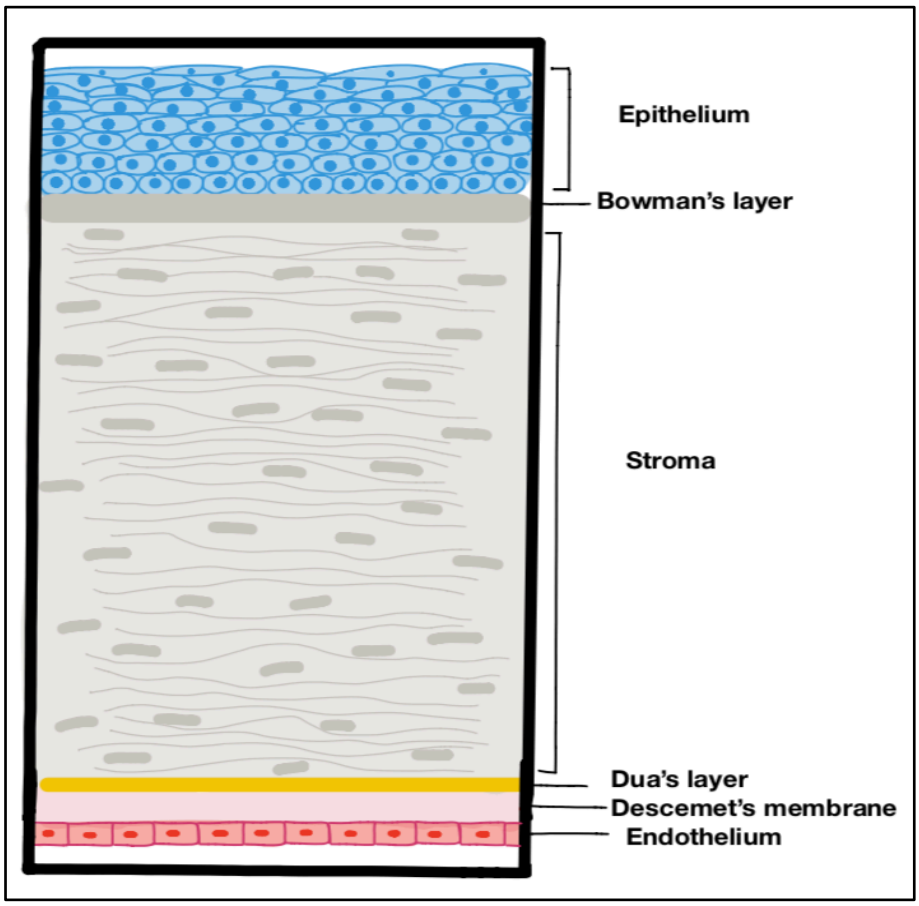

Figure 1-4 Cross-sectional structure of the human cornea.

1.3.1 Corneal epithelium

The corneal epithelium in humans is the outermost layer at the anterior of the cornea, with a thickness of about 50 μm. It comprises the intermediate layer of the epithelium (known as wing cells), sub-basal nerve plexus, superficial epithelial cells and basal epithelial cells (Alzubaidi *et al.*, 2016; Klausner *et al.*, 2007). The main purpose of the epithelium is to block foreign materials like dust and bacteria from entering the eye and the corneal stroma below, and provides a surface for absorbing

nutrients directly from the tear film before distributing the nutrients to the other parts of the cornea (Sridhar, 2018; Masterton and Ahearne, 2018). The corneal epithelium comprises between five and seven layers of stratified squamous epithelial cells, starting with basal cells in the deepest layer, and non-keratinized layers of cells such as the polyhedral wing cells in the second layer and squamous cells with flattened nuclei at the top. The cells undergo continuous cell division, with the basal cells and wing cells migrating to the corneal interior to differentiate into the squamous, which eventually mature fully and drop off into the tear film (Sridhar, 2018; Masterton and Ahearne, 2018).

1.3.2 Bowman's layer

The Bowman's layer is an acellular membrane which separates the stromal layers and the epithelium and is 12 μm thick. It comprises proteoglycans and collagen (Klausner *et al.*, 2007). A search of the literature shows no clear consensus on the physiological function of the membrane, but it is hypothesised that it serves as a physical barrier to protect the nerve plexus and stimulates epithelial nerve supply and sensory recovery.

1.3.3 Corneal stroma

The corneal stroma, which comprises 90% of the thickness of the human cornea, mainly comprises an extracellular matrix

(ECM) of collagen fibres and proteoglycans. The cells within the stroma are known as keratocytes which repair and regenerate ECM (Klausner *et al.*, 2007). Stromal wound healing is associated with the sequential action of growth factors on keratocytes. During the healing process of a corneal wound, released growth factors include the following: fibroblast growth factor-2 (FGF-2), transforming growth factor-beta (TGF-β), platelet-derived growth factor (PDGF), and insulin-like growth factor (IGF) activate keratocytes. These multiply and differentiate into myofibroblasts or fibroblasts, and subsequently migrate (Etheredge, Kane and Hassell, 2009). Similarly, *in vitro*, the growth factors IGF-I and IGF-II lead to the proliferation of keratocytes whilst retaining their dendritic morphology. ECM provides the transparency required for the cornea to transmit the light to the retina and provides the required structural strength for the cornea (Etheredge, Kane and Hassell, 2009). The components and organization of the ECM is imperative for the structure and function of the corneal stroma, regulated by a process the control collagen fibril formation or stromal fibrillogenesis. Some of the key components of the stromal ECM include the fibril forming collagens, network forming collagens, and leucine-rich proteoglycans.

1.3.4 Dua's Layer

Dua et al. have recently recognised a new layer in the human corneal tissue known as “Dua's Layer (DL)” or Pre-Descemet’s Layer (Shafaie *et al.*, 2016; Dua *et al.*, 2013). It is positioned between Descemet's membrane and the stroma. Although the DL is thin, it is characterized by its unique strength and airtight properties, which allows it to withstand pressure. The strength of the DL is attributed to the close packaging of collagen fibres (Dua, Faraj and Said, 2015). The findings by Dua *et al*. (2013) suggest that the DL is separated from the deep stroma and extend to the cornea periphery as indicated by the extension of stress lines. However, Dua *et al.* (2015) reveal that there are variations in the DL from one patient to another based on age, with the line of cleavage differing between adults and children in histological examinations.

1.3.5 Descemet’s membrane

This is a basal membrane of the corneal endothelium with a thickness of about 8 to 10 μm. The Descemet’s membrane consists of an interfacial matrix extending to the corneal stroma. The membrane contains a variety of collagen molecules, as well as laminin (Klausner *et al.*, 2007). The function of the Descemet’s membrane is to provide additional protection against physical injury to the eye or infections, protecting the endothelial

cells lying below it. Damage to the membrane leads to corneal opacity and may require a corneal transplant because the membrane has poor regeneration potential (de Oliveira and Wilson, 2020).

1.3.6 Corneal endothelium

The corneal endothelium is a layer of cells with thickness of approximately 5 μm. It occupies an important function as a barrier to fluid movement by regulating stromal hydration and transferring electrolytes and nutrients from the aqueous humour (Klausner *et al.*, 2007). The endothelium allows solutes including nutrients to move from the aqueous humour to the corneal shallow layers while also pumping water from the stroma to the aqueous humour, a process that averts corneal oedema developing which may lead to visual loss. This is especially important because corneal endothelial cells are lost with age, yet the cells do not regenerate. Overall, the main function of the endothelium is to regulate corneal hydration and nutrition (Klausner *et al.*, 2007).

1.4 Human infections caused by *Acanthamoeba*

1.4.1 Acanthamoeba keratitis (AK)

AK, which is a result of *Acanthamoeba* spp is a corneal disease that is sight threatening. It results in serious inflammation and

intense pain and can cause reduced vision leading to blindness if untreated (Stapleton *et al.*, 2009; Dart, Stapleton and Minassian, 1991). Contact lenses are a major risk element in developing AK. However, other conditions, such as a poor standard of personal hygiene can also lead to developing AK. These risk elements cause bacterial contamination and formation of biofilms which are a rich nutrient source for *Acanthamoeba* (Carnt and Stapleton, 2016; Dart, Stapleton and Minassian, 1991). Corneal trauma caused by injury due to foreign materials and followed by exposure to contaminated water is another potential risk factor associated with AK.

1.4.1.1 Life cycle of Acanthamoeba keratitis

During Acanthamoeba keratitis, the presence of *Acanthamoeba* on the ocular surface is completely incidental, probably caused by using contaminated contact lenses, or exposure of accidentally injured corneas being exposed to environmental sources contaminated with *Acanthamoeba* (Khan, 2006). Both *Acanthamoeba* cysts and trophozoite stages are able to enter the eyes. However, the cornea can only be infected by *Acanthamoeba* in the infective stage, trophozoite. Therefore, the cyst has to transform into the trophozoite once inside the eye to be infective. Once inside the cornea, trophozoites will multiply continuously and feed on the corneal cells as well as on any

contaminant bacteria (Khan, 2006). This leads to the progressive destruction of the corneal epithelium and Bowman's layer, offering a passage through to the stroma (described in detail in sections 1.5 and 1.4.1.2).

1.4.1.2 The host immune response in Acanthamoeba keratitis

When the eye is exposed to *Acanthamoeba* spp., the amoebae attach themselves to corneal epithelial cells by binding to the glycoproteins on the cell surface. *Acanthamoeba* produce a mannose-binding protein (MBP) that mediates adhesion to cells by binding to mannosylated glycoproteins on the cell surface (Marciano-Cabral and Cabral, 2003). The adherence of the organism to the cornea is followed by the invasion and destruction of the host cells, through release of proteases. The organism penetrates the epithelial cells and the Bowman's membrane by utilizing collagenolytic and proteolytic enzymes to allow invasion. *Acanthamoeba* then penetrates the corneal stroma, where invasion and destruction continue through the cytotoxic secretions and the phagocytotic processes.

The human body can react to an infection through either an innate or adaptive immune response. The innate immune response is immediate but not specific to the pathogen, whereas the adaptive response is long-term and specifically targets the pathogen, normally through antibody production. The innate

immune response plays a large part in fighting off initial infection, as described by Clarke and Niederkorn (2006a) The initial defence against *Acanthamoeba* spp is the tear fluid that the lacrimal system generates, as well as the continuous movement of the eyelid (Khan, 2005; Khan, 2006; Cwiklik, 2016). The tear film contains antimicrobial proteins such as lactoferrin, lysozyme, and immunoglobulin A (IgA), that prevent *Acanthamoeba* adherence and invasion (Alsam *et al.*, 2007). If adherence and invasion occur, innate immune cells such as neutrophils and macrophages are activated and infiltrate the cornea after infection and can kill the *Acanthamoeba* trophozoites through release of proteases, preventing infection from progressing.

Macrophages are unable to fight fully formed cysts do exhibit a chemotactic response to cyst lysate and trophozoites. The immune cells release, and induce other cells to produce, chemokines and cytokines. Upregulation of toll-like receptor 4 (TLR4) occurs activates the release of proinflammatory cytokines such as interleukin-8 (IL-8) and tumour necrosis factor-a (TNF-α). These inflammatory cytokines promote the immune responses by encouraging pathogen clearance, recruiting more immune cells and increasing inflammation (Ren, Gao and Wu, 2010). These are early response cytokines that are synthesized

during the acute inflammatory response, and then their levels significantly reduce within 6 hours after infection.

Macrophages generate an inflammatory response by secreting macrophage inflammatory protein (MIP-2), leading to neutrophil recruitment (Hurt *et al.*, 2001). Neutrophils are a key mediator in the innate immune response and are recruited to kill the trophozoites. Neutrophils are also able to eradicate the cyst form of the organism through a myeloperoxidase-dependent mechanism (Clarke and Niederkorn, 2006a).

Although the innate immune system mounts the initial defence against *Acanthamoeba* infection, the adaptive immune response may also be triggered after a lag time in which T and B cells undergo expansion (Clarke and Niederkorn, 2006a). In the adult population, 50-100% of people express specific antibodies for *Acanthamoeba* antigens, suggesting that exposure to *Acanthamoeba spp*. is common and progression of the disease to full infection is rare. In cases where the adaptive immune response fails to irradicate the disease, it may be due to the presence of dominant cysts remaining in the stroma. This is due to the body is being unable to completely eradicate the cyst form, in these cases treatment options are employed, such as mixed therapies using topical antimicrobial agents.

1.4.1.3 Clinical features of Acanthamoeba keratitis

AK is both a painful and progressive disease. The symptoms are clinically associated with the invasion and degradation of corneal components, leading to photophobia, redness and tearing (Lorenzo-Morales, Khan and Walochnik, 2015; Carrijo-Carvalho *et al.*, 2017; Pérez-Santonja *et al.*, 2003). The amoebas are first limited to the corneal epithelium; subsequently, the epithelial cells erode, and the organism punctures and invades the stroma, thereby creating a ring-shaped infiltrate, a common sign of amoebic keratitis. The clinical signs include the formation of an annular abscess, cataract, scleritis, glaucoma, corneal perforation, and secondary microbial infections that could develop as a result of AK. However, changes in the posterior area of the eye; for instance, the optic nerve and retina, are rare (Illingworth and Cook, 1998).

1.4.1.4 Diagnosis of Acanthamoeba keratitis

As AK mimics bacterial, fungal and viral infections, it can be difficult to diagnose. Nevertheless, it can be detected by isolating the micro-organism in culture medium from biopsy or corneal scrapings. The most frequently applied techniques for recognising *Acanthamoeba* infection are histopathological examinations, culture in specific medium, electron/optical microscopy and polymerase chain reaction (PCR) (Marciano-

Cabral and Cabral, 2003; Schaumberg, Snow and Dana, 1998; Khan, Jarroll and Paget, 2001). The most effective, sensitive and dependable technique to detect *Acanthamoeba* infection is PCR. Real-time multiplex PCR simultaneously identifies several genotypes in one sample; moreover, immunofluorescence assays have been applied in clinical samples to recognise *Acanthamoeba* spp. (Siddiqui and Khan, 2012; Qvarnstrom *et al.*, 2006).

1.4.1.5 Treatment of Acanthamoeba keratitis

Acanthamoeba infections are treated by applying various combinations of antimicrobial agents (Roberts and Henriquez, 2010; Lorenzo-Morales, Khan and Walochnik, 2015; Pérez-Santonja *et al.*, 2003). Although the majority of such drugs are effective on trophozoites, they are not effective against cysts. The cyst wall contains a physical barrier against anti-amoebic drugs because of its sturdy attributes (Lorenzo-Morales, Khan and Walochnik, 2015; Khan, 2006). In cases that do not respond well to traditional therapy, recurrent infections can occur (Dart, Saw and Kilvington, 2009). The lack of efficient antimicrobials against all *Acanthamoeba* isolates is among the problems encountered when treating AK (Siddiqui and Khan, 2012). Consequently, there is an urgent requirement for enhancing anti-

Acanthamoeba chemotherapy and alternative methods of developing therapeutic interventions.

Chlorhexidine (CHX) and polyhexamethylene biguanide (PHMB) are broad-spectrum medications that treat a wide range of protozoa, bacteria, and viruses. They are used for treating AK (Marciano-Cabral and Cabral, 2003; Lorenzo-Morales, Khan and Walochnik, 2015). Both the drugs have shown to have good efficacy against both types of *Acanthamoeba*. The CHX and PHMB cationic molecules act on the cell membrane by binding to the cell membrane's negatively charged lipid bilayer, causing cell damage and death. PHMB causes impairment of the cytoplasmic membrane, resulting in increased permeability and fluidity, while CHX causes respiratory enzymes inhibition and cellular components loss, and thus the integrity of the microorganism cell is lost (Hübner and Kramer, 2010; Polat and Vural, 2012). Both drugs are considered generally safe, although CHX requires lows doses of administration to avoid any toxic effect.

Nevertheless, the long-term usage of both drugs, especially at elevated concentrations, may lead to the formation of cataracts, iris atrophy, reduce or zero cornea regeneration, and ulceration of the cornea (Dart, Saw and Kilvington, 2009; Carrijo-Carvalho *et al.*, 2017). Therefore, care must be taken when using these

antiseptics to avoid corneal toxicity. Furthermore, according to Dart (2003), corneal toxicity can be associated with cumulative drug deposition through systematic medications such as chloroquine, indomethacin and amiodarone, which result in deposits within the corneal epithelium.

AK treatment is difficult and requires a long-term usage of pharmaceuticals (Dart, Saw and Kilvington, 2009; Carrijo-Carvalho *et al.*, 2017). Generally, treatment can be given immediately following corneal debridement, in which topical antimicrobials are applied every hour for three days from when therapy commences. It is suggested that this is applied for several days, depending on the response to treatment. The dose can be reduced to being taken every two hours for a minimum period of three to four weeks. Nevertheless, it is common practice to observe patients frequently, during and after treatment in order to avoid a recurrence of infection with resistant cystic forms.

However, the drug may not have the anticipated impact in certain cases in the late stage of AK treatment. Therefore, surgical intervention, such as corneal transplantation and debridement may be needed (Marciano-Cabral and Cabral, 2003; Lorenzo-Morales, Khan and Walochnik, 2015). When patients are not treated, the cornea will become ulcerated and

damaged as the disease progresses, leading to complications such as secondary glaucoma iris atrophy.

1.4.1.6 Epidemiology of Acanthamoeba keratitis

Despite the rarity of this disease, recent studies have indicated a higher rate of AK in those who wear contact lenses. The studies have also revealed that contact-lens wearers are as many as 80 times more likely to develop keratitis because of corneal abrasions, poor contact-lens hygiene and the application of contaminated saline cleaning solutions (Dart, Stapleton and Minassian, 1991). In developed nations, approximately 90% of AK cases are diagnosed in contact-lens wearers (Kilvington and Lam, 2013; Radford, Minassian and Dart, 2002) and in 2010, it was estimated that, from a global perspective, about 140 million people wear contact lenses (Swanson, 2012; Rabiah *et al.*, 2019). This data is valuable because it indicates the potential increase in AK as a public health problem. Since contact lenses are associated with AK, prevention measures focus on decontamination of lens using good storage solutions and eye hygiene. Decontamination should target both the cysts and the trophozoites.

Furthermore, it has been accepted that non-contact lens wearers can also develop keratitis as a result of *Acanthamoeba* (Sharma, Garg and Rao, 2000; Lorenzo-Morales, Khan and Walochnik,

2015; Demirci *et al.*, 2006). Consequently, researchers have been motivated to examine other risk factors which could contribute to developing AK, revealing that certain groups have a greater risk of being infected than do others. For instance, people whose immune system is weak, such as those who have HIV/AIDS and those being given chemotherapy are more susceptible to infections (Friedland *et al.*, 1992; Marciano-Cabral and Cabral, 2003; Fatemeh, Maryam and Zeynab, 2017). The immune system plays an important role in fighting AK because immune-competent individuals can prevent disease recurrence and minimize the risk of development of infection with severe disease or treatment failure involving innate and acquired immunity. However, the role of antibodies in *Acanthamoeba* infection is not fully known and inconsistencies exist in the explanation of immune responses (Marciano-Cabral and Cabral, 2003).

Further research findings reveal that the incidence rate of *Acanthamoeba* varies globally. It has been estimated that in the United States, there are 1.65 to 2.01 cases annually in contact lens wearers (Dart, Saw and Kilvington, 2009; Kolar *et al.*, 2015), and that the corresponding statistic in the United Kingdom is 17.53 to 19.50 per million (Dart, Saw and Kilvington, 2009). The number of parasitic infections in developing nations could be

considerably greater as a result of higher temperatures, outdoor events and the availability of efficient antimicrobials.

1.4.1.7 Control of Acanthamoeba keratitis

The prevalence of these *Acanthamoeba* means that it is impossible to avoid contact with them. Nevertheless, simple precautions can be taken to reduce contact with *Acanthamoeba*, incusing ensuring that corneal injuries are not exposed to soil and water that could have been contaminated by *Acanthamoeba*, and by avoiding swimming pools or hot springs which have not been properly treated. Contact-lens wearers should clean their lenses regularly with a disinfectant solution rather than with tap water and avoid wearing them while swimming. Lastly, in order to avoid progression of this disease, correct diagnosis and efficient treatment should be conducted at an early stage (Illingworth and Cook, 1998; Cohen *et al.*, 1987; Lorenzo-Morales, Khan and Walochnik, 2015).

1.4.2 Other infections caused by *Acanthamoeba*

Acanthamoeba spp. may infect other body systems, thereby resulting in encephalitis and cutaneous infections (Marciano-Cabral and Cabral, 2003; Schuster and Visvesvara, 2004). However, cutaneous infections due to *Acanthamoeba* spp. occur rarely, and only in HIV/AIDS patients or those having

immunosuppression as a result of any other cause, and are characterised by erythematous nodules or ulcerations (Chandrasekar *et al.*, 1997; Marciano-Cabral and Cabral, 2003). Such lesions are possible entry routes for infection of the central nervous system (CNS), In such cases, there is a connection between spreading of *Acanthamoeba* to other sites in the host and cutaneous acanthamebiasis (CA) (Marciano-Cabral and Cabral, 2003). Histologically, cutaneous lesions appear on the skin, and where *Acanthamoeba* is present, it is located especially in perivascular spaces or blood vessels (Marciano-Cabral and Cabral, 2003; Friedland *et al.*, 1992).

Granulomatous Amoebic Encephalitis (GAE), which is regarded as being a CNS infection, is a life-threatening and unexpected disease which occurs as a result of *Acanthamoeba* spp. and other free-living amoebae species (Martinez and Visvesvara, 1997; Julio Martinez, 1991). *Acanthamoeba*, in this situation, functions as an opportunistic pathogen because most currently reported cases are in immunologically debilitated persons, such as those who have HIV/AIDS, those receiving chemotherapy or broad spectrum antibiotics, pregnant women and chronic alcoholics (Martinez and Visvesvara, 1997; Julio Martinez, 1991).

The possibility of this infection is higher in patients with illnesses such as renal failure, haematological disease, hepatic disease, pneumonitis, cirrhosis of the liver, diabetes, transplant receivers and AIDS (Julio Martinez, 1991; Siddiqui and Khan, 2012; Martinez and Visvesvara, 1997). The long-term application of immunosuppressive drugs required to treat certain cases leads to the breakdown of the body's immune system which may result in secondary infections; for instance, GAE (Khan, 2006). However, this infection's pathogenic mechanisms remain unclear. The pathophysiological complications which involve the CNS cause a proinflammatory response, and an incursion into the blood-brain barrier (BBB) tissue, and subsequently lead to inflammation and neuronal injury (Schuster and Visvesvara, 2004; Siddiqui *et al.*, 2011; Khan, 2007). Consequently, it is necessary to conduct additional studies in order to explore the pathogenic mechanisms connected with such infections.

Studies show that the *Acanthamoeba* trophozoites access the CNS by two routes, namely, cutaneous infection or the lungs through haematogenous dissemination. Infections are caused by inhaling of amoebic cysts that invade the nasal passage mucosa, subsequently migrating to the lungs, and then entering the bloodstream (Visvesvara, Moura and Schuster, 2007; Khan, 2008; Khan, 2007). Following this, they are able to cross the

blood-brain barrier and enter the CNS, leading to infection. As this illness gradually becomes worse, its incubation period may be weeks, or even months, and could be present for an unspecified time.

1.5 Pathogenesis of Acanthamoeba keratitis

Pathogenesis of AK, which is a long procedure, involves numerous factors that cause the disease, and depends on the environment, host and parasite. A characterisation of virulence factors of *Acanthamoeba* is given below. This involves both direct and indirect factors (Lorenzo-Morales, Khan and Walochnik, 2015; Khan, 2006; Ahmed Khan, 2003).

1.5.1 Direct factors

A) Contact-dependent mechanisms:

In order to attach, invade and damage host cells, *Acanthamoeba castellanii* are dependent on contact. This induces secondary events; for instance, secretion of extracellular proteins, adhesion to the host cells and the capability of phagocytosing, resulting in the death of the host cells as shown in figure 1-5.

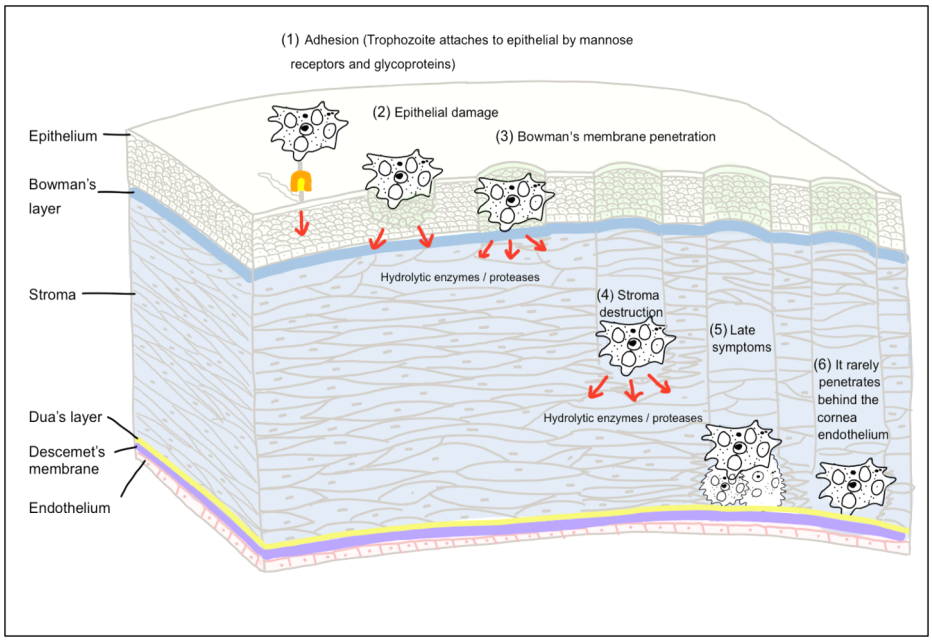

Figure 1-5 Pathogenesis of AK. 1) *Acanthamoeba* trophozoite adheres to the membranes of the corneal epithelial cells through MBP and mannose-glycoproteins. 2) The trophozoites penetrate the corneal epithelium via cytolysis, phagocytosis, and release hydrolytic enzymes in particular proteases. 3) The trophozoites degrade Bowman's layer and continue to produce proteases, which causes cellular tissue damage. 4 and 5) Destruction of stromal cells with the appearance of late symptoms of AK, which leads to secretion of inflammatory cytokines, further increasing cytolysis and cell apoptosis. 6) Infection of the corneal endothelium is rarely detected. The figure adapted from (Clarke and Niederkorn, 2006b).

Adhesion is the initial step of establishing the AK infectious procedure which enables the parasite to cross biological barriers within the host cells. *Acanthamoeba* trophozoite binds itself to the membranes of the host cell through mannose-binding protein (MBP) which binds to mannose-glycoproteins on the corneal epithelial cell (Yang, Cao and Panjwani, 1997; Clarke and Niederkorn, 2006b). This interaction is required in order to penetrate the epithelial cells, causing the disease. Furthermore,

it is thought that the amount of acanthopodia on the trophozoite surface is the second noteworthy element in the adhesion procedure to the surface of the cornea (Lakhundi, Siddiqui and Khan, 2017).

Phagocytosis, which has important functions in *Acanthamoeba* infection pathogenesis, is induced by adhesion of trophozoites with host cells, defined as the ingestion procedure of the host cells (Lorenzo-Morales, Khan and Walochnik, 2015; Khan, 2006; Avery, Harwood and Lloyd, 1995). *Acanthamoeba* employs phagocytosis as a means of feeding by using amoebastomes as food cups even in the incubation stage to promote pathogenesis. Therefore, pseudopods surround the bond particles, which are ingested into the cytoplasm and are then released into the cytoplasmic stream as a phagosome. *Acanthamoeba* phagocytosis is defined as a tyrosine kinase-actin-dependent mechanism associated with the polymerisation into filamentous (F)-actin of monomeric globular actin (G-actin) to enable phagocytosis regulation. As a result, phagocytosis is activated by sodium orthovanadate (an inhibitor of protein-tyrosine phosphatase), whereas Genistein (an inhibitor of protein-tyrosine kinase) inhibits the phagocytosis process. Studies have revealed that *Acanthamoeba*-mediated host cell death has been suppressed by cytochalasin D, which is an actin polymerisation

inhibitor, thereby implying that actin-mediated cytoskeletal modifications have an important role in *Acanthamoeba* pathogenesis (Lorenzo-Morales, Khan and Walochnik, 2015; Khan, 2006).

B) Independent contact factors:

The majority of pathogens, including *Acanthamoeba*, can produce hydrolytic enzymes which can damage host cells. Some enzymes could be required for regular cellular functions, whereas others may be needed for metabolic activities produced under particular conditions (Lorenzo-Morales, Khan and Walochnik, 2015). *Acanthamoeba* uses proteases and phospholipases as contact independent factors.

Proteases are recognised as being a virulence element for viruses, bacteria and numerous protozoa which include *Acanthamoeba* (Lakhundi, Siddiqui and Khan, 2017; Khan, 2006). Subsequent to successful parasitic adhesion, *Acanthamoeba* trophozoites secrete proteases which cause cytopathic impacts. Proteases are proteolytic enzymes capable of degrading the peptide bonds of proteins in order to feed pathogenic organisms (Khan, 2006; Lorenzo-Morales, Khan and Walochnik, 2015). They enhance the feeding during phagocytosis, enabling *A. castellanii* invasion by degrading the corneal epithelial and endothelial cells, iris ciliary body cells,

bowman's membrane, stroma, and even cause macrophage-like cells apoptosis, leading to the development of AK.

The quantity and presence of proteases produced by *Acanthamoeba* have been associated with their invasive ability, possibly as determinants for the virulent phenotype offered by some isolates (Rocha-Azevedo *et al.*, 2010). Aspartic acid proteases, cysteine proteases, serine proteases, and metalloproteases are the most frequently occurring proteases, and *Acanthamoeba* spp. produces all of these with the exception of aspartic acid proteases (Lakhundi, Siddiqui and Khan, 2017; Khan, 2006). Studies have revealed that all *Acanthamoeba* isolates display a greater degree of serine protease activity than others do in every determined genotype. Consequently, further studies are required in order to understand more comprehensively the proteases that have an essential function in *Acanthamoeba* infections.

Phospholipases are a diverse set of hydrolase enzymes connected by glycerophospholipids, which lead to host membrane disorders. The five most frequently occurring phospholipases in consecutive order are: groups A1, A2, B, C and D. Each of these is specifically able to insert a particular ester bond into the substrate at the membrane target (Lorenzo-Morales, Khan and Walochnik, 2015; Khan, 2006).

Phospholipases promote phagocytosis by cleaving phospholipids. Therefore, they disrupt the membrane allowing *A. castellanii* penetration into the eye cells through cell lysis. This encourages degradation of Bowman's membrane and impairment of cellular function, thus the development of AK. Studies imply that the phospholipases and/or lysophospholipases of *Acanthamoeba* have a direct function in the infection risk for the host cell, and also in the induction of immune response and ease of virulence of *Acanthamoeba* (Lorenzo-Morales, Khan and Walochnik, 2015; Khan, 2006).

1.5.2 Indirect factors

Another factor that may enable *Acanthamoeba* pathogenesis is the ability to survive under stressful conditions including salinity, extreme temperatures/pH, lack of food, and the increase in resistance to antimicrobials (Marciano-Cabral and Cabral, 2003; Schuster and Visvesvara, 2004). Pathogenic *Acanthamoeba* is more tolerant of such conditions than weak/non-pathogenic *Acanthamoeba*. However, the exact mechanisms associated with these survival mechanisms need to be elucidated.

The broad distribution of *Acanthamoeba* and capability of survival in numerous habitats contributes considerably to the parasite's pathogenic potential (Khan, 2006). The life-cycle formats of *Acanthamoeba* (trophozoites and cysts) are also

regarded as mechanisms linked to this organism's pathogenic potential. The cysts are resistant to unfavourable temperature and pH, as well as to various antimicrobial drugs which have the potential to cause the disease to recur (Lorenzo-Morales, Khan and Walochnik, 2015; Khan, 2006). Furthermore, the cyst form is able to survive for years while retaining its attributes.

The acanthopodia on the surfaces of the trophozoite infective forms enables them to adhere to the host cells, feed and move (Khan, 2001; Schuster and Visvesvara, 2004). Acanthopodia have a significant function in infections because their presence in pathogenic isolates exceeds that in non-pathogens.

Various factors, for instance, prolonged wearing of lenses, contaminated tap water and home-made lens-cleaning solutions mean that AK is generally linked to contact-lens wearers. Such factors have an impact on the proliferation of micro-organisms such as bacteria, and in certain situations, the formation of biofilms on/under contact lens' surfaces (Carnt and Stapleton, 2016; Marciano-Cabral and Cabral, 2003). However, not all contact lens wearers develop AK. They could be due to personal hygiene behaviour, the type of decontaminant used, environmental conditions as well as disease and genetic factors that affect immune competence.

Biofilms in contact lenses can lead to contamination by *Acanthamoeba* because trophozoites can more easily survive due to the greater availability of nutrients and resistance to disinfectants (Lorenzo-Morales, Khan and Walochnik, 2015; Khan, 2006). Biofilms provide a micro-environment rich in various nutrients, which favours the growth of trophozoites. Furthermore, the biofilm growth, which comprises a broad community of micro-organisms, induces the development of resistance to disinfection because it hampers proper cleaning, thereby promoting the development of resistant variants. Consequently, the research findings suggest that biofilms occupy an essential function in AK in contact-lens wearers.

1.6 Proteases and amino acids and their roles in *Acanthamoeba*

Acanthamoeba exhibits proteolytic activity associated with the need to degrade food substances. There is a correlation between pathogenicity and extracellular protease activity, with pathogenic *Acanthamoeba* exhibiting higher levels of extracellular protease activity (Lorenzo-Morales, Khan and Walochnik, 2015). *A. castellanii* produces serine proteases, cysteine proteases, and metalloproteases, which facilitate host cell invasion.

An approach elucidated in the literature on the characterization and pathogenicity of *A. castellanii* is the use of amino acid analysis of culture media. Several researchers have investigated the changes in amino acids in the culture media of *A. castellanii* and related parasites. Dolphin (1976) investigated the amino acids in a culture media prior to and subsequent to inoculation with *A. castellanii*. The findings indicate that *A. castellanii* exhibits selective utilization of amino acids from culture medium; no amino acid was exhausted during normal population growth.

However, the secretion mechanisms of *A. castellanii* shows variation under different protein availability conditions (Gonçalves *et al.*, 2018). Serine proteases and metalloproteinases were predominant. Although the secretory mechanism of amoebas is not clear, the secretome profile of *A. castellanii* indicates a potential role in pathogenesis.

In another study, Hong et al. (2018) characterized the biochemical and molecular properties of cysteine protease of *A. castellanii*. The findings suggest a potential role for cysteine proteases in *A. castellanii* encystment; however, the biological functions and chemical properties of the cysteine protease remain poorly understood. Therefore, further studies are needed to understand in more detail about proteases and amino acids

that represent an essential role in the pathogenicity of *Acanthamoeba*.

1.7 The role of trace elements in biology and pathogenesis of *Acanthamoeba*

One of the approaches described in the literature for studying how *Acanthamoeba* interacts with human corneal cells entails elemental analysis. A trace element that has received heightened scholarly attention is calcium (Mattana *et al.*, 1997). Different microminerals and trace elements play an important function in the growth of cells, such as calcium, sodium, chlorine, and magnesium among others. Research findings show that calcium ions play a vital role in controlling cellular responses, including cell homeostatic processes, apoptosis, and cell proliferation. Previous *in vitro* studies suggest that *A. castellanii* releases ADP molecules which induces an increase in cytosolic free-calcium concentration in cell cultures as well as cell morphological changes (Mattana *et al.*, 2002; Mattana *et al.*, 2009). The variation in free calcium concentration depends on the trans-membranous influx of Ca^{2+} (Mattana *et al.*, 2002). An increase in the concentration of Ca^{2+} disrupts normal cellular metabolism leading to intoxication and cell death. It is not clear how *A. castellanii* monitors environmental changes and conditions that lead to viable trophozoites. These findings

suggest the need to investigate the effect of the *A. castellanii* and the conditioned medium on calcium concentration.

According to Siddiqui et al. (2019), sodium, calcium, and potassium ion transporters and the proton pump inhibitors plays a vital role in the encystation and excystation of *A. castellanii.* The findings demonstrated that ion transporters play an important role in the cellular differentiation of *Acanthamoeba.* Since trace elements may influence the osmolarity of the media, it is possible that they also affect the encystation in *A. castellanii,* with variations in physiological characteristics. According to Cordingley and Trzyna (2008), the specific molecules responsible for the osmolarity change in axenically grown cultures of *A. castellanii* include inorganic compounds such as sodium chloride and magnesium chloride; however, inorganic compounds do not provide metabolic energy. Since the growth of *Acanthamoeba* in axenic media is problematic, some researchers have examined possible additives to enrich the media, including adjustment of the mineral elements in the culture media and addition of yeast RNA (Megha *et al.*, 2017). These findings demonstrate that elemental analysis of the conditioned medium of *Acanthamoeba* trophozoites and human corneal cells could offer useful insights on the pathogenesis of AK.

1.8 Metabolomic studies

Metabolomics is an “omics” science which aims at study the complete or partial metabolite profile in a biological system at a specific time (Krastanov, 2010; Alvarez-Sánchez, Priego-Capote and Luque de Castro, 2010). A metabolome is defined as the quantitative number of metabolites having a low molecular weight that are present in a cell, organism or biological liquid within a particular physiological environment. Basically, this combines organic species, for example, carbohydrates, lipids and also amino and organic acids. However, inorganic and elemental species can also be studied. Metabolomic techniques can be applied to document various data. These include information associated with the number of metabolites consumed by the system, and also the relative quantitative data regarding the metabolites produced by the organism.

Metabolomics has been applied to an increasing number of studies in order to comprehend protozoan parasites (Jeelani and Nozaki, 2014), and how they interact with their hosts (Kafsack and Llinas, 2010; Olszewski *et al.*, 2009), as well as to assess their susceptibility to drugs (Vincent and Barrett, 2015). The consensus of these studies is that metabolism plays an important role in the parasitism and pathogenesis of protozoan species, with the discovery of novel metabolic biomarkers

providing reliable information for the diagnosis and treatment of parasitic diseases. Additionally, the metabolomics protocol for analysing *Acanthamoeba* trophozoites' metabolome was culture with bacteria or mammalian cells. Notable differences in the metabolites of bacteria, mammalian cells and amoebae were indicated by the results (Hauber *et al.*, 2011; Zhou *et al.*, 2018).

However, evidence suggests that *A. castellanii* T4 genotype prefers to use multiple pathways for energy metabolism (Alves *et al.*, 2017; Wu *et al.*, 2018). Thus, cellulose synthesis, glycolysis, and protein metabolism pathways are employed. In metabolomics, the detection of glucose, urea, and lactate is an indicator of the anaerobic glycolysis pathway. The parasite hydrolyses glucose, the major percussor for cellulose synthesis. Also, cellulose synthesis is crucial for cyst formation, as shown by the increased expression of cellulose synthase and UDP-glucose pyrophosphorylase genes during encystation (Garajová *et al.*, 2019). More so, protein metabolism in *A. castellanii* is identified by detecting metabolites like urea, fumarate, and creatinine (Alves *et al.*, 2017). Wu et al. (2018) note that the key pathways in protein metabolism in *Acanthamoeba* species are the cysteine biosynthesis and the L-serine metabolic pathway, with cysteine synthase and phosphoglycerate dehydrogenase playing key roles in cysteine biosynthesis and serine degradation

(Wu *et al.*, 2018). These pathways provide energy for the organism's development, invasion, and transformation. Findings suggest that the secretion mechanisms of the *Acanthamoeba* vary depending on the protein availability conditions (Gonçalves *et al.*, 2018) and that serine proteases and metalloproteinases are the predominantly found in extracellular vesicles. Although the secretory mechanism of amoebas is unclear, the secretome profile of *A. castellanii* indicates a potential pathogenic role.

1.9 Mode of action for current Anti-*Acanthamoeba* therapy

Acanthamoeba infection management presents many challenges and considerable endeavour has been applied to the development and testing of drugs to combat this infection. These include antibiotics, antiseptics and antimicrobials, which have an impact on several functions and targets in *Acanthamoeba*. The combination strategies of CHX and PHMB have confirmed effectiveness in curing AK patients and are the initial therapeutic option, because they target the amoeba’s plasma membrane, resulting in membrane-damage, lysis, and then death. The antiseptic diamidines, which are effective against nucleic acid and the protein biosynthesis, act against cysts and trophozoites (Marciano-Cabral and Cabral, 2003; Lorenzo-Morales, Khan and Walochnik, 2015; Elsheikha, Siddiqui and Khan, 2020).

The cyst wall functions as a physical barrier for the drugs that target *Acanthamoeba*. Targeting the cyst wall is a helpful strategy for controlling *Acanthamoeba* (Anwar, Khan and Siddiqui, 2018; Siddiqui and Khan, 2012; Elsheikha, Siddiqui and Khan, 2020). The molecular structure of the cyst walls generally contains cellulose. Therefore, targeting cellulose biosynthesis with a specific inhibitor, such as 2,6-dichlorobenzonitrile (DCB), can prevent encystment. Following the breaking of the cellulose component, the parasite will be prone to therapeutic compounds, and become unable to survive on the host.

The impact of drugs that target intracellular calcium levels against Acanthamoeba keratitis has been revealed by past studies (Baig, Iqbal and Khan, 2013; Elsheikha, Siddiqui and Khan, 2020). Amlodipine, which is used to treat *Acanthamoeba* represents a drug target for a dihydropyridine calcium channel blocker. Calcium is necessary for molecule movements in and out of the cell, thereby feeding the cell and enabling other functions. Therefore, the parasite is unable to survive when such pathways are targeted by certain therapeutic agents.

Nucleic acids are necessary molecules in the cell that control the cellular procedures. Drugs that suppress the *Acanthamoeba's* DNA or RNA stop the functioning of such processes, enabling this pathway to be a good target for *Acanthamoeba* (Siddiqui,

Aqeel and Khan, 2016). Another significant aim for certain anti-amoebae drugs is reduction of protein synthesis. Povidone-iodine (PVP-I) disinfectant damages nucleic acid and protein synthesis, affecting cellular activity (Visvesvara, Moura and Schuster, 2007; Elsheikha, Siddiqui and Khan, 2020).

There are other important therapeutic targets for *Acanthamoeba* including proflavine and antiseptics acriflavine, which bind the cellular and nuclear membranes, and also compromise the membrane integrity and lipid bilayer, in both cysts and trophozoites (Elsheikha, Siddiqui and Khan, 2020; Roberts and Henriquez, 2010). It has been demonstrated that phospholipid analogues have trophicidal and restricted cysticidal activities. These analogues repress phospholipid biosynthesis and also disrupt the induction of apoptosis as well as intracellular signalling and cellular membranes (Julia *et al.*, 2002; Elsheikha, Siddiqui and Khan, 2020; Roberts and Henriquez, 2010). Further research is required to understand in more detail the mode of action of novel drugs that may allow the development of more effective therapeutic interventions.

1.10 Prospects for using nanoparticles in the treatment

Nanoparticles (NPs) are usually defined as matter particles whose sizes range from 1 to 100 nm (Ivask *et al.*, 2014; Yah,

Simate and Iyuke, 2012). The unique properties and features of NPs including small size, amenability to improved solubility, and a multi-functionality that enables them to interact with complex cellular functions (Singh and Lillard, 2009). They are classified as organic and inorganic. Organic nanoparticles, which are comprised of organic compounds such as polymersomes and liposomes (Kumar and Lal, 2014; Khalid *et al.*, 2020), are more suited for biological applications and environmentally friendly since they usually degrade readily. By contrast, inorganic nanoparticles exhibit outstanding electrical, magnetic, heat conduction, size-dependent physicochemical and optical properties, which enhances their strength (Khalid *et al.*, 2020). Inorganic nanoparticles such as those manufactured using silver, gold and cerium have received a great deal of attention from scholars for their antimicrobial activities. Inorganic NPs can kill microbes by several mechanisms, including disruption of cell membrane integrity, inhibition of enzymes, and disruption of energy metabolism (Shaikh *et al.*, 2019; Babenko *et al.*, 2012).

An example of a redox NP is cerium oxide (CeO_2NPs), which can be naturally sourced from flora, evaporating water, and soil erosion (Aderibigbe, 2017; Farias, Santos and Sampaio, 2018). CeO_2NPs have been described as both pro-oxidant and anti-oxidant; this can be due to manufacturing causing different

physicochemical parameters and the levels of Ce^{3+}/Ce^{4+} on the surface. CeO_2NPs can self-generate, which is enabled by redox-cycling between 3+ and 4+ states (Xue *et al.*, 2012; Cassee *et al.*, 2011). This gives CeO_2NPs variable properties of both being an effective scavenger of reactive oxygen species and cause extensive elevation of reactive oxygen species (ROS), leading to cell death or apoptosis. Furthermore, CeO_2NPs show powerful absorption of ultraviolet radiation (UV).

CeO_2NPs' specific design gives beneficial physiochemical properties, thereby facilitating their medical application (Farias, Santos and Sampaio, 2018) and use as an antimicrobial (Kannan and Sundrarajan, 2014; Babenko *et al.*, 2012). CeO_2NPs may also be utilised for the delivery of drugs, medical equipment coatings, and in pathogen diagnosis (Zhang *et al.*, 2018; Charbgoo, Ramezani and Darroudi, 2017). Recently, the mimetic and multi-enzyme properties of CeO_2NPs have been identified, thereby increasing their potential application in biological disciplines, including biosensor design, bio-analysis and biomedicine (Charbgoo, Ramezani and Darroudi, 2017). Their integration into biosensors potentially enables biomarkers to be recognised continuously, even under hypoxia, which was notably challenging when detection relied on oxidising reactions.

The versatility of CeO_2NPs in scavenging numerous ROS gives them an advantage over conventional antioxidants. This has motivated scholars to explore whether CeO_2NPs can be used to treat conditions associated with oxidative stress (Xu and Qu, 2014; Zhou *et al.*, 2020). The latter refers to a situation whereby the excessive production of ROS exceeds the antioxidant scavenging capacity, or antioxidant availability decreases (Adeoye *et al.*, 2018). The antioxidative properties of CeO_2NPs are caused by the various ionisation states of Ce^{+4} and Ce^{+3}, which facilitate the scavenging of ROS and can effectively ameliorate oxidative stress and reduce chronic inflammation (Xu and Qu, 2014; Estes *et al.*, 2021). CeO_2NPs have exhibited potential for the treatment of retinal diseases connected with oxidative stress, such as retinal degeneration, diabetic retinopathy, and retinal detachment (Chen *et al.*, 2006). Research has demonstrated that CeO_2NPs are non-toxic in human lens epithelial (HLEC) cells when used in high concentrations up to 200 µg/mL, and they have protective effects toward oxidative stress (Hanafy *et al.*, 2020; Hanafy *et al.*, 2019). While they may be useful in the treatment of certain ocular conditions, knowledge regarding the extent to which CeO_2NPs are toxic in corneal cells is limited.

Oxidative stress-induced by nanoparticles is associated with particle surface, size, and the presence of metals. Damage from ROS is associated with cellular responses, such as immune cell activation, systems toxicity, and mitochondrial respiration (Manke, Wang and Rojanasakul, 2013). CeO_2NPs can be designed to reduce oxidative stress in cells, thereby benefiting the therapeutic potential for human inflammation (Hirst *et al.*, 2009), as well as anti-cancer impacts (Renu *et al.*, 2012). CeO_2NPs can also serve as ROS-scavengers because surface oxygen vacancies allow the reduction of Ce^{4+} to Ce^{3+}, which contributes to reduced ROS levels.

Existing evidence highlights the potential environmental and health risks of CeO_2NPs. For example, research has shown that *A. castellanii* readily takes up CeO_2NPs from the environment through phagocytosis, which are then released back into the environment through other organisms along the food chain (Palmieri *et al.*, 2011). Furthermore, ingestion of CeO_2NPs by *Acanthamoeba* spp. may produce microorganisms that are resistant to therapeutic interventions (Palmieri *et al.*, 2011). Thus, it is essential to conduct an extensive assessment of CeO_2NPs to determine the margin of safety with respect to their ROS-based protective effects on one hand and environmental safety concerns on the other.

Consequently, CeO_2NPs are regarded as being non-toxic for humans even though certain studies have revealed that nanoparticles have a certain degree of toxicity (Xia *et al.*, 2008; Renu *et al.*, 2012), based on their concentration, exposure time or synthesis method (Dhall and Self, 2018). At high concentrations and lower pH, CeO_2NPs exhibits pro-oxidant properties, whereas in other environmental conditions this can be reversed. Additionally, the body has no CeO_2NPs clearance systems; hence, the body can suffer systemic toxicity when treated with CeO_2NPs (Dhall and Self, 2018). However, it is possible to systematically alter NPs for the purpose of controlling size of the particle, morphology and coating substance of the generated NPs. This can cause significant changes in their behaviour by altering their physicochemical characteristics and interactions with biosystems (Albanese, Tang and Chan, 2012; Chen and Chang, 2005). Thus, it is essential that the method of synthesis selected is appropriate for the targeted application. There is now an urgent need to develop non-toxic CeO_2NPs so that their antioxidant properties can be employed to eradicate infections.

1.11 Research hypothesis and aims

It will be helpful to examine the impact of *A. castellanii*-conditioned medium (ACCM) on corneal cells, as this will enable an understanding of the pathogenicity of *A. castellanii*, and the potential role of *A. castellanii* secretome in the structural damage and functional changes that accompany their infection. The recognition of such changes, and finding molecular constituents of the *Acanthamoeba* secretome, may disclose novel insights into the mechanism utilised by *A. castellanii* in damaging the ocular tissues. In this thesis, the hypothesis that ACCM causes structural, functional and metabolomic changes in ocular cells will be tested, by which we recognised the following aims:

- To evaluate structural and cytotoxic changes in human SV40 immortalised corneal epithelial cells (ihCECs) and primary human corneal stromal cells (CSCs) in response to ACCM infection by applying a series of viability assays (alamarBlue®, SRB, MTT), cell toxicity studies (LDH), immunofluorescent staining of cell actin and protease inhibitor assays. Transmission electron microscope (TEM) was used to reveal the ultrastructural changes at the single-cell level following ACCM treatment.

- To determine metabolomic changes that occur in CSCs before and after exposure to ACCM by applying LC-MS/MS and bioinformatic analysis.
- To perform inductively coupled plasma-mass spectrometry (ICP-MS) elemental profiling to compare the changes within the elemental composition of CSCs in response to ACCM.
- To test the effect of CeO_2NPs on *Acanthamoeba* and corneal cells, and also understand mechanisms of action of these CeO_2NPs against *Acanthamoeba.*

2. Chapter Two: Materials and Methods

This study was conducted at the University of Nottingham, UK. Preparation and culture of the human SV40 immortalised corneal epithelial cells (ihCECs) and primary human corneal stromal cells (CSCs) was carried out at the tissue culture laboratory in Academic Ophthalmology, School of Medicine, Queen's Medical Centre (QMC). Parasite-related experiments were performed at the Parasitology Laboratory, School of Veterinary Medicine, Sutton Bonington. Work with *A. castellanii* or any materials derived from this parasite, such as culture medium, represent biological hazards (i.e., category 2 agents) and have been treated as potentially infectious. Therefore, all experiments were conducted following the local health and safety regulations and using a laminar flow hood.

2.1. Cell lines and culture conditions

2.1.1 Culture of ihCECs

The human SV40 immortalized corneal epithelial cell line (ihCECs) was established in 1995 by Araki-Sasaki from primary human corneal epithelial cells (Araki-Sasaki *et al.*, 1995). This cell line was kindly provided by Prof. Felicity Rose (School of Pharmacy, University of Nottingham, UK) to Academic Ophthalmology Department. IhCECs were transformed using the

early region of the simian virus (SV) 40 genome. The cells were cultured in EpiLife™ medium **(**Life Technologies, UK), supplemented with antibiotic-antimycotic solution to prevent possible contamination with fungi or bacteria, containing penicillin (20 Units/mL), streptomycin (20 µg/mL) and amphotericin B (50 ng/mL) (Sigma Aldrich, UK), and 1% (v/v) human keratinocyte growth supplement (HKGS) (Life Technologies, UK). Cell cultures were maintained in a humidified atmosphere at a temperature of 37°C with 5% CO_2. Culture medium was changed twice a week.

2.1.2 Isolation and culture of CSCs

Anonymized corneoscleral rims left as a waste product after penetrating keratoplasty were obtained via materials transfer agreement from Nottingham University Hospitals Trust. All human tissue work was performed strictly according to the tenets of the UK Human Tissue Act. Human corneal stromal cells (CSCs) were extracted from corneoscleral rims according to techniques described previously (Sidney, McIntosh and Hopkinson, 2015). Briefly, the residual sclera was removed from the corneoscleral rim and the remaining tissue was divided in about 16 pieces and placed into a 1 mg/mL collagenase solution (Sigma-Aldrich, UK), before incubation under agitation at 37°C for 7 h. After filtration through a 40 µm cell strainer for removing

cells debris and centrifugation (Universal 32R, Hettich-Zentrifugen, Germany) at 200 x *g* for 5 min, the resulting cell pellet was cultured in M199 basal medium containing 20% (v/v) fetal bovine serum (FBS) (Sigma Aldrich, UK), 2 mM L-Glutamine (Sigma Aldrich, UK), and antibiotic-antimycotic solution. Cells were incubated in a humidified atmosphere at a temperature of 37°C within 5% CO_2, and cultured medium was changed twice a week.

2.1.3 Passaging of CSCs and ihCECs

Both CSCs and ihCECs were passaged at the point when they reached 90% confluency. The medium was then discarded from the T-75 cm^2 flask and the cell monolayers were washed twice with 5 mL of phosphate-buffered saline (PBS). Then, 2 mL of TrypLE-Express dissociation reagent (TrypLE; Life Technologies, UK) was added into the flask, and incubated at 37°C for 5 min. TrypLE-treated cells were checked under an inverted microscope for cell detachment from the bottom of the culture flask. The TrypLE was deactivated with 3 mL of a serum-containing M199 medium. The cells were harvested and subjected to centrifugation for 5 min at 200 x *g*, and supernatants were removed leaving a cell pellet. Cell pellets of ihCEC were suspended in an EpiLife™ medium and seeded into T-75 cm^2 flasks at a passage rate of 1:3 (12 mL of EpiLife™

medium/flask). The CSCs pellets were suspended in a M199 medium and seeded into T-75 cm^2 flasks at a ratio of 1:4 (11 mL of M199 medium/flask). All flasks were incubated at a temperature of 37°C in a humidified atmosphere with 5% CO_2, with media refreshment twice a week. All media were freshly prepared.

2.1.4 Cryopreservation of CSCs or ihCECs

CSCs or ihCECs were harvested from the flasks as mentioned above in section 2.1.3. Following the centrifugation process, the supernatant was discarded, and the ihCECs or CSC pellets were resuspended in a 1 mL cryopreservation medium in labelled cryovials. Cryopreservation medium was prepared by adding 5 mL dimethylsulfoxide (DMSO) (Sigma, USA) to 45 mL FBS, and filtered through a 0.2 µm filter into a new tube for the sterilisation. The labelled cryovials were then put inside a cell-freezing box (CoolCell LX, Corning, UK), and left overnight to freeze at a constant –1°C/min rate. Subsequently, the labelled cryovials were transferred and placed into a storage box where they were stored at –80°C to maintain cells viability.

2.1.5 Recovery of cells from cryopreservation

To recover the CSCs or ihCECs, the frozen cryovials were removed from the storage box, rapidly defrosted in a water bath

at 37°C, and subsequently transferred into universal tubes filled with 9 mL of the corresponding pre-warmed culture medium. The cells were centrifuged for 5 min at 200 x *g*, the supernatant was removed and the ihCEC and CSC pellets were suspended in either 10 mL EpiLife™ and M199 medium respectively. Following this, cells were seeded in T-75 cm^2 flasks and incubated in a humidified atmosphere at a temperature of 37°C with 5% CO_2. Each culture medium was replenished after 48 to 72 h.

2.2. Parasite strain and maintenance conditions

2.2.1 *Acanthamoeba castellanii* culture

A. castellanii trophozoites were maintained within T-75 cm^2 culture plastic flasks at a density of $1x10^6$ trophozoites/flask. The trophozoites were axenically cultured in PYG [proteose peptone (0.75%; w/v, Sigma-Aldrich, Germany), yeast extract (0.75%; w/v, Sigma-Aldrich, USA), and glucose (1.5%; w/v, Sigma-Aldrich, Germany)] growth medium according to a previously described method (Ortega-Rivas *et al.*, 2016; Khan, Jarroll and Paget, 2001). The culture flasks were incubated at 25°C. The PYG medium was replaced twice a week.

2.2.2 Preparation of conditioned medium (ACCM)

Following 24 hours of seeding at a density of $1x10^6$ trophozoites/flask as illustrated in section 2.2.1. *A. castellanii* trophozoites, routinely maintained in PYG medium, were adapted to grow in the culture medium of corneal cells (M199 for CSCs or Epilife™ for ihCECs) by incubating *A. castellanii* in the corresponding medium for 48 h prior to obtain a conditioned medium that contained the secreted metabolites and used in the experiment. In this growth medium, antibiotic-antimycotic solution containing amphotericin B was used in the human cell cultures to prevent fungal contamination. It is possible that amphotericin B may have interfered with *Acanthamoeba* growth. However, in a preliminary time-course experiment using haemocytometer counting, *A. castellanii* was able to grow in human cell medium and PYG medium and their numbers approximately double every 24 h. No adverse effects on the growth of *Acanthamoeba* were observed and there were no signs of apoptosis in the *Acanthamoeba*. This indicates that the human cell growth medium did not prevent proliferation, probably because the amphotericin B was applied at a low dose for *Acanthamoeba*. Subsequently, *A. castellanii* trophozoites were separated from the culture medium by centrifugation at 1000 x *g* (Allegra X-22R centrifuge, Beckman Coulter™) for 5 min. The pellet was discarded, and the supernatant was filtered through a

0.2 μm filter to remove any cell debris or microorganisms from the samples and to avoid potential contamination of cell cultures. Different dilutions of the filtered supernatant (hereafter called *Acanthamoeba castellanii*-derived conditioned medium [ACCM]) were made by mixing the ACCM with M199 or Epilife™ in different volumes [(v/v), 25%, 50%, 75%, and 100%)], which were used to test the cytotoxic effects of ACCM on corneal cells as described below.

2.3. Bicinchoninic acid assay (BCA)

The BCA protein assay was used to quantify the protein concentration of *A. castellanii*-derived conditioned medium (including M199 and Epilife™). The BCA assay was performed according to manufacturer's instructions, using bovine serum albumin (BSA) as standards (Thermo Scientific Pierce, USA). Briefly, 25 μL of each sample was added in triplicate into 96-well microplates, and then 200 μL of working reagent of BCA was added per well. The plate was shaken for 30 seconds, and then incubated for 30 min at 37°C. Absorbance was measured at 562 nm using a microplate reader (BMG Labtech GmbH, Offenburg, Germany).

2.4. Viability assays

The cytotoxic effect of ACCM on the viability of CSCs and ihCECs were examined using three viability assays, namely alamarBlue assay, MTT assay and SRB assay. All viability assays were carried out in triplicates, in 96-well flat bottom (Costar; Corning, USA) microplates, and inside laminar flow hood under aseptic conditions. For all the viability assay, ihCECs and CSCs were harvested from the flasks as described above in section 2.1.3, and seeded in 96-well plastic tissue culture plates at 0.1 mL/well of the respective culture medium at a density of 1 $x10^4$ cells/ well for ihCECs and at 6 $x10^3$ cells/well for CSCs. The numbers of cells were determined using a haemocytometer. After the cells were allowed to attach for 48 h, the media in the wells was replaced with ACCM at various concentrations of (25%, 50%, 75%, and 100%) to a final volume of 100 µL/well. Untreated wells contained 100 µL media/well of Epilife™ for ihCECs and M199 for CSCs were also set up. The plates were incubated at 37 °C and after 3, 24 and 48 h, the plates were subjected to analysis using alamarBlue, MTT and SRB assays as detailed below.

2.4.1 Evaluation of metabolic activity using alamarBlue assay

At incubation time points, the cell viability was measured by addition of 10 µL per well of alamarBlue (Thermo-Fisher Scientific, USA), as previously performed (McBride *et al.*, 2005; Larson *et al.*, 1997). The purpose of this assay is to evaluate the metabolic activity of cells and measure their viability. The plates were incubated for one hour and absorbance was measured at 3, 24 and 48 h after incubation at 492 nm using a microplate reader (Labtech International Ltd, LT- 4000, UK).

2.4.2 MTT cell viability assay

The MTT assay measures viable cells by determining mitochondrial activity. Cell viability was determined by addition of 10 µL/well of MTT [3-(4,5-dimethyl-2-thiazolyl)-2,5-diphenyl-2H-tetrazolium bromide] (5 mg/mL in phosphate-buffered saline [PBS]; Sigma, USA), to each well, followed by incubation for 4 h at 37°C and 5% CO_2. Then, 100 µL of MTT solubilisation solution (10% SDS in 0.01M HCl) was added into each well, and the plate was further incubated for 1 hour at 37°C. The number of live cells is directly correlated to the amount of reduced MTT, which was quantified based on absorbance at 570 nm using a microplate reader (Labtech International Ltd, LT- 4000, UK), (Elsheikha *et al.*, 2014).

2.4.3 Sulforhodamine B assay (SRB)

At 3, 24 and 48 h after incubation with ACCM, the samples were fixed, and subsequently stained with Sulforhodamine B (SRB) assay according to modified techniques described previously (Vanicha and Kanyawim, 2006; Ortega-Rivas *et al.*, 2016). SRB is used for the determination of cell viability by measuring cell protein content. Briefly, the samples were fixed with 25 µL cold (10%, 4˚C) trichloroacetic acid (TCA, Fisher, Belgium), then the samples were kept at 4˚C for a period of one h. After removal of the supernatant, the plate was washed with distilled water, and then dried at an ambient temperature. An SRB solution of 25 µL (v/v, 0.05% SRB dye, dilution of acetic acid within a distilled water up to 1%) was placed into each well to stain the cells. Subsequently, the plates were covered with aluminium foil for the purpose of shielding them from light, and left for 15 min at an ambient temperature. The samples were rapidly washed three-times using 1% (v/v) acetic acid to eliminate surplus cell-unbound SRB dye. The plates were left to air-dry followed by addition of 150 µL of 10 mM tris-base (pH 10.5, tris(hydroxymethyl)aminomethane) for each well to solubilise SRB dye. The plate was then put on a shaker (Stuart, UK) for five min for the purpose of attaining an even distribution of the dye in the well's supernatant. The absorbance was evaluated at

492 nm by a microplate reader (Labtech International Ltd, LT-4000, UK).

2.5. *In vitro* cell toxicity studies

2.5.1 Lactate dehydrogenase (LDH) cytotoxicity assay

The assay measures production of the LDH enzyme, which is released from the plasma membrane of damaged cells into the cell culture medium. The cytotoxicity of ACCM against ihCECs and CSCs was assessed using an LDH cytotoxicity assay according to the manufacturer's instructions (Pierce™ LDH cytotoxicity assay kit; Thermo Scientific, USA). Briefly, ihCECs and CSCs were seeded in 96-well plates at 5 $x10^3$ and 3 $x10^3$ cells/well, respectively. Cells were allowed to attach for 24 h, and the media was removed and replenished with media containing 50% of ACCM or left untreated (control). At 3, 24 and 48 h after exposure to ACCM, an aliquot of 50 µL of culture supernatant per well was collected and transferred into another a 96-well plate in triplicate. Then, 50 µL of reaction mix solution containing substrate mix was added per well, mixed by gentle pipetting, and the plate was covered by aluminium foil for the purpose of shielding it from light, and left for 30 min at ambient temperature. After addition of 50 µL of stop solution, the absorbance was measured at 490 nm with 680 nm corrective background reading using a microplate reader (BMG Labtech GmbH, Offenburg,

Germany). Corrective background readings were subtracted and the percentage cytotoxicity was determined by applying the following formula: (sample or negative control value - total background (*Acanthamoeba*-conditioned medium) / total positive control (treated with 10 µL of Lysis Solution for 30 min at 37℃) x 100 = % cytotoxicity.

2.5.2 Caspase 3 assay

Caspase-3 activity level in CSCs and ihCECs was measured by caspase-3 assay (Caspase-Glo® 3/7 assay kit; Promega, USA) in accordance with the manufacturer's directions. The kit detects the enzymatic activity of caspase-3 in apoptotic cells. Briefly, CSCs and ihCECs were seeded in 96-well plates at 5 $x10^3$ and 3 $x10^3$ cells, respectively for 24 h, followed by addition 50% of ACCM and incubated for 3, 24 and 48 h at 37 °C. After incubation, 100 µL of Caspase-Glo® 3/7 reagent was added to each well (controls and treated groups with 50% ACCM). The plates were covered and shaken for 30 seconds, followed by incubation for 30 min at ambient temperature. The luminescence reading was evaluated at 545-50 nm with a microplate reader (BMG Labtech GmbH, Offenburg, Germany).

2.6. Immunofluorescent staining of actin for corneal cells

CSCs or ihCECs were seeded in 24-well plates at 12 $x10^3$ and 20 $x10^3$ cells, respectively and incubated with ACCM (M199 or Epilife™*)* at various concentrations (100%, 75%, 50% and 25%) for 3, 24 and 48 h at 37°C. The experiment was carried out at room temperature according to protocol described previously (Sidney, McIntosh and Hopkinson, 2015). Briefly, the two types of corneal cells were fixed in 10% buffered formalin (VWR, N. 9713.5000) for 10 min, and washed three times with PBS. Cells were permeabilized, in 0.1% (v/v) Triton X-100 (Sigma Aldrich, UK) diluted in PBS, for 10 min. After washing three times in PBS, blocking buffer (1% (v/v) BSA and 0.3 mol/L glycine [Sigma Aldrich] in PBS) was added to the wells, and incubated for 30 min. Samples were stained for the F-actin with Alexa-Fluor 488 phalloidin (Life Technologies, 1:60 diluted in blocking buffer) for 20 min in the dark before washing once using blocking buffer. Cells were counterstained with DAPI (Life Technologies, 5 µL/5mL in blocking buffer) to stain the nuclei for 10 min. Images were obtained using an inverted wide-field fluorescence microscope (DM-IRB, Leica, Wetzlar, Germany) equipped with a Hamamatsu digital camera (Hamamatsu Photonics, Hamamatsu, Japan).

2.7. Transmission electron microscopy (TEM) for corneal cells

TEM was used to reveal the ultrastructural changes at the single-cell level following ACCM treatment. TEM fires an electron beam through a sample to generate a magnified image. CSCs and ihCECs were seeded in T-*25* flasks at 7 x10^4 and 12 x10^4 cells, respectively for 48 h, followed by addition 50% of ACCM and incubated at 37°C for a period of 48 h. Cells were processed for TEM as described previously (Maradze *et al.*, 2018). Briefly, cells were gently harvested from the flasks with a cell scraper (Greiner, Bio-One, Germany), and fixed with 3% glutaraldehyde within 0.1 M cacodylate buffer (TAAB, Reading, UK) at a temperature of 4°C for a 24 h. Cacodylate buffer was used to wash the fixed cells twice which were then stored in cacodylate wash buffer for 1 day at 4°C. Cells were post-fixed in 1% osmium tetroxide (TAAB, Reading, UK) at 4°C for one hour, then washed in distilled water twice. They were then implanted in 3% (w/v) agarose, followed by dehydration in ascending ethanol series with 50% (v/v), 70% (v/v), 90% (v/v) and 100% (v/v) ethanol twice during each cycle for 10 min, and dehydration with 100% propylene oxide (propox) twice for a period of 15 min. After dehydration, the cells were penetrated with resin (1:3 resin: propox mixed for 1 h, 1:1 resin: propox mixed for 24 h), and then embedded in plastic capsules in 100% resin and incubated for a

period of 48 h at a temperature of 60°C. Ultrathin sections were cut at 90 nm thickness using a Leica EM-UC6 ultramicrotome (Leica, Germany), and placed on gilder copper TEM grids (TAAB, Reading, United Kingdom). The samples were stained with uranyl acetate solution followed by Reynolds' lead citrate (TAAB, UK) for 10 min. Images were obtained through the Tecnai BioTwin-12 TEM (FEI, United States) in cooperation with Ms Denise McLean from the University of Nottingham.

2.8. Protease inhibitor assay

The enzymatic activities in the ACCM were investigated using a protease inhibitor cocktail (Sigma-Aldrich, UK) containing bestatin, aprotinin, leupeptin, pepstatin A and E-64, with a wide specificity for inhibiting cysteine, serine, aminopeptidases and aspartic acid proteases. The protease inhibitor cocktail was added to ACCM (M199 and Epilife™ media) at concentrations 2.5, 5 and 10 µL/mL and incubated for 30 min at 25 °C. Then, 100 µL of treated ACCM were added to CSCs or ihCECs seeded in 96-well plates, which were incubated for 3, 6, 24 and 48 h at 37°C and 5% CO_2. Cells incubated in untreated medium or incubated with 100% ACCM were used as negative and positive controls, respectively. The proliferation rate of the cells subjected to the different concentrations of the protease inhibitor and the

control (untreated) cells was determined using SRB assay as described above.

2.9. Preparation of culture supernatant of CSCs-exposed to ACCM for analysis

CSCs were seeded in T-75 flasks at 5 x10^5 cells for 48 h. The medium was replaced with 10 mL of 50% ACCM (ACCM-M199) and incubated for 0, 3, 24 and 48 h at 37°C and 5%-CO_2. Cells treated with unconditioned M199 medium were utilised as a control. The experiment was performed three times with two replicates per-experiment, as shown in (Figure 2-1). Following incubation, the culture supernatant was transferred into new tubes and stored at -80°C. Assays were then performed to quantify protein concentration and DNA concentrations of the culture supernatant of CSCs-exposed to ACCM. Metabolites from CSCs pellets were also extracted for metabolomics analysis. Samples were subjected to analysis using the techniques detailed in the following sections.

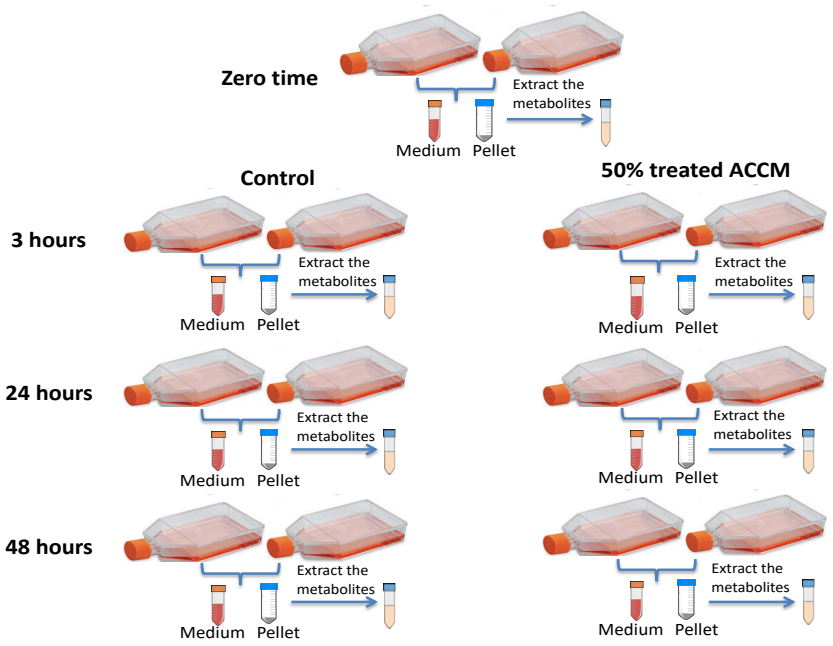

Figure 2-1 Preparation of the culture supernatant of CSCs-exposed to ACCM for analysis. CSCs were incubated with 50% ACCM for 0, 3, 24 and 48 h at 37 °C. Cells treated with unconditioned M199 medium were used as a control. The experiment was performed three times with two replicates per-experiment. The culture supernatant was transferred into new tubes for analysis protein concentration, trace elements and DNA concentrations of the supernatant of CSCs-exposed to ACCM. Cells were gently harvested from the flasks with a cell scraper. Metabolites from CSCs pellets were also extracted for metabolomics analysis.

2.9.1 The DNA concentrations of the culture supernatant of CSCs-exposed to ACCM

DNA from the culture supernatant of CSCs exposed to ACCM was isolated using a ChargeSwitch® gDNA 1mL serum kit in accordance with the manufacturer's recommended protocol (Thermo-Fisher Scientific, USA). 200 µL of supernatant from each sample was placed into 1.5 mL Eppendorf tubes. 140 µL Lysis Buffer (L19), 30 µL of proteinase K and 5 µL RNase were then added to the samples and mixed gently by pipetting 5

times, following which they were incubated at room temperature for 20 min. Following incubation, 50 µL purification buffer (N7) and 6 µL of ChargeSwitch® magnetic beads were placed into each Eppendorf tube. The samples were then mixed gently 5 times and incubated at room temperature for 2 min to allow the DNA to bind to the beads. The tubes were placed in a MagnaRack™ for 3 min and the supernatants removed and discarded. The tubes were removed from the magnet and the pellets resuspended in 200 µL of Wash Buffer (W12) by gently mixing the solution with a pipette 5 times. The tubes were then placed in a MagnaRack™ for 2 min and the supernatants removed and discarded. After washing twice, the tubes were removed from the magnet and the pellets resuspended in a 50 µL elution buffer (E5). The tubes were mixed gently by pipetting 5 times, incubated at room temperature for 2 min, and then placed in a MagnaRack™ for 1 min. The eluates containing the purified DNA were transferred to clean 1.5 mL Eppendorf tubes. Finally, the DNA concentrations (ng/µL) were measured at 260/280 nm using a NanoDrop 8000 Spectrophotometer (Thermo Scientific, USA).

2.9.2 Metabolomics analysis

The extraction of metabolites from CSC pellets was performed according to the modified techniques described previously

(Dettmer *et al.*, 2011). The cells were rapidly washed three times with cold PBS, gently harvested from the flasks with a cell scraper (Greiner, Bio-One, Germany), and transferred into new tubes. Cells were centrifuged at 500 x *g* (Allegra X-22R centrifuge, Beckman Coulter ^{TM}) for 5 min, washed again with PBS, and centrifuged at 1000 x *g* for 5 min. The resulting pellet was transferred into Eppendorf tubes. The metabolites were then extracted twice with 1.5 mL of cold solvent (80% methanol and 20% water, cooled to -48°C on dry ice) with three cycles of freezes, where liquid nitrogen was used to freeze and ice to defrost the samples for 3 min while shaking them. After the extraction of metabolites, the cells were subjected to centrifugation for 5 min at 14,000 x *g*, following which the supernatants were transferred to 15 mL Falcon tubes and stored on dry ice. A further aliquot of 1.5 mL of cold solvent (80% methanol and 20% water) was then added to the pellet. The metabolites were then extracted again utilising the three freeze cycles described previously. The second aliquot of the supernatant was then added to the 15 mL Falcon tubes. The extracted metabolite samples were maintained at –80°C and transported in dry-ice for metabolomics analysis at Glasgow University as described in detail in sections 5.2.3 and 5.2.4.

2.10. Elemental analysis

The culture supernatant of CSCs exposed to ACCM was prepared for analysis as described in detail in section 2.9. Briefly, CSCs were seeded in T-75 flasks at 5 x10^5 cells for 48 h, followed by treatment with 50% ACCM-M199 and incubated for 0, 3, 6, 24 and 48 h at 37°C. Cells treated with unconditioned M199 medium was used as a control. Culture supernatants were harvested from flasks and assessed to determine concentrations of trace elements using ICP-MS (Thermo-Fisher iCAP-Q, Thermo-Fisher Scientific, UK) in accordance with the standard protocol used at Nottingham University and in cooperation with Dr Catherine Williams. Following dilution of 1:20 (0.5 mL in 10 mL) with 4%MetOH - methanol + 0.5%HNO3 - nitric acid + internal standards scandium (25 µg L-1), germanium (10 µg L-1), rhodium (5 µg L-1) and iridium (2.5 µg L-1) were applied to the sample diluent and an analysis of multi-elements performed. External calibration levels are typically in the range 0-100 µg L-1 at part-per-billion (ppb) for micro elements and 0-100 mg L-1 part-per-million (ppm) for macro elements. Samples were assessed using an auto-sampler (Cetac ASX-520) with a perfluoroalkoxy nebulizer ST (PFA-ST) (Elemental Scientific Inc.) (Thermo-Fisher Scientific, UK). The processing of samples was performed using Qtegra software (Thermo-Fisher Scientific, UK).

2.11. Amino acid analysis for ACCM

Trophozoites of *A. castellanii* were cultured as illustrated in section 2.2.1. The trophozoites were then adapted to grow in l 20 mL medium of corneal cells (M199 or Epilife™) and incubated for 3 and 48 h. 3 mL of *A. castellanii*-adapted culture was collected and replaced with the same volume of M199 or Epilife™ medium at each incubation point. The supernatant of ACCM was filtered through a 0.2 µm filter prior to the experiment and stored at -80°C until amino acid analysis was conducted using the modified techniques described previously (Schwarz, Roberts and Pasquali, 2005). The normal medium (NM) (M199 or Epilife) was used as a control. 12 conical centrifuge tubes containing 60 mg of solid 5-sulphosalicylic acid (SSA) were prepared for the deproteinizing of each sample. 980 µL from each sample of ACCM and 20 µL internal standard norleucine (Sigma, MWt = 131.2, UK) were added to each tube. The samples and SSA were mixed gently by pipetting three times, following which the tubes were incubated for one hour at 4ºC. These were then centrifuged at 15,000 x *g* for 15 min at 4ºC to prevent any potential alteration of amino acids. The calibration standard was treated in the same way as the last steps with the samples to ensure both were prepared at the same pH for analysis and to provide similar retention times for corresponding

peaks. The supernatant was collected and filtered through a 0.2 µm filter. 20 µL of treated standards or samples was injected into an amino acid analyser Biochrom 20 plus (Biochrom Ltd, UK) equipped with an ion-exchange column and UV detector in cooperation with Dongfang Li from University of Nottingham. The concentration of amino acids and related compounds were then calculated using EZChrom Elite software.

2.12. Preparation of CeO_2NPs stock solution

Cerium oxide (CeO_2NPs, Sigma Aldrich, UK) used in the present study were obtained as powder nanoparticles (size, 2-5 nm) from the School of Science and Technology, Nottingham Trent University, UK. To prepare the CeO_2NPs stock solution, 2.5 mg of CeO_2NPs nanopowder was added to 50 mL of nanopure water in a 50 mL tube. Probe-sonication was then applied to the suspension in a Fisherbrand® FB 15050 ultrasonicator (Elma Schmidbauer GmbH, Germany) into a nanopure water bath at 80-Watt power and 50/60 Hz frequency for 30 min. The tube was subsequently placed in a UV oven (UVP, CL-1000 Ultraviolet-Crosslinker, USA) for 3 h to kill any microbial contaminants. The tube was stored at 4°C until required.

2.13. *In vitro* toxicity testing of CeO_2 on *Acanthamoeba*

2.13.1 Preparation *Acanthamoeba* for the assessment

A. castellanii trophozoites were cultured in a PYG medium as described in section 2.2.1. The flasks were placed on ice for 5 min before shaking and trophozoites extracted from the culture medium by placing them in a centrifuge for five min at 1000 x *g*. Following centrifugation, the supernatant was removed and the pellet was suspended in 20 mL of the PYG medium. A haemocytometer was used to count the trophozoites, then 1 mL from the suspension containing about 2 $x10^5$ trophozoites was added to 6 mL of the PYG medium, and the mixture was transferred into its respective T-25 flask. This process was repeated until all the trophozoites were placed into 20 flasks. These were then labelled as one control (untreated) and four treated groups for each time point. Following this, the trophozoites were left to become confluent. Subsequently, CeO_2NPs at doses of 100, 200, 300, and 400 µg/mL were utilised to incubate with the trophozoites for 3, 6, 24 and 48 h at 25°C to a volume of 7 mL medium/flask. The control flask was filled with 7 mL of PYG medium. On completion of incubation, the effectiveness of the CeO_2NPs was tested against *A. castellanii* by counting the cells using the haemocytometer, and

cell imaging was performed by using light microscopy at high and lower magnifications as described below. Each experiment was conducted three times.

2.13.1.i Cell counting

As previously described, *Acanthamoeba* trophozoites were treated with CeO_2 at 100, 200, 300 and 400 µg/mL concentrations at 25° C for a period of 3, 6, 24 and 48 h. This enabled the effect of CeO_2 on trophozoites growth to be monitored *in vitro* through cell counting. After incubation, the trophozoites were gathered from the cultures. Following the total number of trophozoites/cysts was determined by utilising a haemocytometer to count them within both central square and the four corner squares in both haemocytometer chambers (Superior Marienfeld, Germany) (Figure 2-2). This cell-counting method was verified by using an inverted microscope (Medline Scientific, CETI, UK). Based on these figures, the average number of cells was computed as $x10^3$ cells/mL. The experiment was conducted three times, with the average overall values being calculated.

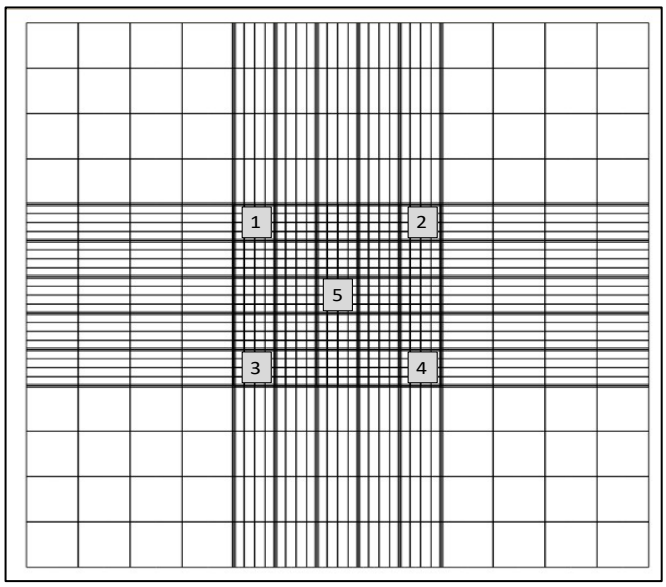

Figure 2-2 Counting chamber of the haemocytometer

2.13.1.ii Imaging light microscope

Following incubation with CeO_2 (as described previously), an inverted microscope at high and lower magnifications (Leica DMIL, CMS, Germany) was employed to obtain images of the trophozoites.

2.13.2 Electron microscopy TEM

Trophozoites were conventionally cultured into a PYG medium, seeded in flasks, and then treated with 400 µg/mL of CeO_2 (as described previously in section 2.13.1) the flasks were incubated at 25°C. The TEM technique was then used to analyse the flasks at 0, 24, and 48 h as detailed above in section 2.7.

2.13.3 Fluorescence microscopy

Sterile 22 x 22 mm round glass-coverslips (Duran Group, Germany) were placed into 24-well cell culture plates. *A. castellanii* trophozoites were then cultured in PYG in each well at a 20 $x10^3$ cell/well density. Once the trophozoites became confluent, without removing their culture supernatants, they were treated with CeO_2 at doses of 100, 200, 300, and 400 µg/mL for 3, 24 and 48 h at 25°C to a volume of 1 mL medium/well. The control well also contained 1 mL of PYG medium/well. Following incubation, trophozoites were fixed with a mixture of 4% paraformaldehyde (40 g/L, pH 6.9, Sigma-Aldrich, Germany) and 0.5 percent glutaraldehyde (TAAB, Reading, UK) in PBS at room temperature for 10 min. Subsequently, they were stained with phalloidin and DAPI as described above in section 2.6. For acridine orange (AO) staining of *Acanthamoeba*, the samples were lightly washed with sterile distilled water three times and stained by adding 250 µL of acridine orange (AO, Acros Organics, USA) to each well. This AO was prepared by dissolving 0.5 g of AO in 50 mL of sterile distilled water. Aluminium foil was then used to cover the plates to protect them from light and incubated for 10 min at room temperature before washing lightly 3 times using sterile distilled water. While preparing the images for both experiments, 1 mL of sterile distilled water was poured into each of the wells, and then

incubated at 4°C. The glass-coverslips containing samples were then extracted with care from a 24-well culture plate by raising it at the edge, and by using a curved needle and grabbing it with a pair of fine forceps. Subsequently, samples were inverted and placed on a drop of sterile distilled water which was placed on a glass slide (76 × 26 mm, Menzel Glaser, Thermo Scientific). Following this, a fluorescence microscope Leica upright PC with a Leica digital camera (Leica, DM5000B; Leica CTR5000; Germany) was then used to obtain images of the samples.

2.13.4 Viability assays

A. castellanii trophozoites were conventionally cultured in a PYG medium before seeding in 96-well plastic tissue culture plates at a density of 3 x10^3 cells. Once confluent, without removing their culture supernatants, the trophozoites were incubated with CeO_2 at concentrations of 100, 200, 300, and 400 ug/mL to a volume of 200 µL medium/well. Control wells contained 200 µL of the PYG medium. Each plate was incubated at 25°C and analysed by utilising SRB assays after 3, 6, 24, and 48 h (as described previously in section 2.4.3).

2.13.5 Encystation assay for *A. castellanii* treated with CeO_2

As described previously in section 2.2.1, *A. castellanii* trophozoites were conventionally cultured within a PYG medium.

When they were confluent, they were extracted from the culture medium, and centrifuged at 1000 x *g* (Allegra X-22R centrifuge, Beckman Coulter™) for 5 min to separate the trophozoites from the culture medium as described in section 2.13.1. The supernatant was removed, and the pellet was suspended in 10 mL of an encystment buffer, which was made via dissolving magnesium chloride (0.48 g) as well as glucose monohydrate (10 g) (Sigma-Aldrich) in 100 mL of PBS. Trophozoites were counted using a haemocytometer and 7 $x10^5$ trophozoites were pipetted into each of the 5 centrifuge tubes containing 2 mL of the suspension. Subsequently, the tubes were labelled as one control (untreated) and four treated groups. Furthermore, 6 mL of a liquid medium: normal control as an encystment buffer and four treated groups of 100, 200, 300 and 400 µg/mL CeO_2 with an encystment buffer were added to the tubes. A vortex mixer was employed to mix the suspension and to detach the trophozoites from the body of the tube. A 10 mL pipette was then utilised to place each suspension into its respective T-25 flask. Following this, the flasks were then labelled and incubated at 25°C. After a period of 48 h, a haemocytometer was utilised to count the control and treatment groups.

These were then gathered and centrifuged again as described previously. The pellets obtained were then treated with an equal

volume of 1% sodium dodecyl sulphate (SDS, cyst digestion buffer) (Fisher Scientific, Japan). They were prepared via dissolving 1 g of SDS in 100 mL of sterile distilled water. To solubilise the remaining trophozoites, the samples were left to stand for 30 min. For post-SDS treatment, a count was applied, and the encystment percentage calculated by following formula (post-digestion total count / pre-digestion total count × 100 = percent encystment). This experiment was conducted three times, and the average overall values computed.

2.14. *In vitro* toxicity testing of CeO_2 on CSCs and ihCECs

2.14.1 Viability assays

As described previously in sections 2.1.3 and 2.4, CSCs or ihCECs were cultured within M199 and Epilife™ medium and then seeded in 96-well plastic tissue culture plates. They were then allowed to attach for 48 h, without removing their culture supernatants, they were incubated with CeO_2 at 100, 200, 300, and 400 µg/mL concentrations to a volume of 200 µL medium/well. The control wells were filled with 200 µL/well of M199 for CSCs and Epilife™ for ihCECs. Following incubation at 37°C, alamarBlue and SRB assays were utilised to analyse the plates after 3, 6, 24, and 48 h (as mentioned in sections 2.4.1 and 2.4.3).

2.14.2 Fluorescence microscopy

As described previously in sections 2.13.3 and 2.6, 24-well cell culture plates were prepared by placing glass coverslips into each well, and ihCECs or CSCs conventionally cultured in M199 and Epilife™ medium. They were seeded at 12 $x10^3$ and 20 $x10^3$ cells respectively and allowed to attach for 48 h, without removing their culture supernatants, they were incubated with CeO_2 at 100, 200, 300 and 400 µg/mL concentrations to a volume of 1 mL medium/well. The control wells were filled with 1 mL of M199 for CSCs and Epilife™ for ihCECs. The plates were then incubated for 3, 24, and 48 h at 37°C. Cells were fixed in 4% paraformaldehyde and stained with phalloidin and DAPI for the immunofluorescent staining of actin as described above in section 2.6. However, in AO analysis, the cells were stained with AO as detailed above in section 2.13.3. A fluorescence microscope, Leica upright PC and a Leica digital camera (Leica, DM5000B; Leica CTR5000; Germany) were then used to obtain the images.

2.15. Statistical analysis

Each experiment was conducted in triplicate and then replicated at least twice. All statistical analysis was undertaken by applying the GraphPad Prism version 7 (GraphPad, San Diego, CA, United States). Analytical styles vary depending on the purpose

of experiments and are outlined in each chapter, including two-way variance analysis (ANOVA). Data are indicated as mean ± SD, with statistical importance being depicted by asterisks; P-value < (0.0001****, 0.001***, 0.01**, 0.05*).

3. Chapter Three: Comparative cytotoxicity of *Acanthamoeba castellanii* derived conditioned medium on human cornea epithelial and stromal cells

3.1 Introduction

Acanthamoeba keratitis (AK) is a severe corneal infection and a poses significant public health issue. Human ocular tissue is considerably damaged in AK, the pathogenesis of which is partially mediated by soluble factors existing in the protozoan *A. castellanii*'s secretome. (Marciano-Cabral and Cabral, 2003; Carnt *et al.*, 2018). *A. castellanii* is an invasive and persistent parasite and expresses various virulence proteins, such as the mannose-binding protein, which mediates adhesion of the organism to mannose-glycoproteins on the surface of the cornea (Garate *et al.*, 2006). Clinical symptoms associated with ocular infection can be attributed to inflammation and cellular damage. Misdiagnosis of fungal or viral infection is also possible, and any delay in initiating appropriate treatment can have sight-threatening consequences (Jiang *et al.*, 2015), and even with the most potent medications, treatment failure can occur.

Previous studies reported that *A. castellanii* trophozoites produce a number of metalloproteinase and serine proteinases

(Cao, Jefferson and Panjwani, 1998). These proteinases possess cytopathic effects, which can kill corneal epithelial cells, and degrade the basement membrane, revealing the stromal matrix, and allowing penetration into the cornea's deeper layers (Mitra *et al.*, 1995). The majority of proteolytic enzymes in protozoal extracts indicates notable activity across a broad scope of a temperature of 8 to 45 °C and pH of between 3 and 9 (Heredero-Bermejo *et al.*, 2015). An earlier study showed that heat-resistant molecules, having low molecular mass (<10 kDa) released by viable trophozoites of *A. castellanii* caused several cytopathic effects in an epithelial (WISH) cell line, such as increase in cytosolic calcium, morphological alterations, cytoskeletal disruption, reduction in cell viability, and increased apoptosis (Mattana *et al.*, 1997). Additionally, *A. castellanii* trophozoites have the capacity to develop contact-dependent cytolysis, thereby destroying phagocytic cells by using cytolytic factors and a finger-like projection (Marciano-Cabral and Toney, 1998). *Acanthamoeba griffin,* an isolate from a contact lens-wearing patient in Spain, induced focal lesions in HeLa cell monolayers which were attributed to the activity of the serine proteases and cysteine proteases secreted by the amoeba (Heredero-Bermejo *et al.*, 2015).

In the present study, we examined the effects of cell-free supernatants from *A. castellanii* culture [*A. castellanii*-conditioned medium (ACCM)], on the viability, apoptosis, actin cytoskeleton and ultrastructure of human SV40 immortalized corneal epithelial cells (ihCECs) and human corneal stromal cells (CSCs). The data showed that ACCM reduced cell viability, increased cell death via apoptosis, disrupted the actin cytoskeleton and caused morphological alterations at subcellular level. We also showed that the cytopathic effects caused by ACCM were mediated by proteases. Together, the results presented herein add further evidence to the extent of the cellular damage that can be caused by the secretome of *A. castellanii*.

3.2 Materials and Methods

3.2.1 Cell culture conditions

ihCECs were cultured in EpiLife™ medium as described above in section 2.1.1. CSCs were also isolated and cultured as mentioned in section 2.1.2.

3.2.2 *A. castellanii* culture and conditioned medium preparation

A. castellanii trophozoites were routinely cultured in PYG medium as described in section 2.2.1. ACCM was prepared with the same protocol that mentioned in section 2.2.2, which were used to test the cytotoxic effects of ACCM on corneal cells as described below.

3.2.3 The bicinchoninic acid (BCA)

BCA assay was used to quantify the protein concentration of ACCM for both M199 and Epilife™ according to the manufacturer's instructions (Thermo Scientific Pierce) (described in detail in section 2.3).

3.2.4 Viability assays

ihCECs and CSCs were seeded in 96-well plates at 1 $\times 10^4$ cells/ well for ihCECs and 6 $\times$ 10^3 cells/well for CSCs and incubated for 48 h at 37 °C and 5% CO_2. the medium in the wells was replaced with ACCM at various concentrations of (25%, 50%,

75%, and 100%) to a final volume of 100 µL/well. Untreated wells contained 100 µL media/well of Epilife™ for ihCECs and M199 for CSCs. The plates were incubated at 37 °C and after 3, 24 and 48 h, the cytotoxic effects of ACCM on the viability and proliferation of CSCs and ihCECs were examined using alamarBlue, MTT and SRB assays as described in detail in sections 2.4.1, 2.4.2 and 2.4.3, respectively.

3.2.5. *In vitro* cell toxicity studies

ihCECs and CSCs were seeded in 96-well plates at 5×10^3 and 3×10^3 cells/well, respectively for 24 h. The cells were then treated with 50% of ACCM or left untreated (control) and incubated for 3, 24 and 48 h at 37°C. After incubation, the cytotoxicity of ACCM against these cells was assessed using LDH cytotoxicity assay as described in section 2.5.1. In addition, the level of caspase-3 activity in CSCs and ihCECs was determined using caspase 3 assay as described in section 2.5.2.

3.2.6. Immunofluorescent staining of actin

CSCs or ihCECs were seeded in 24-well plates at 12×10^3 and 20×10^3 cells, respectively and incubated with ACCM (M199 or Epilife™*)* at various concentrations (100%, 75%, 50% and 25%) for 3, 24 and 48 h at 37°C. Immunofluorescent staining of actin was performed according to technique previously described in section 2.6.

3.2.7. Transmission electron microscopy (TEM)

CSCs and ihCECs were seeded in T-25 flasks at 7 × 10^4 and 12 × 10^4 cells, respectively for 48 h, followed by addition 50% of ACCM. After incubation for 48 h at 37°C, cells were processed for TEM as previously described in section 2.7.

3.2.8. Protease inhibitor assay

A protease inhibitor cocktail was added to ACCM at concentrations 2.5, 5 and 10 µL/mL and incubated for 30 min at 25 °C. 100 µL of treated ACCM were added to CSCs or ihCECs seeded in 96-well plates, and incubated for 3, 6, 24 and 48 h at 37 °C (described in detail in section 2.8). The proliferation rate of the cells was determined using SRB assay as described in section 2.4.3.

3.2.9. Statistical analysis

All statistical analysis was undertaken by applying the GraphPad Prism version 7 (GraphPad, San Diego, CA, United States). The differences between the effects of the various concentrations of ACCM at different incubation times were detected by two-way variance analysis (ANOVA). The results are indicated as mean ± SD, with statistical importance being depicted by asterisks; P-value < (0.0001****, 0.001***, 0.01**, 0.05*).

3.3 Results

3.3.1 The effects of ACCM on the viability of CSCs and ihCECs

The effects of ACCM on the viability and proliferation of CSCs and ihCECs were assessed using alamarBlue®, MTT and SRB assays. Exposure to ACCM caused a decline (i.e. in a dose-dependent manner) in viability and proliferation of CSCs and ihCECs at 3, 24 and 48 h of incubation for all assays (Figures 3-1 and 3-2). As shown in (Figure 3-1 A), the result of the alamarBlue assay showed statistically significant differences in CSCs viability between the incubation groups compared to control at all incubation times. MTT test results also revealed significant differences in CSCs proliferation between treated and control cells at all examined incubation times (Figure 3-1 B). Likewise, the SRB assay revealed significant differences in CSCs proliferation between treated and control at all incubation times (Figure 3-1 C). Regarding the ihCECs, the alamarBlue® results showed that there were not significant differences in ihCECs viability between the incubation groups compared to control at 3 h, however there were significant differences at 24 and 48 h (Figure 3-2 A). The MTT results also showed that the reduction in the viability of ihCECs was significantly different between treated and control cells at 3, 24 and 48 h (Figure 3-2 B). Similarly, based on the cell proliferation rate as determined

by the SRB assay (Figure 3-2 C) there were significance differences between tested concentrations and control at 3, 24 and 48 h.

The BCA protein assay result revealed that a low protein concentration in the ACCM, which was proportional to the percentage of ACCM analysed, compared to the normal culture medium (M199 and Epilife) which had the highest protein concentration (Table 3-1).

Table 3-1 Protein concentrations corresponding to 100%, 50%, and 25% of *A. castellanii*-conditioned medium (ACCM) compared to the protein concentration in the control media. Protein was quantified using the BCA protein assay and the absorbance was measured at 562nm. The experiment was performed three times with four replicates per-experiment.

ACCM Concentrations	Protein Concentration (µg/mL)	
	ACCM_M199 (Mean ± SD)	ACCM_Epilife (Mean ± SD)
100%	366.08 ± 16.71	238.42± 9.53
50%	371.52 ± 5.81	257.41 ± 6.68
25%	434.39 ± 18.38	289.54 ± 11.91
Control*	472.66 ± 17.23	303.21 ± 12.74

* Normal M199 and Epilife™ medium without any contribution from *A. castellanii* secretome

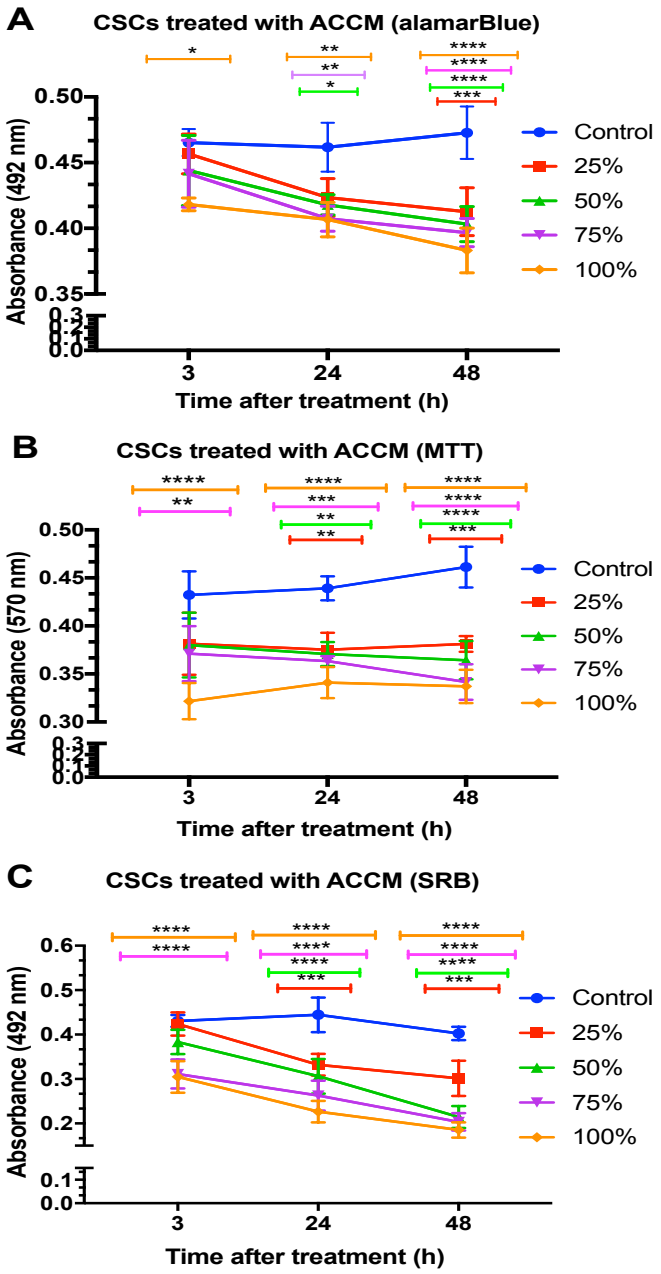

Figure 3-1 Effect of *A. castellanii*-conditioned medium (ACCM) on the viability and proliferation of CSCs using (A) alamarBlue®, (B) MTT and (C) SRB assays. Cultured CSCs were incubated with various concentration of ACCM (25%, 50%, 75%, and 100%) at 37 °C for 3, 24 and 48 h. Cells treated with unconditioned M199 medium was used as a control. The absorbance values obtained at 492 nm were presented as the means ± SDs of 4 technical replicates, and each experiment was replicated three times. Two-way ANOVA detected significant differences between the results for groups treated with ACCM and untreated groups. Significant P-value < (0.0001****, 0.001***, 0.01**, 0.05*), versus the control cells.

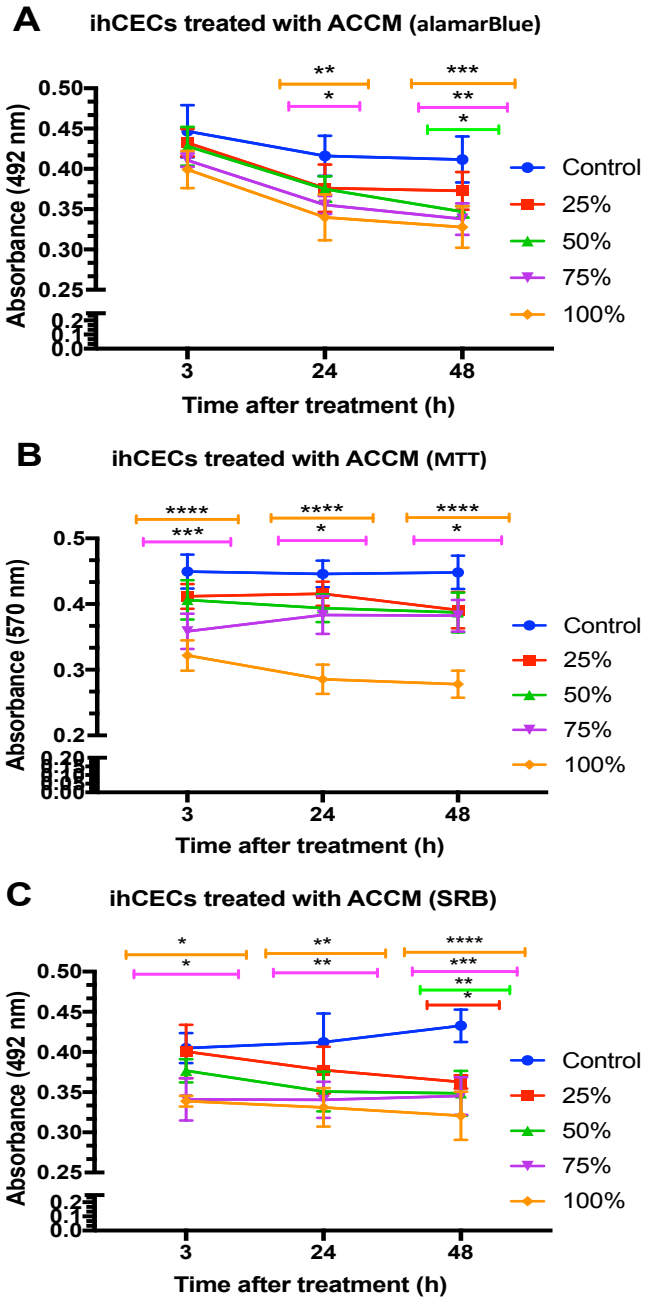

Figure 3-2 Effect of *A. castellanii*-conditioned medium (ACCM) on the viability and proliferation of ihCECs using (A) alamarBlue®, (B) MTT and (C) SRB assays. ihCECs were incubated with ACCM) at 25%, 50%, 75%, and 100% concentrations for 3, 24 and 48 h at 37 °C. Cells treated with unconditioned Epilife™ medium were used as a control. Data are presented as absorbance values at 492 nm relative to untreated (control) cells. Two-way ANOVA showed significant differences between the results for cells subjected to ACCM and untreated cells. Significant P-value < (0.0001****, 0.001***, 0.01**, 0.05*), versus the control cells. Each experiment was performed three times with 4 technical replicates per-experiment.

3.3.2. The cytotoxic effects of ACCM on CSCs and ihCECs

CSCs and ihCECs were incubated with 50% ACCM and the amount of LDH enzyme released into the cell culture medium was quantified. According to our previous results in terms of corneal cells being affected by the high concentrations of ACCM, 50% ACCM was chosen for treatment the corneal cells. The results showed that there were significances differences between treated and control cells, however significant increase and decrease were detected for CSCs at 3 and 24 h, respectively (Figure 3-3 A). Regarding the ihCECs, there were also significant differences between treated and untreated cells at all time points after treatment, with increased level at 3 h, but decreased levels at 24 and 48 h (Figure 3-3 B). We also, examined the apoptotic activity of ACCM by measuring the caspase activity using caspase Glo-3/7 assay. Caspase 3 was activated in CSCs after stimulation with 50% ACCM after 24 h, and more activation was observed at 48 h (Figure 3-4 A). In ihCECs, significant reduction in the level of caspase 3 was observed in cells treated with ACCM at 48 h (Figure 3-4 B).

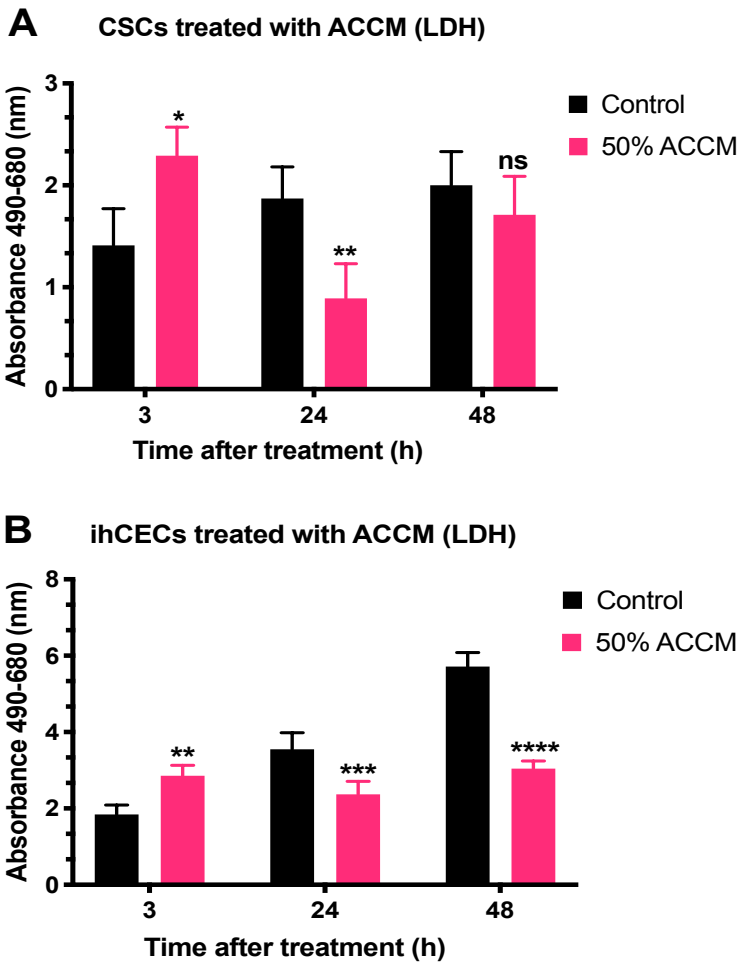

Figure 3-3 Results of the LDH assay. (A) CSCs and (B) ihCECs were incubated with 50% of *A. castellanii*-conditioned medium (ACCM) for 3, 24 and 48 h at 37 °C. The absorbance was measured at 490 and 680nm. Cells treated with unconditioned medium (M199 or Epilife™) was used as a control. The experiment was performed at least three times with 4 technical replicates per experiment. Data are presented as the mean ± SD. Two-way ANOVA detected some significant differences between the results for cells subjected to ACCM and untreated cells. Significant P-value < (0.0001****, 0.001***, 0.01**, 0.05*), versus the control cells.

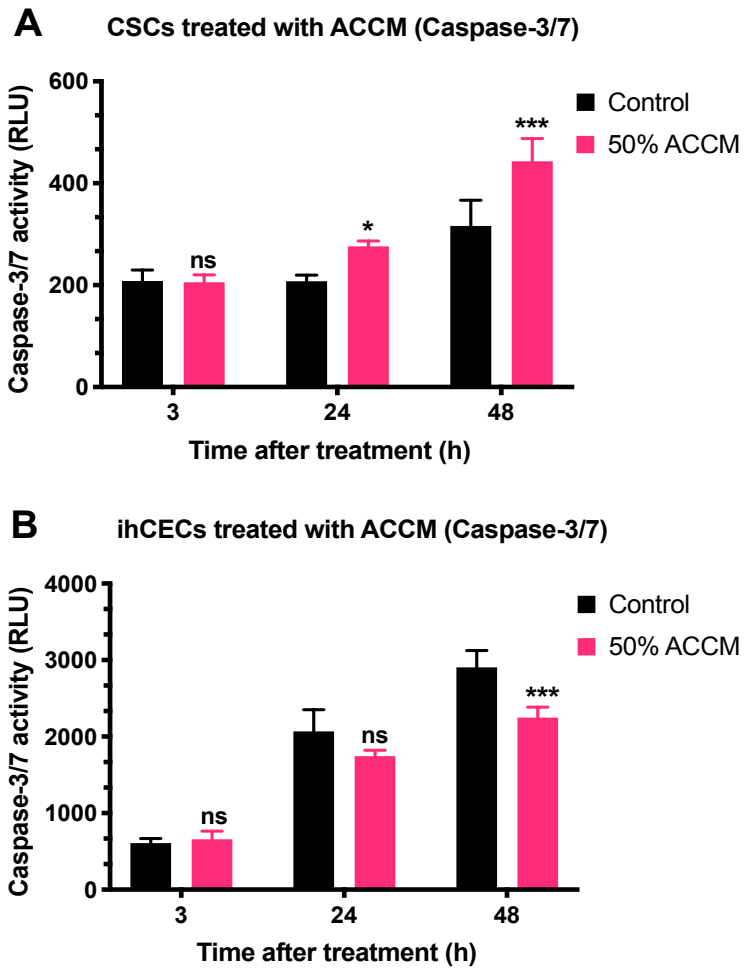

Figure 3-4 Results of the caspase activity in (A) CSCs and (B) ihCECs. Caspase 3/7 activity assay was performed with recombinant human caspase-3 enzyme to test the stimulatory or inhibitory effect of 50% *A. castellanii*-conditioned medium (ACCM) at 3, 24 and 48 h at 37 °C. The bar chart presents the means ± SDs of 4 technical replicates, and each experiment was repeated three times. Data were presented as relative luminescence unit (RLU), which was proportional to caspase 3 activity. Two-way ANOVA detected some significant differences between the results for cells subjected to 50% ACCM and untreated cells. Significant P-value < (0.001***, 0.01**, 0.05*), versus the control cells.

3.3.3 Actin cytoskeleton derangement

The CSCs and ihCECs were stained with phalloidin and DAPI to characterize the morphological alterations in actin arrangement after exposure to different concentrations of ACCM for different incubation times. As shown in Figure 3-5 (A-B) for CSCs and ihCECs respectively, the density of the cell monolayer was high in the control compared to the treated cells, where the integrity of the cell monolayer was compromised in a dose-response manner. We also observed abnormality in the shape of CSCs and ihCECs and derangement of the actin cytoskeleton, particularly at higher concentrations and longer exposure time (i.e. at 24 and 48 h with 50%, 75% and 100% ACCM). Additionally, in ihCECs cultured with 50%, 75% and 100% ACCM, cells became smaller and became more rounded at 3, 24, and 48 h exposure (Figure 3-5 B). However, for both cell types, the number of cells was counted manually in each image of Figure 3-5 (A-B) and a graph of the results has been created and shown in Figure 3-6 (A-B). The results showed a significant decrease in cells density, in a time and concentration-dependant manner.

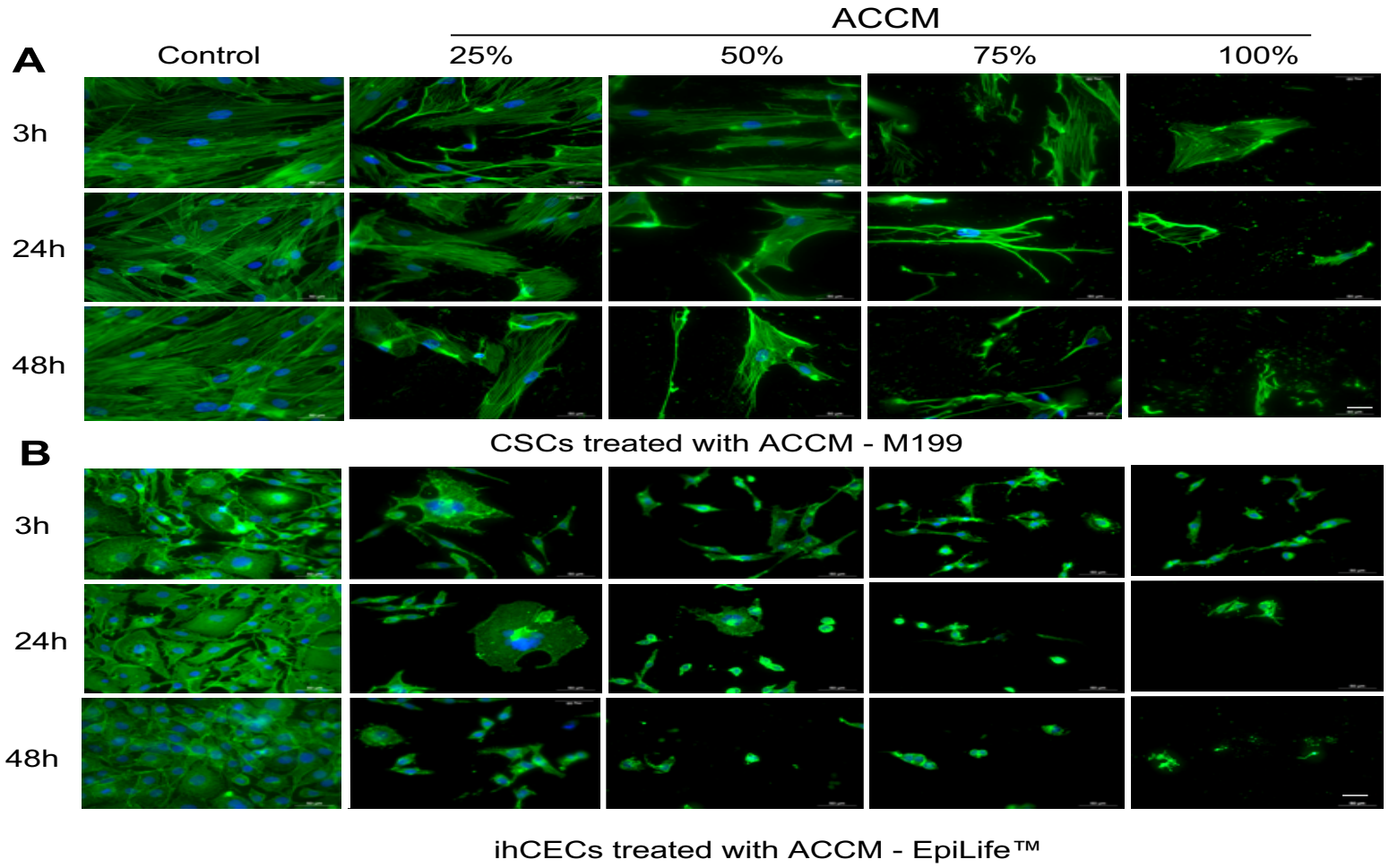

Figure 3-5 Effect of ACCM on fluorescence staining of actin cytoskeleton. (A) CSCs and (B) ihCECs were incubated with ACCM at the indicated concentrations and duration of incubation. Cells were fixed with 10% formalin for 10 min then stained for the F-actin with Alexa Fluor 488 phalloidin and the nuclei were counterstained with DAPI. Images were obtained with an inverted wide-field fluorescence microscope. Scale bar (25 μm) applies to all images. The imaging showed significantly decreased in cells density and disrupted the cell actin cytoskeleton, in a time- and concentration-dependant manner.

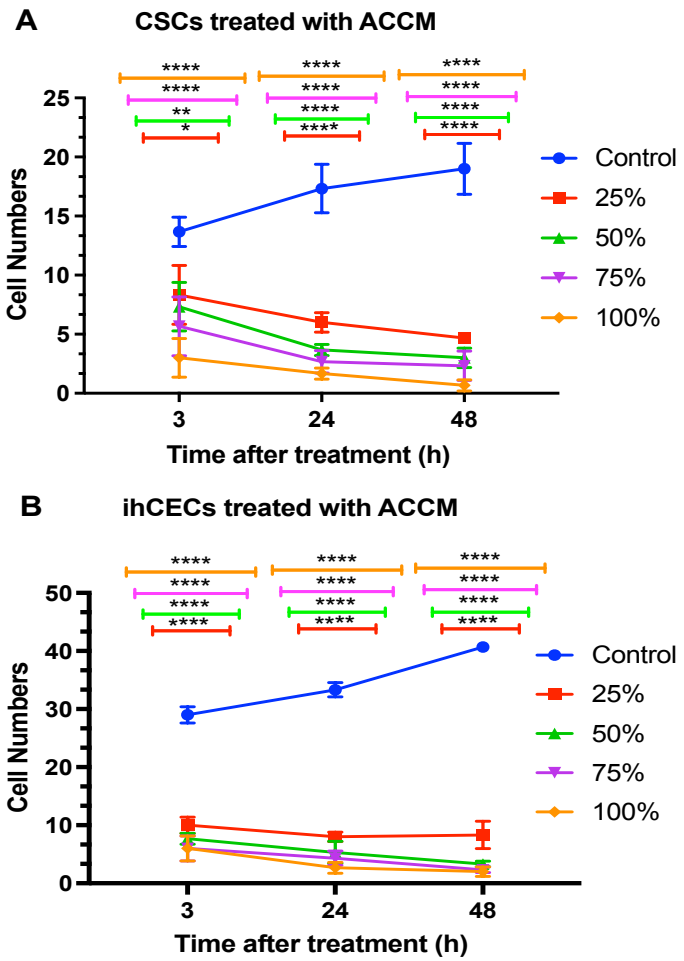

Figure 3-6 The impact of ACCM on the cells density of (A) CSCs and (B) ihCECs were determined by cell counting. The number of cells was counted manually in each image of Figure 3-5 (A-B), (three images for each condition). Data are presented as the mean ± SD. A two-way ANOVA revealed significant differences between the treated cells and the controls. Significant P-value < (0.0001****, 0.001***, 0.01**, 0.05*), versus the control cells.

3.3.4 TEM analysis of ACCM-treated corneal cells

To further elucidate the effects of ACCM on CSCs and ihCECs, TEM was performed to reveal the ultrastructural changes upon 50% ACCM treatment for 48 h. The results showed that cells exhibited normal cellular components in untreated cultures of CSCs (Figure 3-7 A-D) and ihCECs (Figure 3-8 A-D), including a largely convoluted nucleus, conspicuous nucleolus, normal cellular organelles, vacuoles, intact plasma membrane and no sign of cellular or organelle damage. On the contrary, cells treated with 50% ACCM for 48 h showed some damage and morphological changes. The nucleus was less visible or even absent in some cells (Figure 3-7 E-H). Consistent with the results of CSCs, significant damage to cells and more vacuoles were also observed in ihCECs compared to untreated cells (Figure 3-8 E-H).

Based on the previous results, ACCM adversely compromised cell viability and structural integrity of corneal cells in a time- and concentration-dependant manner. ACCM significantly decreased cell viability/proliferation (Figures 3-1 and 3-2), and cytotoxic effects showed significant cell damage within the first 3 h of exposure for ihCECs and extremely significant damage at 24 and 48 h for CSCs (Figures 3-3 and 3-4). Actin cytoskeleton staining showed that derangement of the actin cytoskeleton of

CSCs and ihCECs was observed after exposure to ACCM, particularly at 24 and 48 h (Figure 3-5). TEM analysis showed significant cell damage between 24 and 48 h for both cells (Figures 3-7 and 3-8), corroborating these results. In conclusion, treated CSCs exhibited majority apoptosis, while treated ihCECs exhibited majority cell lysis.

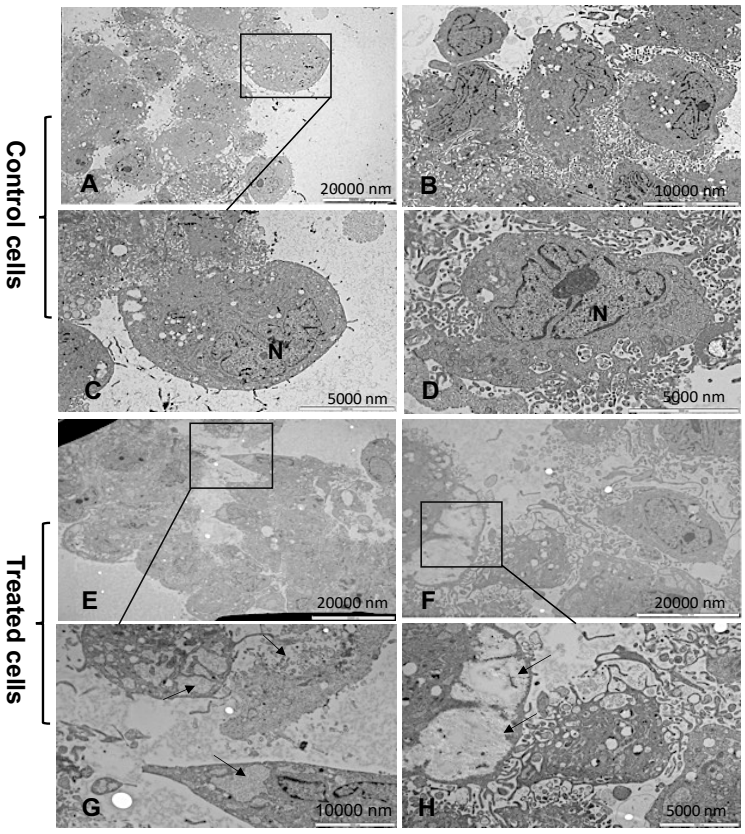

Figure 3-7 Ultrastructural changes in ACCM-treated CSCs. CSCs were incubated with 50% ACCM–M199 for 48 h. (A-D) Control CSCs appeared morphologically normal with a largely convoluted nucleus (N) and conspicuous nucleolus. (E-H) CSCs treated with ACCM showed some of the damages and morphological changes (arrows). Also, there were some cell deaths with no apparent nucleus with cytoplasmic vesicles and lack of cell organelles (arrows).

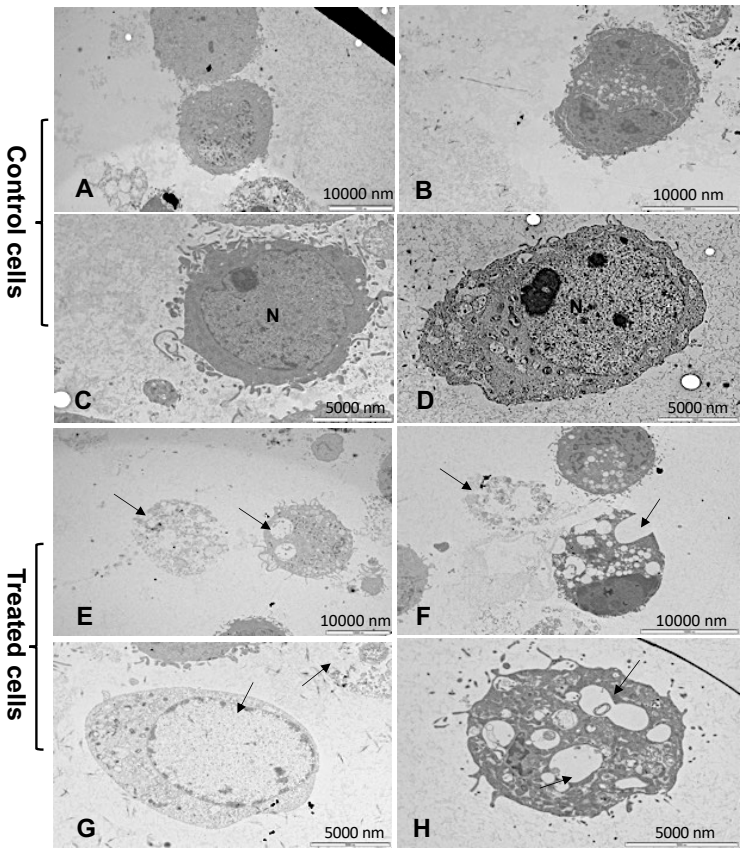

Figure 3-8 Ultrastructural changes in ACCM-treated ihCECs. ihCECs were incubated with 50% ACCM-Epilife™ for 48 h. (A-D) Control ihCECs appeared morphologically normal with a largely convoluted nucleus (N) and conspicuous nucleolus. (E-H) ihCECs treated with ACCM showed some damages and morphological changes (arrows). Also, some cells appeared dead, and lack nucleus and cell organelles (arrows).

3.3.5 Protective effects of enzyme inhibitor cocktail on the cytotoxicity of ACCM

Here, we investigated whether the damaging effect of ACCM was mediated by the presence of proteases known to be secreted by *A. castellanii* (Figure 3-9). A gradual dose-dependent increase in cell proliferation was observed in CSCs treated with protease inhibitor at all concentrations compared to

untreated (control) cells at 3, 6, 24 and 48 h after incubation (Figure 3-9 A). There were significant differences in CSC proliferation between the incubation groups compared to control at 24 and 48 h (Figure 3-9 A). This result suggests that the protease inhibitor cocktail protected corneal cells from the damaging effects of ACCM. Protease inhibition appeared maintain the growth rate of treated ihCECs, where there were significant differences between the incubation groups compared to control at 6, 24 and 48 h (Figure 3-9 B).

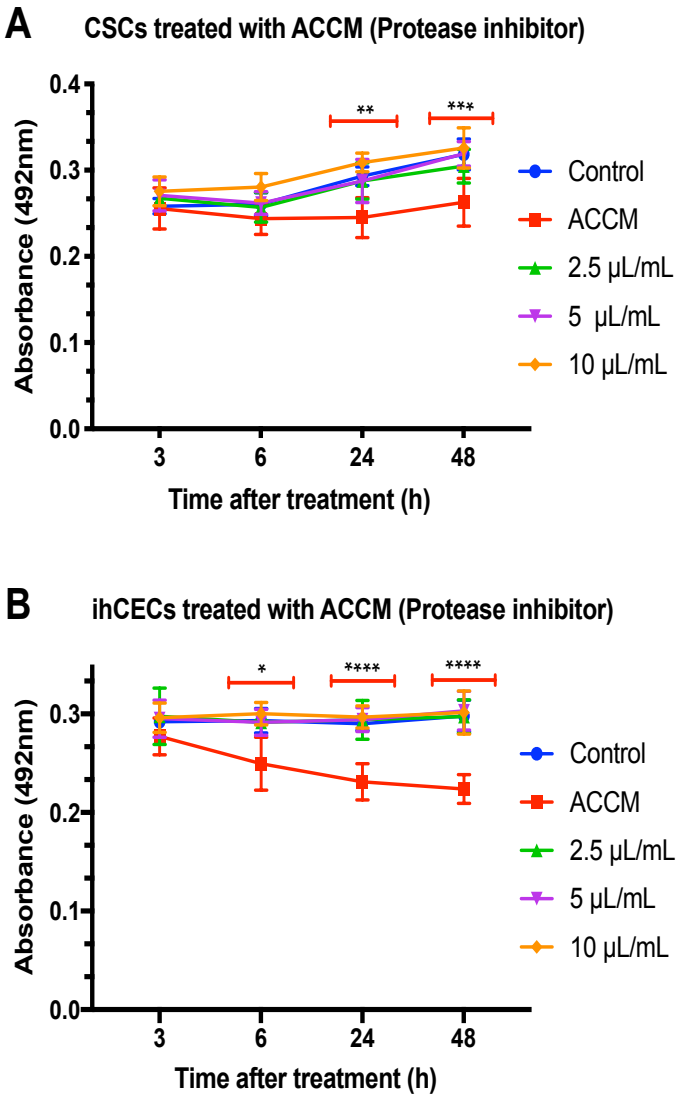

Figure 3-9 Protease inhibitor cocktail protects (A) CSCs and (B) ihCECs from the cytotoxic effect of ACCM. Cells were treated with ACCM that was treated with a protease inhibitor cocktail at various concentrations (2.5, 5 and 10 µL/mL). Cells were then incubated for 3, 6, 24 and 48 h at 37 °C. Cell proliferation was examined using the SRB assay. Data represent the absorbance measured at 492 nm. Two-way ANOVA detected some significant differences between the results for cells subjected to 100% ACCM and untreated cells. Significant P-value < (0.0001****, 0.001***, 0.01**, 0.05*), versus the control cells. Each experiment was performed three separate times with 4 technical replicates per-experiment.

3.4 Discussion

Cellular injury caused by *A. castellanii* infection is related to molecules secreted by the amoeba. The cytotoxic effects of the *A. castellanii* secretome have been demonstrated in some cell types (Khan *et al.*, 2000; Mattana *et al.*, 2002; Mattana *et al.*, 1997). However, the contributions of the cytolytic molecules present in the secretome of *A. castellanii* to the pathophysiology of corneal infection is still not completely known. In this study, we investigated the cellular basis for corneal cell (CSCs and ihCECs) sensitivity to the cytotoxic effects of ACCM. Our findings conformed to past findings (Mattana *et al.*, 2002; Khan *et al.*, 2000; Mattana *et al.*, 1997), Our results also indicated that *A. castellanii* cytotoxicity when against human ocular cells has no necessity of contact with the amoeba host cell; however, cell-free supernatants acquired from trophozoite cultures have the ability to cause cell damage and death.

Various cell viability and proliferation assays were used in this study for assessing the viability and growth kinetics of corneal cells, such as alamarBlue, MTT and SRB assays. AlamarBlue is used to evaluate the metabolic activity and viability of cells. It is a dye that changes from blue to red colour, with more cell growth (Rampersad, 2012). The MTT assay is used for quantifying cellular metabolic activity based on the ability of growing cells to

produce NADPH-dependent oxidoreductase enzymes, which reduces the tetrazolium dye to formazan, a purple insole solid (Berridge, Herst and Tan, 2005). The SRB assay works by binding SRB dye to basic amino acid residues in the intracellular proteins after fixing the cells with trichloroacetic acid (TCA) in mildly acidic conditions (Voigt, 2005). In this study, the effect of ACCM on the viability and proliferation of CSCs and ihCECs by alamarBlue®, MTT and SRB assays showed that ACCM caused a significant decrease in cell viability and proliferation (Figures 3-1, 3-2), suggesting that exposure to ACCM can induce adverse effects on the viability and growth rate of the corneal cells.

The cytotoxicity of ACCM against corneal cells was assessed using an LDH assay. LDH is a stable enzyme, released from the plasma membrane to the cell culture medium when cells are damaged. It is widely used as a marker for cytotoxicity and cell death. The LDH assay determines the damage levels to the plasma membrane by measuring the LDH released by the cells (Parhamifar, Andersen and Moghimi, 2019; Kumar, Nagarajan and Uchil, 2018). The released LDH enhances lactate oxidation resulting in NADH which combines with diaphorase enzyme and transforms the yellow tetrazolium salt into a red formazan. In this experiment, we measured the levels of LDH enzyme in the cell culture medium. Elevated LDH levels in culture medium post

treatment with ACCM reflect leakage in the cell membrane, which seems to depend on the cell type and duration of exposure to ACCM (Figure 3-3). Increased level of LDH seems to occur at an early stage of treatment 3 h, but the opposite was detected at 24 and 48 h. Cell lysis seemed to increase at 3 h in both CSCs and ihCECs, followed by decreased LDH level at 24 h in CSCs, and at 24 and 48 h in ihCECs.

We also determined the changes in the activity of caspase 3. Previous studies have shown that the changes in the mitochondrial membrane possibly cause a cytochrome c release in the cytoplasm, caspase activation (Liu *et al.*, 1996) leading to mitochondrion-initiated apoptosis, mediated by caspase-3 (Thornberry and Lazebnik, 1998). Therefore, we determined whether caspase 3 was activated in CSCs and ihCECs in response to treatment with ACCM. The caspase activity in CSCs and ihCECs was assessed using caspase-3 activity assay (Figure 3-4). In CSCs caspase-3 was activated subsequent to stimulation with 50% ACCM for 24 h, and was highly activated at 48 h. In ihCECs, a significant decrease in caspase-3 level was apparent in cells treated with ACCM after 48 h. The proapoptotic effect of ACCM on CSCs is consistent with previous work (Mattana *et al.*, 2002) suggesting that pathogenic free-living *A. castellanii* by release of adenoside di-phosphate as well as

further metabolites cause death of human monocytic cells within the secretion of proinflammatory cytokines and apoptosis. However, our results indicate significant reduction in caspase compared to the ihCECs control, possibly indicating an anit-apoptotic effect, but or likely due to a reduced cell number in the treated cells due to lysis. The cell line exhibits a lot of natural turnover and apoptosis, leading to both LDH and caspase production in the control. This would not be seen to the same effect if there were fewer cells due to cytotoxicity of the treatment.

The derangement of the actin cytoskeleton is a pathologic manifestation of cell damage because the actin cytoskeleton plays a critical role in maintaining the cell structure, function and adhesion (Soto-Arredondo *et al.*, 2014). In the present study, we assessed the effect of ACCM on the actin cytoskeleton arrangements by investigating the structural changes that occurred in cultured CSCs and ihCECs treated with various doses of ACCM for 3, 24 and 48 h (Figure 3-5 A-B). Smaller concentrations induced mild derangement of the actin cytoskeleton, but exacerbated derangement and deformity of the cell shape was observed at higher concentrations and longer treatment durations. The cytotoxic effects of ACCM on ihCECs was more pronounced than those observed in CSCs. The most

substantial cytotoxic effect of ACCM was detected after 24 h of incubation, resulting in more damage and rounding of cells. Actin fibers do not only contribute to the maintenance of cellular structure but also, adhesion of the *A. castellanii* to target host cells (Soto-Arredondo *et al.*, 2014) and potentially interactions with various structural molecules. Therefore, it is sensible to anticipate that disruption of the actin cytoskeleton caused by ACCM can have a serious consequences on the integrity, function and survival of host cells.

Further evidence to support the adverse effects of ACCM on corneal cells was achieved by ultrastructural microscopic analysis (Figures 3-7, 3-8). Treated cells showed significant damage and became irregular, which seemed to cause leakage of intracellular contents. Based on the previous results, apoptosis and cell lysis were observed in treated cells, suggesting that ACCM is likely to induce cell death via apoptosis and necrosis (cell lysis) in the host cells. These observations were also reported in previous studies (Pettit *et al.*, 1996; González-Robles *et al.*, 2006), however cell damage was detected in host cells due to direct physical contact with *A. castellanii* trophozoites.

The proteases in protozoan organisms are known to contribute to the destruction of host tissue as well as pathogenesis and

digestion of phagocytosed food (Heredero-Bermejo *et al.*, 2015; Klemba and Goldberg, 2002). In *A. castellanii*, it has become apparent that proteases play a role in the parasite pathogenesis by functioning as virulence factors (Serrano-Luna *et al.*, 2006; Kim *et al.*, 2006), contributing to the amoeba encystation process (Moon *et al.*, 2008), and adhesion (Singh *et al.*, 2012). The use of proteinase inhibitors showed that the proteinase activity is essential for the development of focal lesions in the cellular monolayers of HeLa cells (Heredero-Bermejo *et al.*, 2015), and with a corneal endothelial cell line (Khan *et al.*, 2000). These authors also showed that the enzymes found in amoeba extracts were mainly cysteine and serine proteases. However, the prominent role of serine and cysteine proteases was shown when *Acanthamoeba* was incubated with a serine inhibitor (PMSF, phenylmethylsulfonyl fluoride) and a cysteine inhibitor (2S,3S)-trans-epoxysuccinyl-L-leucylamido-3-methylbutane ethyl ester (E64d). This blocked proteinase activity, suggesting the key role played by proteinase activity in the pathogenesis of *A. castellanii* (Leitsch *et al.*, 2010). In our study, we neutralized the enzymatic activities in the ACCM using protease inhibitor cocktail with wide specificity for inhibiting cysteine, serine, aminopeptidases and aspartic acid proteases (Figure 3-9). By inhibiting the enzymatic activities in the ACCM using protease inhibitor cocktail, we confirmed the previous observation that *A.*

castellanii expresses proteases, which play roles in the pathogenesis of *A. castellanii* infection.

The overall trends from of the present results showed that ACCM causes a significant detrimental effect on both types of corneal cells, but the severity of damage to ihCECs ultrastructure was much more than that observed in CSCs. This differential cell sensitivity may largely be explained by variations in cell -specific functions influencing response to ACCM. CSCs are primary cells, whereas ihCECs are a cell line, and thus they are expected to differ in their metabolic activity, natural antioxidant activity and proliferative capacity. In fact, primary cells seem to have a better apoptotic balance and more stable metabolism compared to cell lines (Joris *et al.*, 2013). In line with this assumption, when comparing primary cells to cell lines in our study, CSCs seem to exhibit consistent results in most experiments. In contrast, ihCECs showed slight varying results, particularly when cells were seeded in large plates and flasks, where their growth seemed slow, and they were strongly affected by ACCM. Considering the aforementioned statements and the present results and given that primary cells are more representative to the *in vivo* situation compared to the transformed cell line, CSCs seem to provide a more relevant system for cytotoxicity assessment of ACCM.

Due to differences between stromal cells and corneal epithelial cells, they have different interaction profiles with *Acanthamoeba.* The pathophysiology during *Acanthamoeba* infection in corneal stromal cells involves a set of sequential changes, starting with the production of pathogenic proteases for degrading extracellular matrix and inducing cytolysis and apoptosis (Marciano-Cabral and Cabral, 2003). These changes culminate into the dissolution of the collagen surrounding corneal stromal cells. Since the human corneal epithelium contains dendritic cells, damage to these cells is a pre-condition for AK (Alzubaidi *et al.*, 2016).

Protein quantification using the BCA protein assay revealed a low protein concentration in the ACCM, which was proportional to the percentage of ACCM analysed, compared to the normal culture medium (including M199 and Epilife) which had the highest protein concentration (Table 3-1). *A. castellanii* trophozoites are metabolically active and survive and replicate outside the host cells because they are auxotrophic for most of their nutrients (Naemat *et al.*, 2018; Schunder *et al.*, 2014; Dolphin, 1976). Thus, the decrease in the protein level in conditioned medium is expected, however, it remains interesting to investigate the impact of *A. castellanii* growth on the metabolic constituents of the culture medium.

In summary, the present study demonstrated that cell-free supernatants from *A. castellanii* T4 genotype strain culture containing soluble factors, such as proteases have adverse impact on the function and structure of CSCs and ihCECs via compromising cell viability, cell proliferation and inducing apoptosis. The loss of cell viability and increased apoptosis were associated with derangement of the actin cytoskeleton and ultrastructural changes. We also found that inhibiting the proteolytic activitiy of ACCM, can rescue cell proliferation, suporting the role of proteases in *A. castellanii* virulence. Further characterization of the molecular mechanisms responsible for this pattern of cytotoxic activity of ACCM may ultimately lead to development of interventions to ameliorate or prevent corneal injury in AK patients.

4. Chapter Four: Investigating changes in the composition of culture supernatant from stromal cells and *Acanthamoeba castellanii*-conditioned medium

4.1. Introduction

The secretome of the *A. castellanii* plays a critical role in the pathogenesis of Acanthamoeba keratitis (AK). However, the detailed mechanisms of host cell responses activated upon *A. castellanii* infection are still incompletely known. Therefore, understanding the pathologic effects of *A. castellanii*-derived conditioned media (ACCM) on the ocular cells, will reveal new insights into the ocular tissue damage caused by *A. castellanii*. Herein, we examined the mechanisms underlying ACCM-induced cytotoxicity in human corneal stromal cells (CSCs) following exposure to 50% concentration of ACCM. CSCs were used based on the results of the previous chapter, which seem to provide a more relevant system for cytotoxicity assessment of ACCM.

A number of microminerals and trace elements are important in cell growth, particularly calcium (Mattana *et al.*, 1997). Calcium ions are vital for controlling cellular responses, including cell homeostatic processes and proliferation. *In vitro* studies suggest

that *A. castellanii* increases the cytosolic free-calcium concentration in cell cultures (Mattana *et al.*, 2009) via releases ADP molecules which secreted by trophozoites. Fluctuations in free calcium concentration depend on the trans-membranous influx of Ca^{2+} (Mattana *et al.*, 2002). It is unclear how *A. castellanii* monitors environmental conditions to produce viable trophozoites.

Sodium, calcium, and potassium ion transporters and proton pump inhibitors play critical roles in the encystation and excystation of *A. castellanii* (Siddiqui *et al.*, 2019). The former is critical in cellular differentiation of *Acanthamoeba.* Trace elements may influence osmolarity and affect encystation in *A. castellanii,* with varying physiological characteristics. Specific molecules responsible for osmolarity changes in axenic cultures of *A. castellanii* include inorganic compounds like sodium chloride and magnesium chloride (Cordingley and Trzyna, 2008); however, these do not provide metabolic energy. González-Robles et al. (2014) obtained similar results after incubating epithelial monolayers in a conditioned medium for 24 hours. As growing *Acanthamoeba* in axenic media is problematic, researchers have examined additives that can enrich the media, including yeast RNA (Megha *et al.*, 2017).

Changes in amino acids in the culture media of *A. castellanii* and related parasites have been investigated. Dolphin (1976) tested the amino acids in a culture medium before and after *A. castellanii* inoculation. *A. castellanii* exhibited selective utilization of amino acids in both cases; no amino acid was exhausted during normal population growth. Intracellular matrix analysis showed that alanine and proline were the most abundant free amino acids. *A. castellanii* can grow in a minimal medium (AMLIV) enriched with arginine, methionine, leucine, isoleucine, and valine as primary sources of nitrogen and vitamins, in addition to glucose as a carbon source (Dolphin, 1976).

However, the secretion mechanisms of *A. castellanii* vary with the availability of protein (Gonçalves *et al.*, 2018). Characterization of extracellular vesicles using dynamic light scattering analysis identified 179 proteins, with qualitative differences in amino acid metabolism. Serine proteases and metalloproteinases were predominant. Although the secretory mechanism of amoebas is unclear, the secretome profile of *A. castellanii* indicates a potential pathogenic role. Hong et al. (2018) characterized the molecular and biochemical properties of the *A. castellanii* cysteine protease (AcCP). Sequence analysis revealed AcCP is a member of the cathepsin L family of cysteine proteases. The gene encoding AcCP was expressed

excessively during the parasite's encystation phase. Cysteine proteases may have a role in *A. castellanii* encystment although their chemical properties and biological functions are unclear.

In this study, we tested the hypothesis that *A. castellanii* induces functional changes in ocular cells. Identifying these changes might reveal new insights into the mechanism used by *A. castellanii* to infect and damage the ocular tissues. In order to reveal changes in CSCs before and after exposure to ACCM, elemental analysis and measurement of DNA concentration were used to examine changes in the composition of the supernatant from human CSCs-exposed to *Acanthamoeba*-conditioned medium (ACCM). Amino acids analysis of ACCM was used to evaluate the importance of amino acids for parasite viability. Our data showed that ACCM culture had a significant effect on CSCs, resulting in changes in the composition of the supernatant of CSCs-exposed to ACCM, and in ACCM alone as well. These results provide further evidence to the extent of the cellular damage that can be caused by the secretome of *A. castellanii*.

4.2. Materials and Methods

4.2.1 Preparation for analysis of the supernatant from CSCs-exposed to ACCM

The supernatants of CSCs-exposed to ACCM were prepared for analysis as described in detail in section 2.9. Briefly, CSCs were seeded in T-75 flasks at 5 x10^5 cells for 48 h, followed by treatment with 50% ACCM-M199 and incubated for 0, 3, 24 and 48 h at 37°C. Cells cultured in the normal M199 medium were used as a control. Subsequently, the supernatants were harvested from culture flasks and transferred into new tubes, then stored at -80°C until required for analysis as detailed below.

4.2.1.i Bicinchoninic acid assay (BCA)

Following incubation times, a BCA protein assay was used to quantify the protein concentration in all cultures. Supernatants were obtained from both treated and untreated samples according to the manufacturer's instructions (BCA/BSA, Thermo Scientific, USA) and described above in section 2.3.

4.2.1.ii The DNA concentrations

DNA concentrations from CSCs cultures were isolated using a ChargeSwitch® gDNA 1mL serum kit as per the manufacturer's protocol (Thermo-Fisher Scientific, USA) and is described in section 2.10.

4.2.2 Elemental analysis

Supernatants from CSCs-exposed to ACCM were prepared for analysis as described in section 2.9. Briefly, CSCs were seeded in T-75 flasks at 5 x10^5 cells/flask and incubated for 48 h, Cultures were then treated with 50% ACCM-M199 and incubated for a further 0, 3, 6, 24 and 48 h at 37°C. Cells treated with unconditioned M199 medium were used as controls. Subsequently, the culture supernatants were harvested and assessed for trace elements using ICP-MS (Thermo-Fisher iCAP-Q, Thermo-Fisher Scientific, UK) in accordance with the standard protocol used The University of Nottingham. This method was described in detail in section 2.12.

4.2.3 Amino acid analysis for ACCM

A. castellanii trophozoites were cultured as detailed in section 2.2.1. The trophozoites were then adapted and grown in a normal medium of corneal cells (M199 or Epilife™) and incubated for 3 and 48 h. 3 mL of ACCM was collected and replaced with the same volume of medium at each incubation time. The supernatant of ACCM was filtered through a 0.2 µm filter and stored at -80°C until use. Trophozoites cultured in normal medium (NM) (M199 or Epilife) were used as controls. Amino acid analysis of ACCM was performed according to modified techniques described earlier (Schwarz, Roberts and

Pasquali, 2005). The method used in this experiment is described in section 2.13.

4.2.4 Statistical analysis

All statistical analyses were undertaken using GraphPad Prism version 7. Differences between mean concentrations of treated and untreated groups were determined by two-way variance analysis (ANOVA). Data are shown as mean ± SD, with statistical importance indicated by asterisks; P-value < (0.0001****, 0.001***, 0.01**, 0.05*).

4.3. Results

4.3.1 Protein concentrations

Data from the analysis of supernatant from CSCs-exposed to ACCM are shown in Table 4-1 and Figure 4-1. These results revealed a significant decrease in protein concentration in supernatants from treated cultures, particularly after 48 h, when compared with controls (M199 medium) (p-value = 0.0132).

Table 4-1: Protein concentration in the supernatant of CSCs-exposed to 50% ACCM, compared with control media, obtained using a BCA protein assay. The experiment was performed three times with four replicates per-experiment.

Conditioned medium	Protein Concentration (µg/mL)	
	Mean	Standard Deviation
Zero time (Baseline)	637.35	± 18.47
*** Control – 3h**	672.06	± 21.97
Treated – 3h	658.41	± 6.90
Control - 24h	796.24	± 1.00
Treated - 24h	787.072	± 6.901
Control - 48h	797.66	± 7.06
Treated - 48h	759.10	± 8.19

* M199 medium without any *A. castellanii* secretome

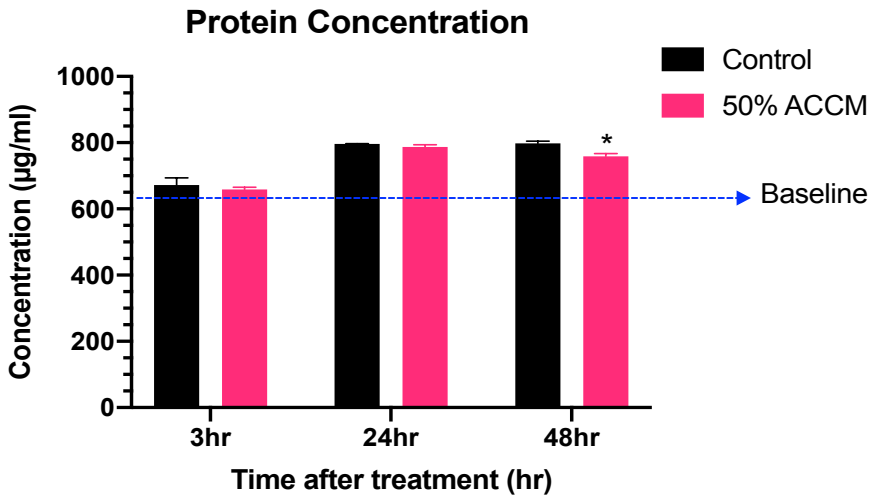

Figure 4-1. Protein concentration in the supernatant of CSCs-exposed to 50% ACCM. CSCs were incubated in 50% ACCM for 0, 3, 24 and 48 h at 37°C. Cells cultured in normal M199 medium were used as controls. Protein was quantified using a BCA protein assay, and absorbance was measured at 562nm. Two-way ANOVA detected a significant difference in the concentration of protein compared with untreated control at 48 hours (p-value = 0.0132). The experiment was performed three independent times with four replicates per-experiment.

4.3.2 DNA concentrations in the supernatant of CSCs-exposed to ACCM

CSCs were incubated in 50% ACCM for 0, 3, 24 and 48 h at 37°C. DNA concentration in the supernatant of CSCs-exposed to ACCM were measured to evaluate the effect of ACCM on CSCs and to see if any DNA was released from unhealthy stromal cells into the conditioned medium. The results showed that the DNA concentration in the supernatant of CSCs-exposed to ACCM was higher in the treated than the control medium throughout the 48 h. However, no significant differences were detected when the incubation groups were compared to controls (Table 4-2 and Figure 4-2). These results illustrate that the concentration of

DNA in the treated media increased slightly above baseline from 4.22 ng/µL after 3 h, to 4.44 ng/µL after 24 h and decreased to 3.13 ng/µL after 48 h. DNA concentration in untreated controls followed the same trend over 48 h, but the remained below the baseline concentration of 2.28 ng/µL.

Table 4-2: DNA concentration in the supernatant of CSCs-exposed to 50% ACCM, compared with controls, obtained using a ChargeSwitch® gDNA 1mL serum kit. The experiment was performed three times with three replicates per-experiment.

Conditioned Medium	DNA Concentration (ng/µL)	
	Mean	Standard Deviation
Zero time (Baseline)	2.28	± 1.14
* **Control - 3h**	2.17	± 1.06
Treated - 3h	4.22	± 2.09
Control - 24h	2.09	± 0.86
Treated - 24h	4.44	± 1.48
Control - 48h	1.19	± 0.04
Treated - 48h	3.13	± 1.73

* M199 medium without any *A. castellanii* secretome.

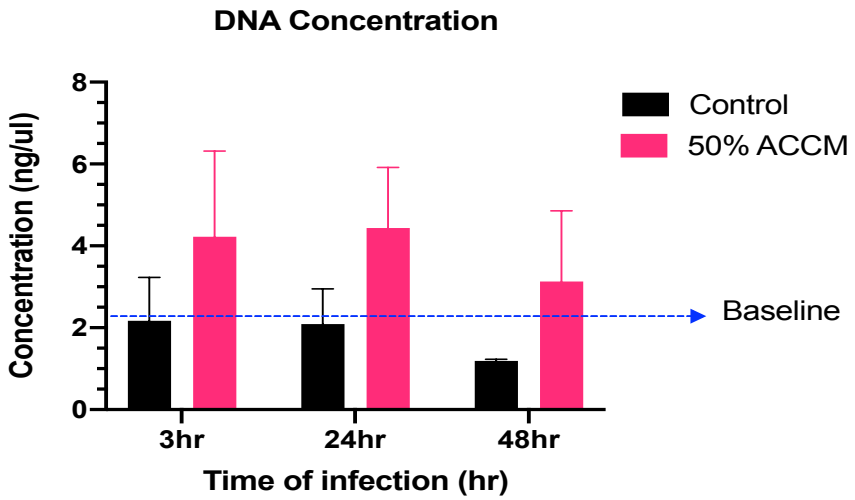

Figure 4-2. The concentration of DNA in the supernatant of CSCs-exposed to 50% ACCM. CSCs were incubated in 50% ACCM for 0, 3, 24 and 48 h at 37 °C. Cells cultured in normal M199 medium were used as controls. The DNA concentrations were quantified using a ChargeSwitch® gDNA 1mL serum kit and measured by NanoDrop. Two-way ANOVA showed no significant differences between the concentration of DNA and the untreated controls. The experiment was performed three independent times with three replicates per-experiment.

4.3.3 Elemental analysis

Analysis results of the macro- and micro- elements in the supernatant of CSCs-exposed to ACCM, were determined using ICP-MS and shown in figures 4-3, 4-4 and 4-5. Statistical analyses revealed significant differences between the treated groups and untreated controls, including the macro-elements magnesium, phosphorus, sulphur, potassium, calcium and titanium (Figure 4-3 A and B), and the micro-elements lithium, vanadium, manganese, iron, cobalt, strontium, caesium and barium (Figure 4-4 A and B). The highest concentration of elements was recorded for sodium, potassium and calcium,

while titanium and iead had the lowest concentrations (Figures 4-3, 4-4 and 4-5).

Significant differences in the concentrations of magnesium, phosphorus, calcium and titanium were detected between the control and treated media; being higher in the controls than the treated media throughout the 48 h. There was an increase in the concentration of sodium and potassium, but no significant differences were detected between the treated groups and controls after 3-48 h (figure 4-3 A and B). In figure 4-4 A and B, the concentration of manganese, iron, strontium and barium were higher in the controls than treated media throughout the 48 h, but the opposite results were recorded for the concentration of vanadium and cobalt, which were significantly higher in treated groups than controls. The concentrations of potassium and caesium were also significantly higher in the treated groups than controls during the initial 0-3 h of exposure. No significant differences were observed between the treated and control groups for the other micro elements, which also showed either low or non-detectable concentrations (figure 4-5 A-C).

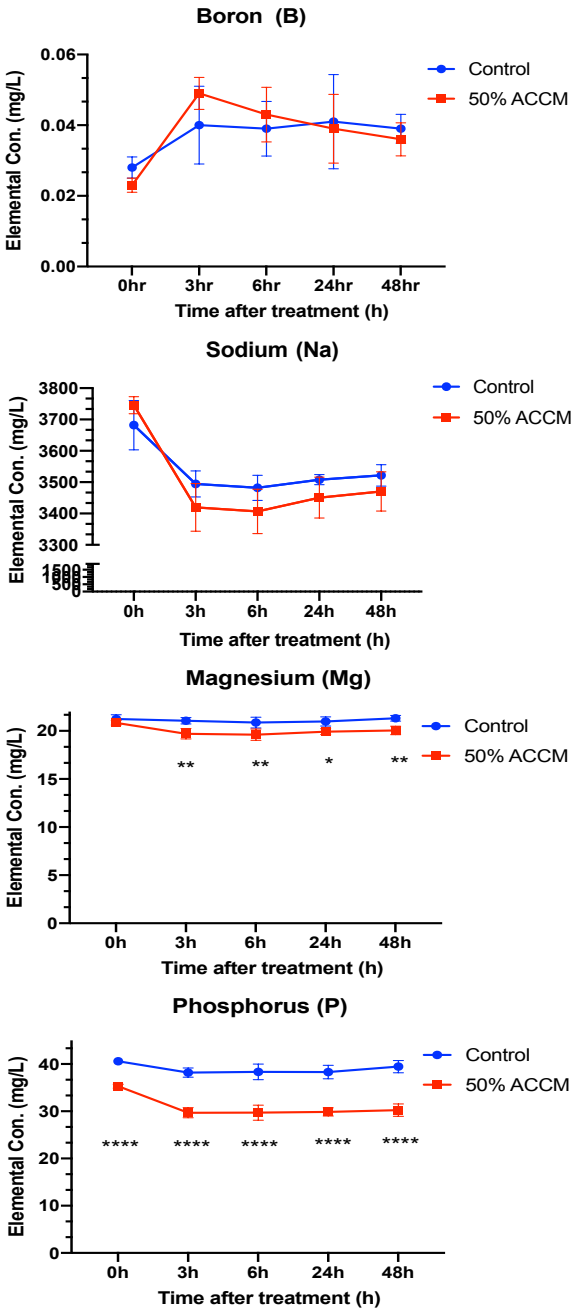

Figure 4-3 A. Analysis of the elements in the supernatant of CSCs-exposed to 50% ACCM. CSCs were incubated in 50% ACCM for 0, 3, 6, 24 and 48 h at 37 °C. Cells treated with unconditioned M199 medium were used as controls. The elemental analysis of culture supernatant was measured using ICP-MS. External calibration levels are in the range 0-100 mg L-1 at (ppm) for macro-elements. Two-way ANOVA detected some significant differences between the treated groups and untreated controls. The experiment was performed three times with 4 technical replicates per-experiment.

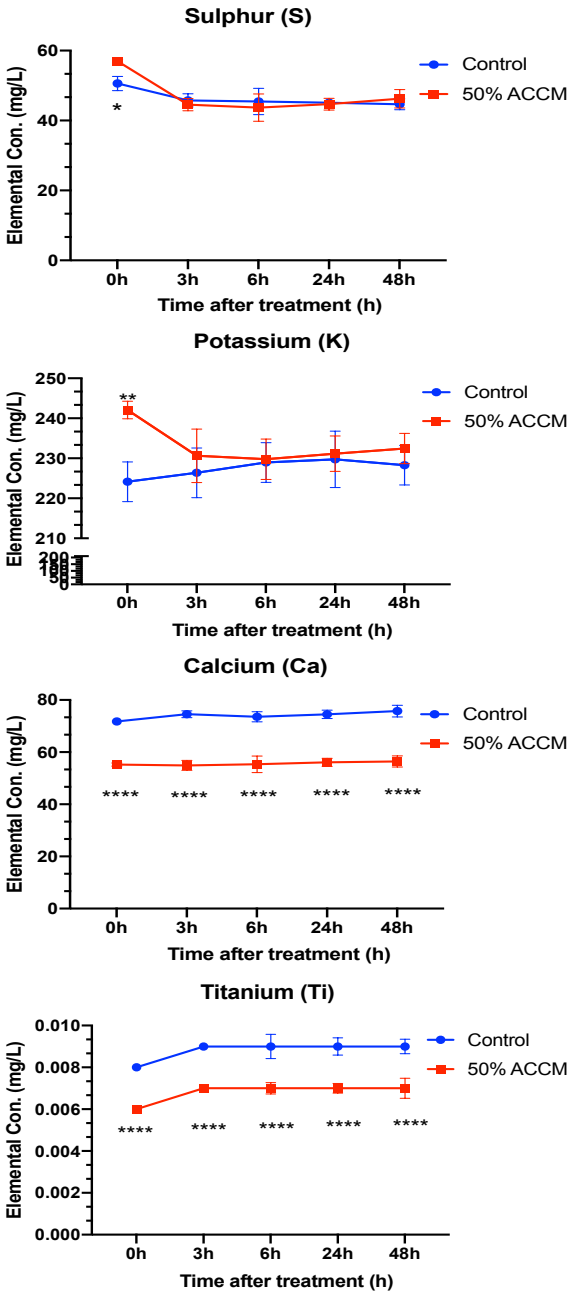

Figure 4-3 B. Analysis of the elements in the supernatant of CSCs-exposed to 50% ACCM. CSCs were incubated in 50% ACCM for 0, 3, 6, 24 and 48 h at 37 °C. Cells treated with unconditioned M199 medium were used as controls. The elemental analysis of culture supernatant was measured using ICP-MS. External calibration levels are in the range 0-100 mg L-1 at (ppm) for macro-elements. Two-way ANOVA detected some significant differences between the treated groups and untreated controls. The experiment was performed three times with 4 technical replicates per-experiment.

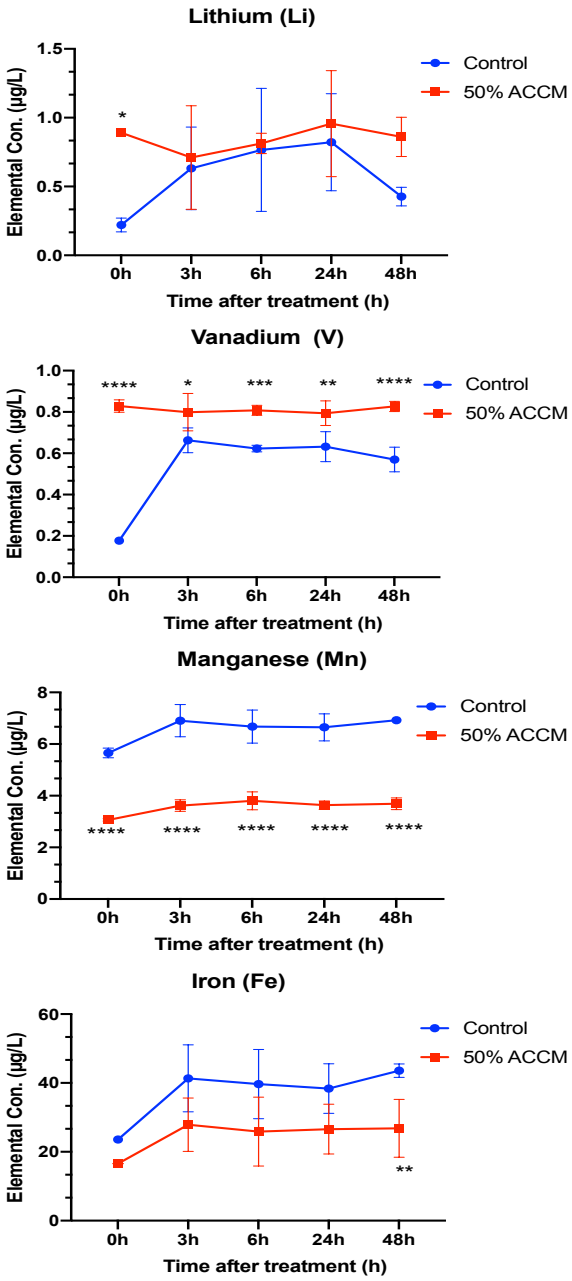

Figure 4-4 A. Analysis of the elements in the supernatant of CSCs-exposed to 50% ACCM. CSCs were incubated in 50% ACCM for 0, 3, 6, 24 and 48 h at 37 °C. Cells cultured in normal M199 medium were used as controls. The elemental analysis of culture supernatant was measured using ICP-MS. External calibration levels are in the range 0-100 µg L-1 at (ppb) for micro-elements. Two-way ANOVA detected significant differences between the treated groups and untreated controls. The experiment was performed three times with 4 technical replicates per-experiment.

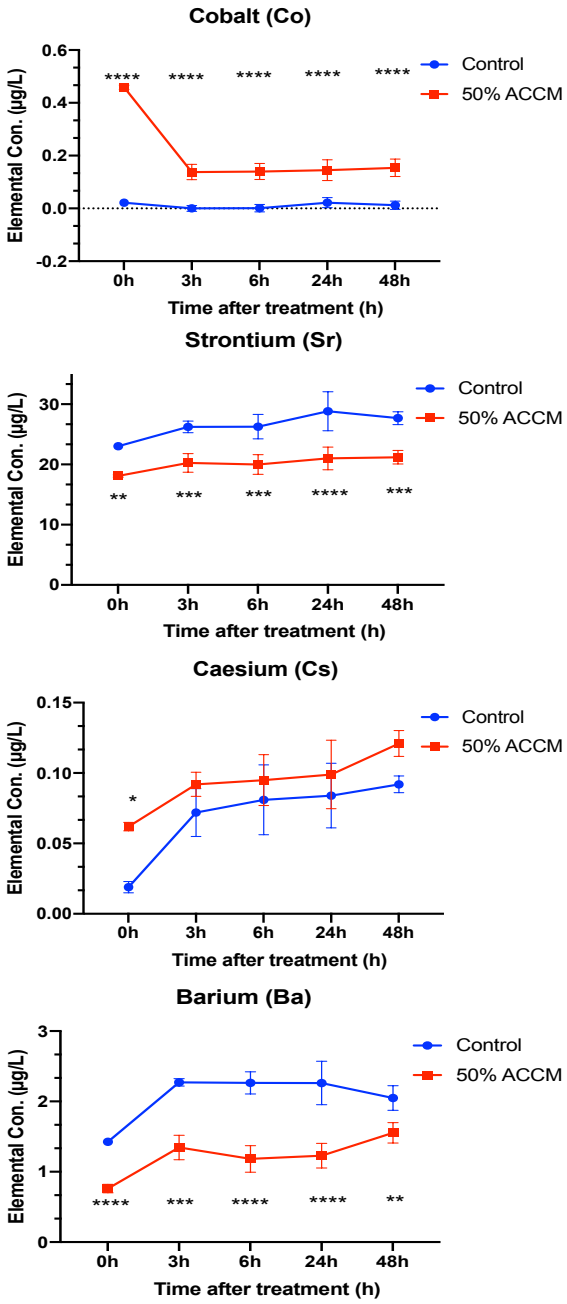

Figure 4-4 B. Analysis of the elements in the supernatant of CSCs-exposed to 50% ACCM. CSCs were incubated in 50% ACCM for 0, 3, 6, 24 and 48 h at 37 °C. Cells cultured in normal M199 medium were used as controls. The elemental analysis of culture supernatant was measured using ICP-MS. External calibration levels are in the range 0-100 µg L-1 at (ppb) for micro-elements. Two-way ANOVA detected significant differences between the treated groups and untreated controls. The experiment was performed three times with 4 technical replicates per-experiment.

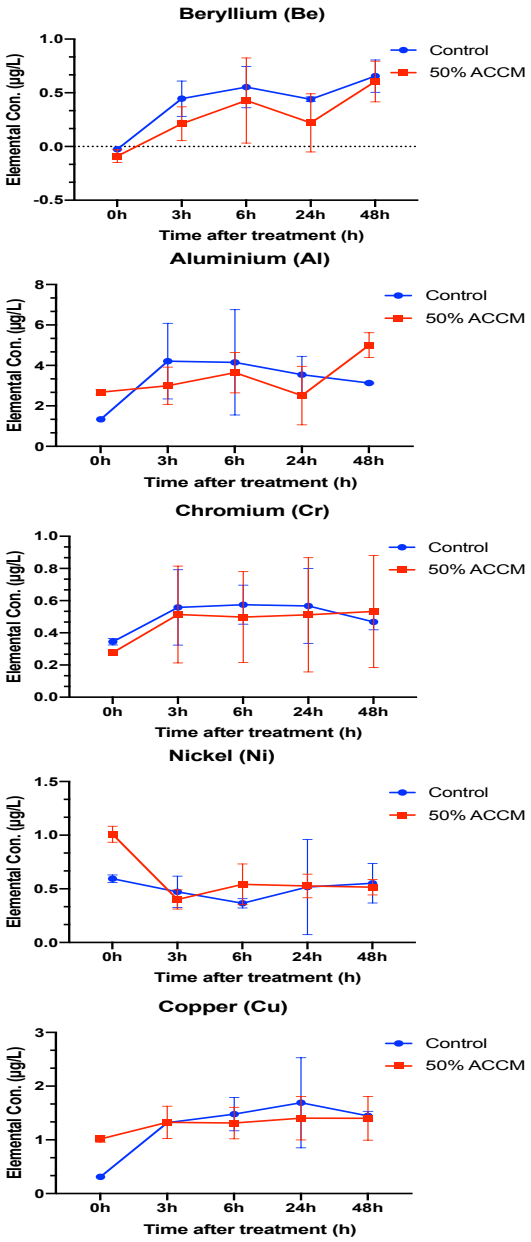

Figure 4-5 A. Analysis of the elements in the supernatant of CSCs-exposed to 50% ACCM. CSCs were incubated in 50% ACCM for 0, 3, 6, 24 and 48 h at 37 °C. Cells cultured in normal M199 medium were used as controls. The elemental analysis of culture supernatant was measured using ICP-MS. External calibration levels are in the range 0-100 µg L-1 at (ppb) for micro-elements. Two-way ANOVA detected no significant differences between the treated groups and untreated controls. The experiment was performed three times with 4 technical replicates per-experiment.

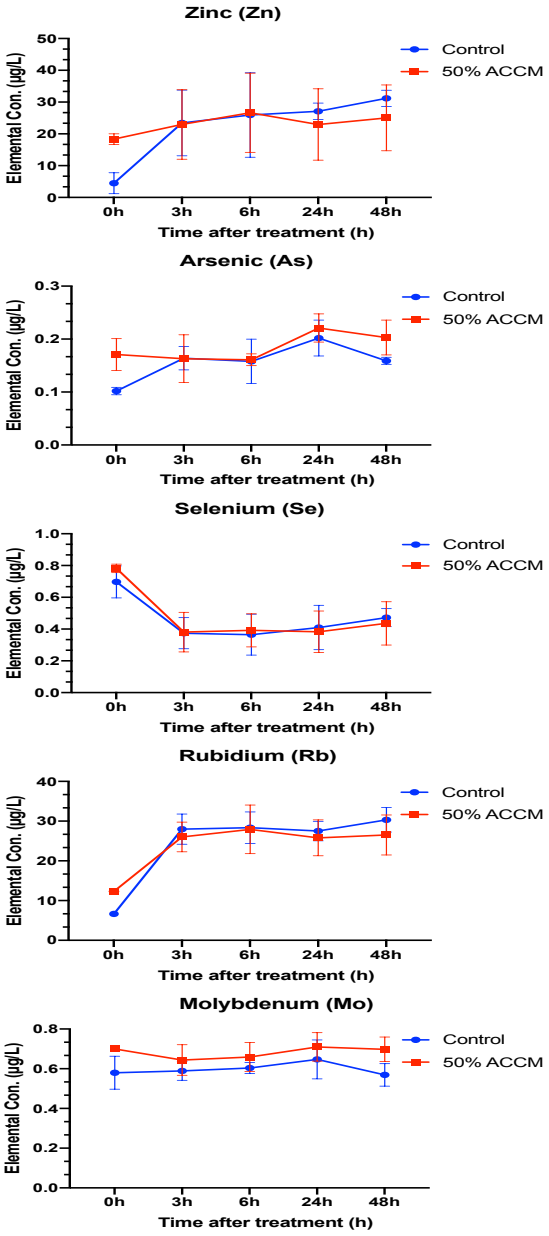

Figure 4-5 B. Analysis of the elements in the supernatant of CSCs-exposed to 50% ACCM. CSCs were incubated in 50% ACCM for 0, 3, 6, 24 and 48 h at 37 °C. Cells cultured in normal M199 medium were used as controls. The elemental analysis of culture supernatant was measured using ICP-MS. External calibration levels are in the range 0-100 µg L-1 at (ppb) for micro-elements. Two-way ANOVA detected no significant differences between the treated groups and untreated controls. The experiment was performed three times with 4 technical replicates per-experiment.

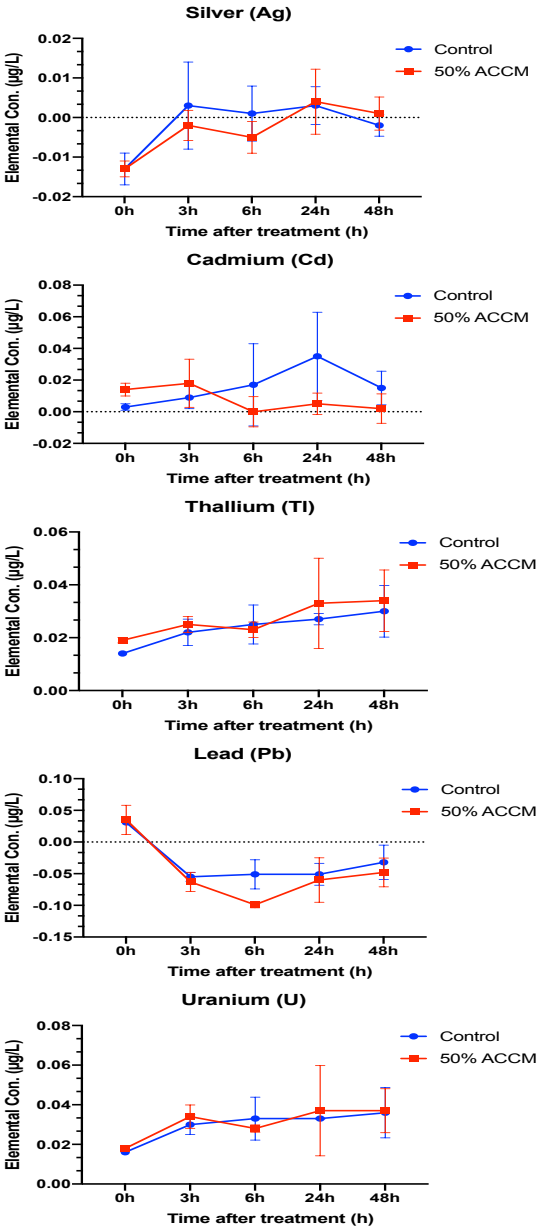

Figure 4-5 C. Analysis of the elements in the supernatant of CSCs-exposed to 50% ACCM. CSCs were incubated in 50% ACCM for 0, 3, 6, 24 and 48 h at 37 °C. Cells cultured in normal M199 medium were used as controls. The elemental analysis of culture supernatant was measured using ICP-MS. External calibration levels are in the range 0-100 µg L-1 at (ppb) for micro-elements. Two-way ANOVA detected no significant differences between the treated groups and untreated controls. The experiment was performed three times with 4 technical replicates per-experiment.

4.3.4 Analysis of amino acid in ACCM

Amino acid analysis was carried out on ACCM that was generated using either M199 or Epilife medium. Following this, ACCM was collected in order to determine the amino acid content at 3 and 48 h, the normal medium (NM) (M199 or Epilife) was used as a control (Figures 4-6 A-B). The highest concentrations of amino acids found in ACCM-M199 were glycine, glutamic acid and leucine, accounting for approximately half of the total volume. These concentrations were higher after 3 h, then decreased after 48 h of incubation, with significant differences between the incubation groups and control NM (Figures 4-6 A-B). The results also revealed that there were other amino acids in ACCM-M199 with different concentrations, including threonine, serine, asparagine, alanine, valine, cysteine, phenylalanine, lysine, methionine, isoleucine, and proline with significant differences between the treated groups and controls (Figures 4-6 A-B).

However, the highest amino acid concentrations in ACCM-Epilife medium were glutamine and arginine - accounting for more than half of the total volume of ACCM-Epilife. There was an increase in the amount of arginine after 3 and 48 h incubation, but a decrease in amount of glutamine after 3 and 48 h. However, no significant differences were detected when the incubation groups

were compared to controls (Table 4-4 A, see Appendix A). Other amino acids were detected in ACCM-Epilife with different concentrations, including threonine, serine, asparagine, alanine, valine, citrulline, cysteine, phenylalanine, lysine, methionine, isoleucine, leucine, proline, glycine and glutamic acid. There were significant differences between the treated groups and controls (Figures 4-6 A-B). The remaining concentrations of amino acids and components containing amino acid in ACCM-M199 or ACCM-Epilife were either present in small amounts, or not at all (Tables 4-3, 4-4, A-B, Appendix A).

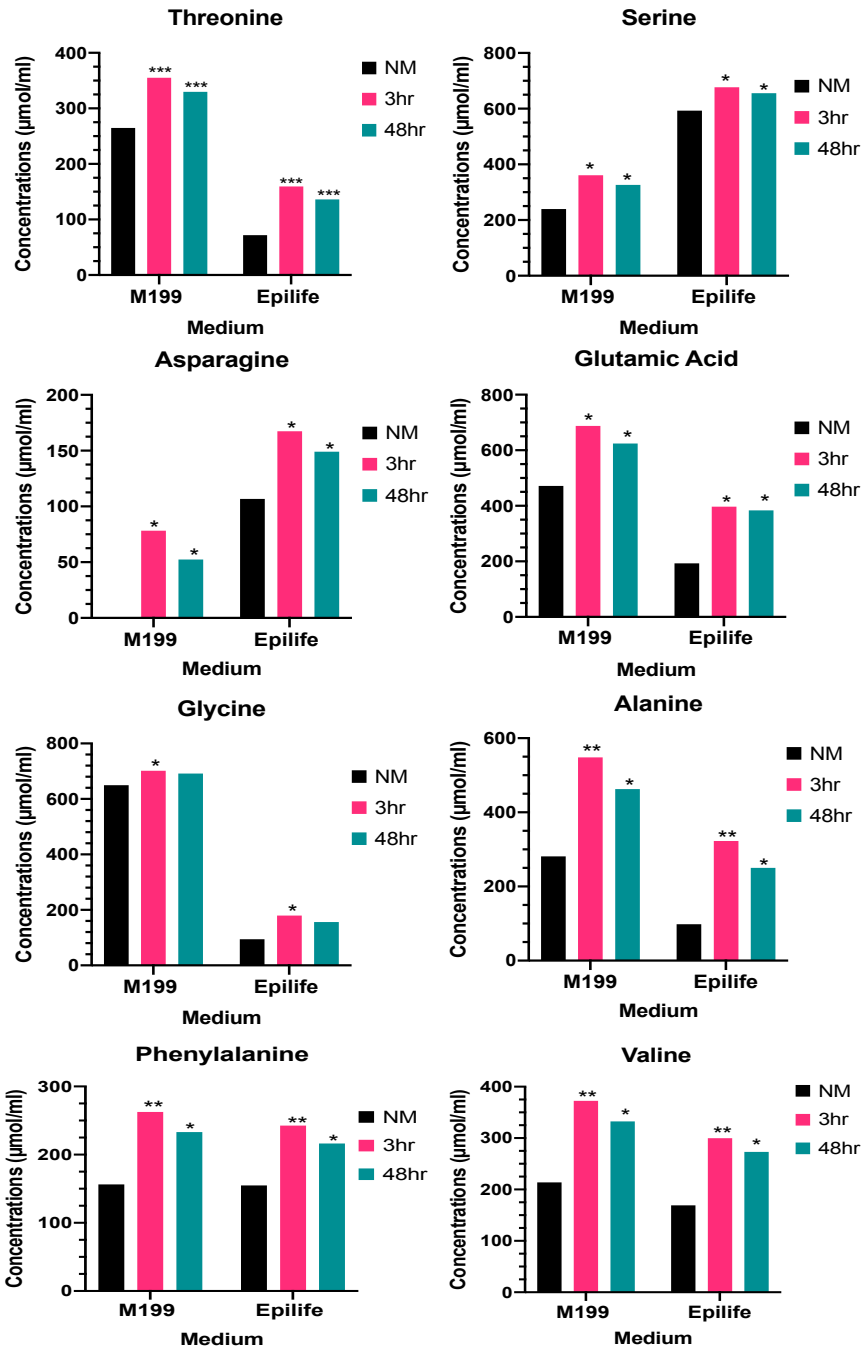

Figure 4-6 A. Amino acid analysis of ACCM generated using either M199 or Epilife medium. ACCM was collected for determining the amino acid content at 3 and 48 h, the normal medium (NM) (M199 or Epilife) was used as a control. Two-way ANOVA detected some significant differences between the treated groups and control media. The experiment was performed three times with 2 technical replicates per-experiment.

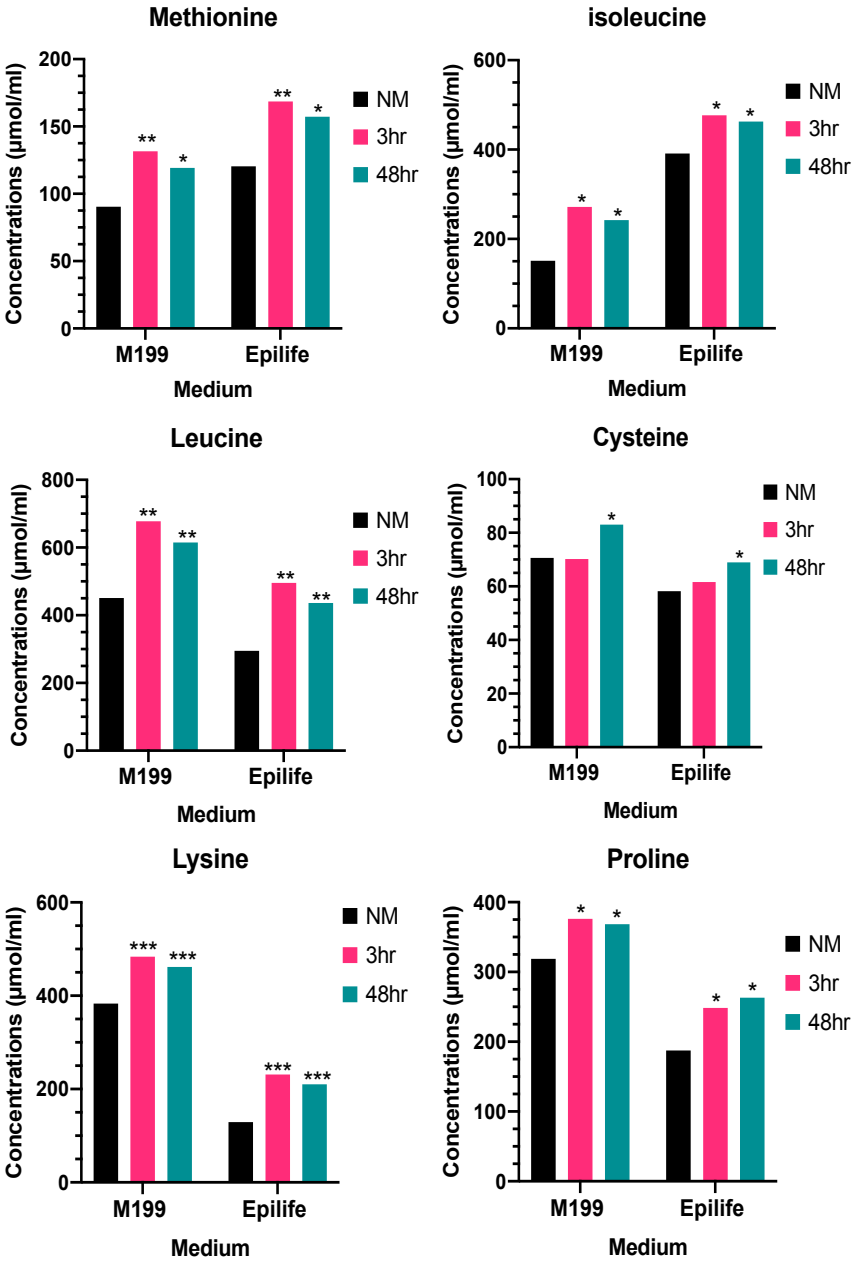

Figure 4-6 B. Amino acid analysis of ACCM generated using either M199 or Epilife medium. ACCM was collected to determine the amino acid content at 3 and 48 h, the normal medium (NM) (M199 or Epilife) was used as a control. Two-way ANOVA detected some significant differences between the treated groups and control media. The experiment was performed three times with 2 technical replicates per-experiment.

4-4. Discussion

Acanthamoeba is a pathogenic protozoan that is capable of inducing cytotoxic effects on ocular cells. *Acanthamoeba* are metabolically active protozoa, and it is impossible to separate the metabolites of corneal cells and trophozoites post-infection, making it impossible to determine the effects of live *Acanthamoeba* trophozoites on the metabolism in corneal cells. The purpose of this study was to examine any functional changes in CSCs before and after exposure to ACCM. Elemental and DNA concentration analysis was used to compare changes in the composition of the conditioned medium from CSCs-exposed to ACCM. Although co-culture systems of different somatic cells have demonstrated beneficial effects in *in vitro* cultures, there is limited evidence on the effects of conditioned media on culture cells. Preliminary research has shown that co-culture systems are powerful *in vitro* tools for analysing tissue/cellular interactions and function; however, they often lack spatial resolution and fail to simulate the physiological environment (Wilson, Yang and El Haj, 2014). Ex-vivo organ culture can provide a more powerful model system for analysing the interactions of the parasites and human corneal cells, but drawbacks like cell migration, cell death, and the requirements of highly rich culture media limits the applications of these complex

techniques (Janin-Manificat *et al.*, 2012; Deshpande *et al.*, 2015). Therefore, despite the limitations of co-culture systems, ex-vivo organ culture systems would be unfeasible for this study.

The supernatant from CSCs-exposed to ACCM was examined for protein quantification using a BCA protein assay. Results revealed a low protein concentration in the culture supernatants of treated groups compared with untreated groups, particularly at 48 h. This significant decrease in the concentration of protein suggests that exposure to ACCM may induce a reduction in the protein concentration of CSCs, or that the number of metabolically active CSCs has reduced, reducing the overall protein production by the cells compared to control. As mentioned earlier, proteases or proteolytic enzymes of pathogenic organisms have the ability to degrade several substrates of peptide bonds and protein for nutritional purposes (Lorenzo-Morales, Khan and Walochnik, 2015; Khan, 2006). Therefore, a reduced protein concentration in the conditioned medium of CSCs may be expected due to the degradation by ACCM, but the effects of *A. castellanii* growth on metabolic constituents of the culture medium remains an important matter to investigate.

DNA concentration analysis was used to compare any changes in the composition of the supernatant of CSCs-exposed to

ACCM. Results revealed an increase in DNA concentration in the CSCs treated with ACCM, when compared with cells treated with the normal M199 medium throughout the 48 hours; however, a statistical analysis demonstrated that no appreciable difference was apparent between the DNA concentrations of the treated cells and the controls. From these findings, we can infer that ACCM did not directly affect the DNA concentration of CSC, but DNA concentrations in CSCs could be affected when treatment with ACCM at concentrations greater than 50%. An increase in DNA concentration would indicate DNA replication while a decrease would suggest the presence of DNases in the media or apoptosis (Nagata, 2000). Our results are consistent with previous research findings, which suggested that *A. castellanii* produce a cytopathic effect on human corneal fibroblasts after direct adhesion in ex vivo conditions, but not through chemical mediators (Takaoka-Sugihara *et al.*, 2012). Cytopathic effects involve structural changes on the corneal cells as part of the pathogenesis, whereas cytotoxicity refers to the destruction of the cells due to exposure to chemicals and other agents. Takaoka-Sugihara et al. (2012) argues that the cytopathic effect correlates with DNA loss rather than DNA degradation or loss of viability. The ability to adhere to host cells and produce the cytopathic effect is directly correlated with the expression of proteins. However, this study went further to

determine that *A. castellanii* mainly killed corneal fibroblasts by apoptosis. This study involved determination of apoptotic corneal fibroblasts through the detection of DNA fragmentation. Further research has shown that major DNA fragmentation is a late event in apoptosis (Kim *et al.*, 2003). Studies have also shown that conditioned culture medium was unable to lyse cells of the corneal epithelium by itself, since there was no evidence of cell damage or disorganization (Omaña-Molina *et al.*, 2013). There was no analysis of DNA fragmentation in this study, which means that the DNA could have still been there in the same concentration. This is due to ineffective anti-apoptotic activities (Sixt *et al.*, 2012) that may inhibit fragmentation, or the apoptosis process was still in the early stages. The decision was taken that elemental analysis may provide more in-depth insights on the structural changes in CSCs following incubation with ACCM.

Elemental analysis of the supernatant from CSCs-exposed to ACCM revealed a significant difference between the CSCs cells treated with ACCM and cells cultured in normal M199 medium. The findings revealed a significant difference in the concentration of trace elements, with the un-conditioned media (control) exhibiting higher concentrations of magnesium, phosphorus, calcium, titanium, manganese, iron, strontium and barium, whereas the conditioned (treated) media contained higher concentrations of vanadium and cobalt. Additionally, the

highest concentrations of elements were for sodium, potassium and calcium, respectively. This indicates that ACCM alters the concentration of elements in the supernatant of CSCs, with a decrease in the concentrations of sodium and calcium, and an increase in potassium. Trace elements may affect cell growth in cultures, indicating the importance of monitoring elemental impurities and any changes that may affect the growth of target cells. Yet, it is unclear how different trace elements in the cell culture media affect metabolism and other upstream processes.

According to Khan et al. (2000), proteases are powerful markers of differentiation in *Acanthamoeba*, both the pathogenic and the non-pathogenic species. However, Khan et al. (2000) demonstrated a clear distinction between protease activity in pathogenic and non-pathogenic *A. castellanii*, with the pathogenic species exhibiting higher protease activity compared to the non-pathogenic species. However, the findings in this study do not show whether ACCM induced the cells to release the trace elements into the medium. The existing literature shows that *A. castellanii* induces damage to different cell types via different mechanisms, for example, trophozoites of the pathogenic *A. castellanii* rapidly lyse various cells *in vitro* (Mattana *et al.*, 1997). Their findings suggest that *A. castellanii* induces the release of soluble factors that elicit a cytosolic

increase in calcium ions in target cells. Low molecular weight amoeba metabolites induce the increase in calcium ions, but the phenomenon depends upon the transmembrane influx of extracellular calcium. Since calcium ions play a critical role in cell homeostasis, and the control of cellular responses such as apoptosis and cell proliferation, the findings indicate that elevated free calcium in the ACCM might play a critical role in damaging of the cells during infections with *A. castellanii*. Other pathogenic mechanisms include the alteration of in cytosolic calcium concentrations in *A. castellanii*, although the relative changes in trace elements are poorly characterized.

Amino acid analysis of ACCM was also examined in this study to evaluate the importance of amino acids for parasite viability. We found that ACCM alone produced significant differences in the concentration of amino acids, when compared with either M199 or Epilife, over a period of 48 hours. The highest concentration was obtained for glycine, glutamic acid and leucine representing approximately a half of the total volume of ACCM-M199. There were significant differences between the incubation groups and controls. However, the highest concentrations of amino acids in ACCM-Epilife medium were glutamine and arginine which represented more than half of the total volume of ACCM-Epilife, but with no significant differences between the incubation groups

and controls. These amino acids are considered essential amino acids for *Acanthamoeba* growth.

The amino acid profile of ACCM revealed an increase after 3 hours and a decrease at 48 hours in most of the treated samples. This may have been due to the increase in the relative amount of amino acid produced by *Acanthamoeba* over the incubation time, but it may also result from increased growth rates. Only the amino acid concentration of glutamine showed a gradual decrease after 3 and 48 h in both ACCM-M199 and ACCM-Epilife media. This finding indicates that *Acanthamoeba* has a potential role to consume or remove amino acid glutamine from ACCM.

Acanthamoeba species exhibit proteolytic activity associated with the need to degrade food substances. However, there is a correlation between pathogenicity and extracellular protease activity; with pathogenic *Acanthamoeba* exhibiting higher levels of extracellular protease activity (Lorenzo-Morales, Khan and Walochnik, 2015). *A. castellanii* produces serine proteases, cysteine proteases and metalloproteases, all of which facilitate host cell invasion. In this study, serine and cysteine, which play important roles in the pathogenesis of *A. castellanii* infection, are found in high concentrations in both ACCM-M199 and ACCM-Epilife media.

These findings concur with other research literature which show that *A. castellanii* produce important proteases. A search of the literature reveals that several serine proteases, with molecular weights ranging from less than 20 kDa to over 200 kDa, have been identified; including MIP 133, a 133 kDa serine protease which plays a critical role in the pathogenic damage of keratocytes by *A. castellanii* (Tripathi and Alizadeh, 2014; Huang *et al.*, 2017). Another study found that proteolytic enzymes secreted by *A. castellanii* are the key virulence factor influencing the severity of AK (Sant'ana *et al.*, 2015). They found that the unique properties of serine proteases enhanced the invasion of corneal stroma by *A. castellanii* and facilitated the degradation of keratocytes. The observation of an elevated serine concentration in ACCM points to a direct functional role for serine proteases in *A. castellanii* infection (Dudley, Alsam and Khan, 2008). Overall, these findings demonstrate a strong link between extracellular serine protease and the pathogenesis, and virulence, of *A. castellanii.*

Cysteine proteases also play a pivotal role during the early stages of *A. castellanii* infection (Leitsch *et al.*, 2010). These findings are consistent with the observation that proteases present in trophozoites mediate proteolytic processes during the early stages of encystment. The use of a serine inhibitor (PMSF)

and a cysteine inhibitor (E64d) completely blocked proteolytic activity, showing the prominent role played by proteolytic activity in the pathogenesis of *A. castellanii.* Moreover, these findings suggest that protease could be a viable marker for the differentiation of *A. castellanii.*

In summary, this study has examined potential functional changes in ocular cells following infection with *A. castellanii*. DNA concentration and elemental analyses indicated that ACCM culture had no direct influence on DNA concentration of CSCs cells. ACCM altered the elements in CSCs, with a change in the abundance of intracellular sodium, potassium and calcium. Results from the amino acid analysis revealed that *A. castellanii* secretes serine and cysteine proteases. In conclusion, ACCM from cultures of *A. castellanii* had a significant effect on CSCs, resulting in changes in the composition of the supernatant of CSCs-exposed to ACCM and in ACCM alone.

5. Chapter Five: Metabolomic changes in human primary corneal stromal cells following exposure to the secretome of *Acanthamoeba castellanii*

5.1 Introduction

Acanthamoeba keratitis, a severe sight-threatening corneal infection, is caused by *Acanthamoeba castellanii* T4 genotype (Marciano-Cabral and Cabral, 2003). In earlier chapters, the *A. castellanii* secretome was found to cause functional and structural changes in human stromal corneal cells (CSCs). Identifying the metabolic mechanism underpinning these changes may provide new insight into how *A. castellanii* damages ocular tissues. In the present study, a metabolomic analysis was undertaken to examine the metabolic changes that occur in CSCs exposed to the secretome of *A. castellanii* for 48 hours.

Metabolomic analysis focuses on nucleotides: purines and pyrimidines (Gerasimovskaya *et al.*, 2008), which are both nitrogenous bases; purines are two-carbon nitrogen ring bases and pyrimidines are one-carbon nitrogen ring bases (Phillips, 2018; Fragoso and Brooks, 2015). Nucleotides interact with various ocular structures including the aqueous humor and tears,

and high concentrations of nucleotides in ocular secretions may suggest disease states (Guzman-Aranguez *et al.*, 2013). These nucleotides modulate the physiological and pathophysiological responses of ocular cells, even *in vitro*. As cells proliferate, synthesis of nucleotides increases to permit DNA replication and RNA production during various stages of the cell cycle (Guzman-Aranguez *et al.*, 2013; Sanderson *et al.*, 2014; Lane and Fan, 2015). Consequently, nucleotide biosynthesis consumes a lot of energy and ATP in multiple metabolic pathways which rely on nitrogen and carbon as basic organic precursors (Lane and Fan, 2015).

Studies of the regulation of mammalian nucleotide metabolism have shown that biosynthesis is allosterically regulated at both the transcription and enzyme levels (Lane and Fan, 2015). Studying the uses and interconversion of purine and pyrimidine bases can offer valuable information on nucleotide metabolism in human corneal stromal cells. It is also worth noting that amino acids serve as nutrients to maintain cell survival, and mediate various regulatory pathways that control cell proliferation and cell death–although there is a paucity of information on this. Therefore, analysis of amino acid metabolism may help to determine how cell proliferation and cell death affect nucleotide metabolism under different growth conditions. Previous research

has shown that many of the factors regulating these processes interact with metabolic enzymes (Okumura *et al.*, 2017; Marijnen *et al.*, 1989; Quéméneur *et al.*, 2003) finding that cysteine was necessary for the growth and survival of human corneal cells.

Other studies have provided insight into the metabolomics of human corneal cells under various growth conditions (Kryczka *et al.*, 2013; Snytnikova *et al.*, 2017). It is possible for the intracellular metabolome, which is necessary to maintain tissue and cellular functions in physiological conditions, to change because of infectious and pathological conditions. It is also possible for observable changes in the metabolomic composition of the eye tissues to reveal the development of ophthalmic pathologies (Snytnikova *et al.*, 2017).

Metabolomic analysis of parasites and host organisms has specific relevance for explaining various features of parasitic biology along with how they interact with the host, and has been demonstrated to have significant benefits for identifying therapeutic targets and the biomarkers of disease, as well as determining the mode of action of drugs (Jeelani *et al.*, 2012; Paget *et al.*, 2013). Metabolomic analysis has the potential to generate beneficial data, facilitating the understanding of organisms' molecular structure and the diseases they cause.

Hence, understanding metabolomics has particular importance and can be instrumental in identifying therapeutic targets.

In this study, we tested the hypothesis that the *A. castellanii* secretome induces metabolic changes in ocular cells. Identifying these metabolic changes may provide new insight into the mechanism used by *A. castellanii* to infect and damage ocular tissues. A metabolomic analysis was used to detect changes in the metabolism in human CSCs after 48 hours, in the presence or absence of *A. castellanii*-conditioned medium (ACCM). The data showed elevated nucleotide metabolism after 48 hours in both the control and treated samples, when compared with samples at zero time (baseline). Metabolites in the treated samples were generally higher by 48 hours. We also detected a decrease in amino acids in the control samples after 48 hours, when compared with the baseline, which is suggestive of protein synthesis. Additionally, there was an increase in free amino acids by 48 hours in the treated samples, compared with the baseline, suggesting protein degradation.

5.2 Materials and Methods

5.2.1 Experimental design

The experimental design involved three biological groups: Time=0 group (T0), Time=48 h control group (T48hCTRL), and Time=48 h treated/infected group (T48hINF). The differences in metabolite levels between T0 and T48, for both control and treated samples, was assessed. The samples were separated into groups for analysis: T0 (A); T48hCTRL (B); T48hINF (C); a pooled sample, containing an aliquot from each sample, for quality control analysis (pooled); and a Matrix blank (blank samples).

5.2.2 Experimental procedure and analytical methods

CSCs were seeded in T-75 flasks at 5 $x10^5$ cells per flask and incubated for 48 h. The medium was then replaced with 10 mL of 50% ACCM (ACCM-M199) and incubated for a further 0 h or 48 h at 37°C. Cells treated with unconditioned M199 medium were used as controls. This method was detailed in section 2.9. Following incubation, the extraction of metabolites from CSC pellets was performed as described in section 2.9.2. The extracted metabolite samples were maintained at –80°C and transported in dry-ice for metabolomics analysis at Glasgow University.

5.2.3 Analytical platform

Hydrophilic-interaction liquid chromatography was conducted by an Ultimate™ 3000-RSLC technique (Dionex™, Thermo Scientific, UK). This was undertaken with a ZIC®-pHILIC analytical column (150mm x 4.6mm, 5µm, Merck Sequant) (Villanueva *et al.*, 2018). Samples were then eluted by a linear gradient (20 mM ammonium carbonate in water) for 26 min at a 0.3 mL/min flow rate, while the column was maintained at 25°C. Prior to the 10 µL volume injection process the samples were kept at 5°C. For the mass spectrometry analysis, Thermo Orbitrap Q-Exactive (Thermo Fisher Scientific) was performed in polarity switching mode. To cover small metabolites, the calibration mass range was extended by including low-mass calibrants. Furthermore, the lock-mass correction was applied to each analytical run in order to improve calibration stability (Villanueva *et al.*, 2018).

5.2.4 Data processing

The raw files, which were converted to negative and positive ionisation mode mzXML files, were subsequently analysed using IDEOM and PiMP with fragmentation data analysis software (Schwendner *et al.*, 2018; Villanueva *et al.*, 2018). All samples were loaded into the instrument by Dr Shellie Walsh and analysed by Dr Gavin Blackburn at Glasgow University.

5.3 Results

5.3.1 Quality control (QC)

The pooled samples were evaluated for reproducibility to assess the accuracy of the MS instrument used. Pooled samples containing an aliquot from every sample submitted for analysis. Figure 5-1 shows the minimum and maximum signals seen in the pooled samples, and the interquartiles to demonstrate the range, in both the negative and positive ionisation modes. This demonstrates the high reproducibility of the instrument over time.

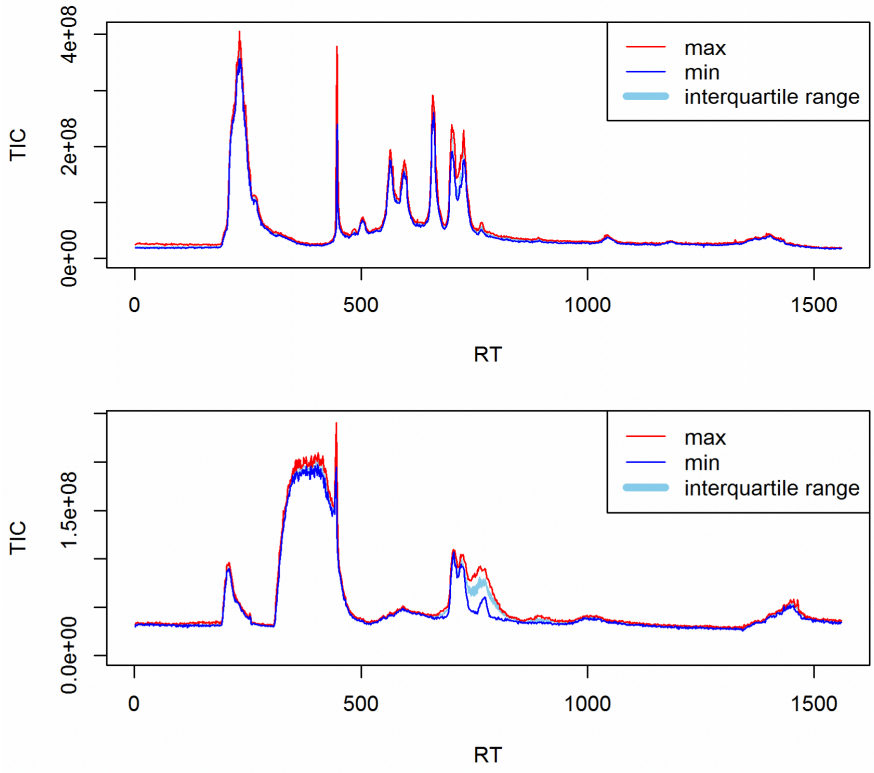

Figure 5-1. Total ion chromatograms for the pooled samples in positive ionisation mode (top) and negative ionisation mode (bottom) showing the high reproducibility of the instrument over time. The experiment was performed three times with 2 technical replicates per-experiment.

5.3.2 Principal Component Analysis (PCA)

To examine biological variation and the reproducibility of the analysis, PCA was performed using the 686 signals identified as likely metabolites for the complete sample set. Figure 5-2 shows all the biological replicates/samples; Figure 5-3 shows the experimental groups.

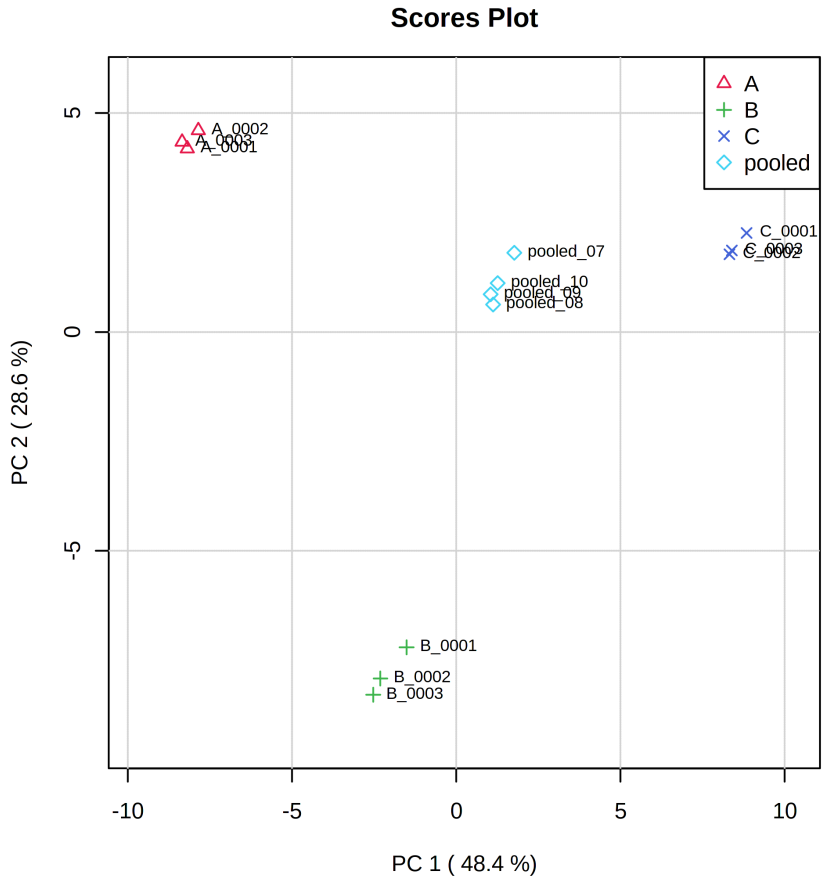

Figure 5-2. The PCA plot of first and second main components computed for the full dataset. The graph was generated using MetaboAnalyst 4.0 on generalized log (glog), the transformed data was obtained using IDEOM. The samples were separated into groups for analysis: T0 (A); T48hCTRL (B); T48hINF (C); a pooled sample (pooled) for quality control analysis. The experiment was performed three times with 2 technical replicates per-experiment.

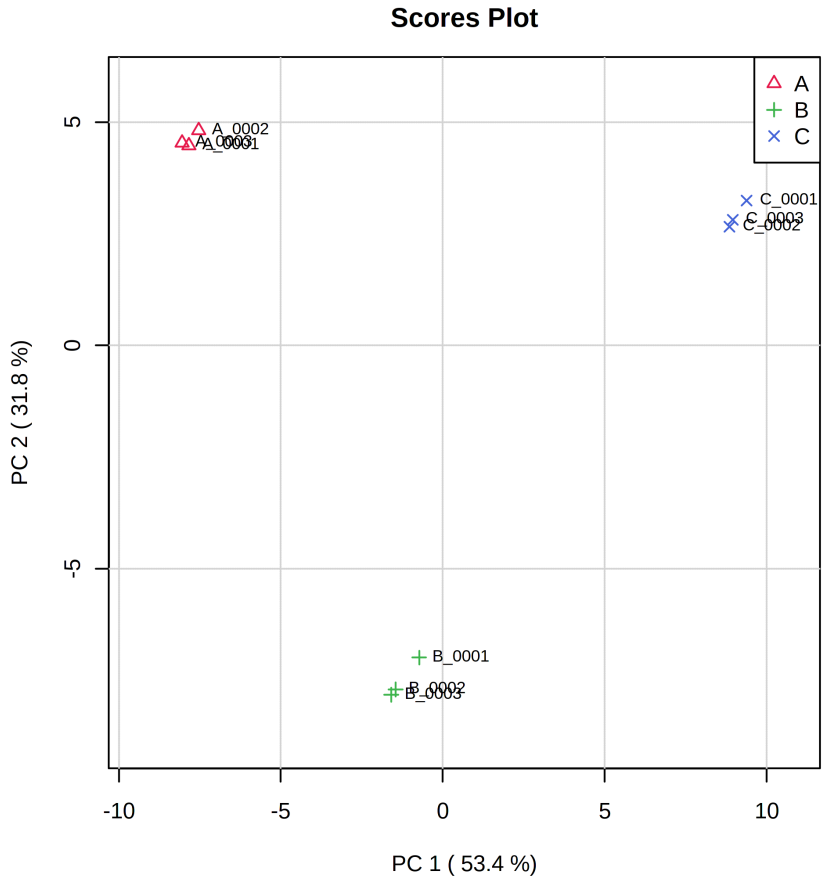

Figure 5-3. The PCA plot of first and second main components computed for the experimental samples. The graph was generated using MetaboAnalyst 4.0 on generalized log (glog); the transformed data was obtained using IDEOM. The samples were separated into groups for analysis: T0 (A); T48hCTRL (B); T48hINF (C); a pooled sample (pooled) for quality control analysis. The experiment was performed three times with 2 technical replicates per-experiment.

The PCA plot in Figure 5-2 demonstrates the reproducibility of results from the pooled samples. Results from the biological samples also appear to be reproducible–as can be seen in the PCA in Figure 5-3.

5.3.3 Comparison of Time 0 (T0), Time 48h control (T48hCTRL), and Time 48h infected (T48hINF)

We determined the difference in the metabolites of CSCs, prior to, and 48 h after exposure to *A. castellanii* secretome. Data was processed using the Polyomics integrated Metabolomics Pipeline (PiMP), and the pathway analysis tool was used to identify areas of difference in the metabolite profiles between the samples. The most relevant pathways were determined based on the PALS p-value and the assigned formulae were compared to the total pathway formulae. These values identify the pathways which are different between the two groups. The pathways are based on the KEGG maps.

5.3.4 Nucleotide Metabolism

Differences in nucleotide levels between the two time points were evident. In general, the pyrimidine and purine pathways, and their related metabolites, were higher in the T48hCTRL samples than in the T0 samples. These changes corroborate with the results of pathway analysis where aminoacyl-tRNA biosynthesis was the most affected pathway based on the PALS p-value (2.3E-04). Coverage of this pathway is good, with ~70% identified metabolites. Several of these metabolites were identified based on comparison to reference standards. These results, together with the annotated metabolites that cannot be

confirmed due to lack of standards, are listed in Table 5-1 including their logFC values.

A similar trend for these metabolites was observed when T0 and T48hCTRL were compared with T48hINF; however, the trend was more pronounced as shown in Table 5-1. The same differences were also observed using the pathway analysis, with aminoacyl-tRNA being the most affected pathway for T0 compared with T48hINF (PALS p-value = 3.2E- 04); the second most-altered pathway for T48hCTRL compared with T48hINF (PALS p-value = 3.0E-05). These large increases may suggest cell death and DNA degradation.

The abundance of some of the metabolites in Table 5-1 was lower in the 48hCTRL samples compared with the T0 samples due to the CSC metabolism. Notably, glutamine showed a significant reduction (logFC = –3.02). Glutamine plays a key role in energy metabolism, while some of its reduction may be attributed to increased production of nucleotides, it is likely that the cells are consuming any reserves of glutamine metabolite for various activities. Similarly, with the identified signal in the pentose phosphate pathway, the reduction is likely to be due to the depletion of the metabolic sources. This correlate with the reduction in ATP, one of the annotated metabolites. It should also be noted that several of these metabolites, such as CMP,

have low signal intensity and some caution should be exercised when drawing any conclusions from these results. It is likely that these small increases are due to cell proliferation.

The opposite was observed for glutamine and CMP when comparing 48hINF with the T0 and 48hCTRL samples. Levels of both metabolites were higher in the 48hINF sample than in the other samples, whereas ATP, ADP and AMP levels were lower than those in the 48hCTRL samples, suggesting a reduction in glutamine usage and possibly a reduced energetic demand. This indicates that the smaller increase in nucleotides observed in 48hCTRL samples, when compared with T0, may be due to nucleotide synthesis, with the large increase in the 48hINF samples being due to nucleotide degradation.

Table 5-1. The differences in nucleotide metabolism for the three sample groups.

Name	Formula	Log Fold Change (logFC)			Identification
		T48hCTRL (B) /Baseline (A)	T48hINF (C) /Baseline (A)	T48hINF (C) / T48hCTRL (B)	
Cytosine	C4H5N3O	3.19	4.38	1.19	Identified
Cytidine	C9H13N3O5	2.58	3.65	1.07	Identified
IMP	C10H13N4O8P	1.84	0.87	-0.97	Annotated
AMP	C10H14N5O7P	1.68	1.1	-0.58	Identified
dGMP	C10H14N5O7P	1.68	1.1	-0.58	annotated
3'-AMP	C10H14N5O7P	1.68	1.1	-0.58	annotated
UDP	C9H14N2O12P2	1.16	0.24	-0.92	annotated
Inosine	C10H12N4O5	1.13	1.35	0.22	identified+fragment
Adenosine	C10H13N5O4	1.11	2.69	1.58	Identified
Deoxyguanosine	C10H13N5O4	1.11	2.69	1.58	annotated
Uracil	C4H4N2O2	1.03	1.21	0.18	annotated
Adenine	C5H5N5	1.01	2.32	1.31	annotated+fragment
Guanosine	C10H13N5O5	0.99	2.49	1.5	Identified
Pseudouridine	C9H12N2O6	0.95	1.25	0.3	Annotated
Uridine	C9H12N2O6	0.95	1.25	0.3	Identified
Guanine	C5H5N5O	0.8	1.9	1.11	Identified
UDP-glucose	C15H24N2O17P2	0.74	-0.6	-1.34	annotated
dGDP	C10H15N5O10P2	0.4	0.13	-0.27	annotated+fragment
Adenosine 3',5'- bisphosphate	C10H15N5O10P2	0.4	0.13	-0.27	annotated+fragment
ADP	C10H15N5O10P2	0.4	0.13	-0.27	annotated+fragment
3-Ureidopropionate	C4H8N2O3	-0.05	1.62	1.67	annotated
Hypoxanthine	C5H4N4O	-0.17	0.25	0.42	identified+fragment
GDP	C10H15N5O11P2	-0.22	0.16	0.39	Annotated
alpha-D-Ribose 1-phosphate	C5H11O8P	-0.34	-0.19	0.15	Annotated
D-ribose 5-phosphate	C5H11O8P	-0.34	-0.19	0.15	Identified
CMP	C9H14N3O8P	-0.72	0.87	1.59	Identified
3'-CMP	C9H14N3O8P	-0.72	0.87	1.59	Annotated
Guanosine triphosphate	C10H16N5O14P3	-0.8	-0.81	-0.01	Annotated
CTP	C9H16N3O14P3	-0.95	-0.81	0.14	Annotated
UTP	C9H15N2O15P3	-0.97	-1.53	-0.55	Annotated
ATP	C10H16N5O13P3	-1.17	-1.12	0.05	Annotated
dGTP	C10H16N5O13P3	-1.17	-1.12	0.05	Annotated
L-Glutamine	C5H10N2O3	-3.02	0.69	3.71	Identified
3-Ureidoisobutyrate	C5H10N2O3	-3.02	0.69	3.71	Annotated

5.3.5 Amino Acid Metabolism

Amino acid metabolism was investigated in the treated and untreated samples to determine if changes in nucleotide metabolism were due to cell proliferation or cell death. The growth medium was not changed throughout the course of the experiment meaning that finite resources were available to the cells. Therefore, any direction of change in levels of the amino acids may be indicative of protein synthesis (a reduction in the abundance of amino acids) or protein degradation (an increase in the abundance of amino acids). In general, there was a reduction in the abundance amino acids observed at T48hCTRL when compared with T0 (see Table 5-2). This correlates well with the changes observed in nucleotide biosynthesis, with cell proliferation being the likely cause.

The opposite was generally seen for the 48hINF samples, when compared with both the T0 and 48hCTRL samples. Amino acid levels were higher than in T0 including valine, methionine, phenylalanine, lysine, leucine and tryptophan–all identified using authentic standards. As these are all essential amino acids for humans, this is indicative of protein degradation and likely cell death. In addition, the most changing amino acid metabolisms were D-Glutamine, L-Glutamine, and isoglutamine in T48INF after 48 hours when compared with both T0 and T48hCTRL

(Table 5-2). These large increases of amino acids in T48hINF may suggest cell death and DNA degradation.

The metabolite oxoadipic acid which showed a small increase in the 48hCTRL samples compared with T0, and a much larger increase in 48hINF samples compared with T0 and T48hCTRL.

Table 5-2 Log fold-change data of differential amino acid metabolites of the three sample groups, identified and annotated in the dataset by PiMP. (see appendix B for the complete table).

Name	Formula	Log Fold Change (logFC)			Identification
		T48hCTRL (B) /Baseline (A)	T48hINF (C) / Baseline (A)	T48hINF (C) / T48hCTRL (B)	
L-Glutamine	C5H10N2O3	-3.02	0.69	3.71	identified
D-Glutamine	C5H10N2O3	-3.02	0.69	3.71	annotated
Isoglutamine	C5H10N2O3	-3.02	0.69	3.71	annotated
Betaine	C5H11NO2	-2.69	1	3.69	identified+fragment
Creatinine	C4H7N3O	-2.27	-1.54	0.73	identified
5-Oxo-D-proline	C5H7NO3	-2.21	0.25	2.46	annotated
L-Glutamate	C5H9NO4	-1.66	-0.66	1.01	identified+fragment
DL-Glutamate	C5H9NO4	-1.66	-0.66	1.01	annotated+fragment
D-Glutamic acid	C5H9NO4	-1.66	-0.66	1.01	annotated+fragment
O-Acetyl-L-serine	C5H9NO4	-1.66	-0.66	1.01	identified+fragment
L-Threonine	C4H9NO3	-1.54	0.48	2.02	identified+fragment
L-Allothreonine	C4H9NO3	-1.54	0.48	2.02	annotated+fragment
L-Proline	C5H9NO2	-1.53	0.19	1.72	identified+fragment
D-Proline	C5H9NO2	-1.53	0.19	1.72	annotated+fragment
Taurine	C2H7NO3S	-1.14	1.3	2.44	identified
L-Histidine	C6H9N3O2	-1.11	0.42	1.54	annotated
L-Serine	C3H7NO3	-0.98	-0.3	0.67	identified
D-Serine	C3H7NO3	-0.98	-0.3	0.67	annotated
S-Adenosyl-L-methionine	C15H22N6O5S	-0.96	-0.24	0.72	annotated+fragment
L-Leucine	C6H13NO2	-0.9	0.21	1.1	identified
(3R)-beta-Leucine	C6H13NO2	-0.9	0.21	1.1	annotated
Beta-Tyrosine	C9H11NO3	-0.78	0.39	1.17	annotated+fragment
N-Hydroxy-L-phenylalanine	C9H11NO3	-0.78	0.39	1.17	annotated+fragment
L-Tyrosine	C9H11NO3	-0.78	0.39	1.17	annotated+fragment
L-Tyrosine	C9H11NO3	-0.66	0.38	1.04	annotated
L-Arginine	C6H14N4O2	-0.53	0.04	0.57	identified
D-Arginine	C6H14N4O2	-0.53	0.04	0.57	annotated
L-Methionine	C5H11NO2S	-0.42	0.85	1.26	identified+fragment
L-Tryptophan	C11H12N2O2	-0.41	0.32	0.73	identified
L-Valine	C5H11NO2	-0.38	0.33	0.72	identified
L-Phenylalanine	C9H11NO2	-0.35	0.72	1.07	identified+fragment
D-Phenylalanine	C9H11NO2	-0.35	0.72	1.07	annotated+fragment
L-Asparagine	C4H8N2O3	-0.05	1.62	1.67	identified
L-Lysine	C6H14N2O2	-0.03	0.43	0.47	identified
D-Lysine	C6H14N2O2	-0.03	0.43	0.47	annotated
Glutathione	C10H17N3O6S	0.72	0.84	0.12	annotated+fragment
Oxoadipic acid	C6H8O5	2.74	5.75	3.01	annotated
Citraconic acid	C5H6O4	2.96	6.16	3.2	annotated
2,5-Dioxopentanoate	C5H6O4	2.96	6.16	3.2	annotated

5.3.6 Clustering analysis of the identified metabolites

The amino acid metabolism heat map (Figure 5-4), defined by KEGG, was used to filter the differentially identified metabolites within PiMP. This data was exported to an Excel file and modified to match the format required for Metaboanalyst upload. Once uploaded the data was log transformed and range scaled. The heatmap was then plotted using a Euclidean distance measure, the Ward clustering algorithm, of the original data with no normalisation and was standardised by autoscaling across the features. Figure 5-5 shows the heatmap of the metabolites involved in nucleotide metabolism, as defined by KEGG depending on the most differentially abundant metabolites. As shown in figures 5-4 and 5-5, the obtained results are divided into three groups, T0, T48h control and T48h treated samples. Metabolites indicated by a dark brown colour are upregulated, while the metabolites indicated by a dark blue colour are downregulated. In these figures, the rows represent the list of metabolites and columns represent the number and types of the analysed samples. Differences in amino acid and nucleotide levels between the two time points were evident, when T0 and T48hCTRL were compared with T48hINF (Figures 5-4 and 5-5). The general trend shows a decrease in amino acid and nucleotide levels and their related metabolites at T48h in the

treated sample. For instance, the amino acids with the most altered metabolisms were D-Glutamine, L-Glutamine, and isoglutamine at 48 h post treatment when compared with both base line T0 and control samples at 48 h post treatment (Figure 5-4). These significant increases of amino acids at 48 h post treatment suggest cell death and DNA degradation. However, as shown in figure 5-5, the levels of glutamine and CMP were higher in the 48hINF sample than in the other samples, whereas ATP, ADP and AMP levels were lower than those in the 48hCTRL samples, suggesting a decrease in glutamine usage and possibly a reduced energetic demand. This indicates that the smaller increase in nucleotides observed in the 48hCTRL samples, when compared with T0, may be attributed to nucleotide synthesis, with the large increase in the 48hINF samples possibly being due to nucleotide degradation.

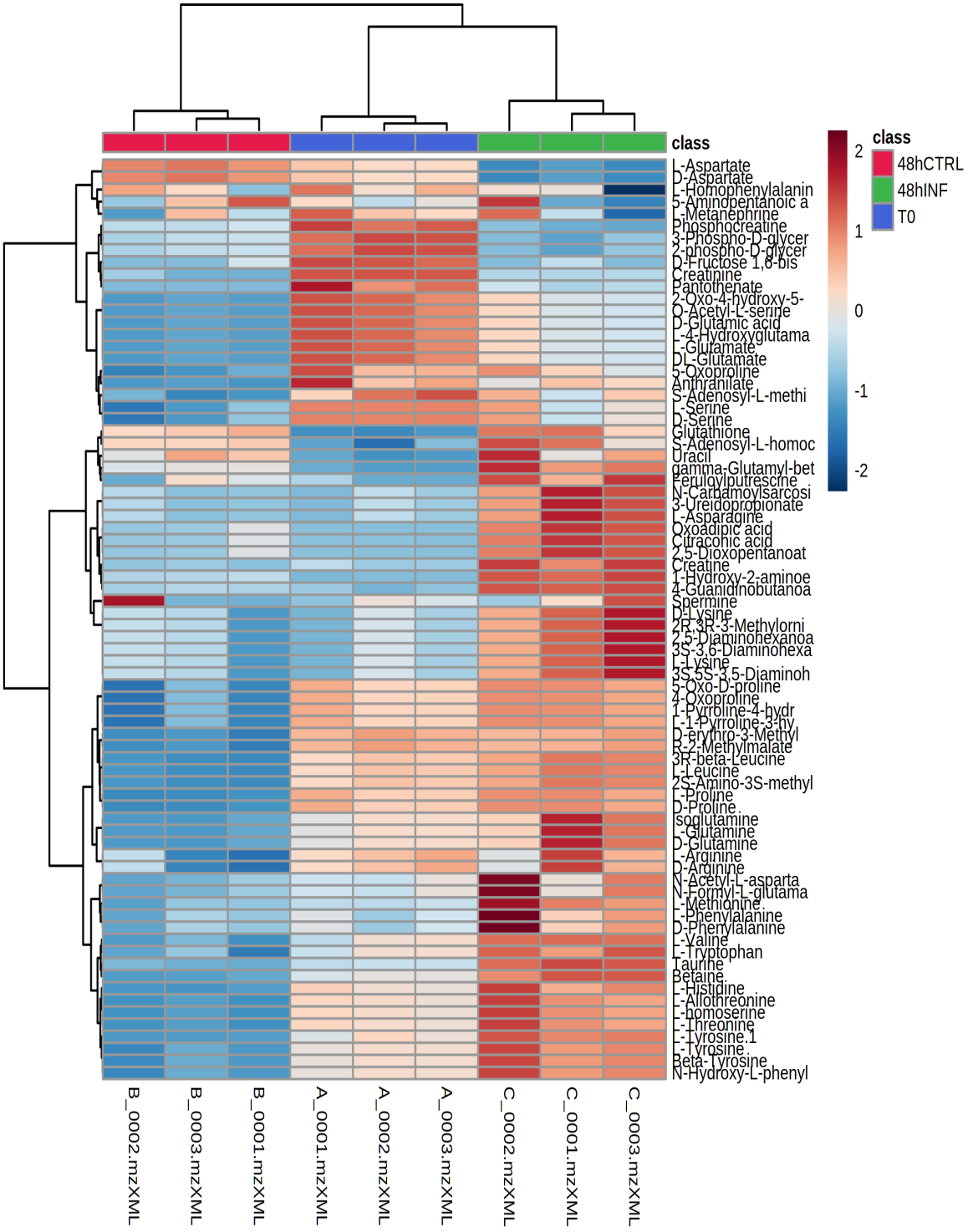

Figure 5-4. Heatmap showing the clustering of metabolites involved in amino acid metabolism. Rows represent the list of metabolites and columns represent the number of analysed samples. The experiment was performed three times with 2 technical replicates per-experiment.

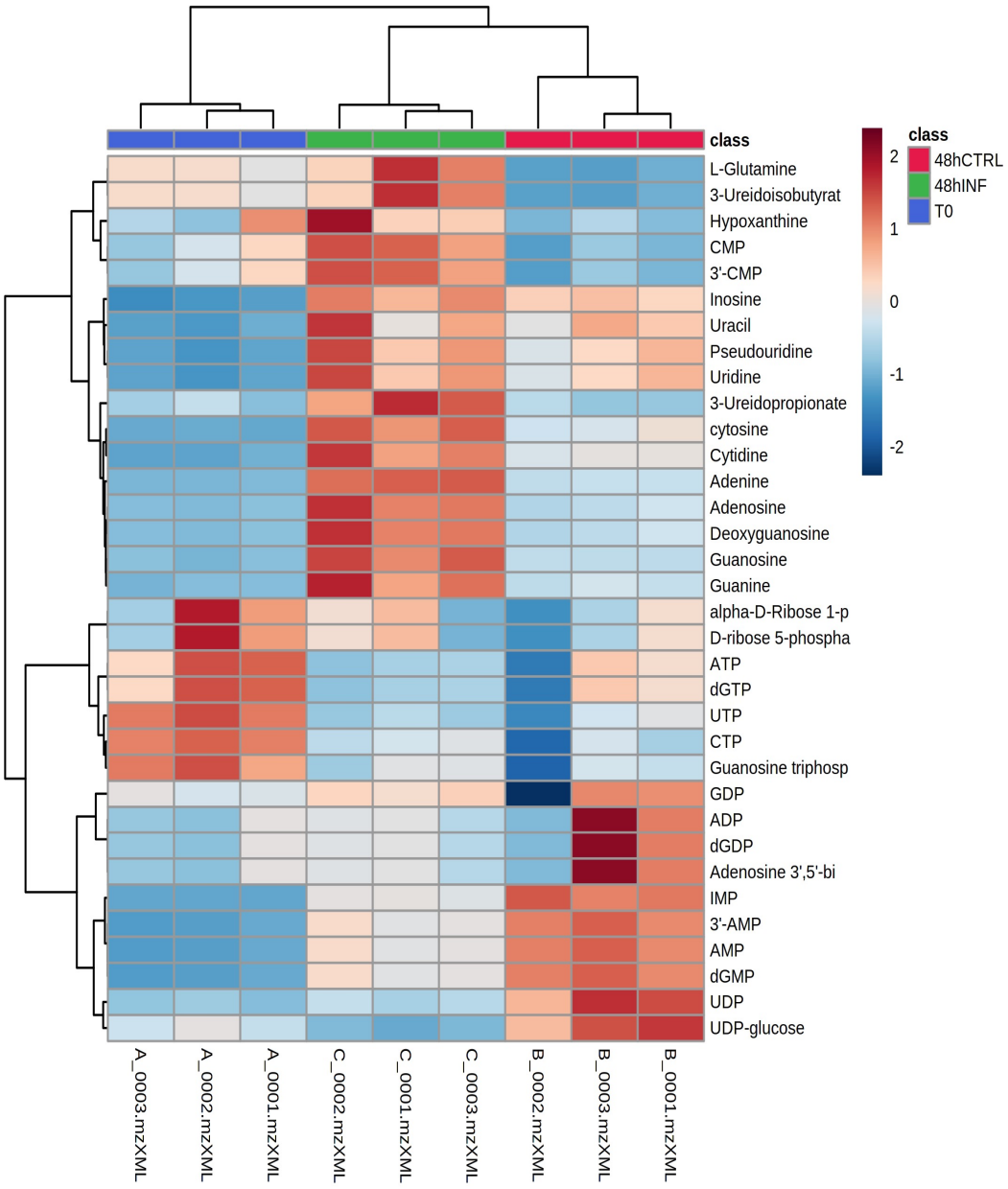

Figure 5-5. Heatmap showing the clustering of metabolites involved in nucleotide metabolism. Rows represent the list of metabolites and columns represent the number of analysed samples. The experiment was performed three times with 2 technical replicates per-experiment.

5.4 Discussion

This research aimed to detect changes in the metabolism of CSCs following 48 hours incubation with the secretome of *A.*

castellanii. We tested the hypothesis that exposure of CSCs to *A. castellanii* secretome would result in alterations in cellular metabolism. In the present study, significant changes were detected in the metabolites related to nucleotides and amino acids. We also detected an increase in nucleotide metabolites after 48 hours, in both the control and treated CSCs, which was generally greater in 48hINF. This finding is consistent with the results for pathway analysis based on the PALS p-value, which shows that the most changing pathway was aminoacyl-tRNA (aa-tRNA) biosynthesis (Table 5-1). Studies of aa-tRNA synthesis have led to a deeper understanding of the synthesis of these translation substrates, from both chemical and structural perspectives (Ibba and Söll, 2000). Every amino acid has a specific aa-tRNA synthetase which catalyzes the coupling of tRNA to the cognate amino acid. The biosynthesis of aa-tRNA involves two steps: adenylation of amino acids to form aminoacyl-AMP and transferring the amino acid moiety to tRNA (Ibba and Söll, 2000). However, opposing evidence suggests that, whereas free amino acids act as precursors for protein synthesis, cells poorly utilize exogenous aa-tRNAs. This may be because of the structural organization of cells *in vivo*, rather than leakage from the cells, cellular instabilities or cell damage (Negrutskii and Deutscher, 1991). Unfortunately, as noted in

Table 5-1, the lack of a standard for annotated metabolites makes it difficult to confirm the results.

Similar results, though more pronounced, were detected for the metabolites when T0, T48hCTRL, and T48hINF were compared. The results concurred with the findings from the pathway analysis. The aa-tRNA exhibited the highest variation in T0 compared with T48hINF; with the second-highest variation in T48hCTRL compared with T48hINF. The large increase in aa-tRNA levels may indicate cell death and DNA degradation (Hou and Yang, 2013). However, glutamine, which plays an essential role in energy metabolism, decreased significantly in samples at 48 hours (see Table 5-1). The decreasing levels of glutamine may have been due to increased cellular uptake, as well as its utilization for nucleotide biosynthesis. However, the identification of the pentose phosphate pathway signal suggested that the depletion of glutamine in the medium could explain the reduced levels observed in these experiments. These findings are consistent with the observed reduction in ATP, as ATP synthesis is the primary source for glucose metabolism in cells (Fan *et al.*, 2013).

In this study, an analysis of amino acid metabolism was necessary to determine if there was an association between the changes in nucleotide metabolism and cell proliferation or death.

The corneal cells were incubated with or without ACCM without changing the growth medium for 48 hours, which created a condition of limited nutrient resources available to the cells. The limitation of resources meant that any change in amino acid levels would be indicative of either protein synthesis (if the amino acid levels decreased) or protein degradation (if amino acids were abundant). Our results revealed a decrease in amino acid levels in 48hCTRL compared with T0 (Table 5-2), which suggests protein consumption by the growing healthy/control cells. These findings correlate with the observed changes in nucleotide biosynthesis which result from cell proliferation. However, the 48hINF samples showed an increase in amino acid levels compared with T0–including those essential for humans such as valine, methionine, phenylalanine, lysine, leucine, and tryptophan (Table 5-2). These results are indicative of protein degradation due to cell death. The finding was informative as it showed cell death after 48 hours of infection. In general, there was an increase in the abundance of amino acids observed in 48hINF when compared with both the T0 and 48hCTRL. For instance, glutamine level in 48hINF was higher than in T0 or 48hCTRL. This suggesting that ACCM induces protein degradation in T48INF by utilizing serine proteases (Dudley, Alsam and Khan, 2008; Sant'ana *et al.*, 2015), increasing amino acids. This is indicative of protein degradation

and likely cell death. The opposite is seen for ACCM analysis in chapter four. Generally, the concentrations of most amino acids were highest in the first 3 hours. However, they decline within 48 hours of incubation, but the glutamine level was decreased at both 3 and 48 hours, suggesting that *Acanthamoeba* utilizes amino acids particularly glutamine for rapid growth, development, and multiplication.

Oxoadipic acid is one of the annotated metabolites of special interest in this study. Our results revealed a small increase in the oxoadipic acid metabolite in the 48hCTRL samples, when compared with T0, and a much larger increase in 48hINF samples compared with T0 and T48hCTRL. Existing research shows that patients with Kearns-Sayre Syndrome (KSS), a progressive condition caused by defects in mitochondria that mainly affects the eyes leading to retinopathy, tend to present with 2-oxoadipic aciduria (Barshop *et al.*, 2000). The 2-oxoadpic aciduria in KSS patients could be attributed to abnormally high levels of protein in the cerebrospinal fluid (CSF), perhaps due to disorders in the metabolism of amino acids. However, it was unclear whether this was related to AK because retinopathy involves the back of the eye and not the cornea. The clinical signs of AK include the degradation of corneal components (Lorenzo-Morales, Khan and Walochnik, 2015). Changes in the

posterior region of the eye, such as the retina and optic nerve, are rare (Illingworth and Cook, 1998). The annotation of the oxoadipic acid signal and the relationship of this metabolite to eye disease in other research merits further investigation.

In summary, the present study demonstrated that cell-free secretomes from *A. castellanii* T4 genotype strain cultures induced metabolic changes in CSCs, causing a reduction in cell viability and increased cell death. We found a decrease in amino acid levels in control samples at 48 hours compared with baseline samples, suggesting more protein turnover as cell grow; while increased levels of free amino acids at 48 hours in treated samples compared with baseline samples suggested protein degradation and cell death. We also observed an increase in nucleotide metabolism at 48 hours in both the control and treated samples, when compared with samples at baseline. This increase was much greater in the treated samples. The metabolite oxoadipic acid is known to be associated with ophthalmoplegia, retinopathy, and elevated CSF protein, was detected in this study. In conclusion, secretomes from *A. castellanii* cultures caused a significant impact on CSCs, resulting in changes in the levels of metabolites related to nucleotides and amino acids that ultimately led to a reduction in cell viability and increased cell death.

6. Chapter Six: Differential effects of nanoparticles on *A. castellanii* and human corneal cells

6.1 Introduction

Acanthamoeba keratitis (AK) is a serious infection of the cornea, for which there are no standard treatment procedures (Marciano-Cabral and Cabral, 2003; Lindsay *et al.*, 2007). Treatment requires prolonged dosage regimens and the use of multiple drugs in some cases, with various drugs being proposed for the treatment of *A. castellanii* infection. However, treatment is limited by a number of challenges including: a prolonged period of therapy; the drugs' toxicity to the cornea; and the fact that trophozoites are morphologically transformed into cysts, which are more difficult to kill (Niyyati, Dodangeh and Lorenzo-Morales, 2016). Treatment outcomes can also fail as some patients may not comply with the lengthy treatment duration. Given the current limitations of anti-Acanthamoebic drugs, there is an urgent need for new therapeutic agents and approaches.

Cerium oxide nanoparticles (CeO_2NPs) have demonstrated antimicrobial properties against bacteria (Kannan and Sundrarajan, 2014; Babenko *et al.*, 2012), protozoa (Jacob Inbaneson and Ravikumar, 2013) and viruses (Zholobak *et al.*,

2010). This nanoparticle metal oxide is regarded to have significant antimicrobial action activities, and it offers plausible efficiency in removing pathogens from different environments. This is due to the ability of CeO_2NPs to self-generate, which is enabled by redox-cycling between 3+ and 4+ states (Xue *et al.*, 2012; Cassee *et al.*, 2011). This gives CeO_2NPs variable properties of both being an effective scavenger of reactive oxygen species and cause extensive elevation of reactive oxygen species (ROS), leading to cell death or apoptosis. These characteristics of CeO_2NPs are significant in biomedical applications.

In order to detect intracellular antimicrobial activities, a cell must first be permeabilized. It has been shown that CeO_2NPs induce permeabilization of biological membranes (Bellio *et al.*, 2018), permeabilization allows an increase in the diffusion of antimicrobials, which enhances the availability of the therapeutic agent. In addition, due to their smaller size, CeO_2NPs can more easily penetrate the microbial cell membrane and interact with the intracellular components and enhance their antimicrobial efficacy. This includes changing and damaging the microbial cell membrane and generating ROS, obstructing cellular proteins and reducing replication of DNA, ultimately killing the pathogen (Aderibigbe, 2017; Farias, Santos and Sampaio, 2018).

However, there are other factors to consider in the treatment of *A. castellanii* using CeO_2NPs, such as how to target the encystment process to interrupt the organism encystaion or prevent the formation of cysts.

CeO_2NPs effectiveness as an antimicrobial been demonstrated, and they have been suggested for treating numerous diseases. CeO_2NPs have exhibited antioxidant activities in various mammalian cell lines, due to their ability to scavenge ROS in an enzyme-mimetic manner, and have demonstrated a potential for treating a number of ocular conditions – including cataract and retinal diseases (Chen *et al.*, 2006; Hanafy *et al.*, 2019). CeO_2NPs can reduce oxidising stress within cells, indicating a therapeutic potential for treating human inflammation (Zheng *et al.*, 2019; Hirst *et al.*, 2009), and treating neovascularization-related ophthalmic diseases.

Nevertheless, potential risks connected with CeO_2NPs are apparent in environmental and biomedical areas (Booth *et al.*, 2015; Schwotzer *et al.*, 2017; Koehlé-Divo *et al.*, 2018). The cause of these is usually the greater surface-to-volume ratio, dose and time dependency, which have the potential to increase the particles' reactivity or catalytic impacts. Studies that have explored CeO_2NPs' effects on human/animal cells have found varying levels of vulnerability to cytotoxicity (Schwotzer *et al.*,

2017; Rajeshkumar and Naik, 2018). These studies claim that inhaling CeO_2NPs carries a greater risk than does ingesting, because the intestine has some ability to absorb them, but the lungs do not. However, there is a possibility of these particles penetrating the inner cellular constituents due to intercellular agglomeration and/or the size of the particle (Pešić *et al.*, 2015). It is necessary to test the potential cytotoxicity of many cultured cells with CeO_2NPs *in vitro*, as well as to conduct *in vivo* studies for assessing the particles' biosafety and biocompatibility.

Despite the therapeutic value of CeO_2NPs, no research has been published on their activity against *A. castellanii* and corneal cells. The current study is the first to examine the effect of cerium oxide nanoparticles (CeO_2NPs) on both *A. castellanii* and corneal cells cultured *in vitro*. We examined the effect of CeO_2NPs on *A. castellanii* and corneal cells viability using an alamarBlue® assay, and on cell proliferation using a SRB assay, absolute cell counting of *A. castellanii*, immunofluorescent staining of actin and acridine orange (AO) staining. Transmission Electron Microscopy (TEM) was used for tracking the accumulation of the particles, and identifying changes in cellular ultrastructure in *A. castellanii*, following exposure to CeO_2NPs. The data showed a significant dose-dependent reduction in cell proliferation and viability; and effects on the morphology, of *A.*

castellanii. Interestingly, CeO_2NPs had no significant effect on corneal cells, and up to 200 µg/mL with no indications of a decrease in viability, proliferation or damage to actin.

6.2 Materials and Methods

6.2.1 Corneal cell culture

CSCs, or ihCECs, were cultured in M199, or EpiLife™ medium, respectively, as described in sections 2.1.2.and 2.1.1.

6.2.2 *Acanthamoeba castellanii* culture

A. castellanii trophozoites were cultured in PYG media as described in section 2.2.1.

6.2.3 Antimicrobial activity of nanoparticles

All nanoparticles (NPs) used in the present study were obtained as powder nanoparticles (size, 2-5 nm) from the School of Science and Technology, Nottingham Trent University, UK.

6.2.3.i Preparation of NP stock solutions

Silver (AgNP), cerium oxide (CeO_2NP) and selenium (SeNP) nanoparticle stock solutions were prepared using the protocol described in section 2.12. These NPs were used to test their effects on *A. castellanii* and corneal cells as described below.

6.2.3.ii *In vitro* anti-Acanthamoebic activities of NPs

We examined the effect of NPs on *A. castellanii* trophozoites and corneal cells using the methods described in sections 2.13.4 and 2.14.1. *A. castellanii,* or corneal cells, were incubated in AgNPs, CeO_2NPs and SeNPs at doses of 100, 200 and 400 µg/mL in 96-

well plates for 3, 6, 24 and 48 h, at 25 °C for *A. castellanii* and at 37 °C for corneal cells. Untreated wells were used as controls. Following incubation, SRB assays were employed to measure the proliferation rate of *A. castellanii* as detailed in section 2.4.3.

6.2.4 *In vitro* anti-Acanthamoebic efficacy of CeO_2NPs

A. castellanii trophozoites were cultured in PYG media as detailed in section 2.2.1. Trophozoites were into T-25 flasks at a density of 2 $x10^5$ trophozoites and 96-well plates at 3 $x10^3$ trophozoites. They were then incubated in various concentrations of CeO_2NPs (100, 200, 300, and 400 µg/mL) at 25°C for 3, 6, 24, and 48 h as detailed in section 2.13.1 for cell-counting and imaging/microscopy, and section 2.13.4 for the SRB assay. Following incubation, the effects of CeO_2NPs were tested in *A. castellanii* as described below.

6.2.4.i Viability assay

Following incubation, the effect of CeO_2NPs on the proliferation rate of *A. castellanii* was determined using a SRB assay as described in section 2.4.3.

6.2.4.ii Trophozoite counting

Cell counting was performed using a haemocytometer and verified with an inverted microscope (Medline Scientific, CETI, UK) as described in section 2.13.1.i.

6.2.4.iii Microscopic examination

Following incubation in CeO_2NPs, as described in section 2.13.1, the effects of CeO_2NPs on the viability rate of *A. castellanii* were determined by microscopy and imaging at high and lower magnification (500 µm and 100 µm), using an inverted microscope (Leica DMIL, CMS, Germany).

6.2.5. Transient exposure of *A. castellanii* to CeO_2NPs

The short-term effects of high and low concentrations of CeO_2NPs on *A. castellanii* were investigated using SRB assays and cell counting. Trophozoites were cultured in T-25 flasks at 2 $x10^5$ trophozoites, and 96-well plates at 3 $x10^3$ trophozoites. They were then exposed to different concentrations of CeO_2NPs (100, 200, 300 and 400 µg/mL) for a period of 1 h. The dose-effects at these concentrations were determined in earlier experiments using a SRB assay and cell counting. Trophozoites were cultured in T-25 flasks and 96-well plates (Nunc, Thermo Fisher Scientific, USA), as described above, and then exposed to high concentrations of CeO_2NPs (500 and 1000 µg/mL) for one h. Following incubation, the supernatants were discarded and trophozoites were gently rinsed twice with PBS to remove residual external CeO_2NPs, and re-incubated in fresh PYG medium for 48 h at 25°C. For examining *A. castellanii* cells'

proliferation, SRB assays and cell counting were conducted as described in sections 2.4.3 and 2.13.1.i, respectively.

6.2.6. Tracking the intra-acanthamoebic accumulation of CeO_2NPs with TEM

A. castellanii trophozoites were conventionally cultured in a PYG medium, seeded into T-75 cm^2 flasks, and then treated with 400 µg/mL of CeO_2NPs, as mentioned in section 2.13.1. The flasks were then incubated at 25°C for 0, 24, and 48 h. Following incubation, TEM analysis was performed to characterise the changes in ultrastructure that occurred in trophozoites after 0, 24, and 48 h of CeO_2NP treatment, as detailed in section 2.7.

6.2.7. The effect of CeO_2NPs on actin and the cellular structure of *A. castellanii*

The effect of CeO_2NPs on the *A. castellanii* cytoskeleton was determined using immunofluorescent staining of *A. castellanii* actin. Acridine orange (AO) staining was used to detect changes in the nucleus, as described in sections 2.13.3.

6.2.8. Anti-encystation effect of CeO_2NPs

The inhibition of *A. castellanii* encystation following exposure to various doses of CeO_2NPs (100, 200, 300 and 400 µg/mL) at 25°C for 48 h was examined using the encystation assay described in section 2.13.5.

6.2.9. *In vitro* toxicity of CeO_2NPs in CSCs and ihCECs

6.2.9.i Viability assays

ihCECs or CSCs were seeded in 96-well plates, as described in sections 2.1.3 and 2.4., then incubated in various concentrations of CeO_2NPs (100, 200, 300, and 400 µg/mL) at 37°C for 3, 6, 24, and 48 h, as described in section 2.14.1. Following incubation, the cytotoxic effects of CeO_2NPs on the viability of CSCs and ihCECs were examined using alamarBlue® as detailed in section 2.4.1. SRB assays were used to assess proliferation as described in section 2.4.3.

6.2.9.ii Transient exposure of corneal cells to CeO_2NPs

The short-term effect of high and low concentrations of CeO_2NPs on corneal cells was examined using both the alamarBlue® and SRB assays. CSCs or ihCECs were cultured and then seeded in 96-well plates as described in sections 2.1.3 and 2.4. They were then exposed to different concentrations of CeO_2NPs (100, 200, 300 and 400 µg/mL) for a period of 1 h. Both corneal cell types were also seeded in 96-well tissue-culture plates, as above, and exposed to high concentrations of CeO_2NPs (500 and 1000 µg/mL) for 1 h. Following incubation, the supernatants were removed. Samples were gently rinsed twice with PBS to remove residual external CeO_2NPs, then re-suspended in fresh media (M199 for CSCs or Epilife™ for

ihCECs) and incubated for 48 h at 37°C. AlamarBlue® and SRB assays were used to examine cell viability and proliferation, as described in sections 2.4.1 and 2.4.3.

6.2.9.iii The effect of CeO_2NPs on actin and the cellular structure of CSCs and ihCECs

The effects of CeO_2NPs on CSCs and ihCECs were examined using immunofluorescent staining of actin and AO staining of the nucleus, as previously mentioned in section 2.14.2.

6.2.10 Statistical analysis

Data analysis was undertaken by applying the GraphPad Prism version 7. A two-way variance analysis ANOVA was used to reveal statistical differences between mean concentrations of treated and untreated groups. Data are indicated as mean ± SD, with statistical importance being depicted by asterisks; P-value < (0.0001****, 0.001***, 0.01**, 0.05*).

6.3 Results

6.3.1 Differential toxic effects of NPs on *A. castellanii* and corneal cells

The toxic effects of NPs on *A. castellanii* and both types of corneal cells were examined using a SRB assay to measure the level of proliferation of trophozoites following 3, 6, 24 and 48 h of exposure to AgNPs, CeO_2NPs and SeNPs (100, 200 and 400 µg/mL) (Figures 6-1, 2 and 3 A-D). All three concentrations up to 400 µg/mL (with the exception of CeO_2NPs) had no significant effect on the proliferation of *A. castellanii* after 3 h of exposure (Figure 6-1, A). Significant reductions in proliferation were observed in *A. castellanii* exposed to CeO_2NPs and SeNPs, at 200 and 400 µg/mL, after 6 h of exposure (Figure 6-1, B). Significant changes in the proliferation of *A. castellanii* were observed following 24 and 48 h exposure to most concentrations of all NPs (Figure 6-1, C-D). These results demonstrated that the effects of CeO_2NPs on *A. castellanii* proliferation were strongest, followed by SeNPs and weakest for AgNPs (Figure 6-1, A-D).

The SRB assay results for ihCEC proliferation revealed non-significant differences between controls and treated groups at 3 and 6 h for all NPs, except AgNPs and SeNPs after 6 h in 400 µg/mL (Figure 6-2, A-B). SRB assay results also detected

significant differences between treated and control cells at 24 and 48 h, particularly at higher concentrations (Figure 6-2, C-D). The SRB assay also revealed non-significant differences in CSCs proliferation between treated and control cells after 3 and 6 h for all NPs, however the reduction in the proliferation of CSCs was significantly greater between treated and control groups after 24 and 48 h in higher concentrations for all NPs (Figure 6-3, A-D). Based on these results we conclude that the effects of NPs on corneal cells were strongest with SeNPs, followed by AgNPs, and weakest with CeO_2NPs. The subsequent experiments were only conducted with CeO_2NPs at various doses (100, 200, 300 and 400 µg/mL) to identify any dose-dependent effect.

However, the data in figures 6-2 and 6-3 were used to calculate the selectivity index (SI) of all NPs for evaluating the toxic effect of NPs on corneal cells, and the results has been shown in Tables 6-1 (A-B). The EC_{50} and IC_{50} concentration were determined through nonlinear regression analysis by GraphPad Prism. Subsequently, the efficacy of NPs was determined by SI ($SI = IC_{50}/EC_{50}$). The results showed that the CeO_2NPs are not very safe for the corneal cells. The SI at all time points analysed is either below 1 or just more than 1.

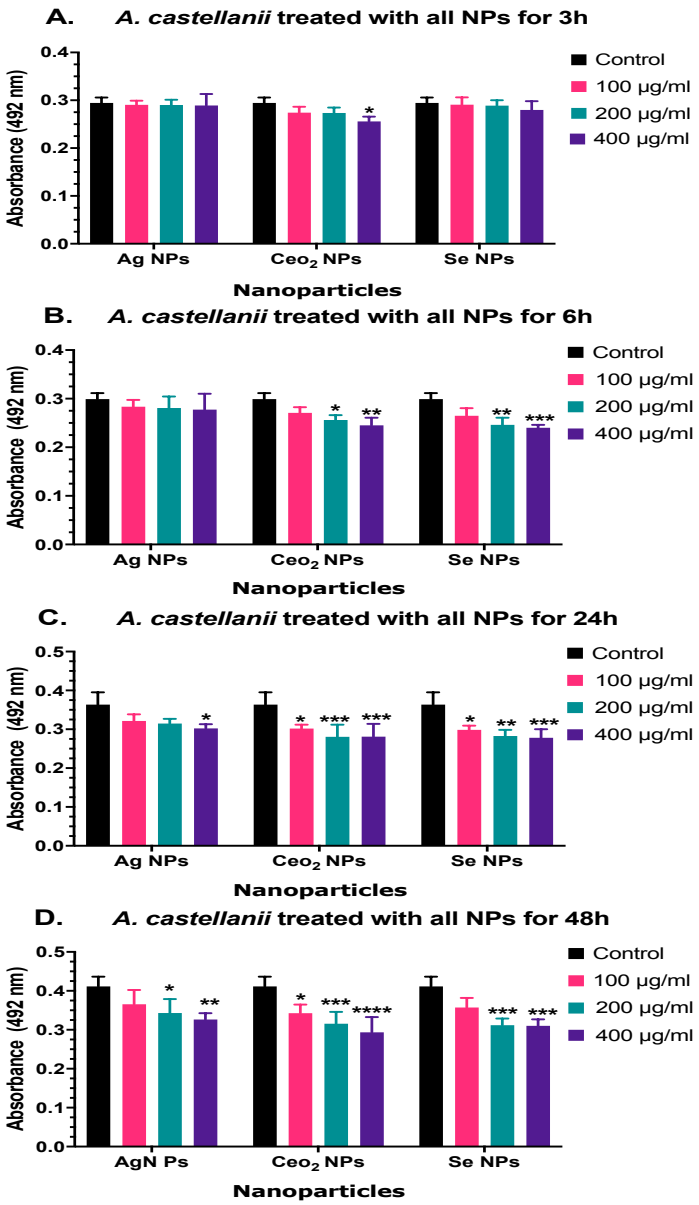

Figure 6-1. The effects of AgNPs, CeO_2NPs and SeNPs on the proliferation of *A. castellanii* determined using SRB assays. Cultured *A. castellanii* trophozoites were incubated in various concentrations of NPs (100, 200 and 400 µg/mL) at 25 °C for 3, 6, 24 and 48 h. Trophozoites treated with PYG medium were used as control. Absorbance values (at 492 nm) are presented as mean ± SDs of 4 technical replicates, and each experiment was replicated three times. A two-way ANOVA revealed significant differences between the results for cells treated with NPs and untreated cells.

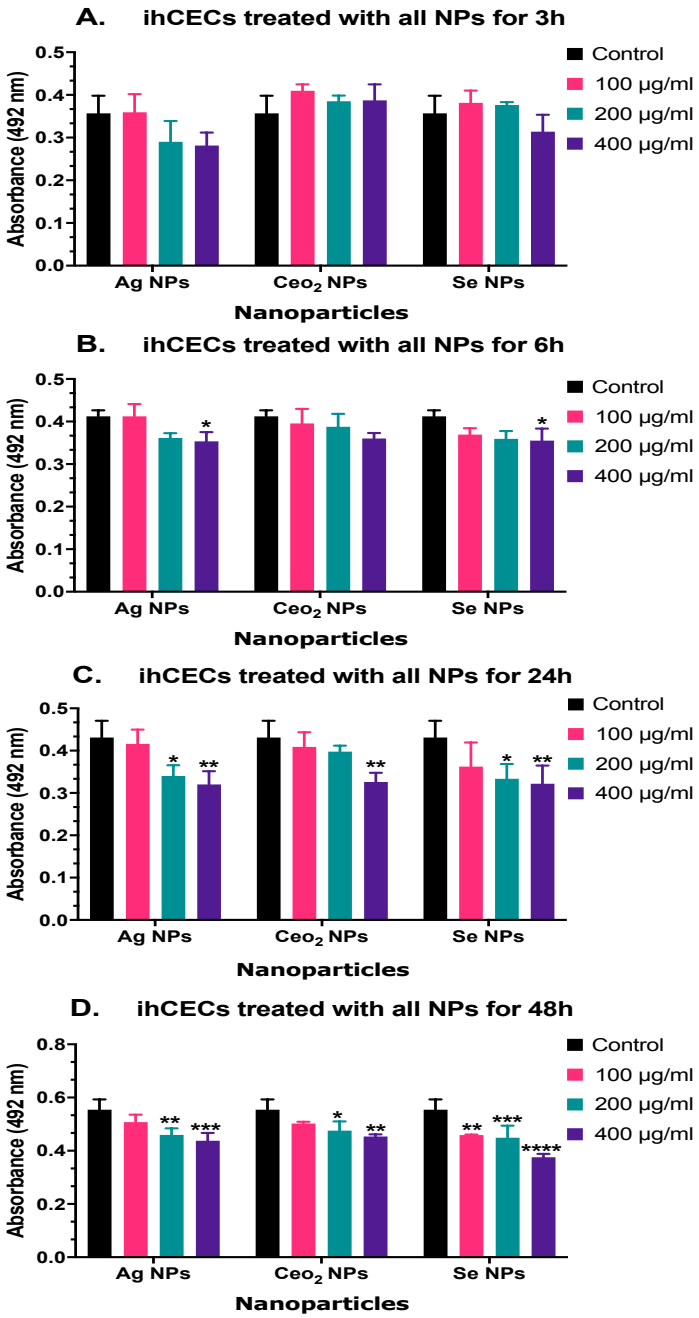

Figure 6-2. The effects of AgNPs, CeO_2NPs and SeNPs on the proliferation of ihCECs determined using SRB assays. Cultured ihCECs were incubated in various concentrations of NPs (100, 200 and 400 µg/mL) at 37 °C for 3, 6, 24 and 48 h. Cells treated with PYG medium were used as control. Absorbance values (at 492 nm) are presented as mean ± SDs of 4 technical replicates, and each experiment was replicated three times. A two-way ANOVA revealed significant differences between the results for cells treated with NPs and untreated cells.

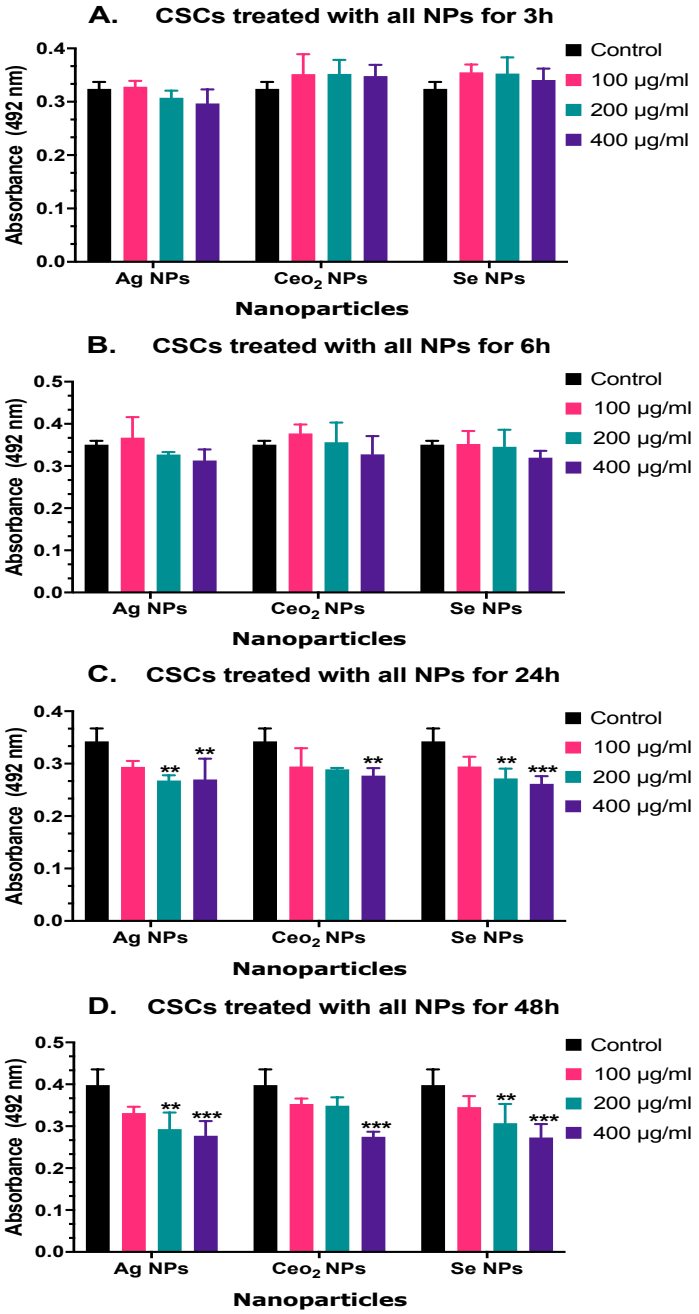

Figure 6-3. The effects of AgNPs, CeO_2NPs and SeNPs on the proliferation of CSCs determined using SRB assays. Cultured CSCs were incubated in various concentrations of NPs (100, 200 and 400 µg/mL) at 37 °C for 3, 6, 24 and 48 h. Cells treated with PYG medium were used as control. Absorbance values (at 492 nm) are presented as mean ± SDs of 4 technical replicates, and each experiment was replicated three times. A two-way ANOVA revealed significant differences between the results for cells treated with NPs and untreated cells.

Table 6-1 A: The effects of AgNPs, CeO_2NPs and SeNPs on ihCECs were determined using the selectivity index (SI), (SI = IC_{50}/EC_{50}).

	AgNPs			CeO_2NPs			SeNPs		
	IC_{50} µg/mL	EC_{50} µg/mL	SI	IC_{50} µg/mL	EC_{50} µg/mL	SI	IC_{50} µg/mL	EC_{50} µg/mL	SI
3 h	183.4	156.2	1.17	2.90	2.90	1	214.5	292.5	0.73
6 h	185.9	157.9	1.18	162.5	178.3	0.91	61.43	66.87	0.92
24 h	146.5	153.3	0.96	227.9	254.0	0.90	80.74	79.40	1.02
48 h	119.2	128.1	0.93	99.83	97.83	1.02	107.3	95.04	1.13

IC_{50} (50% inhibition concentration)
EC_{50} (50% effective concentration)
SI (selectivity index)

Table 6-1 B: The effects of AgNPs, CeO_2NPs and SeNPs on CSCs were determined using the selectivity index (SI), (SI = IC_{50}/EC_{50}).

	AgNPs			CeO_2NPs			SeNPs		
	IC_{50} µg/mL	EC_{50} µg/mL	SI	IC_{50} µg/mL	EC_{50} µg/mL	SI	IC_{50} µg/mL	EC_{50} µg/mL	SI
3 h	196.4	176.4	1.11	1.07	1.07	1	4.63	4.63	1
6 h	193.9	167.7	1.16	202.1	117.2	1.72	208.5	274.5	0.76
24 h	98.76	88.72	1.11	69.50	76.82	0.90	100.5	99.97	1.01
48 h	92.59	90.65	1.02	172.6	233.4	0.74	118.4	125.9	0.94

IC_{50} (50% inhibition concentration)
EC_{50} (50% effective concentration)
SI (selectivity index)

6.3.2 The impact of CeO_2 on the viability of *A. castellanii*

The effect of CeO_2NPs on the viability of *A. castellanii* was examined by cell counting, light microscopy and by SRB assay. The cell count and SRB tests showed a dose-dependent decline in the viability and proliferation of *A. castellanii* after 3, 6, 24 and 48 h of incubation in CeO_2NPs. As shown in Figure 6-4, A, the cell count revealed significant differences in treated groups when compared with controls for all incubation periods. SRB assay results also revealed a significant difference in treated groups when compared with controls for all incubation periods, except after 3 h which did not appear to be significantly different (Figure 6-4, B). However, light microscopy revealed that the density of *A. castellanii* trophozoites was higher in controls than treated groups, and gradually declined in a dose-dependent manner (Figures 6-5, A-B). The high and low magnification images also showed that the numbers of trophozoites were significantly lower in treated samples, particularly at higher concentrations and over longer exposure periods (i.e. after 6, 24 and 48 h in 200, 300 and 400 µg/mL CeO_2NPs).

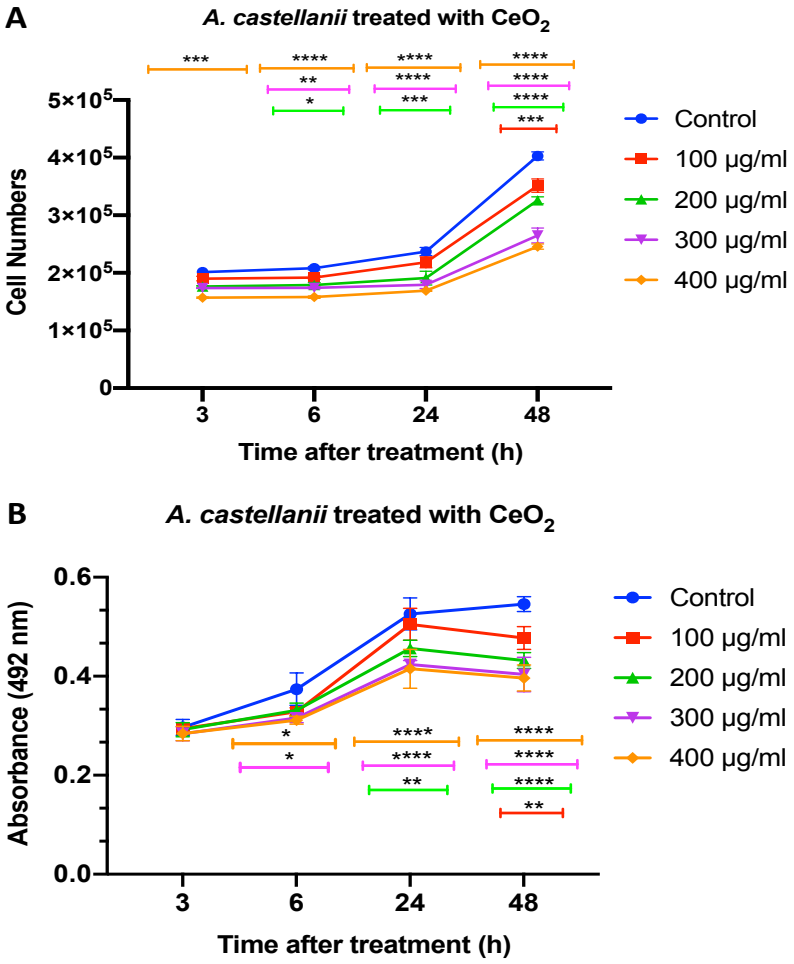

Figure 6-4. The impact of CeO_2NPs on the viability and proliferation of *A. castellanii* determined by cell counting (A) and SRB assays (B). Cultured *A. castellanii* trophozoites were incubated in various concentrations of NPs (100, 200, 300 and 400 µg/mL) at 25 °C for 3, 6, 24 and 48 h. Trophozoites treated with PYG medium were used as control. A two-way ANOVA revealed significant differences between the treated cells and the controls. Each experiment was performed three times with 4 technical replicates per-experiment.

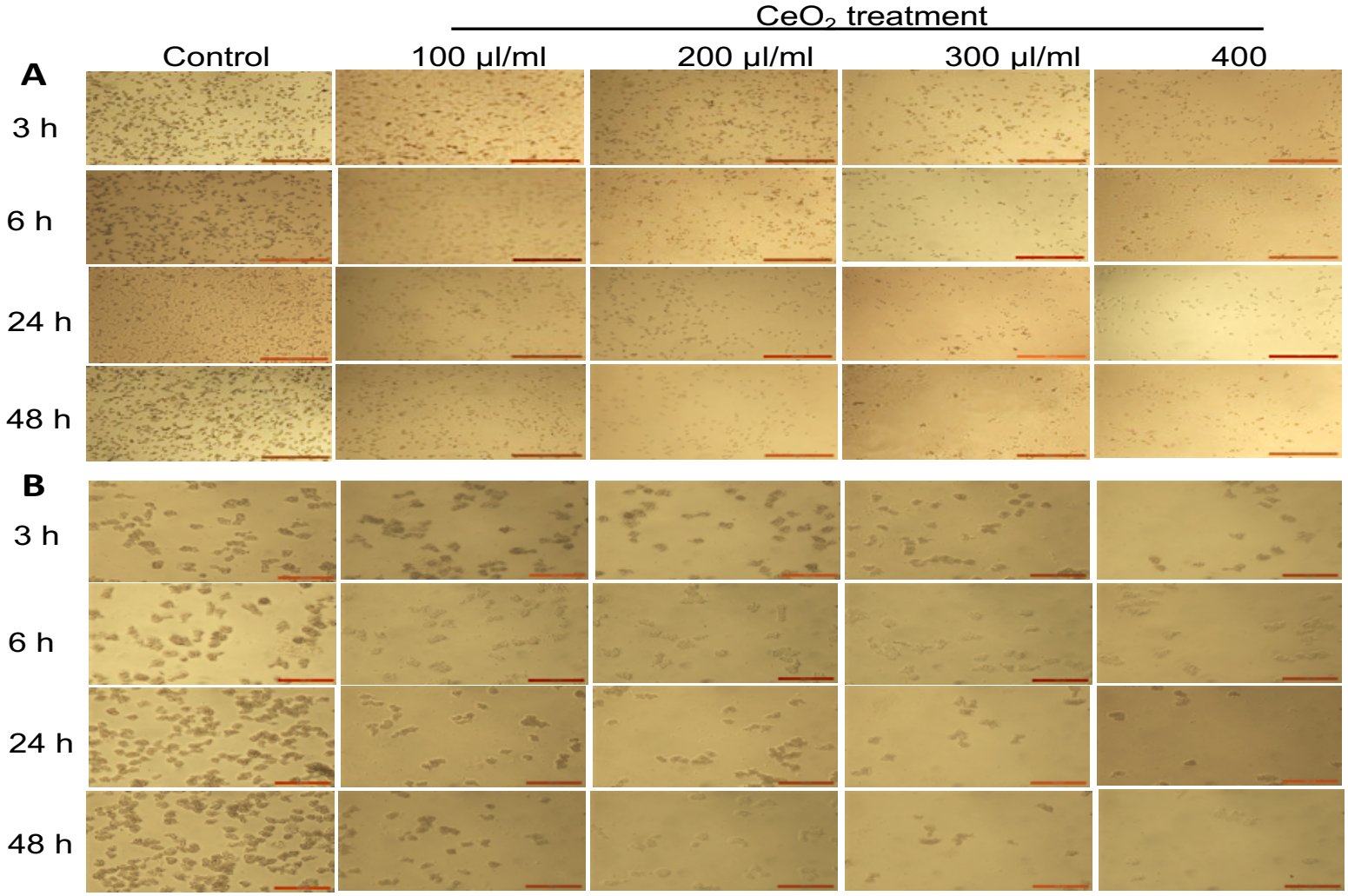

Figure 6-5. The effect of CeO_2NPs on the viability of *A. castellanii* determined by light microscopy at low (A) and high (B) magnification. Cultured *A. castellanii* trophozoites were incubated in various concentrations of NPs (100, 200, 300 and 400 µg/mL) at 25 °C for 3, 6, 24 and 48 h. Trophozoites treated with PYG medium were used as control. Images were captured using an inverted microscope. Scale bar (500µm, A) and (100µm, B) applies to all images. The experiment was performed three times with 4 technical replicates per-experiment.

6.3.3 Short-term toxicity of CeO_2NPs in *A. castellanii*

Toxicity caused by transient exposure (one hour) to various doses of CeO_2NPs (100, 200, 300 and 400 µg/mL) on *A. castellanii* was investigated by cell counting and SRB assay following 48 h of re-incubation. The results revealed a gradual concentration-dependent reduction in growth rate of *A. castellanii* trophozoites treated with CeO_2NPs at all doses except 100 µg/mL, when compared with controls, following 48 h of re-incubation (Figures 6-6, A-B).

Toxicity of high concentrations of CeO_2NPs (500 and 1000 µg/mL) to *A. castellanii* after 1 h was also examined by cell counting and SRB assay. Significant reductions in the growth-rate of *A. castellanii* trophozoites were seen after 48 h of re-incubation for all concentrations, when compared with controls (Figures 6-7, A-B).

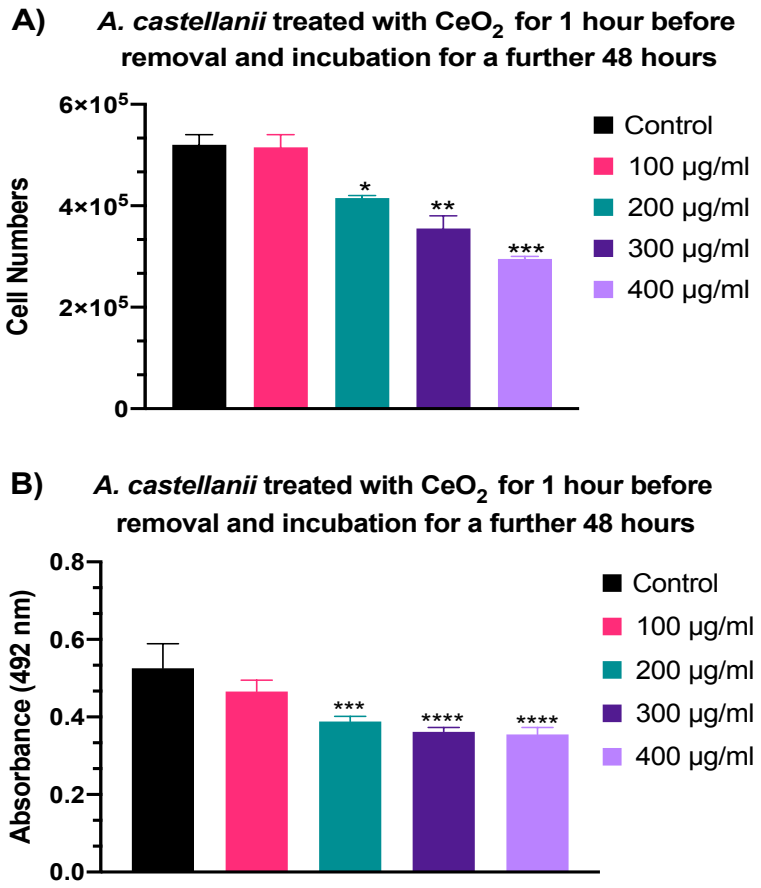

Figure 6-6. The impact of CeO_2 nanoparticles (NPs) on the viability and proliferation of *A. castellanii* determined by cell counting (A) and SRB assays (B). Cultured *A. castellanii* trophozoites were incubated in various concentrations of CeO_2NPs (100, 200, 300 and 400 µg/mL) at 25°C for short-term (one hour) exposure; then re-incubated in fresh PYG medium at 25°C for 48 h. Trophozoites treated with PYG medium were used as control. A two-way ANOVA revealed significant differences between the treated cells and the controls. Each experiment was performed three times with 4 technical replicates per-experiment.

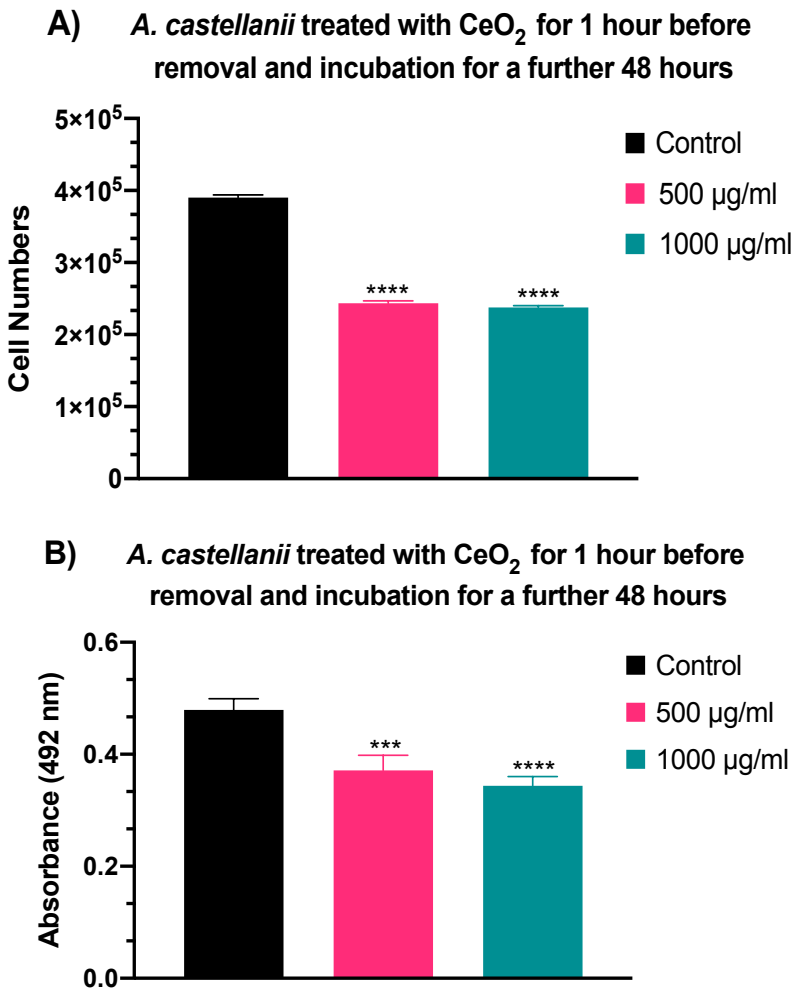

Figure 6-7. The effects of CeO_2 nanoparticles (NPs) on the viability and proliferation of *A. castellanii* was determined by cell counting (A) and SRB assays (B). Cultured *A. castellanii* trophozoites were incubated in high concentrations of CeO_2NPs (500 and 1000 µg/mL) at 25 °C for 1 h; then re-incubated in fresh PYG medium at 25°C for 48 h. Trophozoites treated with PYG medium were used as control. A two-way ANOVA revealed significant differences between the treated cells and the controls. Each experiment was performed three times with 4 technical replicates per-experiment.

6.3.4 TEM analysis of CeO_2NP -treated *A. castellanii*

TEM was performed to further elucidate the effects of CeO_2NPs on the ultrastructure of *A. castellanii*, following 48 h incubation in 400 µg/mL of CeO_2NPs. In untreated cultures of *A. castellanii*

(Figure 6-9) trophozoites exhibited normal components, including a large nucleus, conspicuous nucleolus, vacuoles and no signs of organelle damage. The morphological examination of *A.castellanii* treated with CeO_2NPs at zero time showed a distinct structure of nucleus, vacuoles and other organelles (Figure 6-8). CeO_2NPs were also observed inside the vacuoles as small granules and in large quantities. Trophozoites treated with CeO_2NPs for 24 h showed nuclear damage, morphological changes and organelle degeneration (Figure 6-8). Consistent with the results obtained after 24 h of exposure, significant damage to trophozoites was detected at 48 h, when compared with untreated trophozoites, and more nuclear damage was also observed – with the nucleus even absent in some trophozoites (Figure 6-9).

Based on the results of TEM, the mechanism of entry of CeO_2NPs into *A. castellanii* is shown in Figure 6-10, A-B. According to our results, CeO_2NPs were detected on the *A.castellanii* membrane's outer surface. Subsequently, they were readily phagocytosed by *Acanthamoeba*, thereby allowing them to accumulate in vesicles and permitting subcellular targeted effects. After CeO_2NPs enter the vesicles and accumulate there, they transfer to directly-targeted specific subcellular organelles causing further effects. CeO_2NPs were subsequently located

within the nucleus of the cell, thereby showing a necessity to enter this organelle in order to exert their toxic effects. According to our experimental results, the scheme depicted in figure 6-10, A-B shows the CeO_2NPs' mechanism of action inside the cell, and their effective targeting of the cell nucleus. Consequently, both the nucleic acid components and proteins could be significantly damaged.

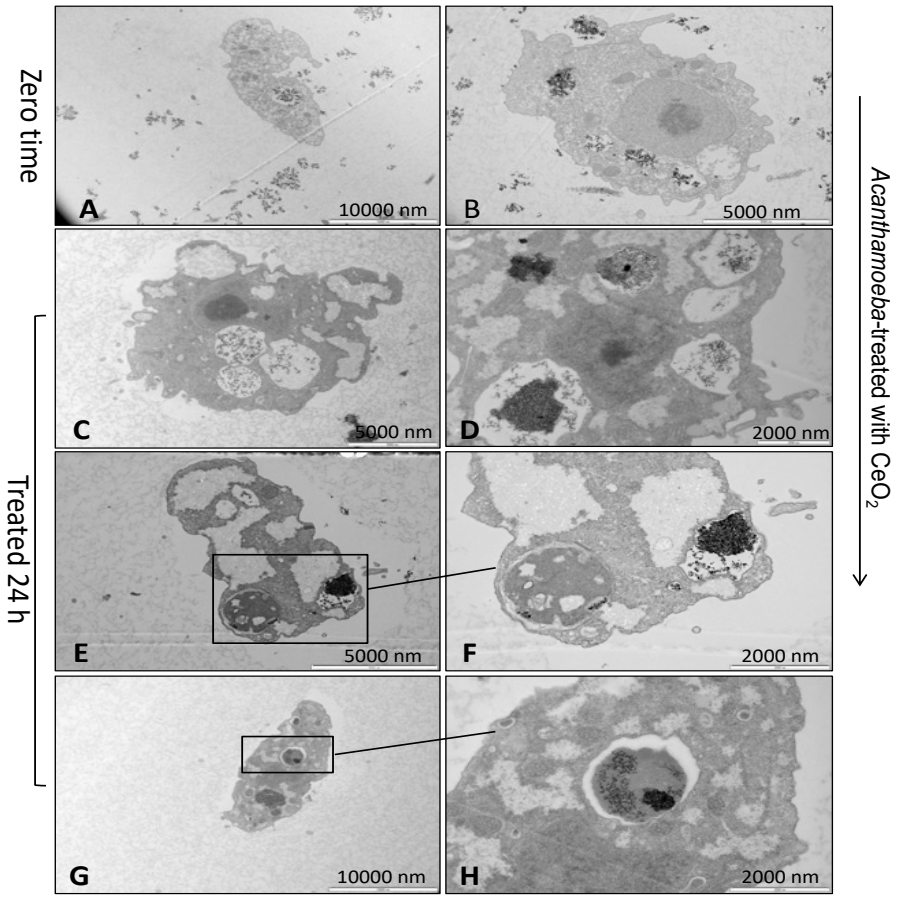

Figure 6-8. Ultrastructural changes in CeO_2NP-treated *A. castellanii*. Trophozoites were incubated in 400 µg/mL of CeO_2NPs for 48 h. At zero time (A-B), trophozoites absorbed the CeO_2NPs via phagocytosis. Treated trophozoites at 24 h (C-H) showed some damage and morphological changes. There were some dead trophozoites with cytoplasmic vesicles, but no apparent nucleus and lacking organelles. The experiment was performed three times with 2 technical replicates per-experiment.

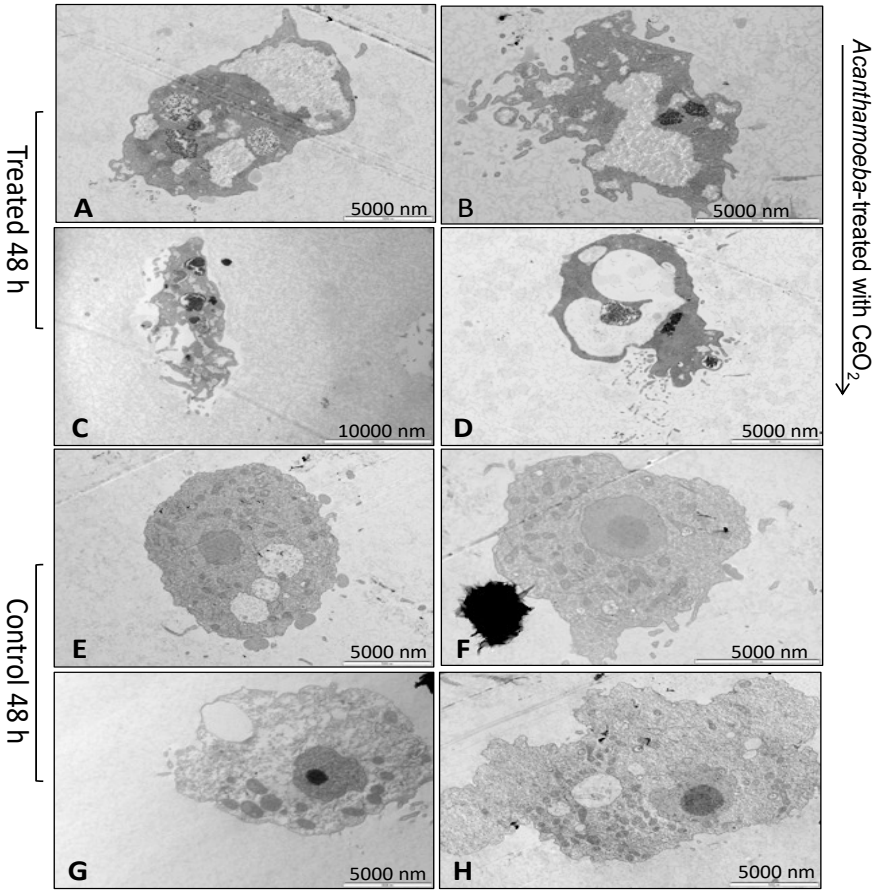

Figure 6-9. Ultrastructural changes in CeO_2NP-treated *A. castellanii*. Trophozoites were incubated in 400 µg/mL of CeO_2NPs for 48 h. Treated trophozoites at 48 h (A-D) showed significant damage and morphological changes. Most of the trophozoites appeared dead with the loss of their nucleus and some organelles. Control trophozoites (E-H) appeared morphologically normal with a largely convoluted nucleus and conspicuous nucleolus. The experiment was performed three times with 2 technical replicates per-experiment.

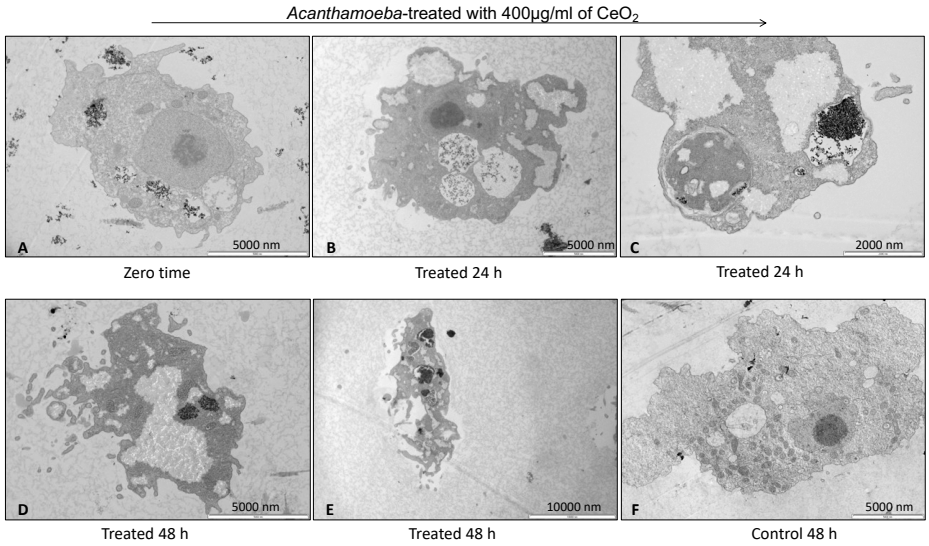

Figure 6-10, A. Illustrative images of the mechanism of CeO_2NPs in *A. castellanii* trophozoites. CeO_2NPs acted as an anti-acanthamoebic agent via the following mechanism: trophozoites absorbed the CeO_2NPs via phagocytosis and then accumulate within vesicles. The CeO_2NPs were then transported to the cell's nucleus where they caused damage.

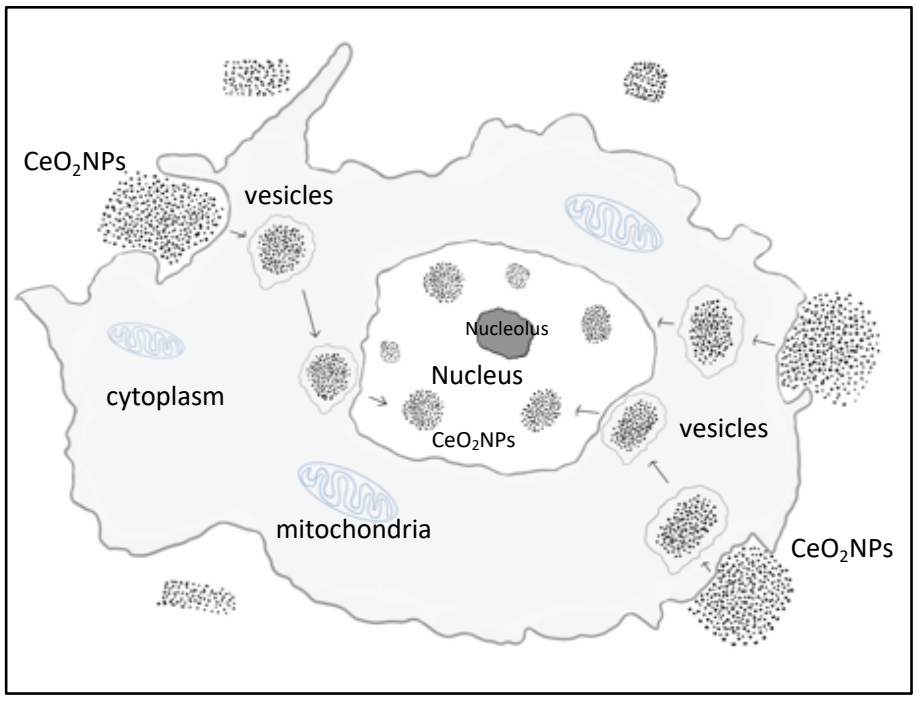

Figure 6-10, B. Illustrative scheme of the mechanism of CeO_2NPs in *A. castellanii* trophozoites.

6.3.5 CeO_2NPs induce actin cytoskeleton disruption in *A. castellanii*

Fluorescence microscopy was used to examine the morphological changes in actin arrangement after incubation in various CeO_2NP concentrations for various periods of time. *A. castellanii* trophozoites were stained with DAPI and phalloidin. Figure 6-11 shows that the trophozoites' density was greater in controls than in treated trophozoites, indicating a steady dose-dependent reduction in the trophozoites' density. Furthermore, figure 6-12 A-C illustrates that control trophozoites had a well-distributed actin cytoskeleton, a normal nucleus. An abnormal arrangement of the actin cytoskeleton and shape of the trophozoites was observed, particularly at higher concentrations over longer exposure periods (e.g.,24-48 h in 200, 300 and 400 µg/mL CeO_2NPs). Moreover, the number of treated trophozoites was notably less after 24 and 48 h of culture (Figure 6.-12, B-C) and an altered actin cytoskeleton and damaged nucleus were detected in the remaining trophozoites.

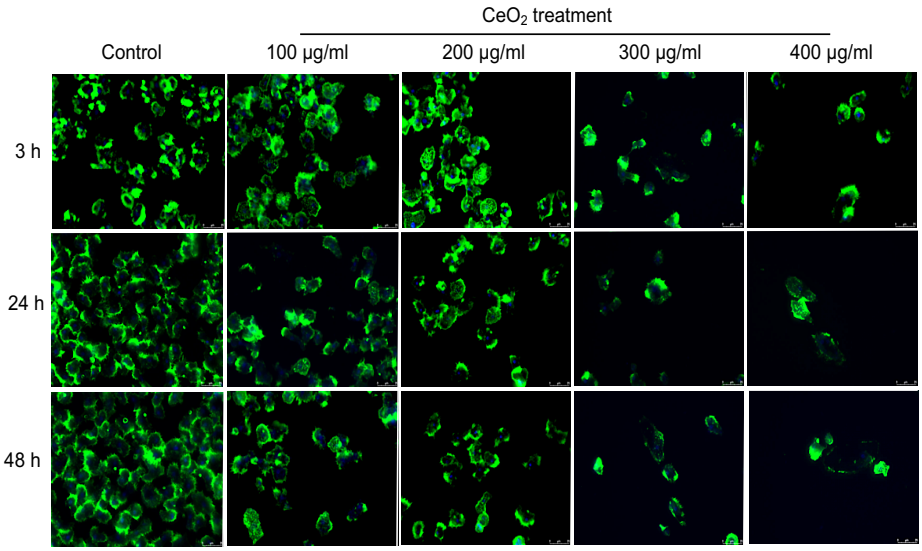

Figure 6-11. The effect of CeO_2NPs on fluorescence staining of the actin cytoskeleton. *A. castellanii* trophozoites were incubated with CeO_2NPs at the indicated concentrations and duration. Trophozoites were fixed with paraformaldehyde and glutaraldehyde (4% and 0.5%) for 10 min, then stained with phalloidin (actin) and DAPI (nucleus). Images were obtained with an inverted wide-field fluorescence microscope. Scale bar (25 µm) applies to all images. The experiment was performed three times with 2 technical replicates per-experiment.

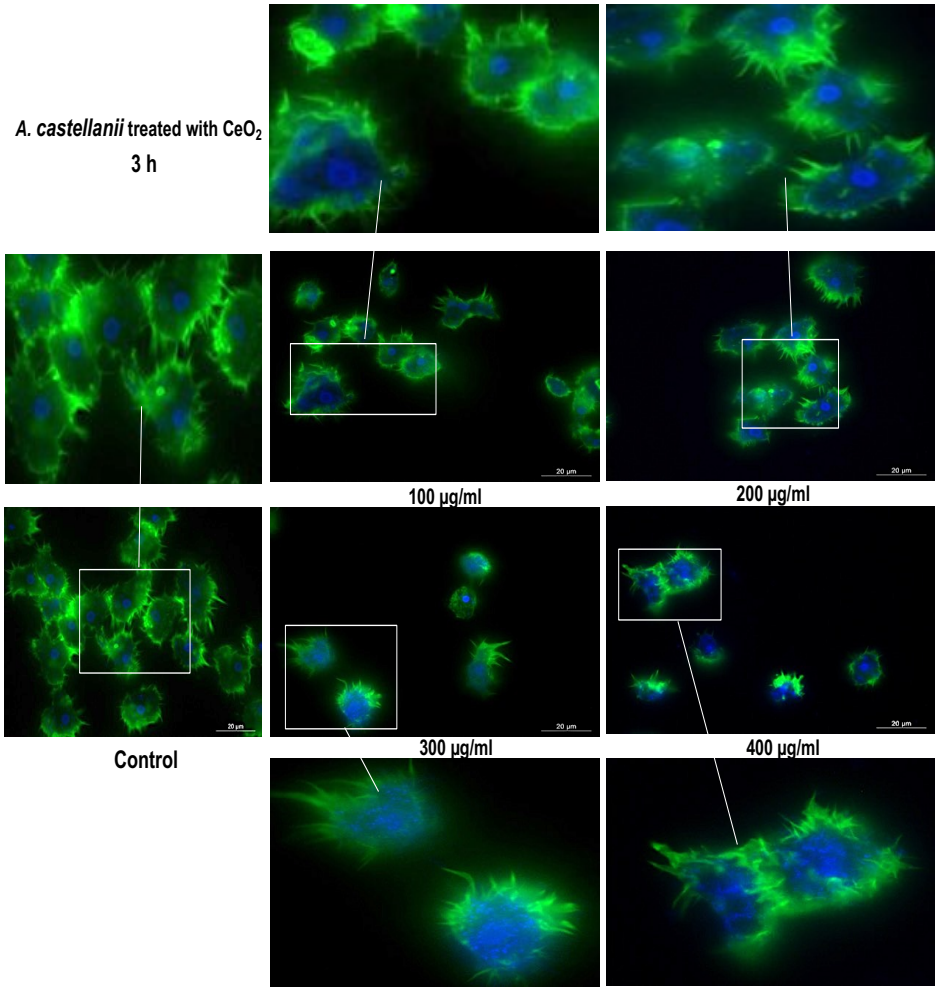

Figure 6-12, A. The effect of CeO_2NPs on fluorescence staining of the actin cytoskeleton. *A. castellanii* trophozoites were incubated CeO_2NPs at the indicated concentrations for 3h (A), 24h (B) and 48h (C). Trophozoites were fixed with paraformaldehyde and glutaraldehyde (4% and 0.5%) for 10 min, and stained with phalloidin (actin) and DAPI (nucleus). Images were obtained using an inverted wide-field fluorescence microscope. Scale bar (20 µm) applies to all images. The experiment was performed three times with 2 technical replicates per-experiment.

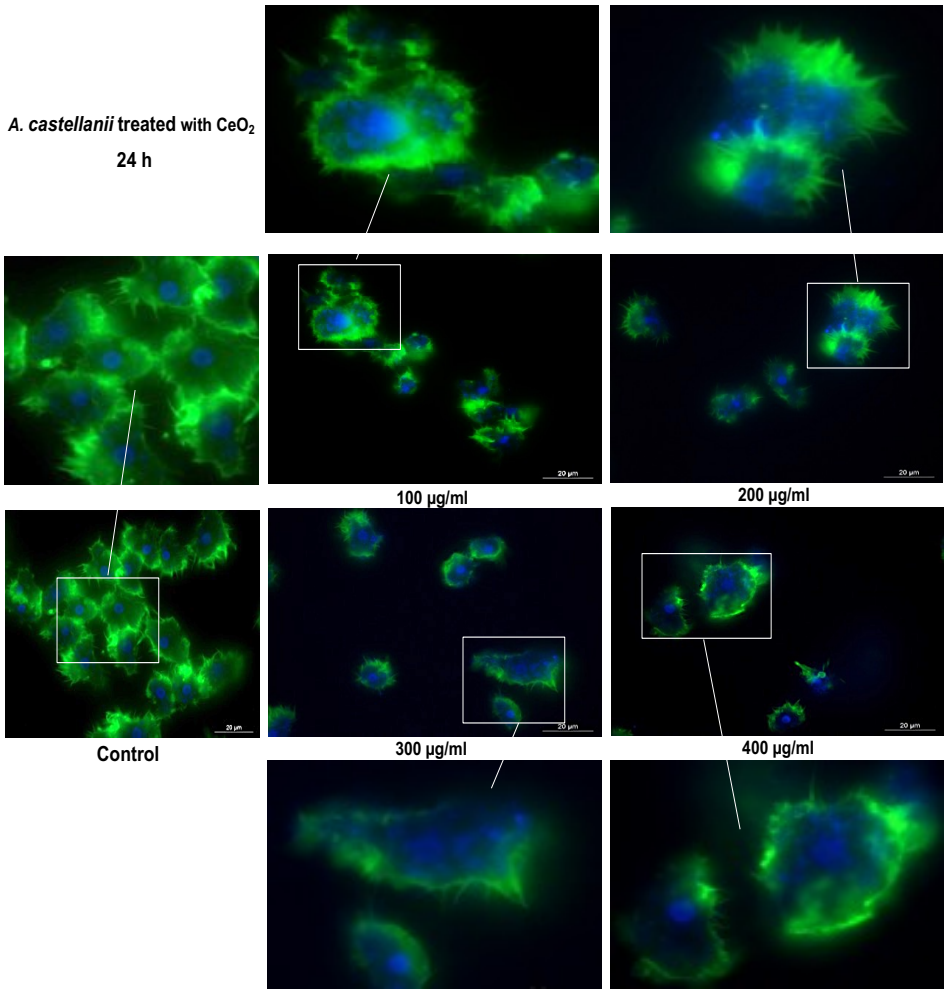

Figure 6-12, B. The effect of CeO_2NPs on fluorescence staining of the actin cytoskeleton and nucleus of *A. castellanii* trophozoites after 24 h.

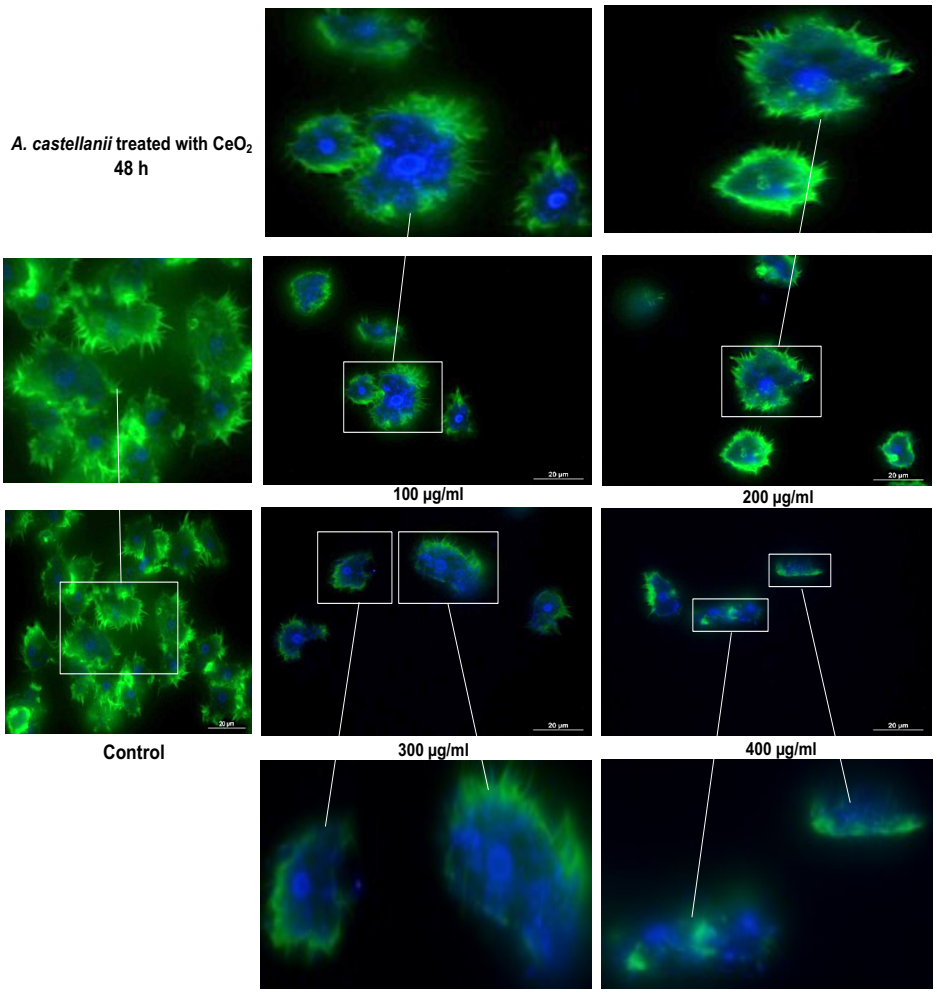

Figure 6-12, C. The effect of CeO_2NPs on fluorescence staining of the actin cytoskeleton and nucleus of *A.castellanii* trophozoites after 48 h.

6.3.6 Acridine orange staining for *A. castellanii*

AO staining was used to test the toxic effects of exposure to various concentrations of CeO_2NPs (100, 200, 300 and 400 µg/mL) on *A. castellanii* for 3, 24 and 48 h (Figures 6-13 and 6-14, A-C). AO, a membrane-permeable cationic dye, selectively binds to RNA or DNA of viable cells, emitted a green fluorescence when binding with DNA, whereas the binding with

RNA in the cytoplasm emitted an orange-red fluorescence, thereby indicating the presence of non-viable cells. These results demonstrated concentration-dependent changes in the fluorescence (green to orange-red) of trophozoites that were treated with CeO_2NPs at all concentrations for 3, 24 and 48 h, when compared with controls.

Trophozoite density was high in controls when compared with treated trophozoites, indicating a gradual concentration-dependent reduction (Figure 6-13). Furthermore, CeO_2NPs caused a significant reduction in the numbers of trophozoites at all investigated incubation times, except for 3 h in 100 µg/mL.

Figure 6-14 (A-C) illustrates the untreated trophozoites (stained green) showing the usual morphology. A fluorescence microscope, with the ability to distinguish viable trophozoites from non-viable ones, was used to view the morphological changes in *A. castellanii*. The green-stained trophozoites indicate intact membranes, organelles and nuclei. However, those that were stained orange, or those that were stained green with the granules in the trophozoites stained red or orange, were either not intact or dead. Moreover, in these specimens, the *A. castellanii* cystic form was rarely observed.

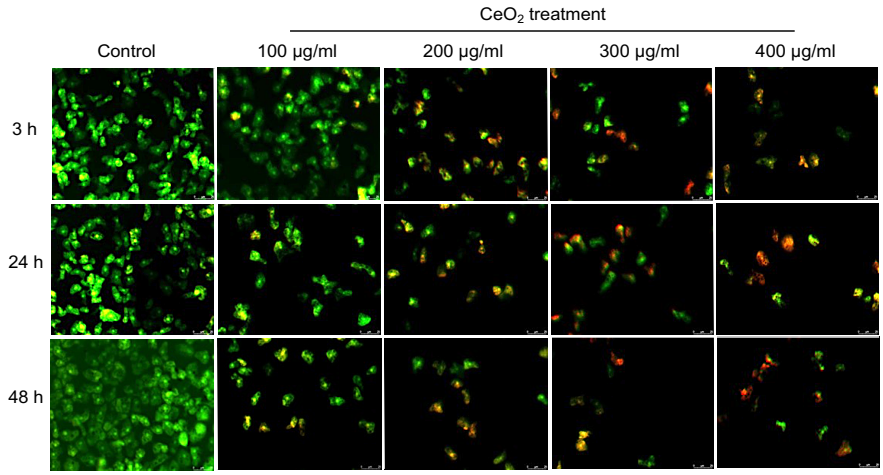

Figure 6-13. The effect of CeO_2NPs on *A. castellanii* revealed by AO fluorescence staining. *A. castellanii* trophozoites were incubated in CeO_2NPs at the indicated concentrations and duration. Trophozoites were fixed with paraformaldehyde and glutaraldehyde (4% and 0.5%) for 10 min, and then stained with AO. Images were obtained with an inverted wide-field fluorescence microscope. Scale bar (25 µm) applies to all images. The experiment was performed three times with 2 technical replicates per-experiment.

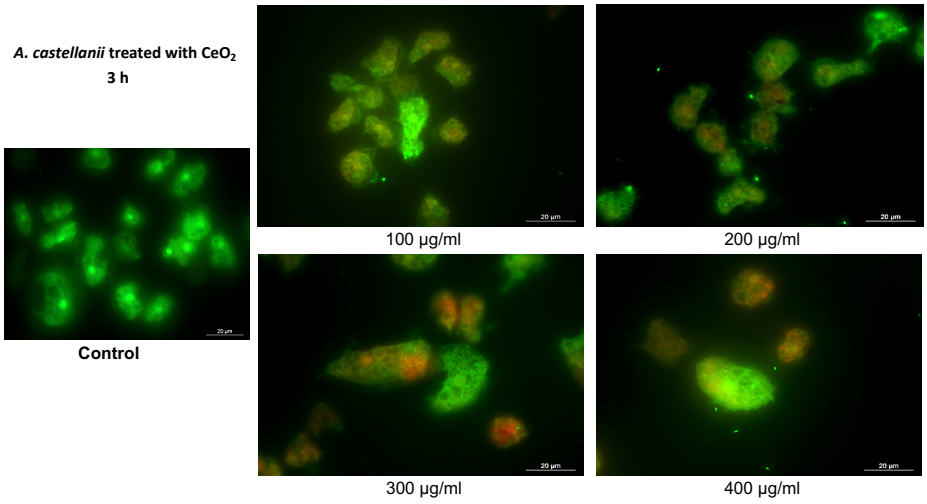

Figure 6-14, A. The effect of CeO_2NPs on *A. castellanii* revealed by AO fluorescence staining. *A. castellanii* trophozoites were incubated in CeO_2NPs at the indicated concentrations for 3h (A), 24h (B) and 48h (C). Trophozoites were fixed with paraformaldehyde and glutaraldehyde (4% and 0.5%) for 10 min, then stained with AO. Cultures emitted either a green fluorescence, indicating healthy trophozoites, or an orange/red fluorescence indicating unhealthy trophozoites. Images were obtained using an inverted wide-field fluorescence microscope. Scale bar (20 µm) applies to all images. The experiment was performed three times with 2 technical replicates per-experiment.

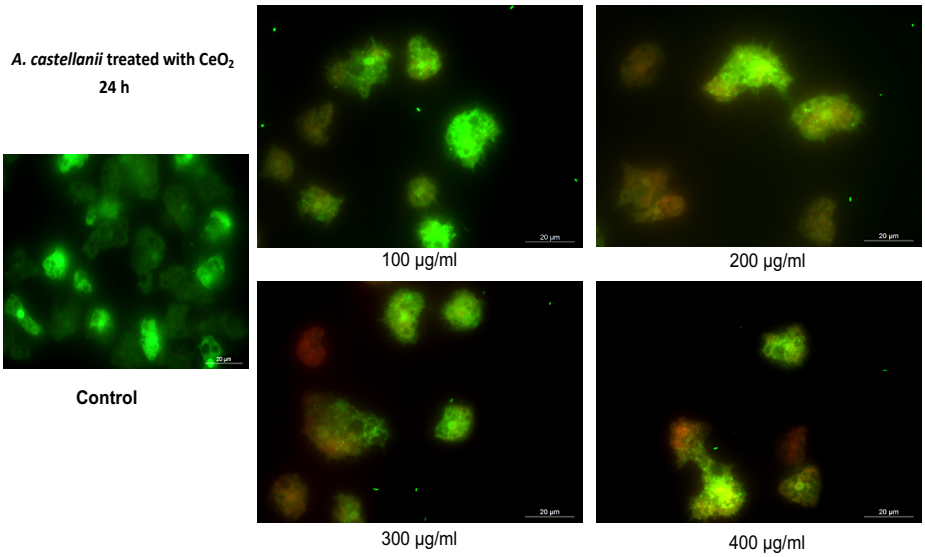

Figure 6-14, B. The effect of CeO_2NPs on *A. castellanii* using AO fluorescence staining for 24 h.

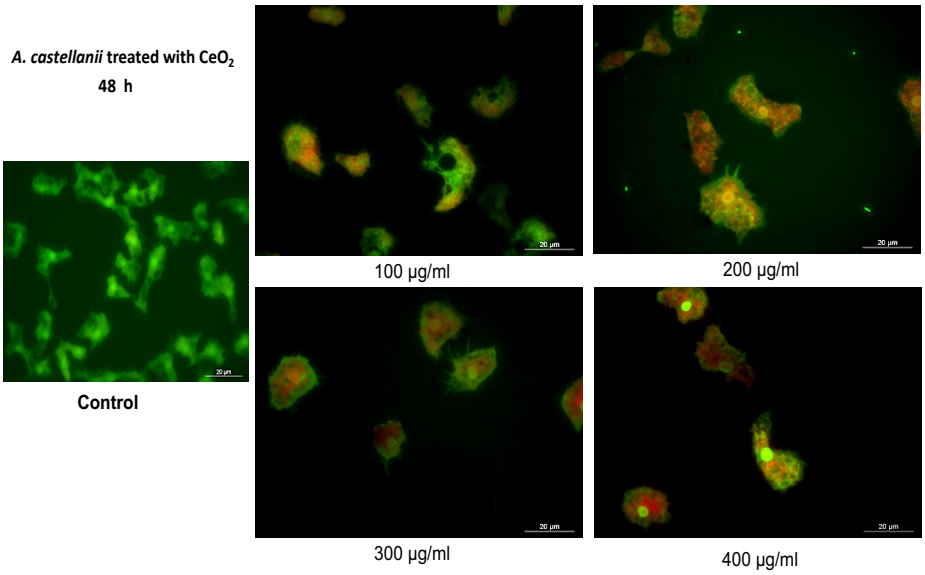

Figure 6-14, C. The effect of CeO_2NPs on *A. castellanii* using AO fluorescence staining for 48 h.

6.3.7 CeO_2NPs inhibit encystation of *A. Castellanii*

We examined the effect of CeO_2NPs on *A. castellanii* encystation following exposure to various doses (100, 200, 300 and 400 µg/mL) at 25 °C for 48 h (Figure 6-15 and Table 6-2). The results showed a gradual concentration-dependent decrease in encystation in the treated *A. castellanii* cultures at all concentrations, compared with the control. Exposure of *A. castellanii* to increasing concentrations of CeO_2NPs (100, 200, 300 and 400 µg/mL) did significantly inhibit encystation after 48 h of incubation. Untreated *A. castellanii* showed 100% encystation; while 100, 200 and 300 and 400 µg/mL concentrations of CeO_2NPs showed 86%, 80%, 69% and 56% encystation, respectively. The results indicated that CeO_2NPs significantly inhibited encystations of *A. castellanii* at all concentrations compared with control.

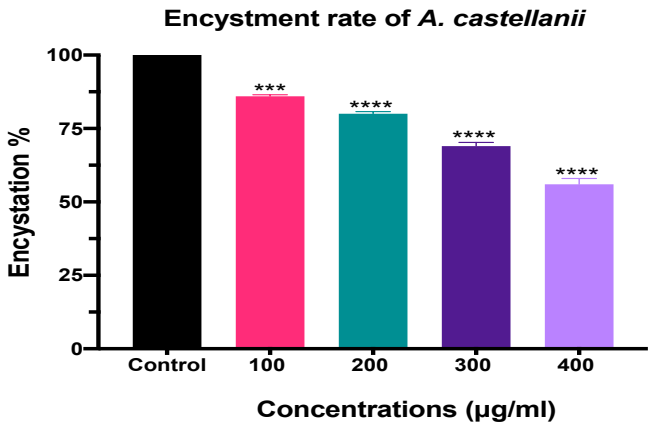

Figure 6-15. The impact of CeO_2NPs on the encystation of *Acanthamoeba castellanii*. Cultured trophozoites were incubated in various concentration of CeO_2NPs (100, 200, 300 and 400 µg/mL) mixed with an encystment buffer, at 25 °C for 48 h. Trophozoites treated with the encystment buffer alone were used as control. Data are presented as percentage of encystation rates relative to untreated (control) trophozoites. A two-way ANOVA showed significant differences between the treated cells and the controls. The experiment was performed three times with 2 technical replicates per-experiment.

Table 6-2. The percentage of encystation rates of *Acanthamoeba*-exposed to CeO_2NPs compared to control. The encystment percentage calculated by (Post-SDS / Pre-SDS × 100) after pre- and post-treatment with sodium dodecyl sulphate (SDS).

CeO_2 µg/ml	Pre-SDS average	Post-SDS average	Mean ± SD	Encystation rate Post-SDS / Pre-SDS * 100
Control*	7	7	7 ± 0	100%
100	7	6	6.5 ± 0.5	86%
200	7.5	6	6.75 ± 0.75	80%
300	8	5.5	6.75 ± 1.25	69%
400	9	5	7 ± 2	56%

Encystment buffer without any contribution from CeO_2 (Control*).

6.3.8 The effects of CeO_2NPs on the viability of CSCs and ihCECs

Figure 6-16 shows the cytotoxic effects of CeO_2NPs on corneal cells. The SRB and alamarBlue® assays showed a gradual concentration-dependent increase in cell proliferation and viability for CSCs and ihCECs treated with CeO_2NPs at all concentrations, when compared with controls, following 3, 6, 24 and 48 h of incubation. However, there was no significant difference between any of the cultures, apart from ihCEC after 48 h in 300 and 400 µg/mL (figure 6-16, D) which were significantly reduced. Cell viability, measured by an alamarBlue® assay, was observed to be a higher in treated cells than in controls.

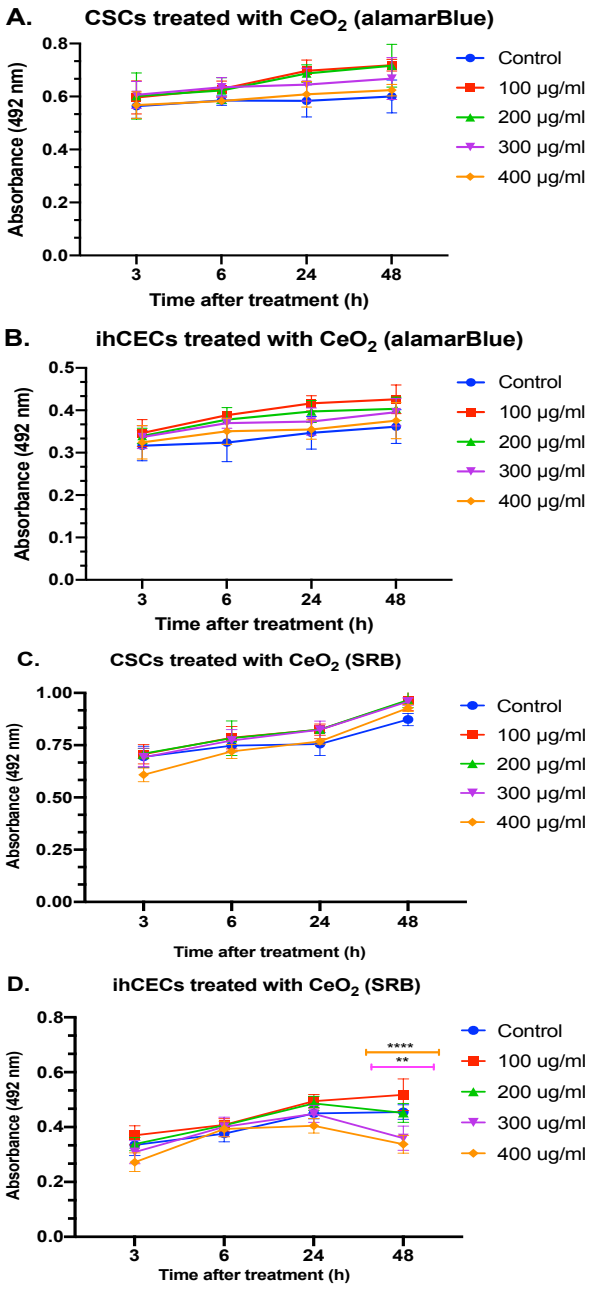

Figure 6-16. The effect of CeO_2NPs on the viability and proliferation of CSCs and ihCECs using alamarBlue (A-B) and SRB (C-D) assays. Cultured CSCs or ihCECs were incubated in various concentration of CeO_2NPs (100, 200, 300 and 400 µg/mL) at 37 °C for 3, 6, 24 and 48 h. Cells treated with M199 or EpiLife™ medium were used as control. Absorbance values (at 492 nm) are presented as mean ± SDs of 4 technical replicates, and each experiment was replicated three times. A two-way ANOVA showed non-significant differences between the treated cells and the controls, except for ihCECs after 48 h in 300 and 400 µg/mL where there was a significant effect.

6.3.9 Short-term cytotoxic effects of CeO_2NPs on CSCs and ihCECs

The cytotoxic effects of CeO_2NPs on CSCs and ihCECs following short-term (one hour) exposure to different concentrations of CeO_2NPs (100, 200, 300 and 400 µg/mL) was examined using alamarBlue® and SRB assays (Figures 6-17, A-D). The results showed a gradual concentration-dependent reduction in cell viability and proliferation of cells treated with CeO_2NPs when compared with controls, particularly at high concentrations with 300 and 400 µg/mL CeO_2NPs. However, exposure of corneal cells to these concentrations of CeO_2NPs showed non-significant differences after 48 h of re-incubation. The cytotoxic effects of CeO_2NPs on CSCs, or ihCECs, in response to high concentrations of CeO_2NPs (500 and 1000 µg/mL) for a period of one hour, was also investigated using alamarBlue® and SRB assays (Figures 6-18, A-D). Non-significant differences were observed in cell viability and proliferation at all concentrations, compared to controls, for both types of corneal cells after 48 h of re-incubation.

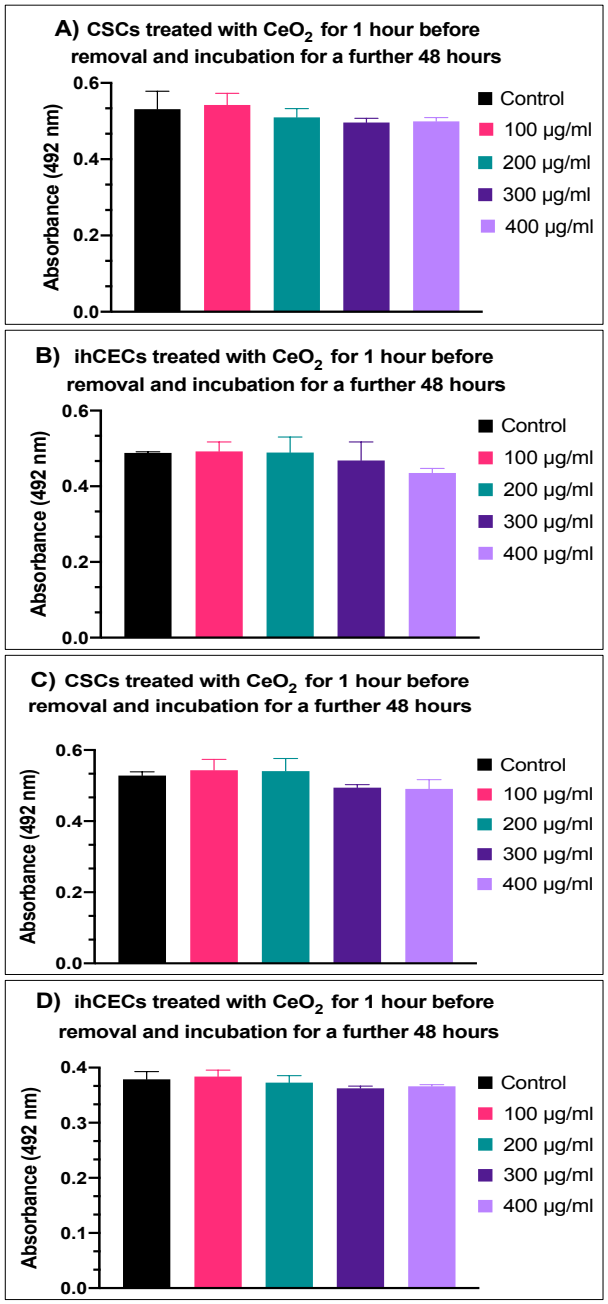

Figure 6-17. The effect of CeO_2NPs on the viability and proliferation of CSCs and ihCECs revealed SRB (A-B) and alamarBlue (C-D) assays. Cultured CSCs or ihCECs were incubated in various concentration of CeO_2NPs (100, 200, 300 and 400 µg/mL) at 37 °C for 1 h, then re-incubated in fresh M199 or EpiLife™ medium at 37 °C for 48 h. Cells treated with M199 or EpiLife™ medium were used as control. Data are presented as mean ± SD of absorbance values (at 492 nm) relative to untreated (control) cells. A two-way ANOVA showed non-significant differences between treated cells and the controls. Each experiment was performed three times with 4 technical replicates per-experiment.

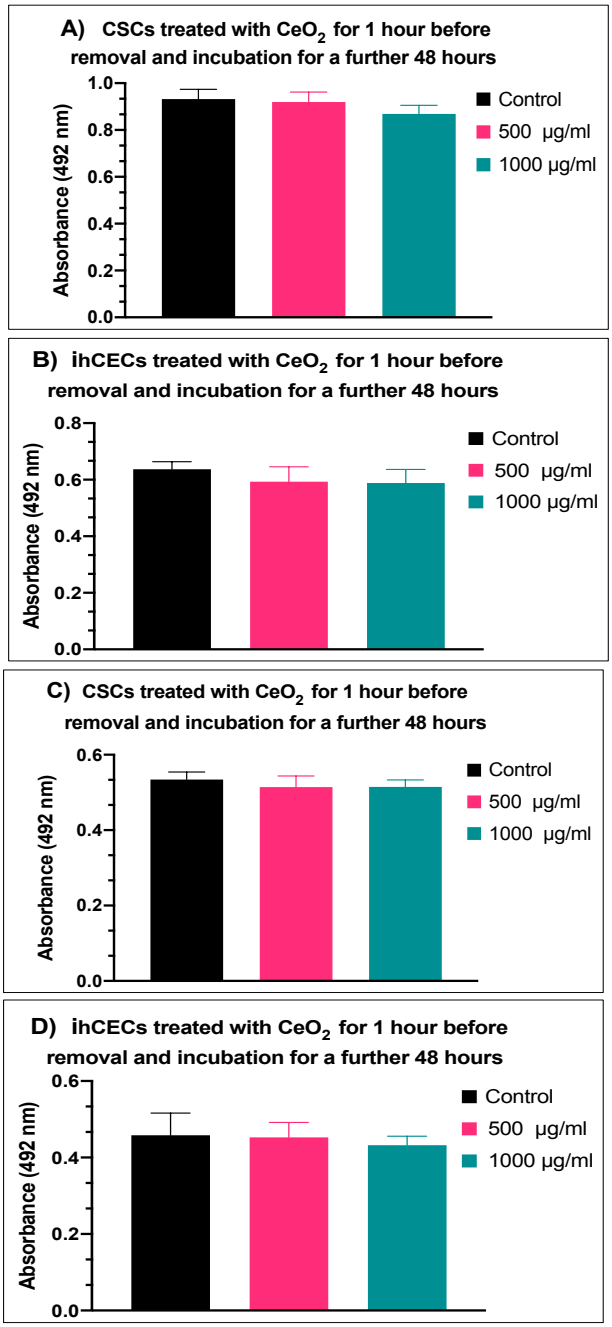

Figure 6-18. The effect of CeO_2NPs on the viability and proliferation of CSCs and ihCECs, determined by SRB (A-B) and alamarBlue (C-D) assays. Cultured CSCs or ihCECs were incubated in high concentrations of CeO_2NPs (500 and 1000 µg/mL) at 37 °C for one h, then re-incubated in fresh M199 or EpiLife™ medium at 37°C for 48 h. Cells treated with M199 or EpiLife™ medium were used as control. Data are presented as mean ± SD of absorbance values (at 492 nm) relative to untreated (control) cells. A two-way ANOVA showed non-significant differences between treated cells and the controls. Each experiment was performed three times with 4 technical replicates per-experiment.

6.3.10 Actin cytoskeleton disruption in CSCs and ihCECs

We examined the effect of CeO_2NPs on the actin cytoskeleton of cultured CSCs and ihCECs exposure to different doses of CeO_2NPs for 3, 24 and 48 h (Figures 6-19 and 6-20, A-C). Cell morphology showed no changes up to 48 h. The treated cells showed a similar morphology to the controls. The surfaces of both treated corneal cell-types were covered with CeO_2NPs but were more clearly seen in ihCECs as nanotubular structures on the cells. Actin images of CeO_2NP-treated ihCECs revealed more detrimental structural changes than seen CSCs, particularly after 48 h with 300 and 400 µg/mL CeO_2NPs.

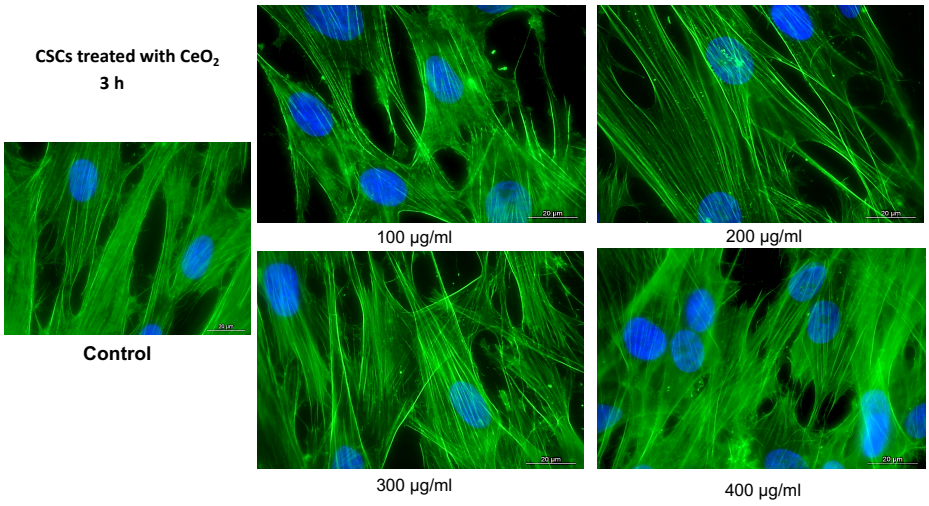

Figure 6-19, A. The effect of CeO_2NPs on fluorescence staining of actin cytoskeleton. CSCs were incubated with CeO_2NPs at the indicated concentrations for 3h (A), 24h (B) and 48h (C). CSCs were fixed with 4 percent paraformaldehyde by 10 min and stained with phalloidin (actin) and DAPI (nucleus). Images were obtained using an inverted wide-field fluorescence microscope. Scale bar (20 µm) applies to all images. The experiment was performed three times with 2 technical replicates per-experiment.

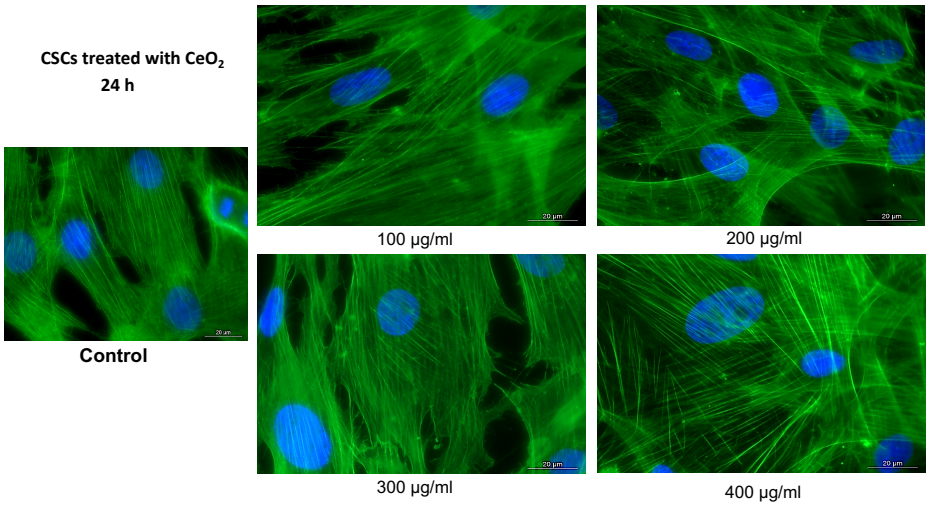

Figure 6-19, B. The effect of CeO_2NPs on fluorescence staining of the actin cytoskeleton and nucleus of CSCs after 24 h.

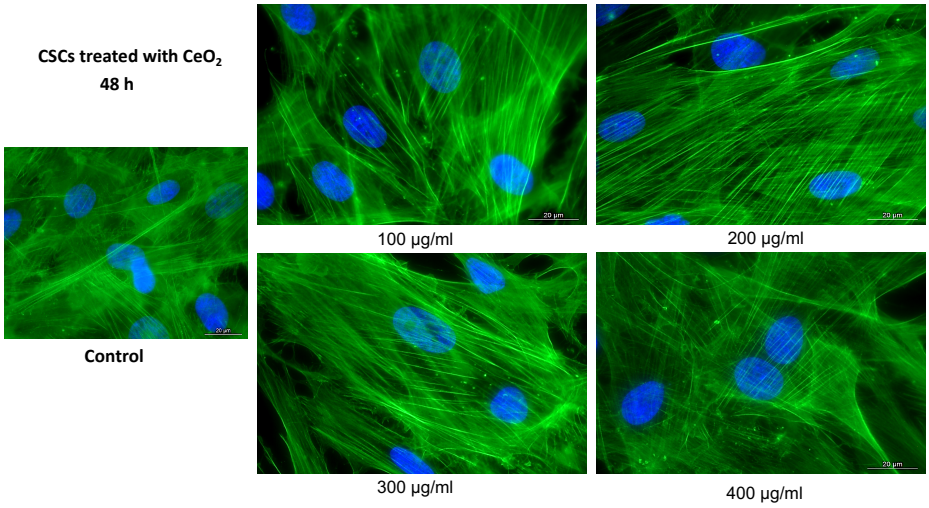

Figure 6-19, C. The effect of CeO_2NPs on fluorescence staining of the actin cytoskeleton and nucleus of CSCs after 48 h.

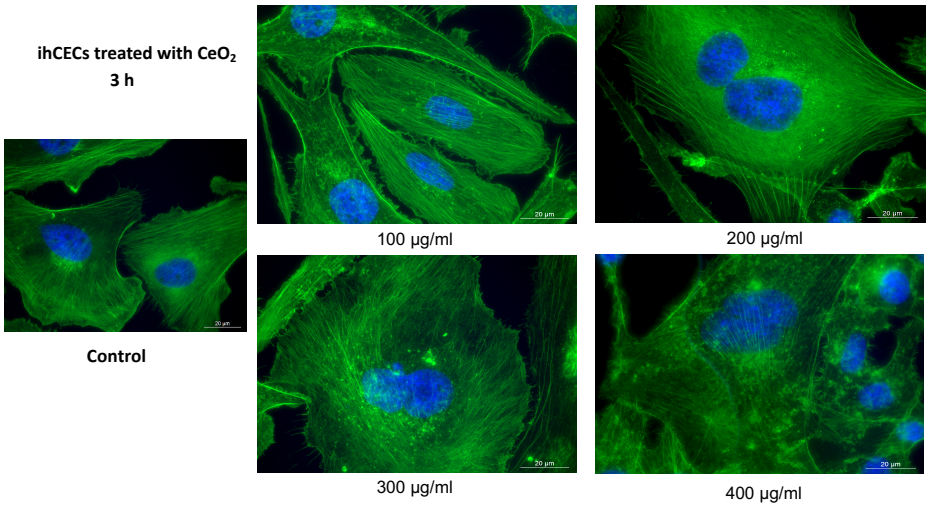

Figure 6-20, A. The effect of CeO_2NPs on fluorescence staining of the actin cytoskeleton of ihCECs incubated in CeO_2NPs at the indicated concentrations for 3h (A), 24h (B) and 48h (C). The ihCECs were fixed with 4 percent paraformaldehyde for 10 min and stained with phalloidin (actin) and DAPI (nucleus). Images were obtained using an inverted wide-field fluorescence microscope. Scale bar (20 µm) applies to all images. The experiment was performed three times with 2 technical replicates per-experiment.

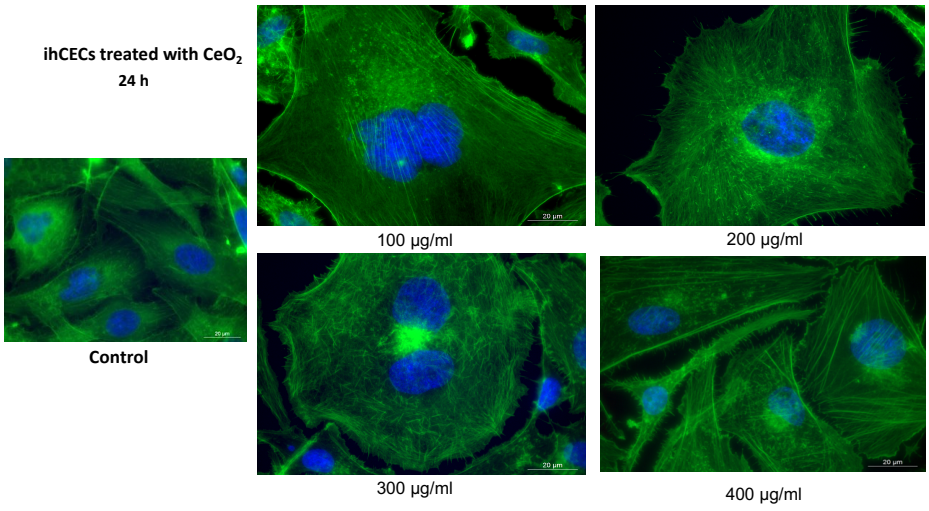

Figure 6-20, B. The effect of CeO_2NPs on fluorescence staining of the actin cytoskeleton and nucleus of ihCECs after 24 h.

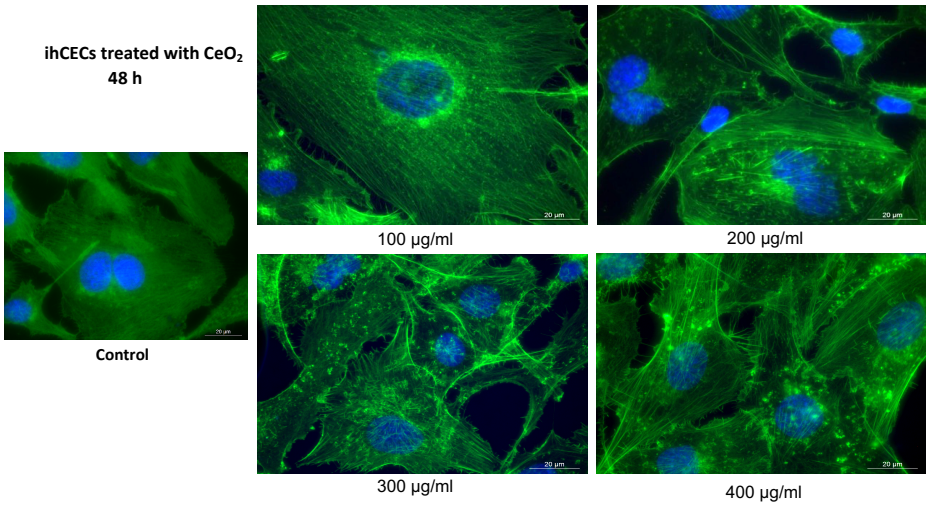

Figure 6-20, C. The effect of CeO_2NPs on fluorescence staining of the actin cytoskeleton and nucleus of ihCECs after 48 h.

6.3.11 Acridine orange staining for the corneal cells

Corneal cells were incubated in various concentrations of CeO_2NPs (100, 200, 300 and 400 µg/mL) for 3, 24 and 48 h, in order to examine cytotoxicity (Figures 6-21 and 6-22, A-B). AO staining characteristics of corneal cells varied according to their stage. Green-fluorescent untreated corneal cells (controls) showed normal cell morphology, indicated by the intact structure of the organelles as illustrated in figures 6-21 and 6-22, A-B.

Moreover, treated corneal cells were stained green, and observed to have normal morphology, particularly after 3 and 24 h in 100, 200, 300 and 400 µg/mL CeO_2NPs. This showed that intracellular organelles were intact, and that CeO_2NPs had no impact on the corneal cells' viability, assessed by morphological criteria following AO staining (Figures 6-21 and 6-22, A-B).

Fluorescence microscopy showed the impact of incubating corneal cells in CeO_2NPs for 48 h, particularly at high concentrations with 300 and 400 µg/mL CeO_2NPs. This included an array of condensation of chromatin and cytoplasm cell shrinkage. Some cells emitted a bright-orange fluorescence and had a round shape, possibly indicating dead cells or cells whose organelles were not intact (Figures 6-21 and 6-22, C).

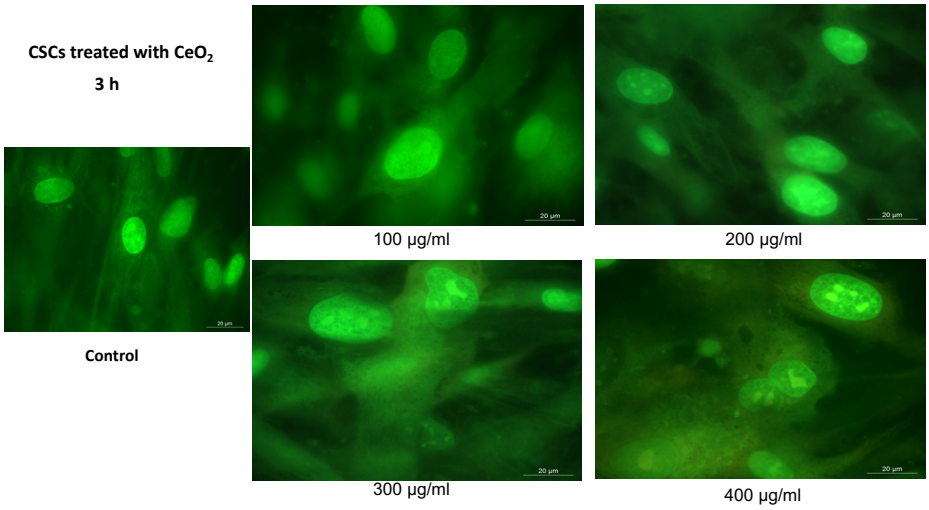

Figure 6-21, A. The effect of CeO_2NPs on CSCs revealed by AO staining. CSCs were incubated in CeO_2NPs at the indicated concentrations for 3 h (A), 24 h (B) and 48 h (C). CSCs were fixed with 4 percent paraformaldehyde for 10 min and stained with AO. Images were obtained with an inverted wide-field fluorescence microscope. Scale bar (25 µm) applies to all images. The experiment was performed three times with 2 technical replicates per-experiment.

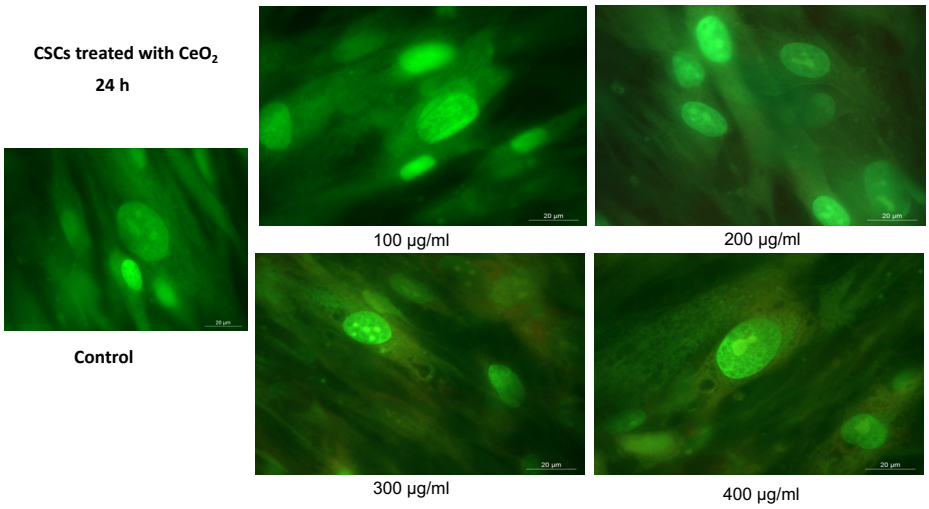

Figure 6-21, B. The effect of CeO_2NPs on CSCs revealed by AO staining after 24 h.

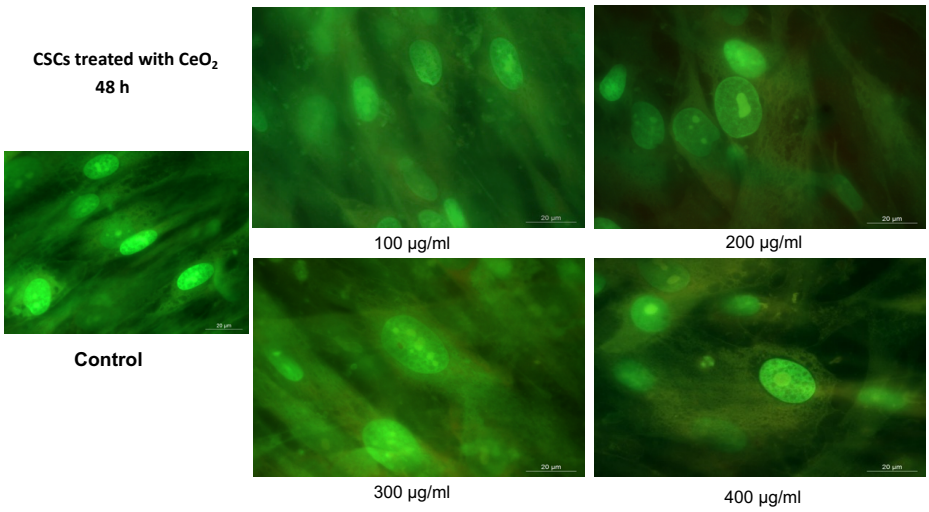

Figure 6-21, C. The effect of CeO_2NPs on CSCs revealed by AO staining after 48 h.

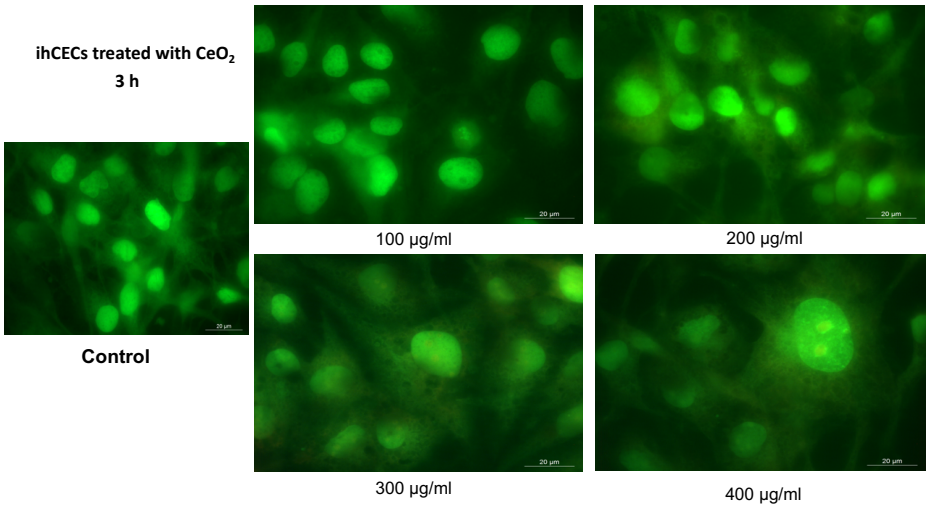

Figure 6-22, A. The effect of CeO_2NPs on ihCECs revealed by AO staining. The ihCECs were incubated in CeO_2NPs at the indicated concentrations for 3h (A), 24h (B) and 48h (C); then fixed with 4% paraformaldehyde for 10 min and stained with AO. Images were obtained using an inverted wide-field fluorescence microscope. Scale bar (25 µm) applies to all images. The experiment was performed three times with 2 technical replicates per-experiment.

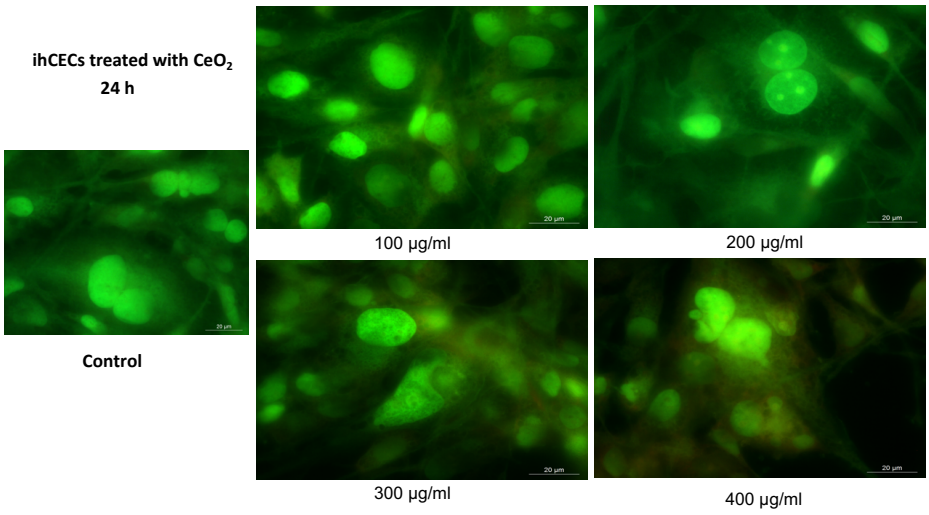

Figure 6-22, B. The effect of CeO_2NPs on ihCECs revealed by AO staining after 24 h.

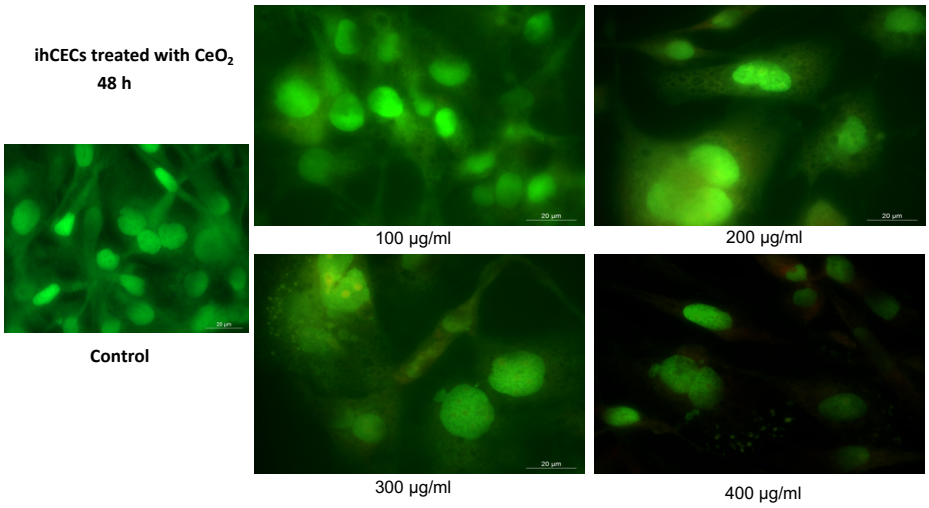

Figure 6-22, C. The effect of CeO_2NPs on ihCECs revealed by AO staining after 48 h.

6.4 Discussion

The effect of CeO_2NPs on *Acanthamoeba castellanii* and corneal cells was assessed *in vitro* by measuring several parameters including cell proliferation, viability and morphology. To date, no study has examined the effect of CeO_2NPs on *A. castellanii* and corneal cells. The data showed a significant dose-dependent reduction in cell proliferation and viability; and effects on the morphology of *A. castellanii* when treated with doses of 200 µg/mL and above. CeO_2NPs had no significant effect on corneal cells, and up to 200 µg/mL with no indications of a decrease in viability, proliferation or damage to actin. This demonstrates that the CeO_2NPs are slightly more effective at killing *Acanthamoeba*

than corneal cells and there may be a dose of around 200 µg/mL where balance of damage can be achieved.

Initial experiences in comparing the toxic effects of nanoparticles (NPs) on *A. castellanii* and corneal cells, using the SRB assay, revealed that all NPs exhibited activity in *A. castellanii* when treated with doses above 100 µg/mL of concentrations examined. The results indicated that the strongest effects were induced by CeO_2NPs, then SeNPs, with the weakest effects being induced by AgNPs. Additionally, SeNPs had the strongest effects on corneal cells, followed by AgNPs and then CeO_2NPs. Based on these findings, further experiments were performed only using various concentrations of CeO_2NPs (100, 200, 300 and 400 µg/mL) as a result of the better balance found between antimicrobial activity against *A. castellanii* and toxic effect corneal cells.

However, further analysis was performed to calculate the selectivity index (SI) of all NPs for evaluating the toxic effect of NPs on corneal cells. Based on this analysis, the results showed that the CeO_2NPs are not very safe for the mammalian host cells. The SI at all time points analysed is either below 1 (which means the NPs are toxic to host cells) or just more than 1 (which is not high enough to consider NPs safe). Perhaps other types of

NPs or modified derivatives of CeO_2NPs might be safer but this requires further research.

In terms of the anti-*Acanthamoeba* activities of CeO_2NPs against cysts and trophozoites, our findings revealed that CeO_2NPs are inhibitors of the replication of *A. castellanii* trophozoites *in vitro*. It was shown by the SRB assay, cell count and light microscopy results a concentration-dependent gradual decrease in the viability and proliferation of *Acanthamoeba castellanii* in treated groups for the majority of treatments, compared with controls, for each of the incubation periods, apart from 3 hours which was not enough to impair trophozoite growth. Recently, the effects of CeO_2NPs on different bacteria have also been studied (Dos Santos *et al.*, 2014; Babenko *et al.*, 2012; Bellio *et al.*, 2018). Taken together these findings indicate that CeO_2NPs exhibit antimicrobial effects *in vitro*.

Our results indicated that CeO_2NPs had toxic effects on *A. castellanii*. We examined the toxic effects on *A. castellanii* after short-term (one hour) exposure to various CeO_2NP doses (100, 200, 300,400,500 and 1000 µg/mL) followed by re-incubation in PYG medium for 48 hours. Cells were then counted and subjected to a SRB assay. The findings show significant reduction in the viability and proliferation of *Acanthamoeba castellanii* following a brief period of exposure to CeO_2NPs

(except for 100 µg/mL) which concur with the results from our extended exposure assay. These findings confirm that *Acanthamoeba castellanii* is sensitive to short-term toxic effects of CeO_2NPs. This may be therapeutically beneficial for preventing infection, while avoiding the toxicity and harm caused to human cells by extended treatment.

A specific problem in anti-acanthamoebic therapy is the cystic stage of *A. castellanii* as a result of its inherent resistance to the majority of drugs. Encystment usually occurs when the parasite is exposed to harsh conditions, such as the use of therapeutic agents, variation in pH, or lack of certain nutrients. According to our findings, CeO_2NPs demonstrated anti-encystment activity by preventing *A. castellanii* trophozoites from forming cysts, leading to a significant reduction in the *A. castellanii* encystment rate. It is possible that the CeO_2NPs could be used to target the encystment process to slow it or prevent the formation of cysts, thus creating an environment that favours the growth of the active form of the parasite, which is the trophozoite. The inhibition of encystment in *A. castellanii* using CeO_2NPs is a potential therapeutic approach, or in combination with chemotherapeutic products for the development of drugs against *A. castellanii*, but it requires further analysis to examine the viability of corneal cells following treatment with the CeO_2NPs.

We conducted experiments to demonstrate the effect of long-term and short-term exposure of corneal cells to CeO_2NPs. The outcomes of these studies demonstrated that CeO_2NPs did not show a toxic effect on corneal cells up to 200 µg/mL, with no significant decrease in viability, proliferation or damage to actin, although some minor damage may have occurred, except for ihCECs in the long-term incubation at 48 hours in concentrations of 300 and 400 µg/mL, where there was a significant effect. Short-term treatment of corneal cells with CeO_2NPs (1 hour, then removed) at concentrations of (300 and 400 µg/mL, 500 and 1000 µg/mL,) exhibited some inhibitory effects on the growth of corneal cells, although these were not significant. This difference between the more acute toxicity on *Acanthamoeba* balanced with less toxicity to corneal cells, after 1 hour treatment, may offer a potential treatment route that control overall damage to the human cells. It should be noted that multiple factors are influential on the toxicity profile, such as the Ce^{+3}/Ce^{+4} ratio, size of the particle, purity, morphology, adsorption, cell line used, as well as aggregation and sedimentation (Lin *et al.*, 2021; Asati *et al.*, 2010). Hence, a formulation of degree of safety must consistently be evaluated according to the specific case.

These outcomes concur with those of other researchers who studied the toxicity of CeO_2NPs in human lens epithelial (HLEC) cells by analysing different indicators of cellular health. The findings revealed that CeO_2NPs did not show cytotoxic effect on the cells up to dose at 200 µg/mL. At an elevated concentration of (400 µg/mL), CeO_2NPs initiated the production of ROS, which acts as a mediator in cellular apoptosis (Hanafy *et al.*, 2020; Hanafy *et al.*, 2019). Regardless of the safety of a formulation, toxic or unwanted effects could be caused by an overdose. There is insufficient knowledge regarding the cytotoxic effects of CeO_2NPs when increased concentrations are utilised. Hence, further research is required to test the potential cytotoxic effects on corneal intracellular components following exposure to CeO_2NPs *in vitro*.

Disruption of the actin cytoskeleton indicates damage to cells, and is also pivotal for infection establishment by a variety of protozoan pathogens. It has been demonstrated that disrupting the actin filament system of protozoans prevented trophozoites from adhering to polymorphonuclear cells (Soto-Arredondo *et al.*, 2014); with a potentially significant impact on the protozoan's integrity, function and survival. In this study, we examined how CeO_2NPs affect actin cytoskeleton arrangement, by investigating structural changes in cultured trophozoites treated with different

doses of CeO_2NPs for 3, 24 and 48 hours. The actin cytoskeleton was mildly disrupted after 3 hours, but disruption increased, with trophozoite shape deformities, at higher concentrations and longer treatment periods. The highest level of cytotoxicity was observed after incubation in CeO_2NPs for 24 hours, which led to increased trophozoite damage. The effect of CeO_2NPs on the actin cytoskeleton arrangement in both types of corneal cells, treated under identical conditions as described, was also investigated. It was seen that the actin cytoskeleton exhibited mild disruption at increased concentrations and longer treatment periods. The cytotoxic effects of CeO_2NPs in ihCECs were more noticeable than those detected in CSCs, particularly with concentrations of 300 and 400 µg/mL. This warrants further investigation as these disruptions could indicate potential long-term cytotoxicity. However, the effect on human cells was less pronounced than seen on *Acanthamoeba*.

Although the pathway of action of CeO_2NPs has been widely investigated, their mechanism of action has yet to be completely described. Previous work on bacteria has shown that cell membranes are destabilised by NPs, and the plasmatic membrane potential collapses. In addition, recent studies have revealed that oxidative damage is caused within cells by NPs, which can be detrimental to the genetic structure of the

microorganism, impacting replication (Aderibigbe, 2017; Wang, Hu and Shao, 2017; Farias, Santos and Sampaio, 2018). It appears that CeO_2NPs exhibit a multi-targeted mode of action that underlies their antifungal, antimicrobial and antiprotozoal properties.

In our study, we demonstrated the mechanism of action of CeO_2NPs in *Acanthamoeba castellanii* using TEM. Our findings confirmed that trophozoites phagocytosed the CeO_2NPs, which then accumulated within their vesicles. The CeO_2NPs were transported to the cell's nucleus for their toxicity to be exerted by causing damage to the nucleus. Hence, CeO_2NPs can enter the nucleus and subsequently exert their toxicity. It is therefore clear that CeO_2NPs can kill *A. castellanii* after 24 and 48 hours.

Several research groups have used TEM to confirm that endocytosis is the most common mechanism for NPs uptake. It has also been identified that all NPs were internalised as agglomerates, which do not appear to have a significant effect on cells as the NP agglomerates' sizes were all approximately the same (~400 nm) (Magdolenova *et al.*, 2012; Xia, Rome and Nel, 2008; Franchi *et al.*, 2015). However, the mechanism of uptake and localisation of CeO_2NPs in human lens epithelial (HLEC) cells were explained. It was shown that non-toxic concentrations of CeO_2NPs rapidly enter HLEC in as little as 15

minutes. The uptake largely continued via energy-dependent endocytosis. Researchers have shown that CeO_2NPs are predominantly localised within the cells' cytoplasm, specifically the mitochondria. As a result of the efficiency with which the CeO_2NPs enter the HLEC, they are able to apply anti-cataract effects (Hanafy *et al.*, 2021).

Our findings indicate that CeO_2NPs significantly affected *A. castellanii* by effectively targeting the nuclei, resulting in damage to the components of the nucleus. These findings differ from tests involving human corneal cells, as the viability and proliferation of the cells were not as significantly impacted, except for ihCECs incubated at 48 hours in concentrations of 300 and 400 µg/mL. Hence, it appears that CeO_2NPs exhibit more toxicity in *A. castellanii* than human corneal cells. This distinction may be explained by the fact that *A. castellanii* is an organism that is capable of easily phagocytosing CeO_2NPs, which facilitates the accumulation of CeO_2NPs within the vesicles and enables subcellular targeted effects. Conversely, CeO_2NPs also have the ability to traverse membranes of the organisms' cells and were predominantly detected in endocytic vesicles (Franchi *et al.*, 2015), or in the mitochondria (Hanafy *et al.*, 2019); although the probability of these particles penetrating the inner components of the cell is negligible as a result of the

particle's size and/or intercellular agglomeration (Pešić *et al.*, 2015). Our findings indicate that CeO_2NPs can potentially be used as therapeutic agents against *A. castellanii*. However, more research is required to further elucidate their mechanism of action and to fully determine the potential level of cytotoxicity of corneal cells and how this may affect the tissue in vivo.

A. castellanii trophozoites were exposed to CeO_2NPs for 3, 24 and 48 hours and then stained with acridine orange (AO). Untreated trophozoites were observed as green fluorescent, indicating cell viability and that the organelles were intact. Conversely, following treatment, the trophozoites showed organelle damage by the orange/red fluorescence within their cytoplasm, which could be differentiated from viable trophozoites that had not been treated. This is caused by the binding of the AO stain to healthy DNA within the nucleus, which produces the detected green fluorescence. Treated trophozoites exhibited organelle damage by the RNA within the cytoplasm exhibiting an orange/red colour. When the DNA within the nucleus of untreated corneal cells was stained, a green fluorescence was produced, whereas an orange/red colour was emitted by the RNA within the cytoplasm in treated samples at increased concentrations and prolonged periods of exposure. Thus, it was demonstrated that the CeO_2NPs used in this study damaged the

organelles of *Acanthamoeba*, but did not affect corneal cells to such a high degree.

In summary, the findings reported in this study show that CeO_2NPs had inhibitory effects against both forms of *A. castellanii* and showed less effects to corneal cells up to 200 µg/mL. Further investigation is required to examine the synergistic effects of CeO_2NPs or in combination with chemotherapeutic products used against *A. castellanii*.

7. Chapter Seven: General Discussion and Conclusion

7.1. Overview of the thesis

Outbreaks of Acanthamoeba keratitis (AK), caused by *Acanthamoeba* infection, frequently cause blindness and are becoming more prevalent, probably as a result of the growing use of contact lenses (Carnt *et al.*, 2018). Nevertheless, it is increasingly acknowledged that *Acanthamoeba* infections represent a significant cause of keratitis in people who do not wear contact lenses (Demirci *et al.*, 2006). Amoebic infection can also arise when the cornea is accidentally injured then exposed to water contaminated with *Acanthamoeba* (Marciano-Cabral and Cabral, 2003). The thesis findings indicate that *A. castellanii*-conditioned medium (ACCM) containing different soluble factors that are crucial virulence factors and contribute to the pathogenesis and cytopathic effect of *Acanthamoeba* infection (Panjwani, 2010). A variety of drugs have been suggested for treating *Acanthamoeba*, such as antimicrobial chemotherapy. However, such treatment is faced with a number of problems including the lengthy time required for therapy and the toxicity of the drugs with regard to the cornea; in addition to the fact that the morphological transformation of trophozoites occurs rendering them harder to kill (Niyyati, Dodangeh and

Lorenzo-Morales, 2016). *In vitro* testing of cerium oxide nanoparticles (CeO_2NPs) has largely been undertaken to determine their activity on pathogenic microorganisms (Dos Santos *et al.*, 2014; Babenko *et al.*, 2012). Therefore, this chapter presents a summary of the work targeted at the characterisation and examination of the effect of ACCM on corneal cells, and the investigation of CeO_2NPs' effects on both *A. castellanii* and corneal cells.

7.2. Key findings:

7.2.1. Comparative cytotoxicity of ACCM on human corneal cells

The mechanism underlying damage induced by *A. castellanii*-conditioned medium (ACCM) in CSCs and ihCECs was examined. Viability/proliferation assays, MTT, alamarBlue and SRB, cytotoxicity assays (LDH) and caspase activity, and fluorescent staining were used to assess changes in corneal cells after exposure to different concentrations of ACCM for 3, 24 and 48 hours. ACCM significantly decreased cell viability/proliferation, triggered apoptosis, disrupted the actin cytoskeleton and changed the ultrastructural features of CSCs and ihCECs in a time- and concentration-dependant manner. Interestingly, the sensitivity of ihCECs to the damaging effects of ACCM was greater than that of CSCs. Additionally, it was

identified that proteases mediated the process by which cellular damage was induced in ihCECs and CSCs by ACCM – as shown by enhanced cell proliferation after ACCM neutralisation utilising a cocktail of protease inhibitors. These results suggest that the *A. castellanii* secretome is a critical factor in the structural, and functional, damage that occur when ocular cells are exposed to a filter-sterilised supernatant from *A. castellanii* culture.

7.2.2. Changes in the composition of culture supernatant of CSCs and ACCM

This study investigated any potential functional changes in ocular cells after infection by *A. castellanii*. DNA concentration analysis and elemental analysis were performed to compare alterations in the composition of supernatant after exposure to 50% ACCM-M199 for 0, 3, 24 and 48 hours. Additionally, amino acid analysis of ACCM was also performed to evaluate the significance of amino acids for parasite viability. The findings indicate that ACCM culture does not directly affect the DNA concentration of CSC cells. Nevertheless, CSC elements were altered by ACCM, with changes in the abundance of potassium, sodium and calcium. Amino acid analysis showed that serine and cysteine proteases are secreted by *A. castellanii*. In summary, ACCM from *A. castellanii* cultures significantly

affected CSCs; thus, changing the composition of CSCs exposed to ACCM, as well as ACCM alone. Additional evidence was also found showing how much cellular damage can be caused by the *A. castellanii* secretome.

7.2.3. Metabolomic alterations in CSCs in response to exposure to ACCM

Metabolomic analysis was performed to identify changes in CSCs metabolism after 48 hours incubation, both with and without the *A. castellanii* secretome. The results indicated that ACCM triggers metabolic changes in CSCs, reducing cell viability and enhancing cell death. Amino acid levels were observed to decrease in control samples after 48 hours, when compared with baseline samples, suggesting protein synthesis and cell growth. However, free amino acid levels in treated samples increased after 48 hours, indicating protein deterioration and cell death. Additionally, nucleotide metabolism was found to increase after 48 hours in both treated and control samples when compared with baseline samples, with a greater increase recorded in treated samples. The metabolite oxoadipic acid, previously linked to ophthalmoplegia, retinopathy and increased CSF protein, was observed in this study. Thus, the secretome from *A. castellanii* cultures significantly affected CSCs, leading to alterations in the metabolites associated with nucleotides and

amino acids that ultimately led to a reduction in cell viability and increased cell death.

7.2.4. Testing effect of nanoparticles on *A. castellanii* and human corneal cells

This thesis examined how CeO_2NPs affect *A. castellanii* and corneal cells. This was accomplished based on an examination of the cell viability/proliferation using alamarBlue; SRB; cell counting; and cell imaging with immunofluorescent staining of actin and AO staining. TEM was used to track the aggregation of particles and identify the molecular mechanism of action of CeO_2NPs. Our results showed a concentration-dependant decrease in both cell viability and proliferation, and changes in the morphology of *A. castellanii.* CeO_2NPs did not significantly affect corneal cells at the lowest doses, however, there was more indication of a toxic effect above 200 µg/mL, but this was not of the same magnitude of that seen affecting the *Acanthamoeba*.

7.3. Discussion of key findings

The main objective of this study was to examine the cytotoxic, structural and functional changes that occur in human CSCs and ihCECs as a reaction to ACCM infection. The results concur with those of other studies (Mattana *et al.*, 2002; Mattana *et al.*,

1997), and also show that it is not always necessary to have contact of amoeba with host cells for *A. castellanii* cytotoxicity in human ocular cells; in fact, cell damage can also be induced by cell-free supernatants acquired from trophozoite cultures.

The general findings obtained from these studies indicated that ACCM significantly affected both kinds of corneal cells, although the damage was more severe to the infrastructure of ihCECs compared with CSCs. This discrepancy in the sensitivity of cells is largely due to differences in cell-specific functions that impact the reaction to ACCM, where CSCs were the primary cell and ihCECs were the cell line, as previously explained in Chapter 3.

It is evident that *Acanthamoeba* organisms are metabolically active protozoa, and corneal cells and trophozoite metabolites cannot be separated post-co-infection; therefore, it was not feasible to examine how live *Acanthamoeba* trophozoites affect the metabolism of corneal cells. Therefore, we analysed the functional changes in the composition of the supernatant from CSCs prior, and subsequent, to exposure to 50% ACCM-M199. The findings of the elemental and DNA concentration analyses indicated that ACCM culture did not directly affect the DNA concentration in CSCs cells. ACCM did alter the elements in CSCs, with changes in the abundance of intracellular sodium, potassium and calcium.

A previous study has demonstrated that corneal fibroblasts were killed by *A. castellanii* predominantly via apoptosis (Takaoka-Sugihara *et al.*, 2012). Further research indicates that primary DNA fragmentation is a delayed occurrence in apoptosis (Kim *et al.*, 2003). Nevertheless, cell growth within these cultures could be affected by trace elements following treatment with ACCM at concentrations greater than 50%; thus, showing the significance of monitoring elemental contaminants and the changes that could impact target cell growth. However, the process by which various trace elements influence metabolism, and other upstream process within the cell culture media, has yet to be determined.

The study findings revealed that the metabolites associated with nucleotides and amino acids were significantly altered. It was necessary to analyse amino acid metabolism to identify whether a relationship existed between nucleotide metabolism changes and the proliferation and death of cells. It was observed that amino acids within the control samples decreased after 48 hours, compared with baseline, suggesting protein synthesis. Furthermore, increases were also observed after 48 hours in samples that had been treated, compared with baseline, suggesting protein deterioration. Nucleotide metabolism was found to increase after 48 hours, in both treated and control

samples, when compared with baseline samples. The findings also revealed a small rise in the metabolite oxoadipic acid– previously associated to ophthalmoplegia and retinopathy in control samples after 48 hours, in comparison to baseline, and a significantly greater increase after 48 hours in treated samples compared with baseline and control samples. However, it was unclear whether this was related to AK because retinopathy involves the back of the eye and not the cornea. Additional studies should be conducted on the annotation of a signal as oxoadipic acid as well as how this metabolite is associated with eye disorders.

In recent studies, *in vitro* testing of CeO_2NPs has predominantly been performed to investigate their actions on pathogenic microorganisms (Dos Santos *et al.*, 2014; Babenko *et al.*, 2012). They can also be used for the treatment of multiple diseases. CeO_2NPs exert antioxidant effects in different mammalian cell lines and have also exhibited potential for the treatment of various ocular disorders, for example cataract and retinal diseases (Chen *et al.*, 2006; Hanafy *et al.*, 2019). CeO_2NPs can reduce oxidising stress inside cells, which is therapeutically beneficial in cases of human inflammation (Zheng *et al.*, 2019; Hirst *et al.*, 2009), and exhibited potential for treating neovascularization-related ophthalmic diseases. Moreover, we

tested the hypothesis that the interactions between CeO_2NPs and CSCs or ihCECs have no impact on the viability of corneal cells when used at low doses. This was the first study to show that CeO_2NPs inhibit the proliferation of *A. castellanii*, with a smaller toxic effect on corneal cells grown *in vitro*. The CeO_2NPs mechanism of action into *A. castellanii in vitro* has also been demonstrated for the first time.

7.4. Limitations of this study

A shortcoming of this research was that two types of corneal cells from different sources were used, namely CSCs and ihCECs, which were generated from primary tissue and immortalised cell line, respectively. The study was also performed in 2D cell cultures and not 3D cultures which would have been more representative of the human eye. Another potential limitation is that I only studied the effect of the conditioned medium/secretome of *Acanthamoeba* on corneal cells and not the direct interaction between *Acanthamoeba* and corneal cell in order to compare the results between the two different infection models. Due to time limitations, it was not possible to process TEM images of the corneal cells after exposure to CeO_2NPs, although the results of the other experiments had high accuracy and were sufficient for achieving the research objective, as demonstrated in chapter 6.

7.5. Implications of this study

As a result of this research, a potentially new class of antimicrobials have been identified that can be critical for generating industrial cooperation. The availability of new antimicrobials, with sufficient potency for the treatment and prevention of Acanthamoeba keratitis, will reduce the economic burden on the NHS in the UK and other health systems abroad. The research will ultimately assist patients at an increased risk of blindness due to *Acanthamoeba* infection via the provision of new, and safer, therapies. This study has also produced valuable new insight into the molecular pathology of Acanthamoeba keratitis.

7.6. Future research

In the future, there is a necessity to develop cellular models of the human cornea that are more representative to human eye. Investigations should be performed in which corneal cells are cultured on three-dimensional (3D) substrates. Testing of ACCM or CeO_2NPs should be performed using the *in vivo* models where feasible. It is necessary for CeO_2NPs to be optimised in order to apply them in the biomedical field. Optimisation of sizes, coatings and stability in aqueous solutions of biological medium must occur to make the results of further biological tests more consistent. Moreover, after CeO_2NPs have been optimised, their

levels of safety and toxicity with respect to corneal cells and corneal tissue in vivo should be investigated thoroughly using a range of assays, including ultrastructural characterisation, and determination of cell viability, activation of caspase and LDH, basal ROS level and cellular ATP level.

CeO_2NPs have shown potential antimicrobial properties via the inhibition of *Acanthamoeba castellanii*. The next step would be to combine CeO_2NPs at low concentrations with chemotherapeutic drugs to examine whether they affect *Acanthamoeba* infection differently. To offer a means of delivering anti-amoebic drugs inside the *Acanthamoeba*. Additionally, when CeO_2NPs are used in the form of a solution or integrated into contact lenses, it can diminish the availability of microbes, and restrict their ability to adhere and reproduce on the lens. This could avert the association between pathogenic microorganisms and contaminated contact lenses.

7.7. Conclusion

This research has shown that ACCM from cultures of *A. castellanii* had a significant effect on ocular cells, changing their function, structure and metabolism, which was mediated by serine and cysteine proteases.

The results of this study also suggest that the possible therapeutic benefits of CeO_2NPs are significant and they show antimicrobial effects against *A. castellanii*. CeO_2NPs exhibited potential anti-acanthamoebic effects while inhibiting encystation. Additionally, the toxic effect of CeO_2NPs on corneal cells was much lower than that on *Acanthamoeba*, up to 200 µg/mL, with no indications of a decrease in viability, proliferation or damage to actin. However, further research should be performed to assess the effects of CeO_2NPs alone and in combination with chemotherapeutic drugs against *A. castellanii*.

Bibliography

Adeoye, O., Olawumi, J., Opeyemi, A. and Christiania, O. (2018) 'Review on the role of glutathione on oxidative stress and infertility', *JBRA assisted reproduction,* 22(1), pp. 61-66.

Aderibigbe, B. A. (2017) 'Metal-based nanoparticles for the treatment of infectious diseases', *Molecules,* 22(8), pp. 1-37.

Ahmed Khan, N. (2003) 'Pathogenesis of *Acanthamoeba* infections', *Microbial Pathogenesis,* 34(6), pp. 277-285.

Albanese, A., Tang, P. S. and Chan, W. C. W. (2012) 'The effect of nanoparticle size, shape, and surface chemistry on biological systems', *Annual review of biomedical engineering,* 14(1), pp. 1-16.

Alsam, S., Ryoul Jeong, S., Dudley, R. and Ahmed Khan, N. (2007) 'Role of human tear fluid in *Acanthamoeba* interactions with the human corneal epithelial cells', *International journal of medical microbiology,* 298(3), pp. 329-336.

Alvarez-Sánchez, B., Priego-Capote, F. and Luque de Castro, M. D. (2010) 'Metabolomics analysis I. Selection of biological samples and practical aspects preceding sample preparation', *Trends in Analytical Chemistry,* 29(2), pp. 111-119.

Alves, D. d. S. M. M., Alves, L. M., da Costa, T. L., de Castro, A. M. and Vinaud, M. C. (2017) 'Anaerobic metabolism in T4 *Acanthamoeba* genotype', *Current microbiology,* 74(6), pp. 685-690.

Alzubaidi, R., Sharif, M. S., Qahwaji, R., Ipson, S. and Brahma, A. (2016) 'In vivo confocal microscopic corneal images in health and disease with an emphasis on extracting features and visual signatures for corneal diseases: a review study', *British Journal of Ophthalmology,* 100(1), pp. 41-55.

Anwar, A., Khan, N. and Siddiqui, R. (2018) 'Combating *Acanthamoeba* spp. cysts: what are the options?', *Parasites & Vectors,* 11(26), pp. 1-6.

Araki-Sasaki, K., Ohashi, Y., Sasabe, T., Hayashi, K., Watanabe, H., Tano, Y. and Handa, H. (1995) 'An SV40-immortalized human corneal epithelial cell line and its characterization', *Investigative ophthalmology & visual science,* 36(3), pp. 614-621.

Asati, A., Santra, S., Kaittanis, C. and Perez, J. M. (2010) 'Surface-charge-dependent cell localization and cytotoxicity of cerium oxide nanoparticles', *ACS nano,* 4(9), pp. 5321-5331.

Avery, S. V., Harwood, J. and Lloyd, D. (1995) 'Quantification and characterization of phagocytosis in the soil amoeba *Acanthamoeba castellanii* by flow cytometry', *Applied And Environmental Microbiology,* 61(3), pp. 1124-1132.

Babenko, L. P., Zholobak, N. M., Shcherbakov, A. B., Voychuk, S. I., Lazarenko, L. M. and Spivak, M. Y. (2012) 'Antibacterial activity of cerium colloids against opportunistic microorganisms in vitro', *Mikrobiolohichnyi zhurnal,* 74(3), pp. 54-62.

Baig, A., Iqbal, J. and Khan, N. (2013) 'In vitro efficacies of clinically available drugs against growth and viability of an *Acanthamoeba castellanii* keratitis isolate belonging to the T4 genotype', *Antimicrobial Agents And Chemotherapy,* 57(8), pp. 3561-3567.

Barshop, B. A., Nyhan, W. L., Naviaux, R. K., McGowan, K. A., Friedlander, M. and Haas, R. H. (2000) 'Kearns–Sayre syndrome presenting as 2-oxoadipic aciduria', *Molecular genetics and metabolism,* 69(1), pp. 64-68.

Baylis, O., Figueiredo, F., Henein, C., Lako, M. and Ahmad, S. (2011) '13 years of cultured limbal epithelial cell therapy: a review of the outcomes', *Journal Of Cellular Biochemistry,* 112(4), pp. 993-1002.

Bellio, P., Luzi, C., Mancini, A., Cracchiolo, S., Passacantando, M., Di Pietro, L., Perilli, M., Amicosante, G., Santucci, S. and Celenza, G. (2018) 'Cerium oxide nanoparticles as potential antibiotic adjuvant. Effects of CeO_2 nanoparticles on bacterial outer membrane permeability', *Biochimica et biophysica acta. Biomembranes,* 1860(11), pp. 2428-2435.

Berridge, M. V., Herst, P. M. and Tan, A. S. (2005) 'Tetrazolium dyes as tools in cell biology: New insights into their cellular reduction', *Biotechnology Annual Review,* 11, pp. 127-152.

Booth, A., Størseth, T., Altin, D., Fornara, A., Ahniyaz, A., Jungnickel, H., Laux, P., Luch, A. and Sørensen, L. (2015) 'Freshwater dispersion stability of PAA-stabilised cerium oxide nanoparticles and toxicity towards Pseudokirchneriella subcapitata', *Science of the Total Environment,* 505, pp. 596-605.

Booton, G. C., Visvesvara, G. S., Byers, T. J., Kelly, D. J. and Fuerst, P. A. (2005) 'Identification and distribution of *Acanthamoeba* species genotypes associated with nonkeratitis infections', *Journal of clinical microbiology,* 43(4), pp. 1689-1693.

Bowers, B. and Korn, E. D. (1968) 'The fine structure of *Acanthamoeba castellanii*. I. The trophozoite', *The Journal of cell biology,* 39(1), pp. 95-111.

Cao, Z., Jefferson, D. M. and Panjwani, N. (1998) 'Role of carbohydrate-mediated adherence in cytopathogenic mechanisms of *Acanthamoeba'*, *The Journal of biological chemistry,* 273(25), pp. 15838-15845.

Carnt, N., Hoffman, J. J., Verma, S., Hau, S., Radford, C. F., Minassian, D. C. and Dart, J. K. G. (2018) 'Acanthamoeba keratitis: confirmation of the UK outbreak and a prospective case-control study identifying contributing risk factors', *British Journal of Ophthalmology,* 102(12), pp. 1621-1628.

Carnt, N. and Stapleton, F. (2016) 'Strategies for the prevention of contact lens ‐ related Acanthamoeba keratitis: a review', *Ophthalmic and physiological optics,* 36(2), pp. 77-92.

Carrijo-Carvalho, L. C., Sant'Ana, V. P., Foronda, A. S., de Freitas, D. and de Souza Carvalho, F. R. (2017) 'Therapeutic agents and biocides for ocular infections by free-living amoebae of *Acanthamoeba* genus', *Survey of Ophthalmology,* 62(2), pp. 203-218.

Cassee, F. R., van Balen, E. C., Singh, C., Green, D., Muijser, H., Weinstein, J. and Dreher, K. (2011) 'Exposure, health and ecological effects review of engineered nanoscale cerium and cerium oxide associated with its use as a fuel additive', *Critical reviews in toxicology,* 41(3), pp. 213-229.

Castellanii, A. (1930) 'An amoeba found in cultures of a yeast: preliminary note.', *Journal of Tropical Medicine London,* 33, pp. 160-160.

Chandrasekar, P. H., Nandi, P. S., Fairfax, M. R. and Crane, L. R. (1997) 'Cutaneous infections due to *Acanthamoeba* in patients with acquired immunodeficiency syndrome', *Archives of Internal Medicine,* 157(5), pp. 569-572.

Chappell, C. L., Wright, J. A., Coletta, M. and Newsome, A. L. (2001) 'Standardized method of measuring *Acanthamoeba*

antibodies in sera from healthy human subjects', *Clinical and diagnostic laboratory immunology,* 8(4), pp. 724-730.

Charbgoo, F., Ramezani, M. and Darroudi, M. (2017) 'Bio-sensing applications of cerium oxide nanoparticles: Advantages and disadvantages', *Biosensors and Bioelectronics,* 96, pp. 33-43.

Chen, H.-I. and Chang, H.-Y. (2005) 'Synthesis of nanocrystalline cerium oxide particles by the precipitation method', *Ceramics international,* 31(6), pp. 795-802.

Chen, J., Patil, S., Seal, S. and McGinnis, J. F. (2006) 'Rare earth nanoparticles prevent retinal degeneration induced by intracellular peroxides', *Nature nanotechnology,* 1(2), pp. 142-150.

Clarke, D. W. and Niederkorn, J. Y. (2006a) 'The immunobiology of Acanthamoeba keratitis', *Microbes and infection,* 8(5), pp. 1400-1405.

Clarke, D. W. and Niederkorn, J. Y. (2006b) 'The pathophysiology of Acanthamoeba keratitis', *Trends in parasitology,* 22(4), pp. 175-180.

Cohen, E. J., Parlato, C. J., Arentsen, J. J., Genvert, G. I., Eagle, R. C., Wieland, M. R. and Laibson, P. R. (1987) 'Medical and surgical treatment of Acanthamoeba keratitis', *American Journal of Ophthalmology,* 103(5), pp. 615-625.

Cordingley, J. and Trzyna, W. (2008) 'Multiple factors affecting growth and encystment of *Acanthamoeba castellanii* in axenic culture', *Acta Protozoologica,* 47(4), pp. 307-316.

Corsaro, D., Walochnik, J., Köhsler, M. and Rott, M. (2015) *'Acanthamoeba* misidentification and multiple labels: redefining genotypes T16, T19, and T20 and proposal for *Acanthamoeba micheli* sp. nov. (genotype T19)', *Parasitology Research,* 114(7), pp. 2481-2490.

Culbertson, C. G., Smith, J. W. and Minner, J. R. (1958) *'Acanthamoeba*: observations on animal pathogenicity', *Science,* 127(3313), pp. 1506-1506.

Cwiklik, L. (2016) 'Tear film lipid layer: A molecular level view', *Biochimica et Biophysica Acta,* 1858(10), pp. 2421-2430.

Dart, J. (2003) 'Corneal toxicity: the epithelium and stroma in iatrogenic and factitious disease', *Eye,* 17(8), pp. 886-892.

Dart, J. K. G., Saw, V. P. J. and Kilvington, S. (2009) 'Acanthamoeba Keratitis: diagnosis and treatment update', *American Journal of Ophthalmology,* 148(4), pp. 487-499.

Dart, J. K. G., Stapleton, F. and Minassian, D. (1991) 'Contact lenses and other risk factors in microbial keratitis', *The Lancet,* 338(8768), pp. 650-653.

de Oliveira, R. C. and Wilson, S. E. (2020) 'Descemet's membrane development, structure, function and regeneration', *Experimental eye research,* 197, pp. 108090-108090.

Demirci, G., Ay, G., Karabas, L. V., Altintas, O., Tamer, G. and Caglar, Y. (2006) 'Acanthamoeba keratitis in a 5-year-old boy without a history of contact lens usage', *Cornea,* 25(3), pp. 356-358.

Deshpande, P., Ortega, Í., Sefat, F., Sangwan, V. S., Green, N., Claeyssens, F. and MacNeil, S. (2015) 'Rocking media over ex vivo corneas improves this model and allows the study of the effect of proinflammatory cytokines on wound healing', *Investigative ophthalmology & visual science,* 56(3), pp. 1553-1561.

Dettmer, K., Nürnberger, N., Kaspar, H., Gruber, M., Almstetter, M. and Oefner, P. (2011) 'Metabolite extraction from adherently growing mammalian cells for metabolomics studies: optimization of harvesting and extraction protocols', *Analytical and Bioanalytical Chemistry,* 399(3), pp. 1127-1139.

Dhall, A. and Self, W. (2018) 'Cerium oxide nanoparticles: A brief review of their synthesis methods and biomedical applications', *Antioxidants,* 7, pp. 1-13.

Dolphin, W. D. (1976) 'Effect of glucose on glycine requirement of *Acanthamoeba castellanii*', *The Journal of protozoology,* 23(3), pp. 455-457.

Dos Santos, C., Passos Farias, I., Reis Albuquerque, A., e Silva, P., Costa One, G. and Sampaio, F. (2014) 'Antimicrobial activity of nano cerium oxide (IV) (CeO_2) against *Streptococcus mutans*', *BMC proceedings,* 8(4), pp. 1-2.

Dua, H. S., Faraj, L. A. and Said, D. G. (2015) 'Dua's layer: discovery, characteristics, clinical applications, controversy and

potential relevance to glaucoma', *Expert review of ophthalmology,* 10(6), pp. 531-547.

Dua, H. S., Faraj, L. A., Said, D. G. and Gray, T. a. L., J., (2013) 'Human corneal anatomy redefined: a novel pre-Descemet's layer (Dua's layer)', *Ophthalmology,* 120(9), pp. 1778-1785.

Dudley, R., Alsam, S. and Khan, N. A. (2008) 'The role of proteases in the differentiation of *Acanthamoeba castellanii*', *FEMS Microbiology Letters,* 286(1), pp. 9-15.

Elsheikha, H. M., Alkurashi, M., Kong, K. and Zhu, X.-Q. (2014) 'Metabolic footprinting of extracellular metabolites of brain endothelium infected with *Neospora caninum* in vitro', *BMC research notes,* 7(1), pp. 1-11.

Elsheikha, H. M., Siddiqui, R. and Khan, N. A. (2020) 'Drug discovery against *Acanthamoeba* infections: Present knowledge and unmet needs', *Pathogens,* 9(5), pp. 1-17.

Estes, L. M., Singha, P., Singh, S., Sakthivel, T. S., Garren, M., Devine, R., Brisbois, E. J., Seal, S. and Handa, H. (2021) 'Characterization of a nitric oxide (NO) donor molecule and cerium oxide nanoparticle (CNP) interactions and their synergistic antimicrobial potential for biomedical applications', *Journal of colloid and interface science,* 586, pp. 163-177.

Etheredge, L., Kane, B. P. and Hassell, J. R. (2009) 'The effect of growth factor signaling on keratocytes in vitro and its relationship to the phases of stromal wound repair', *Investigative ophthalmology & visual science,* 50(7), pp. 3128-3136.

Fan, J., Kamphorst, J. J., Mathew, R., Chung, M. K., White, E., Shlomi, T. and Rabinowitz, J. D. (2013) 'Glutamine‐driven oxidative phosphorylation is a major ATP source in transformed mammalian cells in both normoxia and hypoxia', *Molecular systems biology,* 9(1), pp. 1-11.

Farias, I. A. P., Santos, C. C. L. d. and Sampaio, F. C. (2018) 'Antimicrobial activity of cerium oxide nanoparticles on opportunistic microorganisms: a systematic review', *BioMed Research International,* 2018, pp. 1-14.

Fatemeh, M., Maryam, N. and Zeynab, J. (2017) 'Pathogenic *Acanthamoeba* T4 genotype isolated from mucosal tissue of a patient with HIV infection: a case report', *Iranian Journal of Parasitology,* 12(1), pp. 143-147.

Fragoso, Y. D. and Brooks, J. B. B. (2015) 'Leflunomide and teriflunomide: altering the metabolism of pyrimidines for the treatment of autoimmune diseases', *Expert review of clinical pharmacology,* 8(3), pp. 315-320.

Franchi, L. P., Manshian, B. B., de Souza, T. A. J., Soenen, S. J., Matsubara, E. Y., Rosolen, J. M. and Takahashi, C. S. (2015) 'Cyto- and genotoxic effects of metallic nanoparticles in untransformed human fibroblast', *Toxicology in vitro,* 29(7), pp. 1319-1331.

Friedland, R. L., Raphael, A. S., Deutsch, S. E., Johal, J. J., Martyn, S. L., Visvesvara, W. G. and Lischner, W. H. (1992) 'Disseminated *Acanthamoeba* infection in a child with symptomatic human immunodeficiency virus infection', *The Pediatric Infectious Disease Journal,* 11(5), pp. 404-407.

Fuerst, P. A., Booton, G. C. and Crary, M. (2015) 'Phylogenetic analysis and the evolution of the 18S rRNA gene typing system of *Acanthamoeba'*, *Journal of Eukaryotic Microbiology,* 62(1), pp. 69-84.

Garajová, M., Mrva, M., Vaškovicová, N., Martinka, M., Melicherová, J. and Valigurová, A. (2019) 'Cellulose fibrils formation and organisation of cytoskeleton during encystment are essential for *Acanthamoeba* cyst wall architecture', *Scientific reports,* 9(4466), pp. 1-21.

Garate, M., Marchant, J., Cubillos, I., Cao, Z., Khan, N. A. and Panjwani, N. (2006) 'In vitro pathogenicity of *Acanthamoeba* is associated with the expression of the mannose-binding protein', *Investigative ophthalmology & visual science,* 47(3), pp. 1056-1062.

Gerasimovskaya, E. V., Woodward, H. N., Tucker, D. A. and Stenmark, K. R. (2008) 'Extracellular ATP is a pro-angiogenic factor for pulmonary artery vasa vasorum endothelial cells', *Angiogenesis,* 11(2), pp. 169-182.

González-Robles, A., Castañón, G., Cristóbal-Ramos, A. R., Lázaro-Haller, A., Omaña-Molina, M., Bonilla, P. and Martínez-Palomo, A. (2006) '*Acanthamoeba castellanii*: Structural basis of the cytopathic mechanisms', *Experimental Parasitology,* 114(3), pp. 133-140.

González-Robles, A., Salazar-Villatoro, L., Omaña-Molina, M., Reyes-Batlle, M., Martín-Navarro, C. M. and Lorenzo-Morales, J. (2014) 'Morphological features and in vitro cytopathic effect of

Acanthamoeba griffini trophozoites isolated from a clinical case', *Journal of parasitology research,* 2014, pp. 1-10.

Gonçalves, D. d. S., Ferreira, M. D. S., Liedke, S. C., Gomes, K. X., de Oliveira, G. A., Leão, P. E. L., Cesar, G. V., Seabra, S. H., Cortines, J. R., Casadevall, A., Nimrichter, L., Domont, G. B., Junqueira, M. R., Peralta, J. M. and Guimaraes, A. J. (2018) 'Extracellular vesicles and vesicle-free secretome of the protozoa *Acanthamoeba castellanii* under homeostasis and nutritional stress and their damaging potential to host cells', *Virulence,* 9(1), pp. 818-836.

Guzman-Aranguez, A., Santano, C., Martin-Gil, A., Fonseca, B. and Pintor, J. (2013) 'Nucleotides in the eye: focus on functional aspects and therapeutic perspectives', *The Journal of pharmacology and experimental therapeutics,* 345(3), pp. 331-341.

Hanafy, B. I., Cave, Gareth W. V., Barnett, Y. and Pierscionek, B. (2019) 'Ethylene glycol coated nanoceria protects against oxidative stress in human lens epithelium', *RSC advances,* 9(29), pp. 16596-16605.

Hanafy, B. I., Cave, G. W. V., Barnett, Y. and Pierscionek, B. (2020) 'Treatment of human lens epithelium with high levels of nanoceria leads to reactive oxygen species mediated apoptosis', *Molecules,* 25(441), pp. 1-16.

Hanafy, B. I., Cave, G. W. V., Barnett, Y. and Pierscionek, B. K. (2021) 'Nanoceria prevents glucose-induced protein glycation in eye lens cells', *Nanomaterials,* 11(1473), pp. 1-14.

Hauber, S., Parkes, H., Siddiqui, R. and Khan, N. (2011) 'The use of high-resolution 1 H nuclear magnetic resonance (NMR) spectroscopy in the clinical diagnosis of *Acanthamoeba'*, *Parasitology Research,* 109(6), pp. 1661-1669.

Heredero-Bermejo, I., Criado-Fornelio, A., De Fuentes, I., Soliveri, J., Copa-PatiÑO, J. L. and PÉRez-Serrano, J. (2015) 'Characterization of a human–pathogenic *Acanthamoeba griffini* isolated from a contact lens-wearing keratitis patient in Spain', *Parasitology,* 142(2), pp. 1-11.

Hirst, S. M., Karakoti, A., Tyler, R. D., Sriranganathan, N., Seal, S. and Reilly, C. M. (2009) 'Anti-inflammatory Properties of Cerium Oxide Nanoparticles', *Small,* 5(24), pp. 2848-2856.

Hong, Y., Kang, J.-M., Joo, S.-Y., Song, S.-M., Lê, H. G., Thái, T. L., Lee, J., Goo, Y.-K., Chung, D.-I., Sohn, W.-M. and Na, B.-K. (2018) 'Molecular and biochemical properties of a cysteine protease of *Acanthamoeba castellanii*', *The Korean journal of parasitology,* 56(5), pp. 409-418.

Hou, Y.-M. and Yang, X. (2013) 'Regulation of cell death by transfer RNA', *Antioxidants & redox signaling,* 19(6), pp. 583-594.

Huang, J.-M., Liao, C.-C., Kuo, C.-C., Chen, L.-R., Huang, L. L. H., Shin, J.-W. and Lin, W.-C. (2017) 'Pathogenic *Acanthamoeba castellanii* secretes the extracellular aminopeptidase M20/M25/M40 family protein to target cells for phagocytosis by disruption', *Molecules,* 22(2263), pp. 1-13.

Hurt, M., Apte, S., Leher, H., Howard, K., Niederkorn, J. and Alizadeh, H. (2001) 'Exacerbation of Acanthamoeba keratitis in animals treated with anti-macrophage inflammatory protein 2 or antineutrophil antibodies', *Infection and Immunity,* 69(5), pp. 2988-2995.

Hübner, N. O. and Kramer, A. (2010) 'Review on the efficacy, safety and clinical applications of polihexanide, a modern wound antiseptic', *Skin pharmacology and physiology,* 23(1), pp. 17-27.

Ibba, M. and Söll, D. (2000) 'Aminoacyl-tRNA Synthesis', *Annual review of biochemistry,* 69(1), pp. 617-650.

Illingworth, C. D. and Cook, S. D. (1998) 'Acanthamoeba keratitis', *Survey of ophthalmology,* 42(6), pp. 493-508.

Ivask, A., Kurvet, I., Kasemets, K., Blinova, I., Aruoja, V., Suppi, S., Vija, H., Kakinen, A., Titma, T., Heinlaan, M., Visnapuu, M., Koller, D., Kisand, V. and Kahru, A. (2014) 'Size-dependent toxicity of silver nanoparticles to bacteria, yeast, algae, crustaceans and mammalian cells in vitro', *PloS one,* 9(7), pp. 1-14.

Jacob Inbaneson, S. and Ravikumar, S. (2013) 'In vitro antiplasmodial activity of PDDS-coated metal oxide nanoparticles against *Plasmodium falciparum*', *Applied Nanoscience,* 3(3), pp. 197-201.

Janin-Manificat, H., Rovère, M.-R., Galiacy, S. D., Malecaze, F., Hulmes, D. J. S., Moali, C. and Damour, O. (2012) 'Development of ex vivo organ culture models to mimic human corneal scarring', *Molecular vision,* 18, pp. 2896-2908.

Jeelani, G. and Nozaki, T. (2014) 'Metabolomic analysis of Entamoeba: applications and implications', *Current Opinion in Microbiology,* 20, pp. 118-124.

Jeelani, G., Sato, D., Husain, A., Escueta-de Cadiz, A., Sugimoto, M., Soga, T., Suematsu, M. and Nozaki, T. (2012) 'Metabolic profiling of the protozoan parasite *Entamoeba invadens* revealed activation of unpredicted pathway during encystation', *PloS one,* 7(5), pp. 1-11.

Jiang, C., Sun, X., Wang, Z. and Zhang, Y. (2015) 'Acanthamoeba keratitis: clinical characteristics and management', *The Ocular Surface,* 13(2), pp. 164-168.

Jones, D. B., Visvesvara, G. S. and Robinson, N. M. (1975) *'Acanthamoeba* polyphaga keratitis and *Acanthamoeba* uveitis associated with fatal meningoencephalitis', *Transactions of the Ophthalmological Societies of the United Kingdom,* 95(2), pp. 221-232.

Joris, F., Manshian, B., Peynshaert, K., De Smedt, S. C., Braeckmans, K. and Soenen, S. J. (2013) 'Assessing nanoparticle toxicity in cell-based assays: influence of cell culture parameters and optimized models for bridging the in vitro-in vivo gap', *Chemical Society Reviews,* 42(21), pp. 8339-8359.

Julia, W., Michael, D., Karin, S., Andreas, O., Thomas, H., Gerhard, W., Hansjörg, E. and Horst, A. (2002) 'Cytotoxic activities of alkylphosphocholines against clinical isolates of *Acanthamoeba* spp', *Antimicrobial Agents and Chemotherapy,* 46(3), pp. 695-701.

Julio Martinez, A. (1991) 'Infection of the central nervous system due to *Acanthamoeba'*, *Reviews of Infectious Diseases,* 13(Supplement 5), pp. S399-S402.

Kafsack, B. and Llinas, M. (2010) 'Eating at the table of another: metabolomics of host-parasite interactions', *Cell Host & Microbe,* 7(2), pp. 90-99.

Kannan, S. K. and Sundrarajan, M. (2014) 'A green approach for the synthesis of a cerium oxide nanoparticle: characterization and antibacterial activity', *International Journal of Nanoscience,* 13(3), pp. 1-7.

Khalid, K., Tan, X., Mohd Zaid, H. F., Tao, Y., Lye Chew, C., Chu, D.-T., Lam, M. K., Ho, Y.-C., Lim, J. W. and Chin Wei, L.

(2020) 'Advanced in developmental organic and inorganic nanomaterial: a review', *Bioengineered,* 11(1), pp. 328-355.

Khan, N. (2008) '*Acanthamoeba* and the blood-brain barrier: the breakthrough', *Journal Of Medical Microbiology,* 57(9), pp. 1051-1057.

Khan, N., Jarroll, E. and Paget, T. A. (2001) '*Acanthamoeba* can be differentiated by the polymerase chain reaction and simple plating assays', *Current Microbiology,* 43(3), pp. 204-208.

Khan, N. A. (2001) 'Pathogenicity, morphology, and differentiation of *Acanthamoeba*', *Current Microbiology,* 43(6), pp. 391-395.

Khan, N. A. (2005) 'The immunological aspects of *Acanthamoeba* infections', *American journal of immunology,* 1(1), pp. 24-30.

Khan, N. A. (2006) '*Acanthamoeba*: biology and increasing importance in human health', *FEMS Microbiology Reviews,* 30(4), pp. 564-595.

Khan, N. A. (2007) '*Acanthamoeba* invasion of the central nervous system', *International Journal for Parasitology,* 37(2), pp. 131-138.

Khan, N. A., Jarroll, E. L., Panjwani, N., Cao, Z. and Paget, T. A. (2000) 'Proteases as markers for differentiation of pathogenic and nonpathogenic species of *Acanthamoeba*', *Journal of clinical microbiology,* 38(8), pp. 2858-2861.

Kilvington, S. and Lam, A. (2013) 'Development of standardized methods for assessing biocidal efficacy of contact lens care solutions against *Acanthamoeba* trophozoites and cysts', *Investigative ophthalmology & visual science,* 54(7), pp. 4527-4537.

Kim, T.-i., Tchah, H., Lee, S.-a., Sung, K., Cho, B. J. and Kook, M. S. (2003) 'Apoptosis in keratocytes caused by mitomycin C', *Investigative Ophthalmology & Visual Science,* 44(5), pp. 1912-1917.

Kim, W. T., Kong, H. H., Ha, Y. R., Hong, Y. C., Jeong, H. J., Yu, H. S. and Chung, D. I. (2006) 'Comparison of specific activity and cytopathic effects of purified 33 kDa serine proteinase from *Acanthamoeba* strains with different degree of virulence', *The Korean journal of parasitology,* 44(4), pp. 321-330.

Klausner, E., Peer, D., Chapman, R., Multack, R. and Andurkar, S. V. (2007) 'Corneal gene therapy', *Journal Of Controlled Release,* 124(3), pp. 107-133.

Klemba, M. and Goldberg, D. E. (2002) 'Biological roles of proteases in parasitic protozoa', *Annual Review of Biochemistry,* 71(1), pp. 275-305.

Koehlé-Divo, V., Cossu-Leguille, C., Pain-Devin, S., Simonin, C., Bertrand, C., Sohm, B., Mouneyrac, C., Devin, S. and Giambérini, L. (2018) 'Genotoxicity and physiological effects of CeO_2NPs on a freshwater bivalve (*Corbicula fluminea*)', *Aquatic Toxicology,* 198, pp. 141-148.

Kolar, S. S. N., Manarang, J. C., Burns, A. R., Miller, W. L., McDermott, A. M. and Bergmanson, J. P. G. (2015) 'Contact lens care solution killing efficacy against *Acanthamoeba castellanii* by in vitro testing and live-imaging', *Contact Lens and Anterior Eye,* 38(6), pp. 442-450.

Krastanov, A. (2010) 'Metabolomics-the state of art', *Biotechnology & Biotechnological Equipment,* 24(1), pp. 1537-1543.

Kryczka, T., Ehlers, N., Nielsen, K., Wylegala, E., Dobrowolski, D. and Midelfart, A. (2013) 'Metabolic profile of keratoconic cornea', *Current Eye Research,* 38(2), pp. 305-309.

Kumar, P., Nagarajan, A. and Uchil, P. D. (2018) 'Analysis of cell viability by the lactate dehydrogenase assay', *Cold Spring Harbor protocols,* 2018(6), pp. 465-468.

Kumar, R. and Lal, S. (2014) 'Synthesis of organic nanoparticles and their applications in drug delivery and food nanotechnology: a review', *Journal of Nanomaterials & Molecular Nanotechnology,* 3(4), pp. 1-11.

Lakhundi, S., Siddiqui, R. and Khan, N. A. (2017) 'Pathogenesis of microbial keratitis', *Microbial Pathogenesis,* 104, pp. 97-109.

Lane, A. N. and Fan, T. W. M. (2015) 'Regulation of mammalian nucleotide metabolism and biosynthesis', *Nucleic acids research,* 43(4), pp. 2466-2485.

Larson, E. M., Doughman, D. J., Gregerson, D. S. and Obritsch, W. F. (1997) 'A new, simple, nonradioactive, nontoxic in vitro assay to monitor corneal endothelial cell viability', *Investigative ophthalmology & visual science,* 38(10), pp. 1929-1933.

Leitsch, D., Köhsler, M., Marchetti-Deschmann, M., Deutsch, A., Allmaier, G., Duchêne, M. and Walochnik, J. (2010) 'Major role for cysteine proteases during the early phase of *Acanthamoeba castellanii* encystment', *Eukaryotic cell,* 9(4), pp. 611-618.

Lin, Y. H., Shen, L. J., Chou, T. H. and Shih, Y. H. (2021) 'Synthesis, stability, and cytotoxicity of novel cerium oxide nanoparticles for biomedical applications', *Journal of cluster science,* 32(2), pp. 405-413.

Lindsay, R. G., Watters, G., Johnson, R., Ormonde, S. E. and Snibson, G. R. (2007) 'Acanthamoeba keratitis and contact lens wear', *Clinical & Experimental Optometry,* 90(5), pp. 351-360.

Liu, X., Kim, C. N., Yang, J., Jemmerson, R. and Wang, X. (1996) 'Induction of apoptotic program in cell-free extracts: requirement for dATP and cytochrome c', *Cell,* 86(1), pp. 147-157.

Lorenzo-Morales, J., Khan, N. and Walochnik, J. (2015) 'An update on Acanthamoeba keratitis: diagnosis, pathogenesis and treatment', *Parasite,* 22(10), pp. 1-20.

Magdolenova, Z., Bilaničová, D., Pojana, G., Fjellsbø, L. M., Hudecova, A., Hasplova, K., Marcomini, A. and Dusinska, M. (2012) 'Impact of agglomeration and different dispersions of titanium dioxide nanoparticles on the human related in vitro cytotoxicity and genotoxicity', *Journal of environmental monitoring,* 14(2), pp. 455-464.

Maghsood, A. H., Sissons, J., Rezaian, M., Nolder, D., Warhurst, D. and Khan, N. A. (2005) '*Acanthamoeba* genotype T4 from the UK and Iran and isolation of the T2 genotype from clinical isolates', *Journal of medical microbiology,* 54(8), pp. 755-759.

Manke, A., Wang, L. and Rojanasakul, Y. (2013) 'Mechanisms of nanoparticle-induced oxidative stress and toxicity', *BioMed research international,* 2013, pp. 1-15.

Maradze, D., Musson, D., Zheng, Y., Cornish, J., Lewis, M. and Liu, Y. (2018) 'High magnesium corrosion rate has an effect on osteoclast and mesenchymal stem cell role during bone remodelling', *Scientific reports,* 8(1), pp. 1-15.

Marciano-Cabral, F. and Cabral, G. (2003) '*Acanthamoeba* spp. as agents of disease in humans', *Clinical Microbiology Reviews,* 16(2), pp. 273-307.

Marciano-Cabral, F. and Toney, D. M. (1998) 'The interaction of *Acanthamoeba* spp. with activated macrophages and with macrophage cell lines', *Journal of Eukaryotic Microbiology,* 45(4), pp. 452-458.

Marijnen, Y. M. T., Korte, D. d., Haverkort, W. A., den Breejen, E. J. S., van Gennip, A. H. and Roos, D. (1989) 'Studies on the incorporation of precursors into purine and pyrimidine nucleotides via ‘de novo’ and ‘salvage’ pathways in normal lymphocytes and lymphoblastic cell-line cells', *Biochimica et biophysica acta. Molecular cell research,* 1012(2), pp. 148-155.

Martinez, A. J. and Visvesvara, G. S. (1997) 'Free-living, amphizoic and opportunistic amebas', *Brain pathology,* 7(1), pp. 583-598.

Masterton, S. and Ahearne, M. (2018) 'Mechanobiology of the corneal epithelium', *Experimental eye research,* 177, pp. 122-129.

Mattana, A., Alberti, L., Delogu, G., Fiori, P. L. and Cappuccinelli, P. (2009) 'In vitro activity of *Acanthamoeba castellanii* on human platelets and erythrocytes', *Infection and immunity,* 77(2), pp. 733-738.

Mattana, A., Bennardini, F., Usai, S., Fiori, P., Franconi, F. and Cappuccinelli, P. (1997) '*Acanthamoeba castellanii* metabolites increase the intracellular calcium level and cause cytotoxicity in Wish cells', *Microbial Pathogenesis,* 23(2), pp. 85-93.

Mattana, A., Cappai, V., Alberti, L., Serra, C., Fiori, P. L. and Cappuccinelli, P. (2002) 'ADP and other metabolites released from *Acanthamoeba castellanii* lead to human monocytic cell death through apoptosis and stimulate the secretion of proinflammatory cytokines', *Infection and immunity,* 70(8), pp. 4424-4432.

McBride, J., Ingram, P. R., Henriquez, F. L. and Roberts, C. W. (2005) 'Development of colorimetric microtiter plate assay for assessment of antimicrobials against *Acanthamoeba*', *Journal of clinical microbiology,* 43(2), pp. 629-634.

Megha, K., Gupta, A., Sehgal, R. and Khurana, S. (2017) 'An improvised medium for axenic cultivation of *Acanthamoeba* spp', *Indian Journal of Medical Microbiology,* 35(4), pp. 597-599.

Mitra, M. M., Alizadeh, H., Gerard, R. D. and Niederkorn, J. Y. (1995) 'Characterization of a plasminogen activator produced by

Acanthamoeba castellanii', *Molecular & Biochemical Parasitology,* 73(1-2), pp. 157-164.

Moon, E. K., Chung, D. I., Hong, Y. C. and Kong, H. H. (2008) 'Characterization of a serine proteinase mediating encystation of *Acanthamoeba*', *Eukaryotic Cell,* 7(9), pp. 1513-1517.

Naemat, A., Sinjab, F., McDonald, A., Downes, A., Elfick, A., Elsheikha, H. M. and Notingher, I. (2018) 'Visualizing the interaction of *Acanthamoeba castellanii* with human retinal epithelial cells by spontaneous Raman and CARS imaging', *Journal of Raman Spectroscopy,* 49(3), pp. 412-423.

Nagata, S. (2000) 'Apoptotic DNA Fragmentation', *Experimental Cell Research,* 256(1), pp. 12-18.

Nagington, J., Watson, P. G., Playfair, T. J., McGill, J., Jones, B. and Steele, A. D. M. (1974) 'Amoebic infection of the eye', *The Lancet,* 304(7896), pp. 1537-1540.

Negrutskii, B. S. and Deutscher, M. P. (1991) 'Channeling of aminoacyl-tRNA for protein synthesis in vivo', *Proceedings of the National Academy of Sciences - PNAS,* 88(11), pp. 4991-4995.

Niyyati, M., Dodangeh, S. and Lorenzo-Morales, J. (2016) 'A review of the current research trends in the application of medicinal plants as a source for novel therapeutic agents against *Acanthamoeba* infections', *Iranian journal of pharmaceutical research : IJPR,* 15(4), pp. 893-900.

Okumura, N., Inoue, R., Kakutani, K., Nakahara, M., Kinoshita, S., Hamuro, J. and Koizumi, N. (2017) 'Corneal endothelial cells have an absolute requirement for cysteine for survival', *Cornea,* 36(8), pp. 988-994.

Olszewski, K. L., Morrisey, J. M., Wilinski, D., Burns, J. M., Vaidya, A. B., Rabinowitz, J. D. and Llinás, M. (2009) 'Host-parasite interactions revealed by *Plasmodium falciparum* metabolomics', *Cell host & microbe,* 5(2), pp. 191-199.

Omaña-Molina, M., González-Robles, A., Iliana Salazar-Villatoro, L., Lorenzo-Morales, J., Cristóbal-Ramos, A. R., Hernández-Ramírez, V. I., Talamás-Rohana, P., Méndez Cruz, A. R. and Martínez-Palomo, A. (2013) 'Reevaluating the role of *Acanthamoeba* proteases in tissue invasion: observation of cytopathogenic mechanisms on MDCK cell monolayers and hamster corneal cells', *BioMed research international,* 2013, pp. 1-13.

Ortega-Rivas, A., Padrón, J. M., Valladares, B. and Elsheikha, H. M. (2016) '*Acanthamoeba castellanii*: A new high-throughput method for drug screening in vitro', *Acta Tropica,* 164, pp. 95-99.

Paget, T., Haroune, N., Bagchi, S. and Jarroll, E. (2013) 'Metabolomics and protozoan parasites', *Acta Parasitologica,* 58(2), pp. 127-131.

Palmieri, J. R., Gehring, G., Minichino, C. and Elswaifi, S. F. (2011) 'Uptake of nanoparticles of cerium oxide and yttrium oxide by *Acanthamoeba castellanii* (protozoa) and *Daphnia magna* (Crustacea)', *Virginia Journal of Science,* 62(1), pp. 3-14.

Panjwani, N. (2010) 'Pathogenesis of Acanthamoeba Keratitis', *The ocular surface,* 8(2), pp. 70-79.

Parhamifar, L., Andersen, H. and Moghimi, S. M. (2019) 'Lactate dehydrogenase assay for assessment of polycation cytotoxicity', *Methods in Molecular Biology,* 1943, pp. 291-299.

Pettit, D. A., Williamson, J., Cabral, G. A. and Marciano-Cabral, F. (1996) 'In vitro destruction of nerve cell cultures by *Acanthamoeba* spp.: a transmission and scanning electron microscopy study', *The Journal of parasitology,* 82(5), pp. 769-777.

Pešić, M., Podolski-Renić, A., Stojković, S., Matović, B., Zmejkoski, D., Kojić, V., Bogdanović, G., Pavićević, A., Mojović, M., Savić, A., Milenković, I., Kalauzi, A. and Radotić, K. (2015) 'Anti-cancer effects of cerium oxide nanoparticles and its intracellular redox activity', *Chemico-biological interactions,* 232, pp. 85-93.

Phillips, C. D. (2018) 'A brief discussion of genomic therapeutics', *Global journal of pharmacy & pharmaceutical sciences,* 5(2), pp. 43-44.

Polat, Z., Akin and Vural, A. (2012) 'Effect of combined chlorhexidine gluconate and Neosporin on experimental keratitis with two pathogenic strains of *Acanthamoeba*', *Parasitology Research,* 110(5), pp. 1945-1950.

Pussard, M. and Pons, R. (1977) 'Morphologies de la paroi kystique et taxonomie du genre *Acanthamoeba* (Protozoa, Amoebida)', *Protistologica,* 13, pp. 557-610.

Pérez-Santonja, J. J., Kilvington, S., Hughes, R., Tufail, A., Matheson, M. and Dart, J. K. G. (2003) 'Persistently culture

positive Acanthamoeba keratitis : In vivo resistance and in vitro sensitivity', *Ophthalmology,* 110(8), pp. 1593-1600.

Quéméneur, L., Gerland, L.-M., Flacher, M., Ffrench, M., Revillard, J.-P. and Genestier, L. (2003) 'Differential control of cell cycle, proliferation, and survival of primary T lymphocytes by purine and pyrimidine nucleotides', *The Journal of immunology,* 170(10), pp. 4986-4995.

Qvarnstrom, Y., Visvesvara, G. S., Sriram, R. and Da Silva, A. J. (2006) 'Multiplex real-time PCR assay for simultaneous detection of *Acanthamoeba* spp., Balamuthia mandrillaris, and Naegleria fowleri', *Journal of clinical microbiology,* 44(10), pp. 3589-3595.

Rabiah, N. I., Romaniuk, J. A. H., Fuller, G. G., Scales, C. W. and Cegelski, L. (2019) 'Carbon compositional analysis of hydrogel contact lenses by solid-state NMR spectroscopy', *Solid State Nuclear Magnetic Resonance,* 102, pp. 47-52.

Radford, C. F., Minassian, D. C. and Dart, J. K. G. (2002) 'Acanthamoeba keratitis in England and Wales: incidence, outcome, and risk factors', *British Journal of Ophthalmology,* 86(5), pp. 536-542.

Rajeshkumar, S. and Naik, P. (2018) 'Synthesis and biomedical applications of Cerium oxide nanoparticles – A Review', *Biotechnology Reports,* 17, pp. 1-5.

Rampersad, S. N. (2012) 'Multiple applications of alamar blue as an indicator of metabolic function and cellular health in cell viability bioassays', *Sensors,* 12(9), pp. 12347-12360.

Ren, M., Gao, L. and Wu, X. (2010) 'TLR4: the receptor bridging *Acanthamoeba* challenge and intracellular inflammatory responses in human corneal cell lines', *Immunology and cell biology,* 88(5), pp. 529-536.

Renu, G., Divya Rani, V. V., Nair, S. V., Subramanian, K. R. V. and Lakshmanan, V. K. (2012) 'Development of cerium oxide nanoparticles and its cytotoxicity in prostate cancer cells', *Advanced Science Letters,* 6, pp. 17-25.

Roberts, C. W. and Henriquez, F. L. (2010) 'Drug target identification, validation, characterisation and exploitation for treatment of *Acanthamoeba* (species) infections', *Experimental Parasitology,* 126(1), pp. 91-96.

Rocha-Azevedo, B. D., Jamerson, M., Cabral, G. A. and Marciano-Cabral, F. (2010) '*Acanthamoeba culbertsoni*: Analysis of amoebic adhesion and invasion on extracellular matrix components collagen I and laminin-1', *Experimental Parasitology,* 126(1), pp. 79-84.

Sanderson, J., Dartt, D. A., Trinkaus-Randall, V., Pintor, J., Civan, M. M., Delamere, N. A., Fletcher, E. L., Salt, T. E., Grosche, A. and Mitchell, C. H. (2014) 'Purines in the eye: Recent evidence for the physiological and pathological role of purines in the RPE, retinal neurons, astrocytes, Müller cells, lens, trabecular meshwork, cornea and lacrimal gland', *Experimental eye research,* 127, pp. 270-279.

Sant'ana, V. P., Carrijo-Carvalho, L. C., Foronda, A. S., Chudzinski-Tavassi, A. M., de Freitas, D. and de Carvalho, F. R. S. (2015) 'Cytotoxic activity and degradation patterns of structural proteins by corneal isolates of *Acanthamoeba* spp', *Graefe's Archive for Clinical and Experimental Ophthalmology,* 253(1), pp. 65-75.

Sawyer, K. T. and Griffin, L. J. (1975) 'A proposed new family, Acanthamoebidae n. fam. (order Amoebida), for certain cyst-forming filose amoebae', *Transactions of the American Microscopical Society,* 94(1), pp. 93-98.

Schaumberg, A. D., Snow, K. K. and Dana, R. M. (1998) 'The epidemic of Acanthamoeba keratitis: where do we stand?', *Cornea,* 17(1), pp. 3-10.

Schunder, E., Gillmaier, N., Kutzner, E., Herrmann, V., Lautner, M., Heuner, K. and Eisenreich, W. (2014) 'Amino acid uptake and metabolism of *Legionella pneumophila* hosted by *Acanthamoeba castellanii*', *Journal Of Biological Chemistry,* 289(30), pp. 21040-21054.

Schuster, F. L. and Visvesvara, G. S. (2004) 'Free-living amoebae as opportunistic and non-opportunistic pathogens of humans and animals', *International Journal for Parasitology,* 34(9), pp. 1001-1027.

Schwarz, E. L., Roberts, W. L. and Pasquali, M. (2005) 'Analysis of plasma amino acids by HPLC with photodiode array and fluorescence detection', *Clinica Chimica Acta,* 354(1-2), pp. 83-90.

Schwendner, P., Bohmeier, M., Rettberg, P., Beblo-Vranesevic, K., Gaboyer, F., Moissl-Eichinger, C., Perras, A. K., Vannier, P.,

Marteinsson, V. T., Garcia-Descalzo, L., Gómez, F., Malki, M., Amils, R., Westall, F., Riedo, A., Monaghan, E. P., Ehrenfreund, P., Cabezas, P., Walter, N. and Cockell, C. (2018) 'Beyond chloride brines: Variable metabolomic responses in the anaerobic organism *Yersinia intermedia* MASE-LG-1 to NaCl and MgSO4 at identical water activity', *Frontiers in microbiology,* 9, pp. 1-20.

Schwotzer, D., Ernst, H., Schaudien, D., Kock, H., Pohlmann, G., Dasenbrock, C. and Creutzenberg, O. (2017) 'Effects from a 90-day inhalation toxicity study with cerium oxide and barium sulfate nanoparticles in rats', *Particle and fibre toxicology,* 14(23), pp. 1-20.

Serrano-Luna, J. D., Cervantes-Sandoval, I., Calderon, J., Navarro-Garcia, F., Tsutsumi, V. and Shibayama, M. (2006) 'Protease activities of *Acanthamoeba polyphaga* and *Acanthamoeba castellanii*', *Canadian Journal Of Microbiology,* 52(1), pp. 16-23.

Shafaie, S., Hutter, V., Cook, M. T., Brown, M. B. and Chau, D. Y. S. (2016) 'In vitro cell models for ophthalmic drug development applications', *BioResearch Open Access,* 5(1), pp. 94-108.

Shaikh, S., Nazam, N., Rizvi, S. M. D., Ahmad, K., Baig, M. H., Lee, E. J. and Choi, I. (2019) 'Mechanistic insights into the antimicrobial actions of metallic nanoparticles and their implications for multidrug resistance', *International journal of molecular sciences,* 20(10), pp. 1-15.

Sharma, S., Garg, P. and Rao, G. N. (2000) 'Patient characteristics, diagnosis, and treatment of non-contact lens related Acanthamoeba keratitis', *British Journal of Ophthalmology,* 84(10), pp. 1103-1108.

Siddiqui, R., Aqeel, Y. and Khan, N. (2016) 'The development of drugs against *Acanthamoeba* infections', *Antimicrobial Agents And Chemotherapy,* 60(11), pp. 6441-6450.

Siddiqui, R., Emes, R., Elsheikha, H. and Khan, N. A. (2011) 'Area 51: How do *Acanthamoeba* invade the central nervous system?', *Trends in Parasitology,* 27(5), pp. 185-189.

Siddiqui, R. and Khan, N. (2012) 'Biology and pathogenesis of *Acanthamoeba*', *Parasites & Vectors,* 5(6), pp. 1-13.

Siddiqui, R., Roberts, S. K., Ong, T. Y. Y., Mungroo, M. R., Anwar, A. and Khan, N. A. (2019) 'Novel insights into the potential role of ion transport in sensory perception in *Acanthamoeba*', *Parasites and Vectors,* 12(538), pp. 1-8.

Sidney, L. E., McIntosh, O. D. and Hopkinson, A. (2015) 'Phenotypic change and induction of cytokeratin expression during in vitro culture of corneal stromal cells', *Investigative ophthalmology & visual science,* 56(12), pp. 7225-7235.

Singh, B., Fleury, C., Jalalvand, F. and Riesbeck, K. (2012) 'Human pathogens utilize host extracellular matrix proteins laminin and collagen for adhesion and invasion of the host', *FEMS microbiology reviews,* 36(6), pp. 1122-1180.

Singh, R. and Lillard, J. W. (2009) 'Nanoparticle-based targeted drug delivery', *Experimental and molecular pathology,* 86(3), pp. 215-223.

Sixt, B. S., Hiess, B., König, L. and Horn, M. (2012) 'Lack of effective anti-apoptotic activities restricts growth of Parachlamydiaceae in insect cells', *PloS one,* 7(1), pp. e29565-e29565.

Snytnikova, O., Yanshole, L., Iskakov, I., Yanshole, V., Chernykh, V., Stepakov, D., Novoselov, V. and Tsentalovich, Y. (2017) 'Quantitative metabolomic analysis of the human cornea and aqueous humor', *Metabolomics,* 13(12), pp. 1-9.

Soto-Arredondo, K. J., Flores-Villavicencio, L. L., Serrano-Luna, J. J., Shibayama, M. and Sabanero-LÓPez, M. (2014) 'Biochemical and cellular mechanisms regulating *Acanthamoeba castellanii* adherence to host cells', *Parasitology,* 141(4), pp. 531-541.

Sridhar, M. (2018) 'Anatomy of cornea and ocular surface', *Indian journal of ophthalmology,* 66(2), pp. 190-194.

Sriram, R., Shoff, M., Booton, G., Fuerst, P. and Visvesvara, G. S. (2008) 'Survival of *Acanthamoeba* cysts after desiccation for more than 20 years', *Journal of Clinical Microbiology,* 46(12), pp. 4045-4048.

Stapleton, A. F., Ozkan, A. J., Jalbert, A. I., Holden, A. B., Petsoglou, A. C. and McClellan, A. K. (2009) 'Contact lens-related Acanthamoeba keratitis', *Optometry and Vision Science,* 86(10), pp. E1196-E1201.

Swanson, W. M. (2012) 'A cross-sectional analysis of US contact lens user demographics', *Optometry and Vision Science,* 89(6), pp. 839-848.

Takaoka-Sugihara, N., Yamagami, S., Yokoo, S., Matsubara, M. and Yagita, K. (2012) 'Cytopathic effect of *Acanthamoeba* on human corneal fibroblasts', *Molecular vision,* 18, pp. 2221-2228.

Thornberry, N. and Lazebnik, Y. (1998) 'Caspases: Enemies within', *Science,* 281(5381), pp. 1312-1316.

Tripathi, T. and Alizadeh, H. (2014) 'Role of protease-activated receptors 2 (PAR2) in ocular infections and inflammation', *Receptors & clinical investigation,* 1(6), pp. 1-19.

Vanicha, V. and Kanyawim, K. (2006) 'Sulforhodamine B colorimetric assay for cytotoxicity screening', *Nature Protocols,* 1(3), pp. 1112-1116.

Villanueva, M., García, B., Valle, J., Rapún, B., Ruiz de los Mozos, I., Solano, C., Martí, M., Penadés, J. R., Toledo-Arana, A. and Lasa, I. (2018) 'Sensory deprivation in *Staphylococcus aureus*', *Nature communications,* 9(523), pp. 1-12.

Villemez, C. L., Carlo, P. L. and Russell, M. A. (1985) 'Differentiation in *Acanthamoeba castellanii* is induced by specific monoclonal antibodies', *Journal of cellular biochemistry,* 29(4), pp. 373-379.

Vincent, I. M. and Barrett, M. P. (2015) 'Metabolomic-based strategies for anti-parasite drug discovery', *Journal of biomolecular screening,* 20(1), pp. 44-55.

Visvesvara, G. S. (1991) 'Classification of *Acanthamoeba*', *Reviews of infectious diseases,* 13(Supplement 5), pp. S369-S372.

Visvesvara, G. S., Moura, H. and Schuster, F. L. (2007) 'Pathogenic and opportunistic free-living amoebae: *Acanthamoeba* spp., *Balamuthia mandrillaris*, *Naegleria fowleri,* and *Sappinia diploidea*', *FEMS Immunology & Medical Microbiology,* 50(1), pp. 1-26.

Voigt, W. (2005) 'Sulforhodamine B assay and chemosensitivity', *Methods in molecular medicine,* 110, pp. 39-48.

Wang, L., Hu, C. and Shao, L. (2017) 'The antimicrobial activity of nanoparticles: present situation and prospects for the future', *International Journal Of Nanomedicine,* 12, pp. 1227-1249.

Wilson, S. L., Yang, Y. and El Haj, A. J. (2014) 'Corneal stromal cell plasticity: in vitro regulation of cell phenotype through cell-cell interactions in a three-dimensional mode', *Tissue engineering,* 20(1-2), pp. 1-14.

Wu, D., Feng, M., Wang, Z.-X., Qiao, K., Tachibana, H. and Cheng, X.-J. (2018) 'Molecular and biochemical characterization of key enzymes in the cysteine and serine metabolic pathways of *Acanthamoeba castellanii*', *Parasites & vectors,* 11(1), pp. 604-604.

Xia, T., Kovochich, M., Liong, M., Mädler, L., Gilbert, B., Shi, H., Yeh, J. I., Zink, J. I. and Nel, A. E. (2008) 'Comparison of the mechanism of toxicity of zinc oxide and cerium oxide nanoparticles based on dissolution and oxidative stress properties', *ACS nano,* 2(10), pp. 2121-2134.

Xia, T., Rome, L. and Nel, A. (2008) 'Particles slip cell security', *Nature materials,* 7(7), pp. 519-520.

Xu, C. and Qu, X. (2014) 'Cerium oxide nanoparticle: a remarkably versatile rare earth nanomaterial for biological applications', *NPG Asia materials,* 6(90), pp. 1-16.

Xue, Y., Zhai, Y., Zhou, K., Wang, L., Tan, H., Luan, Q. and Yao, X. (2012) 'The vital role of buffer anions in the antioxidant activity of CeO_2 nanoparticles', *Chemistry: A European Journal,* 18(35), pp. 11115-11122.

Yah, C. S., Simate, G. and Iyuke, S. E. (2012) 'Nanoparticles toxicity and their routes of exposures', *Pakistan journal of pharmaceutical sciences,* 25(2), pp. 477-491.

Yang, Z., Cao, Z. and Panjwani, N. (1997) 'Pathogenesis of Acanthamoeba keratitis: Carbohydrate-mediated host- parasite interactions', *Infection and Immunity,* 65(2), pp. 439-445.

Zhang, Y., Wu, X., Hou, C., Shang, K., Yang, K., Tian, Z., Pei, Z., Qu, Y. and Pei, Y. (2018) 'Dual-responsive dithio-polydopamine coated porous CeO_2 nanorods for targeted and synergistic drug delivery', *International Journal of Nanomedicine,* 13, pp. 2161-2173.

Zheng, Q., Fang, Y., Zeng, L., Li, X., Chen, H., Song, H., Huang, J. and Shi, S. (2019) 'Cytocompatible cerium oxide-mediated antioxidative stress in inhibiting ocular inflammation-associated corneal neovascularization', *Journal of materials chemistry. B, Materials for biology and medicine,* 7(43), pp. 6759-6769.

Zholobak, N. M., Olevinskaia, Z. M., Spivak, N. I., Shcherbakov, A. B., Ivanov, V. K. and Usatenko, A. V. (2010) 'Antiviral effect of cerium dioxide nanoparticles stabilized by low-molecular polyacrylic acid', *Mikrobiolohichnyi zhurnal,* 72(3), pp. 42-47.

Zhou, W., Warrilow, A. G. S., Thomas, C. D., Ramos, E., Parker, J. E., Price, C. L., Vanderloop, B. H., Fisher, P. M., Loftis, M. D., Kelly, D. E., Kelly, S. L. and Nes, W. D. (2018) 'Functional importance for developmental regulation of sterol biosynthesis in *Acanthamoeba castellanii*', *BBA - Molecular and Cell Biology of Lipids,* 1863(10), pp. 1164-1178.

Zhou, Z., Ni, K., Deng, H. and Chen, X. (2020) 'Dancing with reactive oxygen species generation and elimination in nanotheranostics for disease treatment', *Advanced drug delivery reviews,* 158, pp. 73-90.

Appendices

Appendix A:

Table 4-3 A. Analysis of the amino acid content of ACCM - M199.

Abbreviation	Amino acid	Amino acid concentration in control	Amino acid concentration at 3 h	Amino acid concentration at 48 h	Quality control
Taur	**Taurine**	0.0BDL	7.182	7.98	200.189
Asp	**Aspartic acid**	0.0BDL	0.0BDL	0.0BDL	200.905
Thr	**Threonine**	264.985	355.231	329.956	200.97
Ser	**Serine**	239.623	361.151	326.071	201.224
Asn	**Asparagine**	0.0BDL	78.227	52.364	199.84
Glu	**Glutamic Acid**	471.952	687.661	624.429	201.97
Gln	**Glutamine**	557.693	510.795	459.522	196.584
Gly	**Glycine**	649.684	701.355	691.881	199.221
Ala	**Alanine**	281.41	548.228	462.948	199.696
Citr	**Citrulline**	0.0BDL	5.577	4.463	199.126
Val	**Valine**	213.814	372.388	332.569	199.231
Cys	**Cysteine**	70.646	70.23	83.027	99.54
Met	**Methionine**	90.336	131.655	119.182	199.283
Ile	**Isoleucine**	151.299	271.686	242.351	200.329
Leu	**Leucine**	451.091	677.551	614.754	201.695
Tyr	**Tyrosine**	256.469	259.476	265.152	201.531
b-ala	**β-Alanine**	0.0BDL	11.475	6.303	199.207
Phe	**Phenylalanine**	156.366	262.728	233.03	200.581
Homocys	**Homocystine**	0.0BDL	2.029	0.979	201.518
Orn	**Ornithine**	0.0BDL	20.806	13.078	200.758
Lys	**Lysine**	383.19	483.717	461.801	201.586
His	**Histidine**	99.874	116.943	115.047	196.157
Tryp	**Tryptophan**	21.993	23.708	24.869	203.053
Argine	**Arginine**	355.427	390.019	388.835	195.425
Pro	**Proline**	318.677	376.096	368.415	193.93

Table 4-3 B. Analysis of principal components containing amino acid in ACCM - M199.

Abbreviation	Component	Component concentration in control	Component concentration at 3 h	Component concentration at 48 h	Quality control
Phser	**Phospho-serine**	12.048	18.38	12.677	201.273
Pea	**Phosphoethanolamine**	0.0BDL	5.443	0.0BDL	197.845
Urea	**Urea**	0.0BDL	0.0BDL	19.576	197.119
Aaaa	**α-aminoadipic acid**	6.078	7.152	7.341	200.132
Aaba	**α-aminobutyric acid**	0.0BDL	3.196	3.007	200.597
cysth-1	**Cystathionine-1**	0.0BDL	0.073	0.02	85.76
cysth-2	**Cystathionine-2**	0.0BDL	1.136	0.403	114.276
Baiba	**β-aminoisobutyric**	0.0BDL	0.0BDL	0.0BDL	198.244
Homocys	**Homocystine**	0.0BDL	2.029	0.979	201.518
Gaba	**g-Aminobutyric acid**	0.0BDL	0.0BDL	0.0BDL	202.908
Ethamn	**Ethanolamine**	45.041	35.192	37.281	207.964
Amm	**Ammonium**	186.54	367.627	327.271	206.103
hylys 1+2	**Hydroxylysine**	0.0BDL	0.0BDL	0.0BDL	201.065
1-mhis	**1-Methylhistidine**	0.0BDL	2.446	0.0BDL	200.701
3-mhis	**3-Methylhistidine**	0.0BDL	4.229	2.466	198.656
Ans	**L-Anserine**	0.0BDL	0.0BDL	0.0BDL	100.24
Car	**Carnosine**	0.0BDL	0.0BDL	0.0BDL	198.291
Hyp	**Hydroxyproline**	365.467	510.732	471.391	204.593

Table 4-4 A. Analysis of amino acid content of ACCM – Epilife.

Abbreviation	Amino acid	Amino acid concentration in control	Amino acid concentration at 3 h	Amino acid concentration at 48 h	Quality control
Taur	**Taurine**	0.0BDL	1.946	1.765	200.189
Asp	**Aspartic acid**	0.0BDL	0.0BDL	0.0BDL	200.905
Thr	**Threonine**	71.92	159.521	136.038	200.97
Ser	**Serine**	593.298	677.233	655.58	201.224
Asn	**Asparagine**	106.706	167.412	149.007	199.84
Glu	**Glutamic Acid**	193.003	396.746	383.992	201.97
Gln	**Glutamine**	4650.292	4075.608	3946.197	196.584
Gly	**Glycine**	94.505	179.968	156.539	199.221
Ala	**Alanine**	98.118	322.872	250.063	199.696
Citr	**Citrulline**	0.0BDL	5.649	4.998	199.126
Val	**Valine**	169.198	299.849	273.292	199.231
Cys	**Cysteine**	58.225	61.66	68.988	99.54
Met	**Methionine**	120.461	168.634	157.204	199.283
Ile	**Isoleucine**	391.126	476.89	462.883	200.329
Leu	**Leucine**	295.168	495.386	436.653	201.695
Tyr	**Tyrosine**	99.19	116.551	116.418	201.531
b-ala	**β-Alanine**	0.0BDL	10.896	5.496	199.207
Phe	**Phenylalanine**	154.876	242.663	216.484	200.581
Homocys	**Homocystine**	0.0BDL	1.131	1.994	201.518
Orn	**Ornithine**	0.0BDL	16.15	9.723	200.758
Lys	**Lysine**	129.194	231	210.457	201.586
His	**Histidine**	194.758	199.002	200.365	196.157
Tryp	**Tryptophan**	11.301	15.533	15.599	203.053
Argine	**Arginine**	1126.34	1135.079	1148.591	195.425
Pro	**Proline**	187.636	248.552	263.132	193.93

Table 4-4 B. Analysis of principal components containing amino acid in ACCM – Epilife.

Abbreviation	Component	Component concentration in control	Component concentration at 3h	Component concentration at 48h	Quality control
Phser	**Phospho-serine**	3.726	4.753	8.76	201.273
Pea	**Phosphoethanolamine**	93.184	88.342	88.097	197.845
Urea	**Urea**	0.0BDL	0.0BDL	37.88	197.119
Aaaa	**α-aminoadipic acid**	12.157	11.924	12.155	200.132
Aaba	**α-aminobutyric acid**	0.0BDL	2.514	2.253	200.597
cysth-1	**Cystathionine-1**	1.127	0.009	0.0BDL	85.76
cysth-2	**Cystathionine-2**	0.0BDL	0.459	0.0BDL	114.276
Baiba	**β-aminoisobutyric**	0.0BDL	0.0BDL	0.0BDL	198.244
Homocys	**Homocystine**	0.0BDL	1.131	1.994	201.518
Gaba	**g-Aminobutyric acid**	0.0BDL	0.0BDL	0.0BDL	202.908
Ethamn	**Ethanolamine**	93.486	116.666	117.542	207.964
Amm	**Ammonium**	1142.143	1663.627	1728.788	206.103
hylys1+2	**Hydroxylysine**	0.0BDL	0.0BDL	0.0BDL	201.065
1-mhis	**1-Methylhistidine**	0.0BDL	1.278	0.0BDL	200.701
3-mhis	**3-Methylhistidine**	0.0BDL	0.0BDL	0.0BDL	198.656
Ans	**L-Anserine**	0.0BDL	0.0BDL	0.0BDL	100.24
Car	**Carnosine**	0.0BDL	0.0BDL	0.0BDL	198.291
Hyp	**Hydroxyproline**	126.802	266.797	220.746	204.593

Appendix B:

Table 5-2 Log fold-change data for the three comparisons of amino acid metabolism map metabolites, identified and annotated in the dataset by PiMP.

Name	Formula	Log Fold Change (logFC)			Identification
		T48hCTRL (B) /Baseline (A)	T48hINF (C) / Baseline (A)	T48hINF (C) / T48hCTRL (B)	
L-Glutamine	C5H10N2O3	-3.02	0.69	3.71	identified
D-Glutamine	C5H10N2O3	-3.02	0.69	3.71	annotated
Isoglutamine	C5H10N2O3	-3.02	0.69	3.71	annotated
Betaine	C5H11NO2	-2.69	1	3.69	identified+fragment
Creatinine	C4H7N3O	-2.27	-1.54	0.73	identified
1-Pyrroline-4-hydroxy-2-carboxylate	C5H7NO3	-2.21	0.25	2.46	annotated
L-1-Pyrroline-3-hydroxy-5-carboxylate	C5H7NO3	-2.21	0.25	2.46	annotated
4-Oxoproline	C5H7NO3	-2.21	0.25	2.46	annotated
5-Oxo-D-proline	C5H7NO3	-2.21	0.25	2.46	annotated
Anthranilate	C7H7NO2	-2.06	-0.41	1.65	annotated
3-Phospho-D-glycerate	C3H7O7P	-1.75	-2.78	-1.03	identified
2-phospho-D-glycerate	C3H7O7P	-1.75	-2.78	-1.03	identified
L-Glutamate	C5H9NO4	-1.66	-0.66	1.01	identified+fragment
DL-Glutamate	C5H9NO4	-1.66	-0.66	1.01	annotated+fragment
L-4-Hydroxyglutamate semialdehyde	C5H9NO4	-1.66	-0.66	1.01	annotated+fragment
D-Glutamic acid	C5H9NO4	-1.66	-0.66	1.01	annotated+fragment
O-Acetyl-L-serine	C5H9NO4	-1.66	-0.66	1.01	identified+fragment
2-Oxo-4-hydroxy-5-aminovalerate	C5H9NO4	-1.66	-0.66	1.01	annotated+fragment
D-Fructose 1,6-bisphosphate	C6H14O12P2	-1.62	-1.92	-0.3	annotated
L-homoserine	C4H9NO3	-1.54	0.48	2.02	identified+fragment
L-Threonine	C4H9NO3	-1.54	0.48	2.02	identified+fragment
L-Allothreonine	C4H9NO3	-1.54	0.48	2.02	annotated+fragment
L-Proline	C5H9NO2	-1.53	0.19	1.72	identified+fragment
D-Proline	C5H9NO2	-1.53	0.19	1.72	annotated+fragment
Pantothenate	C9H17NO5	-1.46	-2.09	-0.63	annotated
5-Oxoproline	C5H7NO3	-1.36	-0.22	1.14	identified
Taurine	C2H7NO3S	-1.14	1.3	2.44	identified
L-Histidine	C6H9N3O2	-1.11	0.42	1.54	annotated
D-erythro-3-Methylmalate	C5H8O5	-1.07	-0.01	1.06	annotated
(R)-2-Methylmalate	C5H8O5	-1.07	-0.01	1.06	annotated
Phosphocreatine	C4H10N3O5P	-1	-1.66	-0.65	annotated
L-Serine	C3H7NO3	-0.98	-0.3	0.67	identified
D-Serine	C3H7NO3	-0.98	-0.3	0.67	annotated
S-Adenosyl-L-methionine	C15H22N6O5S	-0.96	-0.24	0.72	annotated+fragment
L-Leucine	C6H13NO2	-0.9	0.21	1.1	identified
2S-Amino-3S-methylpentanoic acid	C6H13NO2	-0.9			annotated

			0.21	1.1	
(3R)-beta-Leucine	C6H13NO2	-0.9	0.21	1.1	annotated
Beta-Tyrosine	C9H11NO3	-0.78	0.39	1.17	annotated+fragment
N-Hydroxy-L-phenylalanine	C9H11NO3	-0.78	0.39	1.17	annotated+fragment
L-Tyrosine	C9H11NO3	-0.78	0.39	1.17	annotated+fragment
L-Tyrosine	C9H11NO3	-0.66	0.38	1.04	annotated
L-Arginine	C6H14N4O2	-0.53	0.04	0.57	identified
D-Arginine	C6H14N4O2	-0.53	0.04	0.57	annotated
L-Methionine	C5H11NO2S	-0.42	0.85	1.26	identified+fragment
L-Tryptophan	C11H12N2O2	-0.41	0.32	0.73	identified
L-Valine	C5H11NO2	-0.38	0.33	0.72	identified
L-Metanephrine	C10H15NO3	-0.36	-0.4	-0.03	annotated
L-Phenylalanine	C9H11NO2	-0.35	0.72	1.07	identified+fragment
D-Phenylalanine	C9H11NO2	-0.35	0.72	1.07	annotated+fragment
N-Acetyl-L-aspartate	C6H9NO5	-0.33	0.44	0.77	annotated
N-Formyl-L-glutamate	C6H9NO5	-0.33	0.44	0.77	annotated
L-Homophenylalanine	C10H13NO2	-0.13	-0.34	-0.21	annotated
Creatine	C4H9N3O2	-0.12	0.94	1.06	annotated+fragment
3-Ureidopropionate	C4H8N2O3	-0.05	1.62	1.67	annotated
L-Asparagine	C4H8N2O3	-0.05	1.62	1.67	identified
N-Carbamoylsarcosine	C4H8N2O3	-0.05	1.62	1.67	annotated
L-Lysine	C6H14N2O2	-0.03	0.43	0.47	identified
(3S,5S)-3,5-Diaminohexanoate	C6H14N2O2	-0.03	0.43	0.47	annotated
(3S)-3,6-Diaminohexanoate	C6H14N2O2	-0.03	0.43	0.47	annotated
2,5-Diaminohexanoate	C6H14N2O2	-0.03	0.43	0.47	annotated
(2R,3R)-3-Methylornithine	C6H14N2O2	-0.03	0.43	0.47	annotated
D-Lysine	C6H14N2O2	-0.03	0.43	0.47	annotated
Spermine	C10H26N4	0.04	0.13	0.09	annotated+fragment
5-Aminopentanoic acid	C5H11NO2	0.1	-0.13	-0.23	annotated
L-Aspartate	C4H7NO4	0.28	-0.97	-1.24	identified
D-Aspartate	C4H7NO4	0.28	-0.97	-1.24	annotated
S-Adenosyl-L-homocysteine	C14H20N6O5S	0.58	0.73	0.15	identified
Glutathione	C10H17N3O6S	0.72	0.84	0.12	annotated+fragment
4-Guanidinobutanoate	C5H11N3O2	0.79	3.19	2.39	annotated
Feruloylputrescine	C14H20N2O3	0.86	1.9	1.04	annotated
Uracil	C4H4N2O2	1.03	1.21	0.18	annotated
1-Hydroxy-2-aminoethylphosphonate	C2H8NO4P	2.04	4.21	2.17	annotated+fragment
gamma-Glutamyl-beta-cyanoalanine	C9H13N3O5	2.58	3.65	1.07	annotated
Oxoadipic acid	C6H8O5	2.74	5.75	3.01	annotated
Citraconic acid	C5H6O4	2.96	6.16	3.2	annotated
2,5-Dioxopentanoate	C5H6O4	2.96	6.16	3.2	annotated